



RISING STARS 2021: PATHOLOGY

EDITED BY: Arndt Hartmann and Luca Di Tommaso
PUBLISHED IN: Frontiers in Medicine



frontiers

Frontiers eBook Copyright Statement

The copyright in the text of individual articles in this eBook is the property of their respective authors or their respective institutions or funders. The copyright in graphics and images within each article may be subject to copyright of other parties. In both cases this is subject to a license granted to Frontiers.

The compilation of articles constituting this eBook is the property of Frontiers.

Each article within this eBook, and the eBook itself, are published under the most recent version of the Creative Commons CC-BY licence.

The version current at the date of publication of this eBook is CC-BY 4.0. If the CC-BY licence is updated, the licence granted by Frontiers is automatically updated to the new version.

When exercising any right under the CC-BY licence, Frontiers must be attributed as the original publisher of the article or eBook, as applicable.

Authors have the responsibility of ensuring that any graphics or other materials which are the property of others may be included in the CC-BY licence, but this should be checked before relying on the CC-BY licence to reproduce those materials. Any copyright notices relating to those materials must be complied with.

Copyright and source acknowledgement notices may not be removed and must be displayed in any copy, derivative work or partial copy which includes the elements in question.

All copyright, and all rights therein, are protected by national and international copyright laws. The above represents a summary only. For further information please read Frontiers' Conditions for Website Use and Copyright Statement, and the applicable CC-BY licence.

ISSN 1664-8714

ISBN 978-2-83250-383-6

DOI 10.3389/978-2-83250-383-6

About Frontiers

Frontiers is more than just an open-access publisher of scholarly articles: it is a pioneering approach to the world of academia, radically improving the way scholarly research is managed. The grand vision of Frontiers is a world where all people have an equal opportunity to seek, share and generate knowledge. Frontiers provides immediate and permanent online open access to all its publications, but this alone is not enough to realize our grand goals.

Frontiers Journal Series

The Frontiers Journal Series is a multi-tier and interdisciplinary set of open-access, online journals, promising a paradigm shift from the current review, selection and dissemination processes in academic publishing. All Frontiers journals are driven by researchers for researchers; therefore, they constitute a service to the scholarly community. At the same time, the Frontiers Journal Series operates on a revolutionary invention, the tiered publishing system, initially addressing specific communities of scholars, and gradually climbing up to broader public understanding, thus serving the interests of the lay society, too.

Dedication to Quality

Each Frontiers article is a landmark of the highest quality, thanks to genuinely collaborative interactions between authors and review editors, who include some of the world's best academicians. Research must be certified by peers before entering a stream of knowledge that may eventually reach the public - and shape society; therefore, Frontiers only applies the most rigorous and unbiased reviews.

Frontiers revolutionizes research publishing by freely delivering the most outstanding research, evaluated with no bias from both the academic and social point of view. By applying the most advanced information technologies, Frontiers is catapulting scholarly publishing into a new generation.

What are Frontiers Research Topics?

Frontiers Research Topics are very popular trademarks of the Frontiers Journals Series: they are collections of at least ten articles, all centered on a particular subject. With their unique mix of varied contributions from Original Research to Review Articles, Frontiers Research Topics unify the most influential researchers, the latest key findings and historical advances in a hot research area! Find out more on how to host your own Frontiers Research Topic or contribute to one as an author by contacting the Frontiers Editorial Office: frontiersin.org/about/contact

RISING STARS 2021: PATHOLOGY

Topic Editors:

Arndt Hartmann, Friedrich-Alexander-Universität Erlangen-Nürnberg, Germany

Luca Di Tommaso, Humanitas Research Hospital, Italy

Citation: Hartmann, A., Di Tommaso, L., eds. (2022). Rising Stars 2021: Pathology. Lausanne: Frontiers Media SA. doi: 10.3389/978-2-83250-383-6

Table of Contents

- 05 *Histopathological Evidence of Occipital Involvement in Male Androgenetic Alopecia***
Saranya Khunkhet, Kumutnart Chanprapaph, Suthinee Rutnin and Poonkiat Suchonwanit
- 12 *Gastrointestinal Manifestations of COVID-19 Infection: Clinicopathologic Findings in Intestinal Resections Performed at Single Institution***
Alison E. Burkett, Sophia B. Sher, Chirag R. Patel, Isam Ildin-Eltoum, Deepti Dhall, Camilla Margaroli, Shajan Peter, Goo Lee, Prachi Bajpai, Paul V. Benson, Upender Manne and Sameer Al Diffalha
- 21 *From Macroscopy to Ultrastructure: An Integrative Approach to Pulmonary Pathology***
Stijn E. Verleden, Peter Braubach, Christopher Werlein, Edith Plucinski, Mark P. Kuhnel, Annemiek Snoeckx, Haroun El Addouli, Tobias Welte, Axel Haverich, Florian P. Laenger, Sabine Dettmer, Patrick Pauwels, Veronique Verplancke, Paul E. Van Schil, Therese Lapperre, Johanna M. Kwakkel-Van-Erp, Maximilian Ackermann, Jeroen M. H. Hendriks and Danny Jonigk
- 28 *Up-to-Date Pathologic Classification and Molecular Characteristics of Intrahepatic Cholangiocarcinoma***
Taek Chung and Young Nyun Park
- 46 *Senescence-Associated Molecules and Tumor-Immune-Interactions as Prognostic Biomarkers in Colorectal Cancer***
Franziska Kellers, Aurélie Fernandez, Björn Konukiewicz, Mario Schindeldecker, Katrin E. Tagscherer, Achim Heintz, Moritz Jesinghaus, Wilfried Roth and Sebastian Foersch
- 58 *Myxoinflammatory Fibroblastic Sarcoma of the Parotid Gland: First Case Report and Literature Review***
Changhong Wei, Xuejia Yang, Pingping Guo, Xiaoyu Chen, Chunjun Li, Jun Chen and Sufang Zhou
- 65 *CK5/6 and GATA3 Defined Phenotypes of Muscle-Invasive Bladder Cancer: Impact in Adjuvant Chemotherapy and Molecular Subtyping of Negative Cases***
Florestan J. Koll, Alina Schwarz, Jens Köllermann, Severine Banek, Luis Kluth, Clarissa Wittler, Katrin Bankov, Claudia Döring, Nina Becker, Felix K.H. Chun, Peter J. Wild and Henning Reis
- 74 *The Role of Chronic Liver Diseases in the Emergence and Recurrence of Hepatocellular Carcinoma: An Omics Perspective***
Sofia Zanotti, Gina F. Boot, Mairene Coto-Llerena, John Gallon, Gabriel F. Hess, Savas D. Soysal, Otto Kollmar, Charlotte K. Y. Ng and Salvatore Piscuoglio
- 85 *Investigation of Functional Synergism of CENPF and FOXM1 Identifies POLD1 as Downstream Target in Hepatocellular Carcinoma***
Daniel Wai-Hung Ho, Wai-Ling Macrina Lam, Lo-Kong Chan and Irene Oi-Lin Ng

96 *Ferroptosis in Intrahepatic Cholangiocarcinoma: IDH1^{105GGT} Single Nucleotide Polymorphism Is Associated With Its Activation and Better Prognosis*

Samantha Sarcognato, Diana Sacchi, Luca Fabris, Giacomo Zanus, Enrico Gringeri, Monia Niero, Giovanna Gallina and Maria Guido

105 *Digital Pathology – Rising to the Challenge*

Heather Dawson



Histopathological Evidence of Occipital Involvement in Male Androgenetic Alopecia

Saranya Khunkhet^{1,2†}, Kumutnart Chanprapaph^{1†}, Suthinee Rutnin^{1†} and Poonkiat Suchonwanit^{1*†}

¹ Division of Dermatology, Department of Medicine, Faculty of Medicine, Ramathibodi Hospital, Mahidol University, Bangkok, Thailand, ² Skin Center, Srinakharinwirot University, Bangkok, Thailand

OPEN ACCESS

Edited by:

Luca Di Tommaso,
Humanitas Research Hospital, Italy

Reviewed by:

Leonard Sperling,
Uniformed Services University of the
Health Sciences, United States
Irina Khamaganova,
Pirogov Russian National Research
Medical University, Russia

*Correspondence:

Poonkiat Suchonwanit
poonkiat@hotmail.com

†ORCID:

Saranya Khunkhet
orcid.org/0000-0001-9968-4243
Kumutnart Chanprapaph
orcid.org/0000-0001-7931-3816
Suthinee Rutnin
orcid.org/0000-0001-8268-8790
Poonkiat Suchonwanit
orcid.org/0000-0001-9723-0563

Specialty section:

This article was submitted to
Pathology,
a section of the journal
Frontiers in Medicine

Received: 07 October 2021

Accepted: 02 November 2021

Published: 22 November 2021

Citation:

Khunkhet S, Chanprapaph K, Rutnin S
and Suchonwanit P (2021)
Histopathological Evidence of
Occipital Involvement in Male
Androgenetic Alopecia.
Front. Med. 8:790597.
doi: 10.3389/fmed.2021.790597

Background: The occipital region of the scalp is generally accepted as an unaffected area of androgenetic alopecia (AGA) for both genders. However, evidence of AGA involving the occipital scalp has been demonstrated in women; meanwhile, it is unclear whether occipital involvement also occurs in men.

Objective: We aimed to determine if there is occipital involvement in men with AGA.

Methods: This case-control study compared hair counts of scalp biopsy specimens from the occipital region of 82 men with Hamilton-Norwood III-VII and 82 unaffected men.

Results: The mean ages of men with AGA and controls were 40.1 ± 8.9 and 38.6 ± 10.5 years, respectively ($P = 0.291$). A significant decrease in total hair follicles, terminal hair follicles, follicular units and terminal to vellus (T:V) ratio, along with a significant increase in follicular stela was indicated in the AGA group compared to controls (all $P < 0.05$). Subgroup analyses revealed that average counts of total hair follicles, terminal hair follicles and T:V ratios were also significantly lower in males with Hamilton-Norwood VI and VII than in controls (all $P < 0.05$). There were no correlations between increasing age and hair count parameters, but a significant negative association was found between total follicle numbers and disease duration ($r = -0.23$, $P = 0.02$).

Conclusions: AGA can involve the occipital area of male patients with advanced disease. Therefore, the occiput of particular cases should not be used to determine reference data for normal scalp hair, and preoperative measurements of miniaturized hairs in the donor site are strongly recommended in all persons undergoing hair transplantation.

Keywords: pattern hair loss, transverse section, hair count, donor site, hair transplantation, miniaturization

INTRODUCTION

The most common cause of hair loss in both men and women is androgenetic alopecia (AGA), also known as pattern hair loss, and is characterized by gradual hair thinning within a specific distribution on the scalp in genetically susceptible individuals (1). Male patients typically present with hairline recession in the frontotemporal areas as well as balding of the vertex and mid-scalp whereas female patients usually manifest as diffuse hair thinning over the central scalp with a preserved frontal hairline (2). Androgens are apparently implicated in the pathogenesis of male

AGA; by contrast, the role of androgens in women is much less established (3, 4). Although the etiologies between men and women are not identical, they share similar features which include a miniaturization of hair follicles and a progressive shortening of anagen duration (1, 5).

The diagnosis of AGA is usually straightforward and based upon characteristic clinical findings; however, scalp biopsies, in particular transverse sections, may be required to achieve a definite diagnosis in uncertain cases. The main histopathological features of AGA are as follows: (i) decreased terminal hair follicles and increased vellus hair follicles resulting in a reduced ratio of terminal to vellus (T:V) follicles of $<4:1$; (ii) a slightly increased telogen count, standardly accounting for 15–20%; (iii) the presence of follicular stela below miniaturized hair follicles; and (iv) normal follicular density, apart from long-standing and advanced stages, which reveal an actual decrease in total hair follicles (6, 7).

The occipital region of the scalp has been widely accepted as an uninvolved area of AGA for both sexes, under the concept that affected persons have androgen-sensitive and androgen-insensitive scalp regions. This principle has led to the subsequent introduction of donor dominance theory and hair transplantation as a treatment option. Nonetheless, in our practice, we have observed hair thinning extending toward the occipital scalp in some advanced AGA, with more frequent observations among female patients. This may be partly due to the fact that androgen-independent mechanisms also play a role in many women. Moreover, it was highlighted in the field of hair restoration surgery that hair miniaturization can occur in the back and sides of the scalp (the donor sites), which will negatively influence transplant outcomes (8).

Occipital involvement has been demonstrated in female patients with AGA. Previous phototrichogram studies comparing hair characteristics in the occipital area between female AGA and normal controls showed highly consistent results (9–12). Statistically significant decreases in hair density and thickness relative to controls were confirmed in subjects with Ludwig II and III. Additionally, Ekmekci et al. conducted hair counts in biopsy specimens from the mid-scalp and occipital areas of forty female subjects with Ludwig I and II. A quarter of the subjects possessed occipital findings compatible with AGA (T:V ratios of $<4:1$), and almost 40% of the subjects had findings of suspected AGA in the occipital scalp (T:V ratios ranged from 4:1 to 7:1) (13).

On the contrary, occipital involvement in male AGA has not been proved. The results of phototrichogram studies, performed on the occipital region of men with AGA and normal men, have also been inconsistent. One study showed no significant differences in all hair parameters (14). Another study found statistically significant decreases in hair density and hair diameter in male subjects with the U type of the Basic and Specific classification, corresponding to Hamilton-Norwood VI and VII (15). The aim of our study was to determine whether occipital involvement existed in male patients with AGA.

MATERIALS AND METHODS

Study Design and Participants

This study was approved by the Mahidol University Institutional Review Board for Ethics in Human Research (MURA2020/165) and was conducted in accordance with the principles of the Declaration of Helsinki and in compliance with the International Conference on Harmonization-Good Clinical Practice and local regulatory requirements. Informed consent was obtained from the study participants or their families, as appropriate. All male patients with biopsy-proven AGA, who underwent paired 4 mm punch biopsies from both affected frontal/vertex and clinically normal occipital regions of the scalp for transverse sectioning from 2014 to 2019, were enrolled into this case-control study. Patient demographics and clinical data were collected. Principal exclusion criteria included incomplete medical records and the presence of other hair and scalp disorders. Additional exclusion criteria were documented systemic diseases related to hair loss, the use of medications or energy-based devices which can affect hair growth within 6 months and a history of hair transplantation.

As being considered the most reliable method, histological examination of transverse sections from scalp biopsy specimens was chosen to confirm androgenetic changes. Regarding the biopsy protocol in patients with AGA at our institution, the biopsy landmark on the occipital scalp was the external occipital protuberance of the skull. Paired biopsy specimens from the balding and non-balding occipital scalp were horizontally sectioned using the techniques described by Whiting DA (6). Tissue slides of the biopsy specimen from the occipital scalp in each study subject were reviewed. Two cases were excluded as we were unable to obtain the slides and three cases were excluded on account of tangential cuts, which complicated histologic interpretation. A total of 82 cases remained for analysis.

Control Subjects

The control group consisted of 82 male adult decedents who required an autopsy for legal documentation at our institution. These decedents had no type of hair loss and received a 4 mm punch biopsy on the normal occipital scalp, following our AGA biopsy protocol, for transverse sectioning within 8 h of death to avoid autolysis, after receiving written informed consent from the bereaved relatives. Controls were randomly selected from a pool of male deceased subjects in our previous studies on hair counts from scalp biopsy specimens in the Thai population (16, 17), with an equal number of cases and controls. The biopsy specimens of controls were processed using a protocol identical to those of the study cases. The exclusion criteria used were also indistinguishable.

Assessments

Histology slides of specimens from the occipital scalp of both case and control subjects were re-examined by a blinded dermatopathologist. All follicular structures were identified at various anatomical levels from the epidermis to subcutis. The numbers of total, terminal, and vellus hair follicles, along with the number of follicular units, were recorded. Anagen and telogen

hair follicles, as well as follicular stela were also counted. Catagen hair follicles were included in the group of telogen hair follicles. Half of the intermediate hair follicles were assigned to terminal hair follicles with the other half to vellus hair follicles. Differences in hair parameters between groups were subsequently analyzed.

Statistical Analyses

The minimum sample size for estimation of population mean with a 10% margin of error was 26, calculated using data from the previous study assessing values of hair counts per 4 mm diameter punch biopsy from the occipital scalp of Koreans, demonstrating that the mean number of total hair follicles in male subjects was 15.3 ± 3.9 (18).

Comparisons between study and control groups were performed using the Student's *t*-test, the Mann-Whitney *U* test, or the Chi-squared test as appropriate. For further analyses among study subgroups based on disease severity was conducted using the analysis of variance, the Kruskal-Wallis test, or the Chi-squared test. When the overall comparison $P < 0.05$, pairwise

comparisons of subgroups were performed using the Turkey's honest significance difference test, the Mann-Whitney *U* test, or the Chi-squared test as appropriate. The impact of advancing age on hair changes was determined using the Pearson correlation coefficient. A $P < 0.05$ was considered significant, and all statistical analyses were performed with SPSS software (PASW version 18.0; SPSS Inc., Chicago, IL).

RESULTS

Comparisons of Hair Count Parameters Between AGA and Control Groups

Hair counts from the clinically normal occipital scalp of patients with AGA, compared to controls, are shown in **Table 1**. The mean age of 82 patients with AGA was 40.1 ± 8.9 years whereas the mean age of 82 control subjects was 38.6 ± 10.5 years. The age difference between groups was not statistically significant ($P = 0.291$), representing only 18 months; therefore, an age adjustment was not applied. The mean number of total hair follicles in AGA subjects was 17.6 ± 4.2 (95% confidence interval [CI]: 16.68–18.52), showing a significantly lower number compared with controls (mean: 19.1 ± 6.1 , 95% CI: 18.56–21.24, $P = 0.005$). Average counts of terminal hair follicles and follicular units were also significantly lower in patients with AGA than in controls ($P = 0.001$ and 0.002 , respectively). In addition, there was a significant decrease in T:V ratio and a significant increase in follicular stela in the AGA group ($P = 0.001$ and 0.035 , respectively).

Subgroup Analyses of Subjects With AGA

The summary of hair counts in the control and AGA subgroups based on disease severity are exhibited in **Table 2**. As for the severity of AGA according to Hamilton-Norwood classification, 14 (17%), 18 (22%), 15 (18%), 19 (23%), and 16 (20%) patients were grades III, IV, V, VI, and VII, respectively. The overall comparisons among subgroups revealed statistically significant differences in total hair follicles, terminal hair follicles,

TABLE 1 | Hair counts per 4 mm diameter punch biopsy from the occipital scalp of male patients with androgenetic alopecia and controls.

	Controls	AGA	P-value
Number of cases	82	82	
Age, y, mean (SD)	38.6 (10.5)	40.1 (8.9)	0.291
Total hair follicles, mean (SD)	19.9 (6.1)	17.6 (4.2)	0.005*
Terminal hair follicles, mean (SD)	17.9 (4.2)	15.9 (3.8)	0.001*
Vellus hair follicles, median (range)	2 (0–7)	3 (0–14)	0.359
Follicular units, mean (SD)	9.3 (1.9)	8.4 (1.8)	0.002*
Follicular stela, median (range)	1 (0–4)	3 (0–12)	0.035*
Terminal:vellus ratio	8.9:1	7.4:1	0.001*
Anagen:telogen ratio	92.2:7.8	87.6:12.4	0.889

AGA, androgenetic alopecia; SD, standard deviation; y, year.

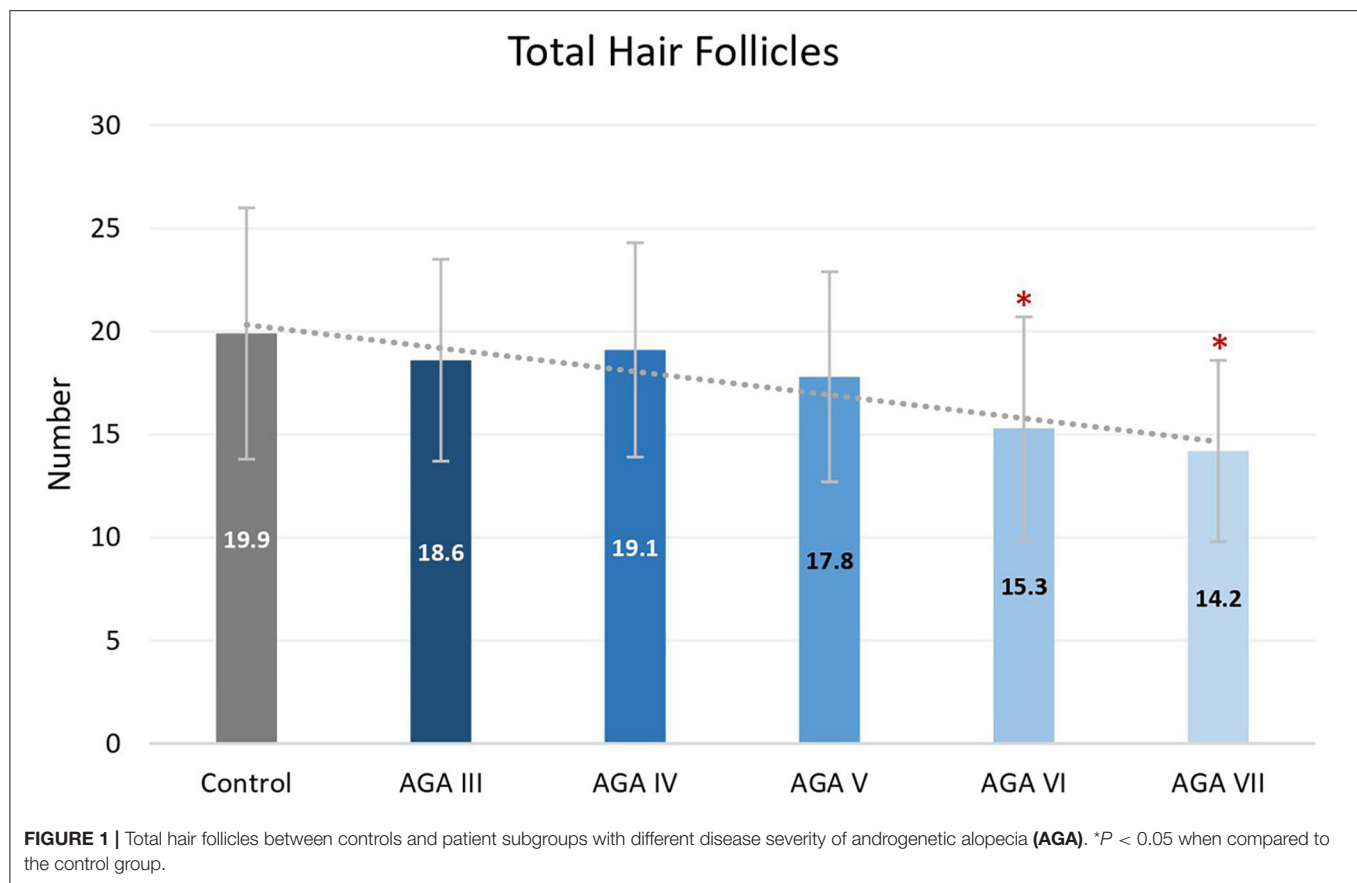
*Statistically significant.

TABLE 2 | Hair counts in the occipital scalp of controls and patient subgroups with different disease severity of androgenetic alopecia.

	Controls	Hamilton-Norwood stages of AGA subjects					P-value
		III	IV	V	VI	VII	
Number of cases	82	14	18	15	19	16	
Age, y, mean (SD)	38.6 (10.5)	40.5 (11.4)	38.2 (12.4)	44.6 (10.2)	38.8 (8.4)	49.5 (7.4)	0.079
Disease duration, y, mean (SD)	–	3.6 (0.8)	5.2 (1.5)	6.5 (2.2)	6.9 (1.9)	8.3 (2.3)	0.001*
Total HF, mean (SD)	19.9 (6.1)	18.6 (4.9)	19.1 (5.2)	17.8 (5.1)	15.3 (5.4)	14.2 (4.4)	0.002*
Terminal HF, mean (SD)	17.9 (4.2)	17.9 (4.8)	18.3 (4.9)	16.1 (5.2)	13.1 (4.2)	11.9 (3.9)	0.002*
Vellus HF, median (range)	2 (0–7)	2 (0–5)	2 (0–8)	3 (0–10)	3 (0–11)	4 (0–14)	0.146
Follicular units, mean (SD)	9.3 (1.9)	8.7 (1.9)	8.8 (2.1)	8.5 (1.6)	7.9 (1.4)	8.1 (2.5)	0.035*
Stela, median (range)	1 (0–4)	1 (0–4)	1 (0–6)	2 (0–8)	2 (0–7)	3 (0–12)	0.294
Terminal:vellus ratio	8.9:1	8.6:1	8.8:1	7.9:1	6.8:1	5.3:1	0.001*
Anagen:telogen ratio	92.2:7.8	90.7:9.3	91.2:8.8	88.6:11.4	85.4:14.6	83.2:16.8	0.294

AGA, androgenetic alopecia; HF, hair follicle; SD, standard deviation; y, year.

*Statistically significant.



follicular units and T:V ratios ($P = 0.002, 0.002, 0.035$ and 0.001 , respectively).

Subgroup analyses showed no significant differences in age between groups; nevertheless, pairwise comparisons displayed significant decreases in the average numbers of total and terminal hair follicles, as well as T:V ratios, in patients with AGA grades VI and VII, when compared to the control group (all $P < 0.05$) (Figures 1–3). There were no significant associations between increasing age and changes in any of the hair parameters; however, a significant negative association between total follicle numbers and disease duration was found ($r = -0.23, P = 0.02$).

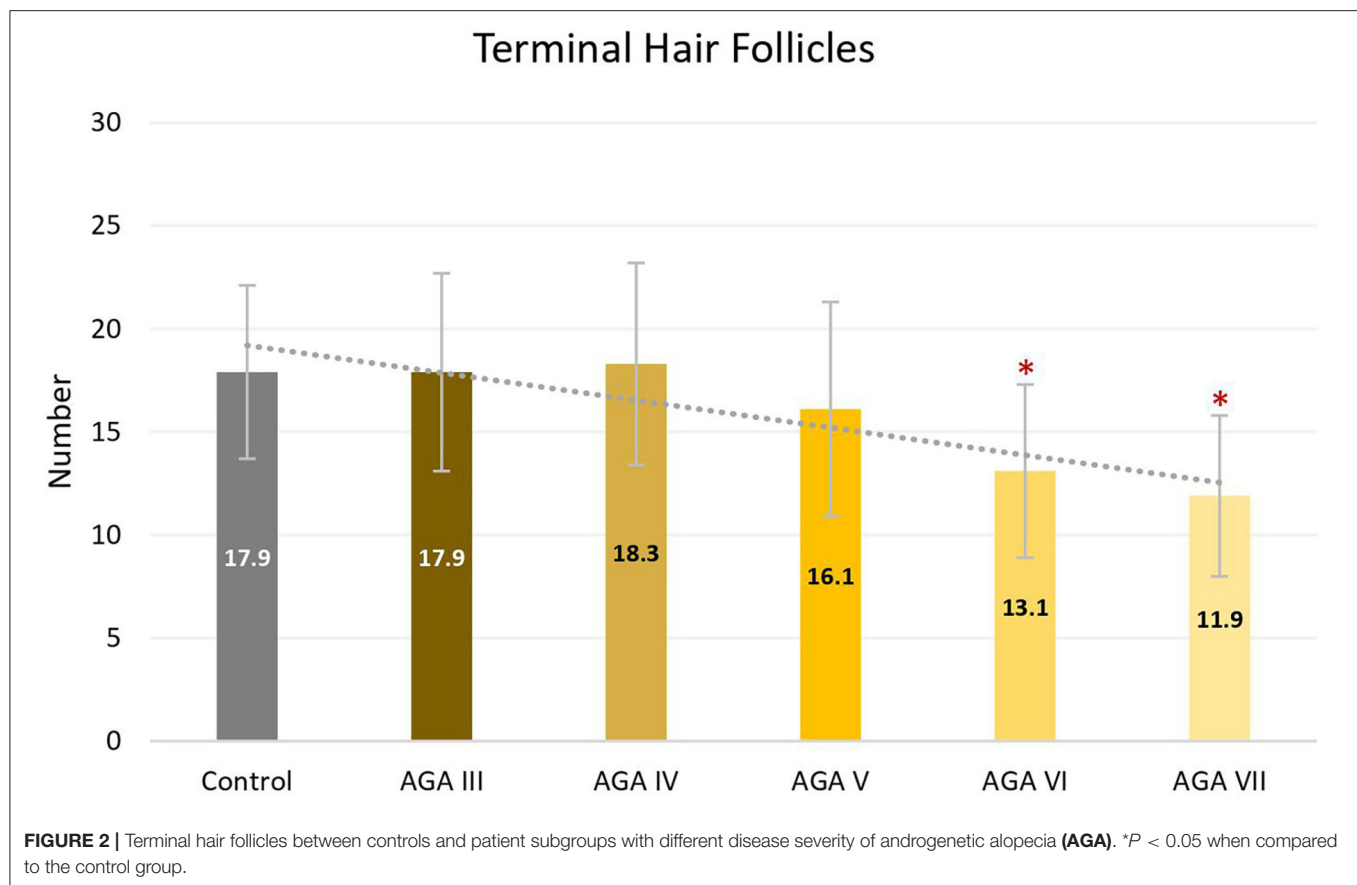
DISCUSSION

We assessed the histopathological changes in the occipital scalp of men with AGA compared with the normal occipital scalp of unaffected men and found a significant reduction in total hair follicles, terminal hair follicles and T:V ratio, along with a significant increase of follicular stela in the occipital scalp of male subjects with AGA. Furthermore, AGA patients had a somewhat wider range of vellus follicle numbers than unaffected men, even though a significant difference in statistics was not achieved among median values. These results parallel the findings from previous histopathological studies analyzing biopsy specimens from the frontal or vertex area of men with

AGA compared to the same scalp sites of normal controls (6, 19, 20).

Based on subgroup comparisons, the more advanced the AGA, the more pronounced the changes in hair parameters, but statistically significant differences from controls were established only in subgroups with advanced disease (Hamilton-Norwood VI–VII). These findings are consonant with two previous comparative studies using phototrichogram analysis on the occipital scalp between male AGA and normal controls. The study showing no significant differences solely recruited subjects with mild to moderate severity (Hamilton-Norwood I–V) (14), whereas the other study revealed a significant change of hair density and diameter in patients with the U type, the most severe type of the Basic and Specific classification, compatible with Hamilton-Norwood VI–VII (15).

Androgenetic changes in the occipital region appear dissimilar to changes in the frontal and vertex regions. An approximate 25% reduction of total follicle numbers in patients with Hamilton-Norwood VI–VII was noticed while the average T:V ratios in these patients were 6.8:1 and 5.3:1, reduced from a normal ratio of 8.9:1 in controls. A noticeable depletion of total hair follicles can be observed in conjunction with an unsubstantial degree of hair miniaturization. In contrast to changes in the frontal and vertex regions, an actual reduction of total follicle numbers is particularly recognized



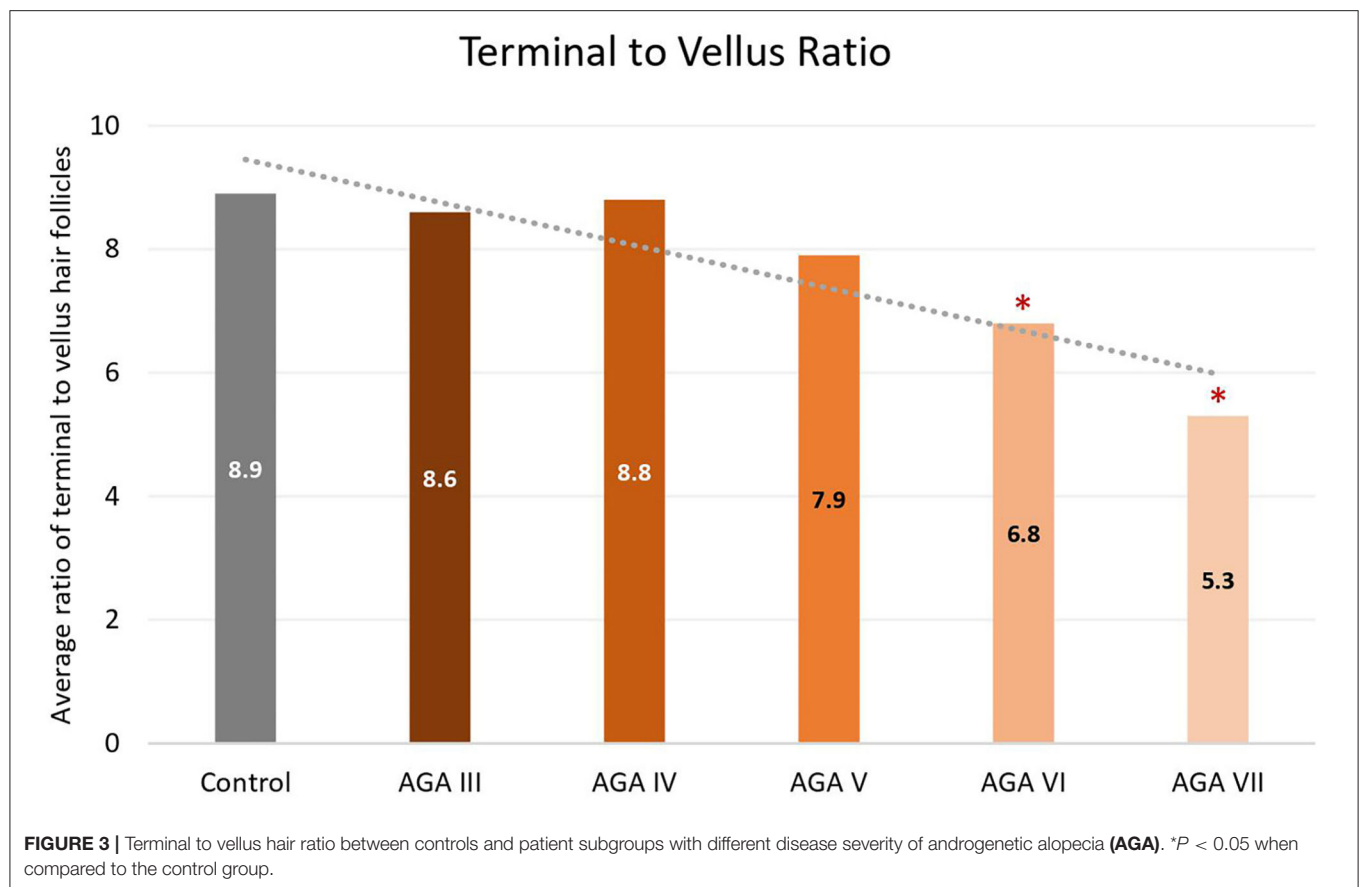
at advanced stages of disease, when a reversal of terminal to vellus hair follicles seems to be obvious (6, 19). Hence, these feature deviations may imply unique characteristics of the occipital scalp in the process of AGA. We hypothesize that occipital hair follicles comprise two populations: one small component influenced by AGA and the unaffected majority. Therefore, clinical changes of AGA in the occipital scalp can be detected only in very advanced disease when the small population experiences pronounced androgenetic changes, including follicular dropout. Meanwhile, the impact on the T:V ratio remains minimal as a large number of normal hair follicles from the unaffected population are included in the ratio calculation.

Distinct anatomical structures and properties related to androgens are suspected to be mainly responsible for site-specific alterations in the occipital scalp of individuals with AGA (21, 22). Accumulating evidence suggests that hair follicles in the occipital area might elicit less androgen-regulated cellular responses than hair follicles in the other scalp areas (22, 23). Frontal hair follicles contained a significantly higher level of androgen receptors and 5 α -reductase enzymes, known for converting testosterone into a more potent androgen called dihydrotestosterone, compared to occipital hair follicles for both genders (24–27). Scalp biopsies also demonstrated a greater amount of aromatase, the enzyme accountable for lowering androgen levels by turning into estrogens, within the occipital

rather than the frontal hair follicles in both men and women (21, 24, 28). Moreover, distinctive characteristics of the occipital scalp are perhaps due to its unique embryological origin. In regard to structural development of the head in vertebrates, a large portion is of neural crest origin while some posterior parts of the head, including the occipital region, are derived from the mesoderm (29).

As no correlation was established in this study between increasing age and total follicle numbers, the follicular dropout that occurred among the men with AGA seems not to result from senescent alopecia. These male patients also displayed an increase of miniaturized hairs and telogen counts, which are not features of age-related alopecia (30–34). On the other hand, a negative correlation between total follicle numbers and disease duration was indicated, showing a coherence with histopathological features of AGA in the original sites where follicular dropout can be observed in long-standing disease (7, 35).

The limitation of this study includes the limited ethnic population. Physical properties of hair, such as hair shapes and density, differ between ethnicities. Our findings might not be generalized to other racial and ethnic groups. Further well-designed prospective studies with diverse racial subjects are required to confirm the present findings.



CONCLUSION

Three main issues and recommendations are derived from this study. First, AGA extendedly involves the occipital area in male patients with advanced disease. Second, androgenetic changes can occur even in the clinically normal occipital scalp; therefore, the occiput of individuals with AGA, especially in advanced stages, should not be used to determine reference data for normal scalp hair. Third, preoperative measurements of miniaturized hairs present in the donor site are strongly recommended in all persons undergoing hair transplantation due to their impact on the success of surgery.

DATA AVAILABILITY STATEMENT

The raw data supporting the conclusions of this article will be made available by the authors, without undue reservation.

REFERENCES

1. Meephansan J, Thummakriengkrai J, Ponnikorn S, Yingmema W, Deenonpoe R, Suchonwanit P. Efficacy of topical tofacitinib in promoting hair growth in non-scarring alopecia: possible mechanism via VEGF induction. *Arch Dermatol Res.* (2017) 309:729–38. doi: 10.1007/s00403-017-1777-5

ETHICS STATEMENT

The studies involving human participants were reviewed and approved by the Mahidol University Institutional Review Board for Ethics in Human Research. Written informed consent to participate in this study was provided by the participants' legal guardian/next of kin.

AUTHOR CONTRIBUTIONS

PS and KC: conceptualization and writing—review and editing. PS and SR: methodology and validation. PS, KC, and SK: formal analysis. PS and SK: investigation and data curation. SK and KC: writing—original draft preparation. All authors have read and agreed to the published version of the manuscript.

2. Leerunyakul K, Suchonwanit P. Asian hair: a review of structures, properties, and distinctive disorders. *Clin Cosmet Investig Dermatol.* (2020) 13:309–18. doi: 10.2147/CCID.S247390
3. Suchonwanit P, Iamsumang W, Rojhirunsakool S. Efficacy of topical combination of 0.25% finasteride and 3% minoxidil versus 3% minoxidil solution in female pattern hair loss: a randomized, double-blind, controlled study. *Am J Clin Dermatol.* (2019) 20:147–53. doi: 10.1007/s40257-018-0387-0

4. Lamsung W, Leerunyakul K, Suchonwanit P. Finasteride and its potential for the treatment of female pattern hair loss: evidence to date. *Drug Des Devel Ther.* (2020) 14:951–9. doi: 10.2147/DDDT.S240615
5. Suchonwanit P, Rujhirunsakool S, Khunkhet S. A randomized, investigator-blinded, controlled, split-scalp study of the efficacy and safety of a 1550-nm fractional erbium-glass laser, used in combination with topical 5% minoxidil versus 5% minoxidil alone, for the treatment of androgenetic alopecia. *Lasers Med Sci.* (2019) 34:1857–64. doi: 10.1007/s10103-019-02783-8
6. Whiting DA. Diagnostic and predictive value of horizontal sections of scalp biopsy specimens in male pattern androgenetic alopecia. *J Am Acad Dermatol.* (1993) 28(Pt. 1):755–63. doi: 10.1016/0190-9622(93)70106-4
7. Olsen EA, Messenger AG, Shapiro J, Bergfeld WF, Hordinsky MK, Roberts JL, et al. Evaluation and treatment of male and female pattern hair loss. *J Am Acad Dermatol.* (2005) 52:301–11. doi: 10.1016/j.jaad.2004.04.008
8. Bernstein R, Rassman W. Densitometry and video-microscopy. *Hair Transplant Forum Int.* (2007) 17:49–51. doi: 10.33589/17.2.0041
9. Ekmekci TR, Koslu A. Phototrichogram findings in women with androgenetic alopecia. *Skin Res Technol.* (2006) 12:309–12. doi: 10.1111/j.0909-752X.2006.00196.x
10. Kang H, Kang TW, Lee SD, Park YM, Kim HO, Kim SY. The changing patterns of hair density and thickness in South Korean women with hair loss: clinical office-based phototrichogram analysis. *Int J Dermatol.* (2009) 48:14–21. doi: 10.1111/j.1365-4632.2009.03795.x
11. Mai W, Sun Y, Liu X, Lin D, Lu D. Characteristic findings by phototrichogram in southern Chinese women with female pattern hair loss. *Skin Res Technol.* (2019) 25:447–55. doi: 10.1111/srt.12672
12. Rujhirunsakool S, Suchonwanit P. Parietal scalp is another affected area in female pattern hair loss: an analysis of hair density and hair diameter. *Clin Cosmet Investig Dermatol.* (2018) 11:7–12. doi: 10.2147/CCID.S153768
13. Ekmekci TR, Sakiz D, Koslu A. Occipital involvement in female pattern hair loss: histopathological evidences. *J Eur Acad Dermatol Venereol.* (2010) 24:299–301. doi: 10.1111/j.1468-3083.2009.03411.x
14. Leroy T, Van Neste D. Contrast enhanced phototrichogram pinpoints scalp hair changes in androgen sensitive areas of male androgenetic alopecia. *Skin Res Technol.* (2002) 8:106–11. doi: 10.1034/j.1600-0846.2002.00329.x
15. Kim JY, Kim MH, Hong SP, Park BC. Characteristics of nonbalding scalp zones of androgenetic alopecia in East Asians. *Clin Exp Dermatol.* (2015) 40:279–85. doi: 10.1111/ced.12554
16. Visessiri Y, Pakornphadungsit K, Leerunyakul K, Rutnin S, Srisont S, Suchonwanit P. The study of hair follicle counts from scalp histopathology in the Thai population. *Int J Dermatol.* (2020) 59:978–81. doi: 10.1111/ijd.14989
17. Rutnin S, Chanprapaph K, Pakornphadungsit K, Leerunyakul K, Visessiri Y, Srisont S, et al. Variation of hair follicle counts among different scalp areas: a quantitative histopathological study. *Skin Appendage Disord.* (2021) 1–7. doi: 10.1159/000518434. [Epub ahead of print].
18. Lee HJ, Ha SJ, Lee JH, Kim JW, Kim HO, Whiting DA. Hair counts from scalp biopsy specimens in Asians. *J Am Acad Dermatol.* (2002) 46:218–21. doi: 10.1067/mjd.2002.119558
19. Aslani FS, Dastgheib L, Banihashemi BM. Hair counts in scalp biopsy of males and females with androgenetic alopecia compared with normal subjects. *J Cutan Pathol.* (2009) 36:734–9. doi: 10.1111/j.1600-0560.2008.01149.x
20. El-Domyati M, Attia S, Saleh F, Abdel-Wahab H. Androgenetic alopecia in males: a histopathological and ultrastructural study. *J Cosmet Dermatol.* (2009) 8:83–91. doi: 10.1111/j.1473-2165.2009.00439.x
21. Suchonwanit P, Triyangkulsri K, Ploydaeng M, Leerunyakul K. Assessing biophysical and physiological profiles of scalp seborrheic dermatitis in the Thai population. *Biomed Res Int.* (2019) 2019:5128376. doi: 10.1155/2019/5128376
22. Chanprapaph K, Sutharaphan T, Suchonwanit P. Scalp biophysical characteristics in males with androgenetic alopecia: a comparative study with healthy controls. *Clin Interv Aging.* (2021) 16:781–7. doi: 10.2147/CIA.S310178
23. Suchonwanit P, McMichael AJ. Alopecia in association with malignancy: a review. *Am J Clin Dermatol.* (2018) 19:853–65. doi: 10.1007/s40257-018-0378-1
24. Sawaya ME, Price VH. Different levels of 5alpha-reductase type I and II, aromatase, and androgen receptor in hair follicles of women and men with androgenetic alopecia. *J Invest Dermatol.* (1997) 109:296–300. doi: 10.1111/1523-1747.ep12335779
25. Suchonwanit P, Iamsung W, Leerunyakul K. Topical finasteride for the treatment of male androgenetic alopecia and female pattern hair loss: a review of the current literature. *J Dermatolog Treat.* (2020) 1–6. doi: 10.1080/09546634.2020.1782324. [Epub ahead of print].
26. Hibberts NA, Howell AE, Randall VA. Balding hair follicle dermal papilla cells contain higher levels of androgen receptors than those from non-balding scalp. *J Endocrinol.* (1998) 156:59–65. doi: 10.1677/joe.0.1560059
27. Chanprapaph K, Mahasaksiri T, Kositkuljorn C, Leerunyakul K, Suchonwanit P. Prevalence and risk factors associated with the occurrence of autoimmune diseases in patients with Alopecia Areata. *J Inflamm Res.* (2021) 14:4881–91. doi: 10.2147/JIR.S331579
28. Suchonwanit P, Triamchaisri S, Wittayakornnerk S, Rattanakaemakorn P. Leprosy reaction in Thai population: a 20-year retrospective study. *Dermatol Res Pract.* (2015) 2015:253154. doi: 10.1155/2015/253154
29. Noden DM, Trainor PA. Relations and interactions between cranial mesoderm and neural crest populations. *J Anat.* (2005) 207:575–601. doi: 10.1111/j.1469-7580.2005.00473.x
30. Leerunyakul K, Suchonwanit P. Evaluation of hair density and hair diameter in the adult Thai population using quantitative trichoscopic analysis. *Biomed Res Int.* (2020) 2020:2476890. doi: 10.1155/2020/2476890
31. Whiting DA. How real is senescent alopecia? A histopathologic approach. *Clin Dermatol.* (2011) 29:49–53. doi: 10.1016/j.clindermatol.2010.07.007
32. Suchonwanit P, Udompanich S, Thadanipon K, Chanprapaph K. Trichoscopic signs in systemic lupus erythematosus: a comparative study with 109 patients and 305 healthy controls. *J Eur Acad Dermatol Venereol.* (2019) 33:774–80. doi: 10.1111/jdv.15421
33. Sriphojanart T, Khunkhet S, Suchonwanit P. A retrospective comparative study of the efficacy and safety of two regimens of diphenylcyclopropenone in the treatment of recalcitrant alopecia areata. *Dermatol Rep.* (2017) 9:7399. doi: 10.4081/dr.2017.7399
34. Suchonwanit P, Hector CE, Bin Saif GA, McMichael AJ. Factors affecting the severity of central centrifugal cicatricial alopecia. *Int J Dermatol.* (2016) 55:e338–43. doi: 10.1111/ijd.13061
35. Chanprapaph K, Udompanich S, Visessiri Y, Ngamjanyaporn P, Suchonwanit P. Nonscarring alopecia in systemic lupus erythematosus: a cross-sectional study with trichoscopic, histopathologic, and immunopathologic analyses. *J Am Acad Dermatol.* (2019) 81:1319–29. doi: 10.1016/j.jaad.2019.05.053

Conflict of Interest: The authors declare that the research was conducted in the absence of any commercial or financial relationships that could be construed as a potential conflict of interest.

Publisher's Note: All claims expressed in this article are solely those of the authors and do not necessarily represent those of their affiliated organizations, or those of the publisher, the editors and the reviewers. Any product that may be evaluated in this article, or claim that may be made by its manufacturer, is not guaranteed or endorsed by the publisher.

Copyright © 2021 Khunkhet, Chanprapaph, Rutnin and Suchonwanit. This is an open-access article distributed under the terms of the Creative Commons Attribution License (CC BY). The use, distribution or reproduction in other forums is permitted, provided the original author(s) and the copyright owner(s) are credited and that the original publication in this journal is cited, in accordance with accepted academic practice. No use, distribution or reproduction is permitted which does not comply with these terms.



OPEN ACCESS

Edited by:

Arndt Hartmann,
Universitätsklinikum
Erlangen, Germany

Reviewed by:

Corinna Lang-Schwarz,
Klinikum Bayreuth GmbH, Germany
Angela Shih,
Massachusetts General Hospital and
Harvard Medical School,
United States

*Correspondence:

Sameer Al Diffalha
saldiffalha@uabmc.edu

†These authors have contributed
equally to this work and share first
authorship

Specialty section:

This article was submitted to
Pathology,
a section of the journal
Frontiers in Medicine

Received: 09 November 2021

Accepted: 17 January 2022

Published: 14 February 2022

Citation:

Burkett AE, Sher SB, Patel CR,
Ildin-Eltoom I, Dhall D, Margaroli C,
Peter S, Lee G, Bajpai P, Benson PV,
Manne U and Al Diffalha S (2022)
Gastrointestinal Manifestations of
COVID-19 Infection: Clinicopathologic
Findings in Intestinal Resections
Performed at Single Institution.
Front. Med. 9:811546.
doi: 10.3389/fmed.2022.811546

Gastrointestinal Manifestations of COVID-19 Infection: Clinicopathologic Findings in Intestinal Resections Performed at Single Institution

Alison E. Burkett^{1†}, Sophia B. Sher^{1†}, Chirag R. Patel¹, Isam Ildin-Eltoom¹, Deepti Dhall¹, Camilla Margaroli², Shajan Peter³, Goo Lee¹, Prachi Bajpai¹, Paul V. Benson¹, Upender Manne^{1,4} and Sameer Al Diffalha^{1,4*}

¹ Department of Pathology, University of Alabama at Birmingham, Birmingham, AL, United States, ² Division of Pulmonary, Allergy and Critical Care Medicine, Department of Medicine, University of Alabama at Birmingham, Birmingham, AL, United States, ³ Division of Gastroenterology, Department of Medicine, University of Alabama at Birmingham, Birmingham, AL, United States, ⁴ O'Neal Comprehensive Cancer Center, Birmingham, AL, United States

It is now known that COVID-19 not only involves the lungs, but other organs as well including the gastrointestinal tract. Although clinic-pathological features are well-described in lungs, the histopathologic features of gastrointestinal involvement in resection specimens are not well characterized. Herein, we describe in detail the clinicopathologic features of intestinal resection specimens in four patients with COVID-19 infection. COVID-19 viral particles by *in situ* hybridization and immunofluorescence studies are also demonstrated. All four patients were males, aged 28–46 years, with comorbidities. They initially presented with a severe form of pulmonary COVID-19 and showed gastrointestinal symptoms, requiring surgical intervention. Histopathologic examination of resected GI specimens, mostly right colectomies, revealed a spectrum of disease, from superficial mucosal ischemic colitis to frank transmural ischemic colitis and associated changes consistent with pneumatosis cystoides intestinalis. Three patients were African American (75%), and one was Caucasian (25%); three patients died due to complications of their COVID-19 infection (75%), while one ultimately recovered from their GI complications (25%), but experienced prolonged sequela of COVID-19 infection including erectile dysfunction. In conclusion, COVID-19 infection, directly or indirectly, can cause ischemic gastrointestinal complications, with predilection for the right colon.

Keywords: COVID-19, gastrointestinal manifestations, pneumatosis cystoides intestinalis, ischemic colitis, ISH

INTRODUCTION

In December 2019, a new human coronavirus (SARS-CoV-2) type emerged in Wuhan, China. COVID-19, the infectious disease caused by SARS-CoV-2, is now a pandemic affecting countries throughout the world. Since spring 2020, the United States has seen a dramatic rise in number of cases, and currently the number of deaths attributable to COVID-19 infection is more than 500,000 (1).

Although the most common presentation of the infection is the development of respiratory symptoms 2–14 days following exposure, gastrointestinal (GI) presentation is

becoming increasingly recognized. The receptor of SARS-CoV-2, angiotensin converting enzyme 2 (ACE2) is highly expressed both in GI epithelial cells and in liver (2). Almost the entire GI tract, including the stomach, small intestine, and rectal epithelial cells express the SARS-CoV-2 nucleocapsid protein and the ACE2 protein (3). The SARS-CoV-2 nucleocapsid protein, which encapsulates the viral genome, is essential for SARS-CoV-2 replication (4). High levels of these two proteins in cells of the GI tracts of SARS-CoV-2 infected patients can explain the concomitant digestive symptoms, including diarrhea, nausea, vomiting, and abdominal pain (3).

TABLE 1 | Patients' demographic, laboratory values and pathologic findings.

Case #	Demographics				Laboratory values					Pathologic findings		
	Age	Sex	Race	Comorbidities	CRP (mg/L)	D-dimer (ng/ml)	LDH (Units/L)	Lactic acid (mMol/L)	Troponin I (ng/L)	Hgb/Hct	Gross findings	Histology
Case 1	47	M	AA	HTN, Obesity (BMI 33.08 kg/m ²)	176.3	4,064	NA	4.0	39	9.9/26	Large patches of erythematous colonic mucosa with focal loss of mucosal folds.	Ischemic colitis showing transmural acute and chronic inflammation and serositis. Features suggestive of pneumatosis.
Case 2	37	M	AA	HTN, Obesity, Insulin Dependent DM	282.6	978	556	NA	44	11/33	Cecum showed several areas of ulceration ranging in size from 0.6 to 1.0 cm	Focal mucosal ulceration, with associated acute and chronic inflammation. Features suggestive of pneumatosis. Focal serositis.
Case 3	40	M	C	Obesity (BMI 33.2 kg/m ²)	NA	>20,000	NA	7.1	1,838	15.6/46	Cecum: Necrotic with dark-brown discoloration. Ascending colon is hemorrhagic and dusky with obvious air bubbles	Mucosal hemorrhagic ischemia, fibrin microthrombi, and pneumatosis cystoides intestinalis
Case 4	28	M	AA	DM	24.87	1,380	681	10.6	98	7.3/22	Small intestine: Granular/gritty brown mucosa with diffuse gray-brown exudate	Transmural ischemia with pseudomembrane formation and acute serositis. Features suggestive of pneumatosis.

Here, we present a series of four SARS-CoV-2 patients who were admitted to the University of Alabama at Birmingham (UAB) Medical Center during June to August 2020 and who underwent GI resections. The course of their SARS-CoV-2 infections was remarkable for the development of GI complications, which necessitated surgical management by right hemicolectomy or segmental small bowel resection; three of the four patients ultimately died as a result of the complications of their COVID-19 infection. The clinical, macroscopic and histopathologic findings are described, which adds to the pathophysiology of SARS-CoV-2 infection and contributes to the ongoing management of the COVID-19 disease.

MATERIALS AND METHODS

The Institutional Review Board of UAB approved the study. A retrospective review of surgical pathology archives for COVID-19 related intestinal resections was performed during the period of June to August 2020. There were four patients with bowel resections, three of whom underwent right hemicolectomies and one a segmental small bowel resection. The hematoxylin and eosin (H&E)-stained slides were reviewed by GI pathologists (SA, IE, DD, and CRP).

In this study, for detection of SARS-CoV2 virus, both immunofluorescence and *in situ* hybridization (ISH) assays were

performed as follows: 5- μ m formalin-fixed paraffin-embedded (FFPE) tissues sections on Plus Slides (VWR, Radnor, PA) were cut at 5 μ m and baked for 2 h at 60°C. Tissues were then deparaffinized and rehydrated with sequential 5-min incubations in xylene (three times), twice in 100% ethanol, and twice in 95% ethanol. Slides were washed three times, for 5 min each, with distilled water. Antigen retrieval was then performed in Tris-EDTA pH-9 buffer at 70°C for 20 min in a steamer, followed by three 5-min washes in distilled water. Tissues were balanced with PBS for 10 min and blocked with 3% w/v bovine serum albumen (BSA) in PBS for 40 min at room temperature. Slides were then blotted dry, and antibody against SARS-CoV-2 nucleocapsid protein (clone GTX135361, GeneTex, Irvine, CA) was applied at a 1:500 dilution in PBS+3% w/v BSA for 1 h at room temperature. Tissues were then rinsed with PBS three times for 5 min under gentle agitation. 4',6-Diamidino-2-phenylindole (100 ng/mL in PBS) staining was performed for 5 min in the dark at room temperature, followed by three 5-min washes in PBS under gentle agitation. Slides were then mounted with ProLong Gold antifade mounting media (Thermofisher) and stored in the dark until image acquisition. Confocal immunofluorescence images were acquired with a Nikon A1R confocal microscope.

ISH assay was performed using RNAscope® kit and ISH probes according to the manufacturer's instructions (Advanced Cell Diagnostics, ACD, Newark, CA). RNA probe, in C2 channel

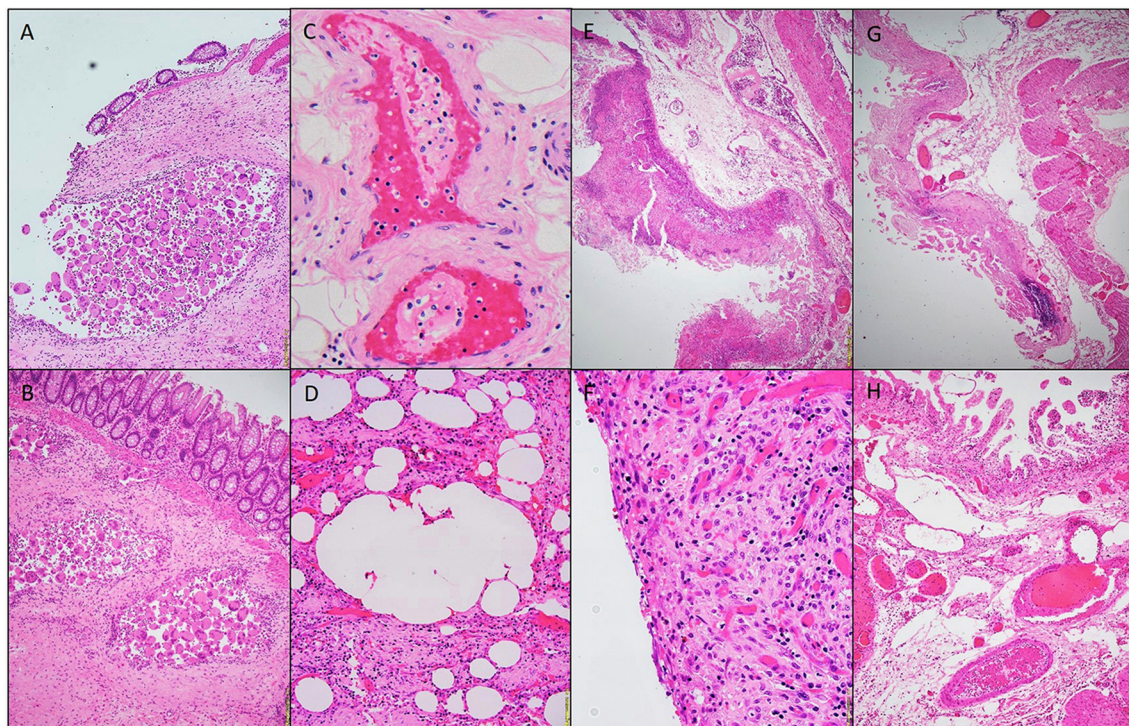


FIGURE 1 | Photomicrographs of a hemicolectomy specimen. Aggregates of multinucleated giant cells lining the cysts. H&E stain 20x (A,B). Fibrin thrombi, H&E staining 40x (C). Micro-cyst lined with multinucleated giant cells, H&E staining 10x (D). Pseudomembrane, H&E 10x (E). Acute serositis, H&E staining 40x (F). Ischemic enteritis, H&E 10x (G). Submucosal thrombi, H&E 10x (H).

targeting SARS-CoV-2 replicative RNA intermediate, was used to detect the replicating virus as red signal (nCoV2019-orf1ab-sense-C2, cat. no. 859151-C2). RNAscope® 2.5 Duplex Reagent Kit (cat. no 322430) along with Human (Hs) Positive Control Probes for housekeeping genes PPIB-C1/ POLR2A-C2, (cat. no 321641) were used to assess the integrity of the RNA. Simultaneously, consecutive sections were probed with probes targeting dihydrodipicolinate reductase B mRNA of a *Bacillus subtilis* strain (DapB) as a negative control, (cat. no. 320751) to assess the specificity of the assay.

RESULTS

Clinical Data

Our cohort included four patients aged 28–46 years with a mean age of 38 years. Three of four patients were African-American (AA); one was non-Hispanic Caucasian. All patients had comorbidities that included essential hypertension (HTN), diabetes mellitus (DM, insulin-dependent or insulin-resistant), and obesity (BMI 33.08–34.8 kg/m²). All patients initially presented with respiratory symptoms, including fever, dyspnea, and/or flu-like symptoms which developed into acute respiratory distress syndrome (ARDS) requiring intubation, ventilation,

and critical care management. The length of time between a positive COVID-19 test and significant GI symptomatology and resection varied widely from 1 to 53 days, with an average of 21.5 days. GI symptoms occurred on a spectrum, beginning as constipation, abdominal pain, or a lower GI bleed before progressing to ischemia and necrosis requiring surgical intervention. COVID-19 infections were confirmed by the presence of SARS-CoV-2 RNA, determined by PCR. The patients were enrolled in a clinical trial of remdesivir. Despite the treatment, they subsequently developed complications, such as lower extremity deep vein thrombosis, pulmonary thromboembolism, septicemia with septic shock (due to *Cutibacterium/Propionibacterium avidum*), multi-organ failure, hypotension, pulseless electrical activity and encephalopathy. For all four patients, acute renal failure was a complication, and all underwent continuous renal replacement therapy. Furthermore, the course of their disease was complicated by the development of GI symptoms, such as GI bleeding in the form of hematochezia, as well as an ileus. All patients underwent CT scans of the abdomen and pelvis, which showed changes compatible with GI bleeding with various degrees of intestinal pneumatosis and bowel ischemia. These findings were corroborated by the frank ischemia, ulceration, cecal dilation, and necrosis

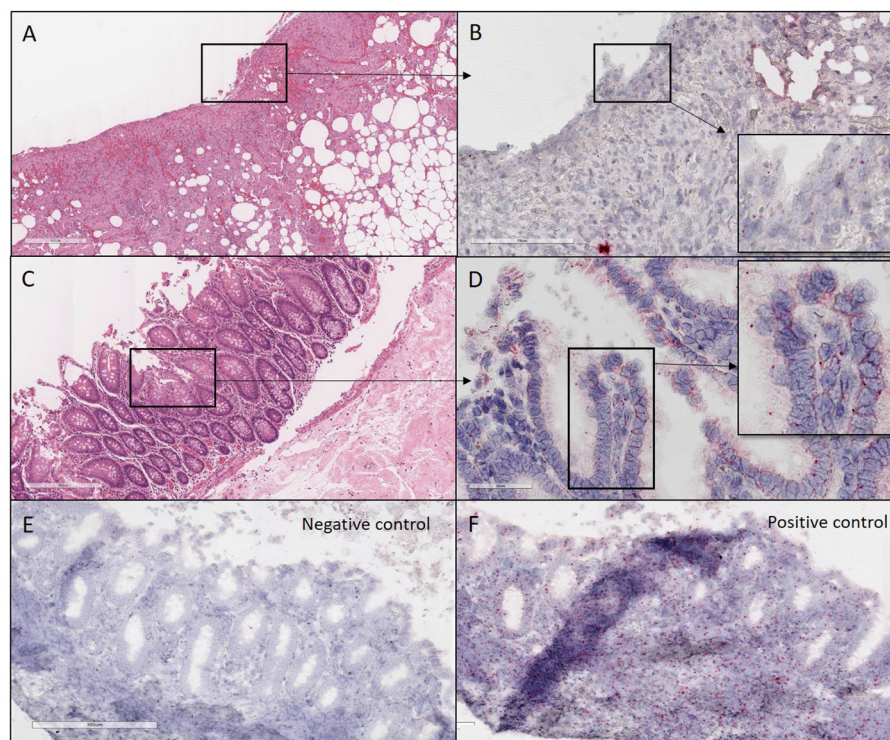


FIGURE 2 | H&E and ISH images of patient #1 in focal mucosal ulcer with granulation tissue formation along with adjacent uninvolved mucosa. **(A)** H&E images of ulcerated colon tissue at 4X magnification **(B)** Images at 20X magnification after *in situ* hybridization using V-nCoV2019—orf1ab—sense probe (cat # 859151-C2), ACD, Bio-technie, detecting replicating SARS-COV-2 RNA (red chromogen) in ulcerated colon tissue sections. **(C)** H&E images at 10x magnification of adjacent uninvolved mucosa **(D)**. Higher magnification images at 40X after *in situ* hybridization using V-nCoV2019—orf1ab—detected as red signal in adjacent uninvolved mucosa. **(E)** Negative control images at 10X after *in situ* hybridization using probe (cat # 320751), ACD, Bio-technie, targeting DapB (*Bacillus subtilis* stain) which did not detect any staining **(F)**. Positive control images at 10X after *in situ* hybridization using probe (cat # 321641), ACD, Bio-technie, demonstrated strong positive staining (red chromogen) in sections probed for the housekeeping gene POLR2A.

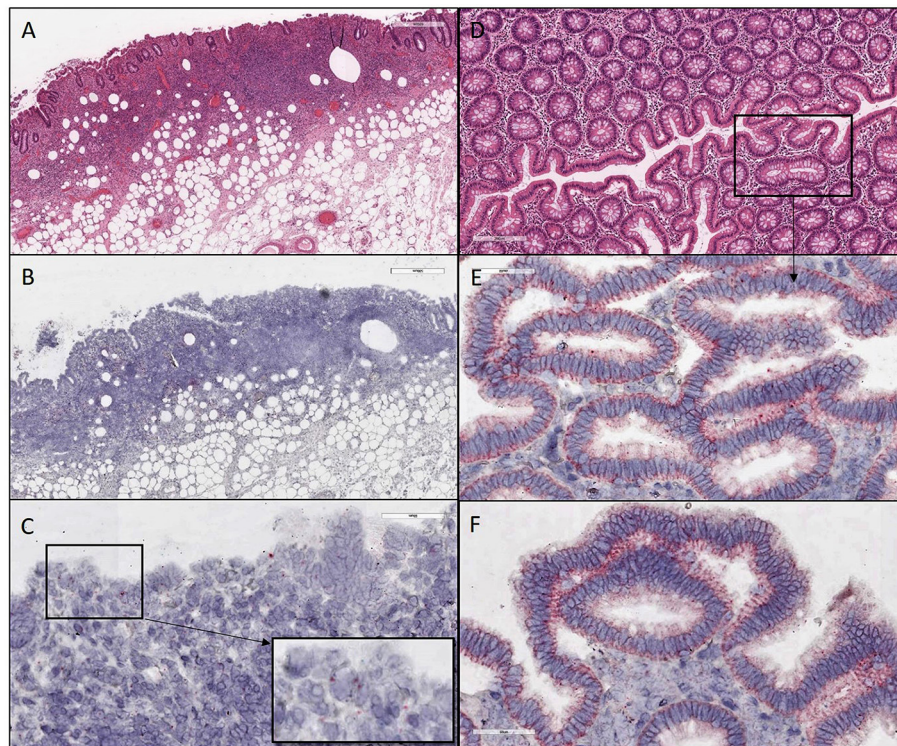


FIGURE 3 | H&E and ISH images of patient #2 in focal mucosal ulcer with granulation tissue formation along with adjacent uninvolved mucosa. **(A)** H&E images of ulcerated colon tissue at 4X magnification **(B,C)** Images after *in situ* hybridization using V-nCoV2019—orf1ab—sense probe (red chromogen) at lower 4X and higher magnification 40x, respectively. **(D)** H&E images at 10X magnification of adjacent uninvolved mucosa **(E,F)** *in situ* hybridization using V-nCoV2019—orf1ab—sense probe detected as red signal in adjacent intact epithelium of uninvolved mucosa at higher magnification images at 40x. Images show pronounced viral load in the surface epithelial lining and the crypts (Basal cytoplasmic localization).

encountered intraoperatively. Additionally, laboratory findings were remarkable for elevated C-reactive protein (ranging from 24.87 to 282.6 mg/L), d-dimer (ranging from 978 to > 20,000 ng/mL), lactate dehydrogenase (556–681 U/L), lactic acid (4.0–10.6 mMol/L), and troponin I (39–1838 ng/L). Most patients were also anemic (Hgb between 7.3 and 11 g/dL; Hct 22–33%). The three patients who expired due to the infection demonstrated the most dramatic clinical courses, with pronounced laboratory, gross, and microscopic abnormalities (**Table 1**). For all four patients with SARS-CoV-2 infection confirmed by nasal swap PCR testing, there was colonic pneumatosis with or without ischemic changes for whom CT scans of the abdomen showed evidence of gas in the mesentery, or features suggestive of lower GI bleeding.

Gross and Microscopic Characteristics

Three patients had right hemicolectomies and one had a segmental small bowel resection. All four specimens showed variable degrees of ischemic changes. Gross examination of one of sample showed transmural ischemic necrosis with hemorrhage, resulting in perforation. The mucosa showed, microscopically, deep ulceration and focal pseudomembrane formation. In an additional patient, there was diffuse transmural

acute and chronic inflammation with necrosis and hemorrhage, and associated acute serositis. The lamina propria demonstrated congestion and edema (in all patients); rare vascular fibrin thrombi were identified (in 2 patients). Pneumatosis cystoides intestinalis (cyst formation with associated multinucleated giant cells lining) were also recognized in two patients (**Figures 1–5** and **Table 1**).

ISH with a V-nCoV2019-sense probe detected replicating SARS-CoV-2 RNA. Furthermore, all four samples were positive on immunofluorescence for antibody against SARS-CoV-2 nucleocapsid protein with a distinctive pattern and a variable viral load (**Figures 2–4**). All patients underwent exploratory laparotomies for GI complications of COVID-19 disease, and three of the four patients underwent a right hemicolectomy procedure. The morphologic findings in all specimens included ischemic changes, acute and chronic inflammation, and fibrin microthrombi in small blood vessels in underlying areas of mucosal ulceration. Moreover, all cases, regardless of extent of the disease, showed changes consistent with pneumatosis cystoides intestinalis, including prominent submucosal edema with occasional cyst formation and aggregates of multinucleated giant cells.

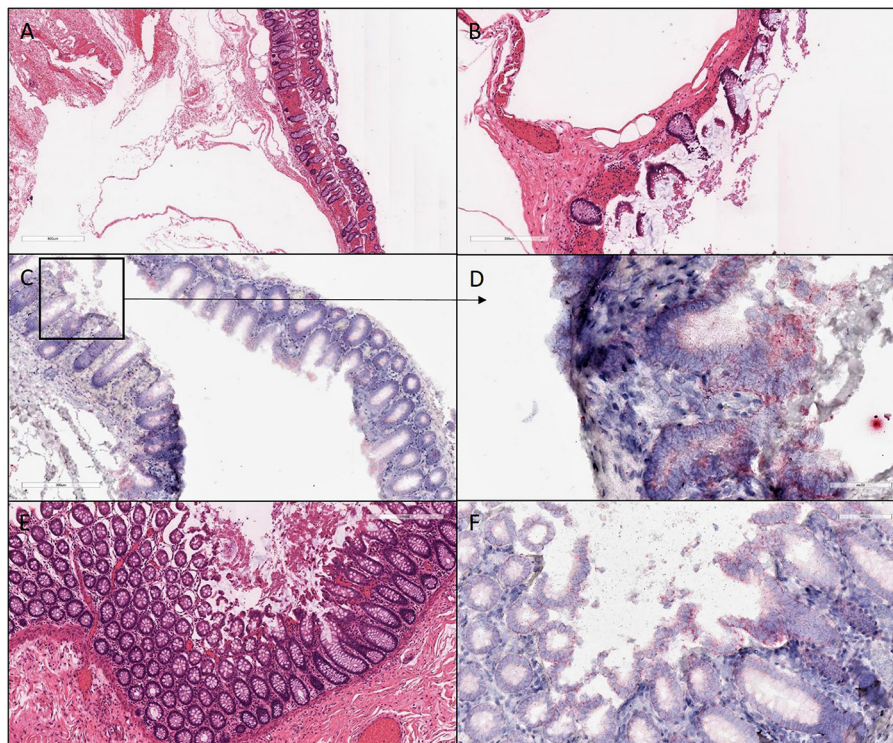


FIGURE 4 | H&E and ISH images of patient #3 in focal mucosal ulcer with granulation tissue formation along with adjacent uninvolved mucosa. **(A,B)** H&E images of ischemic colon tissue sections at 4X and 10X magnification, respectively. **(C,D)** Images at lower (10X) and higher magnification (40X), respectively, after *in situ* hybridization using V-nCoV2019—orf1ab—sense probe (red chromogen). More viral load of replicating SARS-CoV-2 RNA was detected in this ischemic section as compared to its uninvolved mucosa represented in **(F)**. **(E)** H&E images at 10X of adjacent uninvolved mucosa **(F)** *in situ* hybridization using V-nCoV2019—orf1ab—sense probe detected as red signal in adjacent intact epithelium of uninvolved mucosa at 20X magnification.

DISCUSSION

GI symptoms associated with COVID-19 are present in up to 30% of patients, with diarrhea, abdominal pain, and hematochezia occasionally evident as the initial presentation (5). Although patients with significant pulmonary disease have detectable SARS-CoV-2 RNA in fecal samples, a substantial number of patients with GI manifestations also have SARS-CoV-2 RNA in fecal samples (6). Others have now individually established that the virus can be cultured from the feces during an active infection (7). In the present study, we demonstrated by immunofluorescence (**Figure 6**) and ISH studies (**Figures 2–5**) evidence of the virus in affected area of the intestine.

Notably, neither of the patients had a medical history of established GI disease, nor etiology for colitis. Extensive infectious work up including *Clostridium difficile* serology was conducted on two of the four patients, which was negative. Reactivity for CMV IgG was noted in the serum of one patient indicating a previous infection; however, no evidence of viral cytopathic effects were noted on histology. One patient had clinical and microbiological evidence of septicemia due to *Cutibacterium (Propionibacterium) avidum*, the commensal skin microorganism, which is unlikely to be implicated as a primary agent in the etiology of hemorrhagic colitis. One

patient developed HIT following anticoagulation, resulting in septic shock. While this further exacerbated the bowel ischemia and thrombosis, it was a contributing factor rather than a primary cause. Moreover, extensive chart review failed to reveal definitive evidence of mesenteric thrombosis, radiologically or intraoperatively, to explain the segmental ischemic findings.

The target viral receptor for SARS-CoV-2 is ACE2, which is highly expressed on type II alveolar epithelial cells, as well as in glandular cells of gastric, duodenal, and rectal epithelia (8). This suggests that the SARS-CoV-2 gains entry into, and potentially damages, host GI tissue, explaining the digestive symptoms. Microthrombi also contribute to GI insults (9).

Although several studies have attempted to identify histologic findings indicative of SARS-CoV-2 infection, the presentation and expression of SARS-CoV-2 RNA remains variable (10). In our cohort, not all GI specimens demonstrated findings of coagulopathy and ischemia, but all samples revealed changes consistent with pneumatosis cystoides intestinalis. While pneumatosis cystoides is commonly associated with bacterial infection, its pathogenesis is poorly understood and multifocal, and can also be attributed to mechanical and pulmonary causes (11). In our cohort, those patients that underwent infectious work-up for gas producing bacteria were negative. Moreover, these patients were acutely ill, requiring repeated surgical

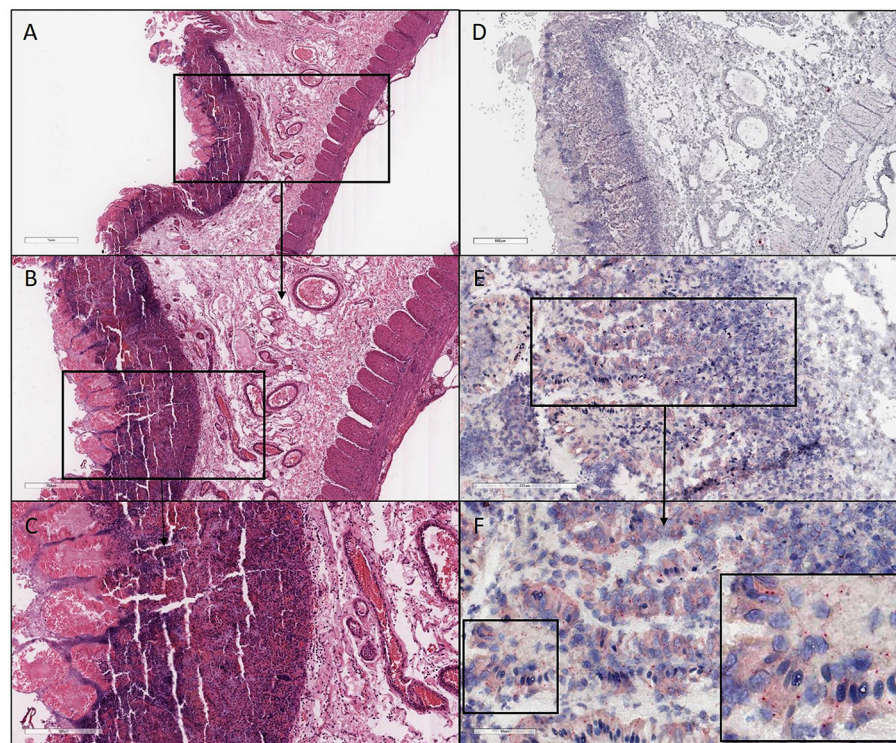


FIGURE 5 | H&E and ISH images of patient #4 in focal mucosal ulcer with granulation tissue formation. **(A–C)** H&E images of ischemic colon tissue sections at 2X, 4X, and 10X magnification, respectively. **(D–F)** Images at lower (4X) and higher magnification (20X and 40X), respectively, after *in situ* hybridization using V-nCoV2019—orf1ab—sense probe (red chromogen) illustrating replicating SARS-CoV-2 RNA was detected.

intervention, intubation and ventilation. This suggested that the etiology of pneumatosis could be the result of iatrogenic trauma or manipulation increasing intraluminal pressure (11), or the result of free air entering the perivascular spaces of the intestinal wall following alveolar rupture in the setting of pulmonary obstruction (12); the clinical significance failed to be elucidated. The pathogenic pathway of COVID-19 remains largely undetermined, and its relationship with the gastrointestinal findings remains a challenge. It is widely accepted that the viral infection results in microthrombi which can lead to ischemic injury; however, in the setting of critical illness, HIT, and intragenic interventions (ECMO) it is difficult to quantify the exact role SARS-CoV-2 virus plays. The clinicopathologic findings in our cohort caused us to consider the relationship between the ischemic enterocolitis and hypercoagulable state of our patients with COVID-19 infection; however, comparison with non-COVID associated acute ischemic bowels should be performed to further characterize and ultimately define the histopathological features of the virus.

Moreover, each GI specimen demonstrated SARS-CoV-2 positivity via ISH, regardless of the extent of disease. Coronaviruses are also found by electron microscopy in intestinal cells of animals (13). Comparable to our study, SARS-CoV-2 RNA ISH is reported to be positive in a few mucosal epithelial cells and lymphocytes of the GI tract in humans (7). Also what supports our findings is that SARS-Cov-2

RNA in stool, determined by amplification is now widely accepted (7).

In a recent study that included a large number of SARS-CoV-2 patients ($n=95$), 58 patients experienced GI symptoms including diarrhea, anorexia and nausea (14). Fecal samples of 65 hospitalized patients were tested for SARS-CoV-2, including 42 patients with and 23 without GI symptoms, of which 22 (52.4%) and 9 (39.1%) were positive, respectively. Six of the patients who had GI symptoms underwent endoscopic examination; one showed erosion/ulcer. In two, SARS-CoV-2 RNA was detected in the esophagus, stomach, duodenum, and rectum (14).

In the present study, there were pathologic findings for the four patients with confirmed SARS-CoV-2, for whom CT scans of the abdomen showed either evidence of colonic pneumatosis with or without ischemic changes and evidence of gas in the mesentery, or features suggestive of lower GI bleeding. All four patients underwent exploratory laparotomies and three of the four were subjected to a right hemicolectomy procedure for COVID-19 GI related complications. The presence of microthrombi in the watershed area suggested that SARS-CoV-2 demonstrates partiality toward the right colon. Moreover, all cases, regardless of extent of the disease, showed pathologic changes consistent with pneumatosis cystoides intestinalis.

For some patients, GI symptoms may be associated with pulmonary SARS-CoV-2 infection, and surgical management of

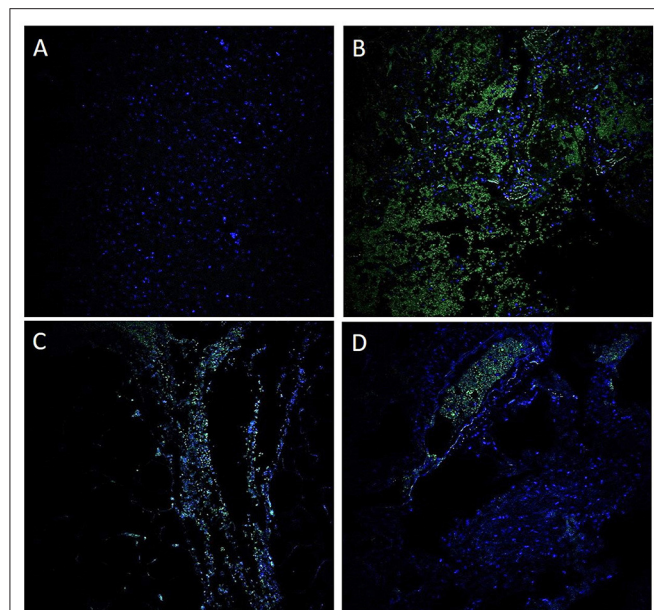


FIGURE 6 | Immunofluorescence for antibody against SARS-CoV-2 nucleocapsid protein. A negative control using a probe targeting DapB (*Bacillus subtilis* strain) did not detect any staining (**A**); a positive control demonstrated strong positive staining in sections probed with the housekeeping gene (**B**). These findings suggest that the GI tract is infected with SARS-CoV-2 (**C**). A unique observation in our case study is the presence of the virus within the blood vessels (**D**).

GI complications, including bleeding, is sometimes necessary. The morphologic findings observed in the resection specimens varied from superficial acute colitis with or without hemorrhage and ischemic changes, to a frank transmural necrotic colitis with fibrin microthrombi. Changes consistent with pneumatosis cystoides intestinalis were also evident. In conclusion, COVID-19 disease, directly or indirectly, can cause ischemic GI complications, with a predilection for the right colon. Awareness of these morphologic changes may prompt pathologists to include potential SARS-CoV-2 infection to the differential diagnosis when the etiology for ischemic colitis is unclear.

REFERENCES

1. Symptoms of COVID-19: The Center for Disease Control and Prevention (2020). Available online at: <https://www.cdc.gov/coronavirus/2019-ncov/symptoms-testing/symptoms.html> (accessed February 22, 2021).
2. Hoffmann M, Kleine-Weber H, Schroeder S, Kruger N, Herrler T, Erichsen S, et al. SARS-CoV-2 cell entry depends on ACE2 and TMPRSS2 and is blocked by a clinically proven protease inhibitor. *Cell*. (2020) 181:271–80 e8. doi: 10.1016/j.cell.2020.02.052
3. Carvalho A, Alqusairi R, Adams A, Paul M, Kothari N, Peters S, et al. SARS-CoV-2 gastrointestinal infection causing hemorrhagic colitis: implications for detection and transmission of COVID-19 disease. *Am J Gastroenterol*. (2020) 115:942–6. doi: 10.14309/ajg.0000000000000667
4. Savastano A, Ibanez de Opakua A, Rankovic M, Zweckstetter M. Nucleocapsid protein of SARS-CoV-2 phase separates into RNA-rich polymerase-containing condensates. *Nat Commun*. (2020) 11:6041. doi: 10.1038/s41467-020-19843-1
5. Buscarini E, Manfredi G, Brambilla G, Menozzi F, Londoni C, Alicante S, et al. GI symptoms as early signs of COVID-19 in hospitalised Italian patients. *Gut*. (2020) 69:1547–8. doi: 10.1136/gutjnl-2020-321434
6. Su S, Shen J, Zhu L, Qiu Y, He JS, Tan JY, et al. Involvement of digestive system in COVID-19: manifestations, pathology, management and challenges. *Therap Adv Gastroenterol*. (2020) 13:1756284820934626. doi: 10.1177/1756284820934626
7. Shi X, Gong E, Gao D, Zhang B, Zheng J, Gao Z, et al. Severe acute respiratory syndrome associated coronavirus is detected in intestinal tissues of fatal cases. *Am J Gastroenterol*. (2005) 100:169–76. doi: 10.1111/j.1572-0241.2005.40377.x
8. Xiao F, Tang M, Zheng X, Liu Y, Li X, Shan H. Evidence for gastrointestinal infection of SARS-CoV-2. *Gastroenterology*. (2020) 158:1831–3 e3. doi: 10.1053/j.gastro.2020.02.055
9. Bhayana R, Som A, Li MD, Carey DE, Anderson MA, Blake MA, et al. Abdominal imaging findings in COVID-19: preliminary

DATA AVAILABILITY STATEMENT

The original contributions presented in the study are included in the article/supplementary material, further inquiries can be directed to the corresponding author.

ETHICS STATEMENT

Ethical review and approval was not required for the study on human participants in accordance with the local legislation and institutional requirements. Written informed consent for participation was not required for this study in accordance with the national legislation and the institutional requirements.

AUTHOR CONTRIBUTIONS

SA principal investigator and corresponding author, conceptualized the study with SS and AB, finalized the manuscript with the assistance of AB. CM, PB, and UM performed the *in-situ* Hybridization and reviewed the results and critically reviewed the manuscript. SP reviewed and revised the manuscript. CP, II, DD, GL, and PVB, contributed in data collection. All authors approved the final manuscript as submitted and agree to be accountable for all aspects of the work.

FUNDING

This work is supported, in part, by the institutional funds to SA and UM.

ACKNOWLEDGMENTS

We thank the UAB Tissue Biorepository (UAB-TBR), UAB Pathology Core Research Laboratory and OCCC Tissue Procurement Shared Resource (TPRO) for their assistance with the processing of the histological specimens, as well Dr. Robert Grabski at the UAB High Resolution Imaging Facility.

- observations. *Radiology*. (2020) 297:E207–E15. doi: 10.1148/radiol.2020201908
10. Westerhoff M, Jones D, Hrycaj SM, Chan MP, Pantanowitz L, Tu H, et al. Gastrointestinal pathology in samples from coronavirus disease 2019 (COVID-19)-positive patients. *Arch Pathol Lab Med*. (2021) 145:1062–8. doi: 10.5858/arpa.2021-0137-SA
 11. Azzaroli F, Turco L, Ceroni L, Galloni SS, Buonfiglioli F, Calvanese C, et al. Pneumatois cystoides intestinalis. *World J Gastroenterol*. (2011) 17:4932–6. doi: 10.3748/wjg.v17.i44.4932
 12. St Peter SD, Abbas MA, Kelly KA. The spectrum of pneumatois intestinalis. *Arch Surg*. (2003) 138:68–75. doi: 10.1001/archsurg.138.1.68
 13. Cimolai N. Features of enteric disease from human coronaviruses: implications for COVID-19. *J Med Virol*. (2020) 92:1834–44. doi: 10.1002/jmv.26066
 14. Lin L, Jiang X, Zhang Z, Huang S, Zhang Z, Fang Z, et al. Gastrointestinal symptoms of 95 cases with SARS-CoV-2 infection. *Gut*. 69:997–1001. doi: 10.1136/gutjnl-2020-321013

Conflict of Interest: The authors declare that the research was conducted in the absence of any commercial or financial relationships that could be construed as a potential conflict of interest.

Publisher's Note: All claims expressed in this article are solely those of the authors and do not necessarily represent those of their affiliated organizations, or those of the publisher, the editors and the reviewers. Any product that may be evaluated in this article, or claim that may be made by its manufacturer, is not guaranteed or endorsed by the publisher.

Copyright © 2022 Burkett, Sher, Patel, Ildin-Eloum, Dhall, Margaroli, Peter, Lee, Bajpai, Benson, Manne and Al Diffalha. This is an open-access article distributed under the terms of the Creative Commons Attribution License (CC BY). The use, distribution or reproduction in other forums is permitted, provided the original author(s) and the copyright owner(s) are credited and that the original publication in this journal is cited, in accordance with accepted academic practice. No use, distribution or reproduction is permitted which does not comply with these terms.



From Macroscopy to Ultrastructure: An Integrative Approach to Pulmonary Pathology

Stijn E. Verleden^{1,2,3†}, Peter Braubach^{4,5†}, Christopher Werlein⁵, Edith Plucinski^{4,5}, Mark P. Kuhnel^{4,5}, Annemiek Snoeckx⁶, Haroun El Addouli⁶, Tobias Welte^{4,7}, Axel Haverich^{4,8}, Florian P. Laenger^{4,5}, Sabine Dettmer^{4,9}, Patrick Pauwels¹⁰, Veronique Verplancke², Paul E. Van Schil^{1,3}, Therese Lapperre^{2,11}, Johanna M. Kwakkel-Van-Erp^{2,11}, Maximilian Ackermann^{12,13}, Jeroen M. H. Hendriks^{1,3} and Danny Jonigk^{4,5*}

OPEN ACCESS

Edited by:

Luca Di Tommaso,
Humanitas Research Hospital, Italy

Reviewed by:

Torsten Goldmann,
Research Center Borstel
(LG), Germany

*Correspondence:

Danny Jonigk
jonigk.danny@mh-hannover.de

†These authors have contributed
equally to this work

Specialty section:

This article was submitted to
Pathology,
a section of the journal
Frontiers in Medicine

Received: 21 January 2022

Accepted: 07 February 2022

Published: 16 March 2022

Citation:

Verleden SE, Braubach P, Werlein C, Plucinski E, Kuhnel MP, Snoeckx A, El Addouli H, Welte T, Haverich A, Laenger FP, Dettmer S, Pauwels P, Verplancke V, Van Schil PE, Lapperre T, Kwakkel-Van-Erp JM, Ackermann M, Hendriks JMH and Jonigk D (2022) From Macroscopy to Ultrastructure: An Integrative Approach to Pulmonary Pathology. *Front. Med.* 9:859337. doi: 10.3389/fmed.2022.859337

¹ Antwerp Surgical Training, Anatomy and Research Centre (ASTARC), Antwerp University, Antwerp, Belgium, ² Division of Pneumology, University Hospital Antwerp, Edegem, Belgium, ³ Department of Thoracic and Vascular Surgery, University Hospital Antwerp, Edegem, Belgium, ⁴ Member of the German Center for Lung Research (DZL), Biomedical Research in Endstage and Obstructive Lung Disease Hannover (BREATH), Hannover, Germany, ⁵ Institute for Pathology, Hannover Medical School, Hannover, Germany, ⁶ Division of Radiology, University Hospital Antwerp and University of Antwerp, Edegem, Belgium, ⁷ Division of Pneumology, Hannover Medical School, Hannover, Germany, ⁸ Division of Thoracic Surgery, Hannover Medical School, Hannover, Germany, ⁹ Department of Radiology, Hannover Medical School, Hannover, Germany, ¹⁰ Division of Pathology, University Hospital Antwerp, Edegem, Belgium, ¹¹ Laboratory of Experimental Medicine and Pediatrics (LEMP), Antwerp University, Antwerp, Belgium, ¹² Institute of Pathology and Department of Molecular Pathology, Helios University Clinic Wuppertal, University of Witten-Herdecke, Witten, Germany, ¹³ Institute of Functional and Clinical Anatomy, University Medical Center of the Johannes Gutenberg University Mainz, Mainz, Germany

Pathology and radiology are complimentary tools, and their joint application is often crucial in obtaining an accurate diagnosis in non-neoplastic pulmonary diseases. However, both come with significant limitations of their own: Computed Tomography (CT) can only visualize larger structures due to its inherent–relatively–poor resolution, while (histo) pathology is often limited due to small sample size and sampling error and only allows for a 2D investigation. An innovative approach of inflating whole lung specimens and subjecting these subsequently to CT and whole lung microCT allows for an accurate matching of CT-imaging and histopathology data of exactly the same areas. Systematic application of this approach allows for a more targeted assessment of localized disease extent and more specifically can be used to investigate early mechanisms of lung diseases on a morphological and molecular level. Therefore, this technique is suitable to selectively investigate changes in the large and small airways, as well as the pulmonary arteries, veins and capillaries in relation to the disease extent in the same lung specimen. In this perspective we provide an overview of the different strategies that are currently being used, as well as how this growing field could further evolve.

Keywords: microCT, lung, histology, lung disease, imaging

INTRODUCTION

Computed tomography (CT), positron emission tomography (PET) and histopathology are major components in the differential diagnosis and follow-up of patients with acute and chronic non-neoplastic respiratory diseases. Given the diversity in CT and histologic presentation and the inherent morphologic differences in strategies of diagnosis between neoplastic and non-neoplastic disease, we will specifically focus on non-neoplastic diseases. Especially as these tend to result in significant day-to-day challenges in the differential diagnosis.

Particularly in the field of interstitial lung diseases (ILD), there is an important diagnostic and prognostic role for CT and histopathology, with a growing emphasis on the relative weight of chest imaging as a diagnostic tool (1). Thus, the need for an invasive video-assisted or robot-assisted thoracic surgery biopsy to confirm differential diagnosis has drastically reduced. Consequently, lung biopsies are currently only recommended for those challenging cases where major discrepancies are observed between CT and clinical findings and a clear diagnosis cannot be rendered. Given this important role of imaging in the management of ILD, it is primordial to integrate the existing clinical, imaging and histopathologic data as much as possible.

Initially, assessment of remodeling and fibrosis patterns by experienced radiologists was the only way to leverage the available imaging data, but gradually and partly due to the large inter-observer variability, automated image analysis tools for characterization and quantification of CT signs and patterns have been developed of which some are on the verge of making their appearance in routine clinical care. CT can provide 3D insight into the (gross) morphological changes in the lung. However, CT patterns are often nonspecific and may change during the evolution of a disease. Importantly, CT changes may also have more than one (histo-) pathological correlate. For example, a study demonstrated that more than 90% of patients presenting with CT findings that were inconsistent with usual interstitial pneumonia demonstrated histological evidence of usual interstitial pneumonia (2). Additionally, *in vivo* resolution is rather limited with a slice thickness of 1 mm most commonly being used for routine patient CT scans due to radiation concerns. This is sufficient to investigate airways and vessels >1 mm in diameter and gross changes in the secondary pulmonary lobule and the lung parenchyma. However, the small airways, the cellular composition and specific smaller sized structures are impossible to address, although morphologic secondary effects of primary changes such as hyperinflation and air trapping may be observed.

Histopathology on the other hand provides the advantage of a detailed analysis of the morphologic and cellular changes within the lung, whereby structures in the micrometer range can be readily resolved. However, (histo-) pathology is limited due to relatively small tissue samples and only allows for a 2D investigation. This can lead to discordance between initial diagnosis made on transbronchial cryobiopsy or surgical lung biopsy and the final diagnosis made in explant lung specimens at the time of transplantation (15–22 and 12.4% respectively) (3, 4). In addition, the lung is considered quite

fragile, making it vulnerable for deformation and distortion during the preparation resulting in histologic artifacts potentially hampering microscopic examination.

As, especially non-neoplastic pulmonary diseases, show a great spatial heterogeneity in disease activity and progression, targeted sampling is essential. It is reasonable to assume that often important patterns/changes in the lung can be overlooked due to sampling bias or sectioning artifacts upon histologic examination.

Proof of concept data of the huge potential of microCT, a tool designed to combine the 3D aspect of CT with almost full histological resolution, to investigate human lung (disease) was provided in 2005. However, at the time, the authors were still struggling to obtain sufficient contrast between air and tissue (5). A subsequent porcine study by Litzlbauer et al. (6) extensively validated the use of microCT with histology, showing great promise in measuring morphological changes such as alveolar surface density and mean linear intercept. Therefore, we and others have further optimized these protocols for *ex vivo* scanning of human lung tissue to bridge the gap between radiology and histopathology, and thus between macroscopy and near-cellular resolution. In this article, we describe a unique approach of air-inflating whole human lung/lobe explants and subjecting these to a wide spectrum of investigations. We propose to use this macro to micro approach leveraging CT and microCT to bridge the gap between radiologic data and histopathology with illustrative examples. Further, we propose to use this approach to selectively investigate changes in the large and small airways, the interstitial compartment as well as the pulmonary arteries, veins and capillaries in relation to the disease extent in the same lung specimen. In addition, other promising tools are discussed in more detail including their potential applications. We acknowledge that a plethora of techniques has also been investigated in animal studies, which can readily be leveraged to combine imaging data with mechanistical insights (7); however, we deliberately focus on studies in humans that can be implemented more easily into routine clinical practice.

METHODOLOGY OF LUNG PROCESSING

Obtaining sufficient contrast between tissue and air is of major importance in the imaging of lung explants. Therefore, immediately following surgical resection, the lung is collected and cannulated via the main stem bronchus. Applying water-controlled air pressure, inflating the lung with 30 cm of water pressure and subsequently lowering the pressure to 10 cm of water pressure allows for an even and uniform recruitment of the lung specimen. The lungs are then mounted in a styrofoam box and frozen in liquid nitrogen vapors. At this moment, the lungs can be safely stored at -80°C until further use. *Ex vivo* CT scanning can be used to correlate with the last available *in vivo* CT, which already allows a higher spatial resolution due to higher radiation doses that can be used. MicroCT scanning of entire lung specimens is more complicated and a dedicated device is needed, where large samples can be mounted while keeping the lung frozen solid inside a styrofoam box. Depending on the size of

the specimen, a resolution of 90–150 micron is feasible, thereby increasing the resolution 6–8 fold compared to conventional *in vivo* CT imaging.

After CT and microCT imaging, which can be used to identify structures of interest, the lung is cut in even slices using a band saw and smaller sized samples with a diameter typically between 12 and 22 mm can be extracted with a core bore or power drill depending on the degree of fibrosis within the samples. These samples can subsequently be re-scanned with high-resolution microCT preferably while keeping the sample frozen (8), where a further increase in resolution can be achieved given the smaller size of the respective specimen, typically up to 5–15 microns.

Subsequently, the lung can be further processed for histopathologic and molecular assessment, e.g., by formalin fixation and dehydration of samples. Our workflow is further illustrated in **Figure 1**. The quality of standard histology is not severely impaired by the prior process of freezing and scanning the lung. Although minor freezing artifacts can be observed, the quality of the histology is much better compared to frozen sections, explained by the fact that the tissue is never in direct contact with ice-cold solutions such as glutaraldehyde. It is very important to emphasize that this process of freezing the lung *in toto* and using microCT also has limited negative impact on further downstream molecular analysis illustrated by e.g., similar gene expression signatures in scanned vs. non-scanned specimens (8). Also bulk RNA-sequencing (9, 10), immunohistochemistry (11), and microbiome sequencing (Einarsson et al. accepted for publication) have already been performed, making ours a valid tool for more molecular-based research.

CT AND MICROCT OF EXPLANT LUNGS

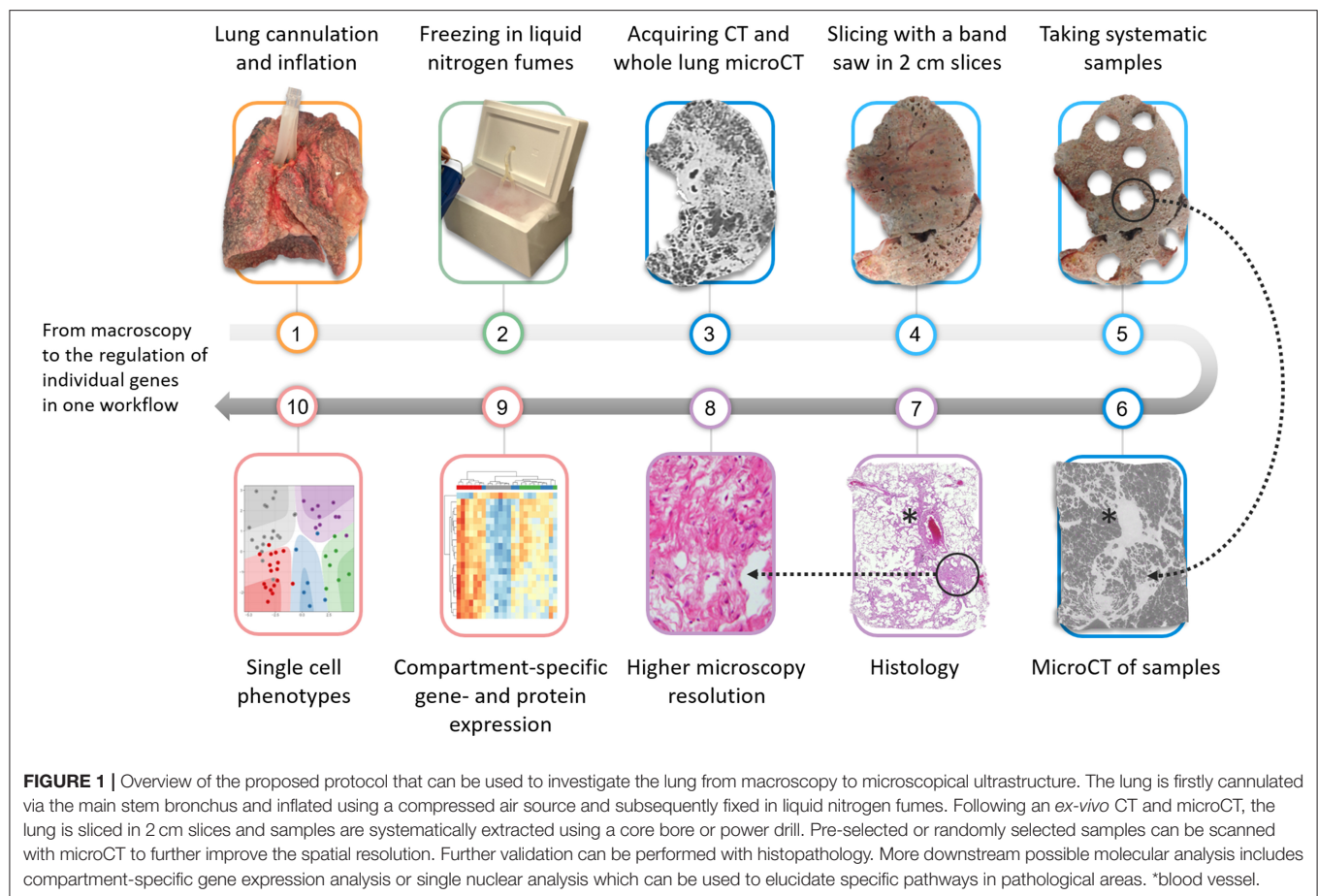
Leveraging CT and whole lung microCT, an easier separation of the lung into morphologically inconspicuous, moderate and severely diseased areas can be made, that can be specifically sampled using the targeted sampling protocol described above. The healthy appearing areas as evident from the imaging can be used as a proxy of early disease. This is valuable given the temporal heterogeneity in non-neoplastic lung diseases, since genuine specimens with early disease features for research purposes are difficult to obtain. There is certainly some ground truth in such a hypothesis as distinct morphological and molecular processes have been demonstrated in minimally affected vs. severely affected regions (9, 10).

Next to pattern and structure analysis, it is also possible to visually identify and segment the entire bronchial tree from the main stem bronchus until the last branch of conducting airways (i.e., terminal bronchioles). This approach can therefore be used to investigate airway abnormalities like airway collapse, airway obstruction or bronchiectasis on a whole lung scale. In addition quantitative data such as the numbers of airways per generation, airway diameters and segment lengths can be generated as has been described already in COPD (12), graft-vs.-host-disease post-allogenic stem cell transplantation (13), lymphangioleiomyomatosis (11) and physiologic aging

(14). The use of a contrast agent, for example osmium staining, also allows for the investigation of (micro-)vascular structures, making the estimation of vascular volumes relative to the total tissue volume possible (15). Specifically in rare pulmonary diseases, whole lung microCT can bridge the gap between research and clinical routine as exemplified in **Figure 2**, where a representative *ex-vivo* CT scan (**Figure 2A**), whole lung microCT scan (**Figure 2B**) and the segmented airway tree based on whole lung microCT (**Figure 2C**) are shown from a patient who underwent pneumonectomy for unilateral congenital emphysema (**Figures 2D,E**). The airway segmentation shows an aberrant airway bifurcation pattern with a marked decrease in the number of visible airways. Remarkably, there are large airway segments without notable airway branching; especially airway segments in severely emphysematous areas show a lack of airway bifurcations (**Figure 2C**).

CORRELATION WITH HISTOPATHOLOGY

Numerous insights can be generated by high-resolution imaging, however the correlation between imaging and histopathology is often difficult, given the inherent differences in spatial resolution. While high-resolution imaging data allows for the investigation of morphological changes, it only provides black and white images and changes at the cellular level or minimal density differences cannot be resolved, making routine pathology still an indispensable tool for both research and routine clinical purposes. Some attempts have, however, been made to correlate imaging with histopathology data, especially with the recent introduction of synchrotron imaging, an extremely powerful source of X-rays, of paraffin embedded samples where sub-stacks of images with (sub)micrometer resolution can be created. Hierarchical phase contrast imaging is another application of synchrotron imaging, where specialized sample preparation and equipment enable the scanning of entire lungs, but also other organs, with a resolution of 25 micron. Furthermore, this technology allows the acquisition of sub-scans with a resolution of 2.5 micron due to the high X-ray photon flux and coherence achieved at modern fourth-generation synchrotron sources (16). This technique has been employed by Ackermann and colleagues to reveal microvascular changes (i.e., broncho-pulmonary shunting) in the bronchial circulation of COVID-19 patients (17). Synchrotron imaging of paraffin embedded samples on the other hand has been used by another group to study morphological changes in the vascularity in pulmonary vascular diseases. Westroo and colleagues leveraged synchrotron imaging to demonstrate a previously unappreciated plexiform lesion heterogeneity, the pathological hallmark of (idiopathic) pulmonary hypertension (18). The same group also used synchrotron-based phase-contrast microCT in combination with vascular dye injection to investigate the vascular morphology in alveolar capillary dysplasia with misaligned pulmonary veins, with vascular dye injection being of significant help in the analysis and further segmentation of the vascular structures (19). A 3D approach for virtual histology and histopathology based on multi-scale phase contrast x-ray tomography has also been



applied to punches of tissue samples with a maximum cross section of 8 mm derived from COVID-19 victims, which allows the segmentation of individual cells with a minimal resolution of 167 nm (20). Lastly, a 36 M-pixel synchrotron radiation microCT has been successfully used to study the secondary pulmonary lobule from a large human lung specimen (21).

However, this approach is not readily available due to the specific nature of the required equipment for both acquisition and analysis, the need for extensive experience with the interpretation of the images and is therefore not (yet) ready for high-throughput screening.

MICROCT IMAGING AS A SCOUTING TOOL

Histopathologic analysis remains the only reliable option for identifying cellular and morphologic patterns keeping the limitation of small tissue samples and the lack of 3D insight in mind. Serial sectioning of paraffin blocks has been used to extensively demonstrate the correlation between microCT and histology (14), however the process of aligning, matching and cutting the samples is tedious and time-consuming. As an alternative, microCT scanning of paraffin blocks or microCT as a scouting tool have been proposed (22). This can especially

be interesting for retrospective studies, in situations where no whole organ is available or when detailed and fast histopathologic assessment is essential for routine patient care such as surgical lung biopsies in the context of a possible interstitial lung disease or suspicion of neoplasms in a resected lung specimen. Interesting and relevant regions can be selected for further sectioning based on the microCT selection which enables time-efficient preparation of conventional histological sections (22). In that aspect, it is also of interest that a novel X-ray microtomosynthesis of unstained pathology tissue samples has also been proposed. Its unique design maximizes the photon flux density through the sample as no rotation is required and therefore samples can be scanned closer to the source resulting in higher resolution (23).

In addition to its potential as a scouting tool, X-ray imaging can also assist in generating a 3D overview of morphological changes in the lung structure. Jones et al. leveraged microCT of paraffin embedded samples to investigate the 3D morphology of fibroblast foci, a key histologic feature of active fibroproliferation in the context of interstitial lung disease. In contrast to the general belief at that time, the fibroblast foci in the lungs of IPF patients were not interconnected and displayed a wide plasticity (24). Wells et al. also used microCT, histopathology, and immunohistochemistry to investigate necrotic granuloma, a characteristic feature of tuberculosis and showed that necrotic

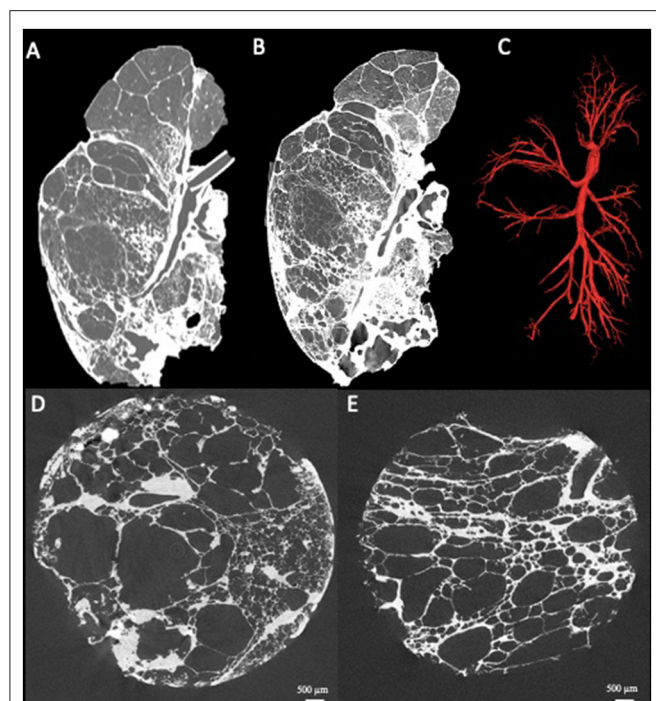


FIGURE 2 | Presentation of a case where clinical routine meets research. Patient with unilateral congenital emphysema that underwent pneumonectomy. The *ex-vivo* clinical CT scan shows severe emphysematous destruction (A) with some fibrosis in the lower lung lobe. The whole lung microCT shows greatly improved details providing near alveolar resolution (B). Airway segmentation of the whole lung by microCT demonstrating the simplification of the airway tree characterized by a low number of visible airways and remarkable long airway segments without airway branching (C). MicroCT imaging of extracted lung specimens showing the severe emphysematous destruction in this lung (D,E).

granulomas exhibit more complex shapes than anticipated, including cylindrical, branched morphologies that are connected to the airways and shaped by the bronchi (25).

The 3D overview provided by microCT is not only helpful to investigate morphologic changes but can also be used to investigate structural changes in the airways. McDonough et al. were the first to employ microCT to quantify the size and number of terminal bronchioles, the last generation of conducting airways before the respiratory bronchioles and alveoli, in tissue samples removed from explanted lungs from COPD patients. Terminal bronchioles can be visually identified on microCT imaging by the loss of the airway wall and appearance of alveolar buds and are of considerable importance in chronic non-neoplastic lung diseases. A significant decrease in the number and size of terminal bronchioles in end-stage COPD lungs was found compared to controls. Given that repeated sampling of the same lung was possible and given that the tissue volume of the sample could be determined, it not only allowed the assessment of the number of terminal bronchioles in the sample, but by carefully measuring the lung volume, these numbers could be extrapolated to the entire lung. This approach provided quantitative data of the actual small airway involvement in COPD

for the first time, something that was always assumed but never conclusively demonstrated in a quantitative way (26). Later on, this approach has also been successfully leveraged to demonstrate small airway involvement in post lung transplantation rejection, cystic fibrosis and idiopathic pulmonary fibrosis (27–30). Over the last years, this approach has been further refined to allow scanning of the samples in frozen condition, making destructive dehydration which was applied at first, unnecessary. In addition, an improvement in the analysis tools has allowed the researchers to extract additional quantitative parameters such as the number of alveolar attachments, the thickness of the airway wall, the circularity of the lumen, but also size and diameter of the preterminal bronchioles (31).

DISCUSSION

Given the above evidence, it is clear that microCT can serve as a complementary, and in the future perhaps even an indispensable tool for routine pathology (32). Although significant technical advances have been made, there is still some work to be done. Indeed, specific microCT devices have already been optimized for 3D imaging of non-stained soft tissue at a resolution of 5–10 micron. These scans could be implemented in routine care and could assist in histology-guided identification of a range of tissue structures and diagnostically relevant histologic criteria and moreover may allow easy quantification of relevant measures such as for example tissue thickness (33). It is our belief that similar advances could also assist in improving the differential diagnosis, particularly in the field of non-neoplastic diseases. However, these approaches could also be leveraged to better understand neoplastic lung diseases such as micro-metastasis, the role of the tumor micro-environment and the role of the vasculature in neoplastic lung disease. Our approach also allows for structurally targeted molecular investigation with both fresh frozen–or formalin fixed tissue being available after non-destructive imaging, allowing panel-based gene expression analysis or broad next-generation sequencing approaches (34). Additionally, microorganisms such as bacteria from biofilms can be recultivated from native flash frozen tissue and used in *in-vitro* assays.

Applying microCT or synchrotron imaging directly to living patients remains an elusive dream, yet a recent study applied propagation-based phase-contrast CT on a human-scale chest phantom prepped with an inflated fresh porcine lung. The authors demonstrated that a resolution of 100 micron could be obtained in a limited local area of interest with significant less radiation than used in conventional CT scanning (35), indicating the possibilities of *in vivo* high resolution scanning. This indicates that we could dream big and hope to apply similar high-resolution imaging *in vivo*, making it perhaps even possible to avoid invasive biopsies. Caution is however needed as rigorous interpretation of the, often immense, imaging data is needed, which could cause a new wave for artificial intelligence based analysis of microCT scans, similar to the current wave of research in the use of artificial intelligence analysis of conventional CT images (36).

Therefore, the imaging-based approaches to close the gap from macroscopy to ultrastructure seems a safe and trustworthy option, which can be relatively fast implemented in the routine care of patients suffering from acute or chronic lung disease and which can facilitate the differential diagnosis.

DATA AVAILABILITY STATEMENT

The original contributions presented in the study are included in the article/supplementary material, further inquiries can be directed to the corresponding author.

ETHICS STATEMENT

The studies involving human participants were reviewed and approved by University Hospital of Antwerp Ethical committee.

REFERENCES

- Raghu G, Remy-Jardin M, Myers JL, Richeldi L, Ryerson CJ, Lederer DJ, et al. Diagnosis of idiopathic pulmonary fibrosis. an official ATS/ERS/JRS/ALAT clinical practice guideline. *Am J Respir Crit Care Med.* (2018) 198:e44–68. doi: 10.1164/rccm.201807-1255ST
- Yagihashi K, Huckleberry J, Colby TV, Tazelaar HD, Zach J, Sundaram B, et al. Radiologic–pathologic discordance in biopsy-proven usual interstitial pneumonia. *Eur Respir J.* (2016) 47:1189–97. doi: 10.1183/13993003.01680-2015
- Unterman A, Wand O, Fridel L, Edelstein E, Pertzov B, Kramer MR. High diagnostic accuracy of transbronchial cryobiopsy in fibrotic interstitial lung diseases compared to final explant diagnosis. *Respiration.* (2019) 98:421–7. doi: 10.1159/000502893
- Panchabhai TS, Arrossi AV, Highland KB, Bandyopadhyay D, Culver DA, Budev MM, et al. A single-institution study of concordance of pathological diagnoses for interstitial lung diseases between pre-transplantation surgical lung biopsies and lung explants. *BMC Pulm Med.* (2019) 19:20. doi: 10.1186/s12890-019-0778-x
- Watz H, Breithecker A, Rau WS, Kriete A. Micro-CT of the human lung: imaging of alveoli and virtual endoscopy of an alveolar duct in a normal lung and in a lung with centrilobular emphysema—initial observations. *Radiology.* (2005) 236:1053–8. doi: 10.1148/radiol.2363041142
- Litzlbauer HD, Neuhaeuser C, Moell A, Greschus S, Breithecker A, Franke FE, et al. Three-dimensional imaging and morphometric analysis of alveolar tissue from microfocal X-ray-computed tomography. *Am J Physiol Lung Cell Mol Physiol.* (2006) 291:L535–45. doi: 10.1152/ajplung.00088.2005
- Tielemans B, Dekoster K, Verleden SE, Sawall S, Leszczyński B, Laperre K, et al. From mouse to man and back: closing the correlation gap between imaging and histopathology for lung diseases. *Diagnostics.* (2020) 10:636. doi: 10.3390/diagnostics10090636
- Vasilescu DM, Phillion AB, Tanabe N, Kinose D, Paige DF, Kantrowitz JJ, et al. Nondestructive cryomicro-CT imaging enables structural and molecular analysis of human lung tissue. *J Appl Physiol.* (1985). (2017) 122:161–9. doi: 10.1152/japplphysiol.00838.2016
- McDonough JE, Ahangari F, Li Q, Jain S, Verleden SE, Herazo-Maya J, et al. Transcriptional regulatory model of fibrosis progression in the human lung. *JCI Insight.* (2019) 4:e131597. doi: 10.1172/jci.insight.131597
- De Sadeleer LJ, McDonough JE, Schupp JC, Yan X, Vanstapel A, Van Herck A, et al. Lung microenvironments and disease progression in fibrotic hypersensitivity pneumonitis. *Am J Respir Crit Care Med.* (2021) 205:60–74. doi: 10.1164/rccm.202103-0569OC
- Verleden SE, Vanstapel A, De Sadeleer L, Weynand B, Boone M, Verbeken E, et al. Quantitative analysis of airway

The patients/participants provided their written informed consent to participate in this study.

AUTHOR CONTRIBUTIONS

SV, PB, CW, MA, JH, TL, JK-V-E, and DJ: responsible for conception and design of the study. EP, MK, AS, HE, TW, AH, FL, SD, PP, VV, and PV: wrote sections of the manuscript. All authors contribute to sample preparation, processing, contributed to manuscript revision, read, and approved the submitted version.

FUNDING

The grants of the European Research Council (ERC); European Consolidator Grant, XHale to DJ (Ref. No. 771883).

- obstruction in lymphangiomyomatosis. *Eur Respir J.* (2020) 56:1901965. doi: 10.1183/13993003.01965-2019
- Everaerts S, McDonough JE, Verleden SE, Josipovic I, Boone M, Dubbeldam A, et al. Airway morphometry in COPD with bronchiectasis: a view on all airway generations. *Eur Respir J.* (2019) 54:1802166. doi: 10.1183/13993003.02166-2018
- Verleden SE, McDonough JE, Schoemans H, Knoop C, Verschakelen J, Dubbeldam A, et al. Phenotypical diversity of airway morphology in chronic lung graft vs. host disease after stem cell transplantation. *Mod Pathol.* (2019) 32:817–29. doi: 10.1038/s41379-019-0203-2
- Verleden SE, Kirby M, Everaerts S, Vanstapel A, McDonough JE, Verbeken EK, et al. Small airway loss in the physiologically ageing lung: a cross-sectional study in unused donor lungs. *Lancet Respir Med.* (2020) 9:167–74. doi: 10.1016/s2213-2600(20)30324-6
- Kampschulte M, Schneider C, Litzlbauer H, Tscholl D, Schneider C, Zeiner C, et al. Quantitative 3D micro-CT imaging of human lung tissue. *Fortschr Röntgenstr.* (2013) 185:869–76. doi: 10.1055/s-0033-1350105
- Walsh CL, Tafforeau P, Wagner WL, Jafree DJ, Bellier A, Werlein C, et al. Imaging intact human organs with local resolution of cellular structures using hierarchical phase-contrast tomography. *Nat Method.* (2021) 18:1532–41. Available online at: <https://www.nature.com/articles/s41592-021-01317-x>
- Ackermann M, Tafforeau P, Wagner WL, Walsh C, Werlein C, Kühnel MP, et al. The bronchial circulation in COVID-19 pneumonia. *Am J Respir Crit Care Med.* (2022) 205:121–5. doi: 10.1164/rccm.202103-0594im
- Westöö C, Norvik C, Peruzzi N, van der Have O, Lovric G, Jeremiasen I, et al. Distinct types of plexiform lesions identified by synchrotron-based phase-contrast micro-CT. *Am J Physiol Lung Cell Mol Physiol.* (2021) 321:L17–28. doi: 10.1152/ajplung.00432.2020
- Norvik C, Westöö CK, Peruzzi N, Lovric G, van der Have O, Mokso R, et al. Synchrotron-based phase-contrast micro-CT as a tool for understanding pulmonary vascular pathobiology and the 3-D microanatomy of alveolar capillary dysplasia. *Am J Physiol Lung Cell Mol Physiol.* (2020) 318:L65–75. doi: 10.1152/ajplung.00103.2019
- Eckermann M, Frohn J, Reichardt M, Osterhoff M, Sprung M, Westermeier F, et al. 3D virtual pathohistology of lung tissue from Covid-19 patients based on phase contrast X-ray tomography. *Elife.* (2020) 9:e60408. doi: 10.7554/eLife.60408
- Umetani K, Okamoto T, Saito K, Kawata Y, Niki N. 36M-pixel synchrotron radiation micro-CT for whole secondary pulmonary lobule visualization from a large human lung specimen. *Eur J Radiol Open.* (2020) 7:100262. doi: 10.1016/j.ejro.2020.100262
- Scott AE, Vasilescu DM, Seal KAD, Keyes SD, Mavrogordato MN, Hogg JC, et al. Three dimensional imaging of paraffin embedded human lung tissue

- samples by micro-computed tomography. Warburton D, editor. *PLoS ONE*. (2015) 10:e0126230. doi: 10.1371/journal.pone.0126230
23. Nguyen DT, Larsen TC, Wang M, Knutsen RH, Yang Z, Bennett EE, et al. X-ray microtomosynthesis of unstained pathology tissue samples. *J Microsc.* (2021) 283:9–20. doi: 10.1111/jmi.13003
 24. Jones MG, Fabre A, Schneider P, Cinetto F, Sgalla G, Mavrogordato M, et al. Three-dimensional characterization of fibroblast foci in idiopathic pulmonary fibrosis. *JCI Insight*. (2016) 1:e86375. doi: 10.1172/jci.insight.86375
 25. Wells G, Glasgow JN, Nargan K, Lumamba K, Madansein R, Maharaj K, et al. Micro-computed tomography analysis of the human tuberculous lung reveals remarkable heterogeneity in three-dimensional granuloma morphology. *Am J Respir Crit Care Med*. (2021) 204:583–95. doi: 10.1164/rccm.202101-0032OC
 26. McDonough JE, Yuan R, Suzuki M, Seyednejad N, Elliott WM, Sanchez PG, et al. Small-airway obstruction and emphysema in chronic obstructive pulmonary disease. *N Engl J Med*. (2011) 365:1567–75. doi: 10.1056/NEJMoa1106955
 27. Verleden SE, Vasilescu DM, Willems S, Rutters D, Vos R, Vandermeulen E, et al. The site and nature of airway obstruction after lung transplantation. *Am J Respir Crit Care Med*. (2014) 189:292–300. doi: 10.1164/rccm.201310-1894OC
 28. Verleden SE, Vasilescu DM, McDonough JE, Rutters D, Vos R, Vandermeulen E, et al. Linking clinical phenotypes of chronic lung allograft dysfunction to changes in lung structure. *Eur Respir J*. (2015) 46:1430–9. doi: 10.1183/09031936.00010615
 29. Boon M, Verleden SE, Bosch B, Lammertyn EJ, McDonough JE, Mai C, et al. Morphometric analysis of explant lungs in cystic fibrosis. *Am J Respir Crit Care Med*. (2016) 193:516–26. doi: 10.1164/rccm.201507-1281OC
 30. Verleden SE, Tanabe N, McDonough JE, Vasilescu DM, Xu F, Wuyts WA, et al. Small airways pathology in idiopathic pulmonary fibrosis: a retrospective cohort study. *Lancet Respir Med*. (2020) 8:573–84. doi: 10.1016/S2213-2600(19)30356-X
 31. Tanabe N, Vasilescu DM, McDonough JE, Kinose D, Suzuki M, Cooper JD, et al. Micro-computed tomography comparison of preterminal bronchioles in centrilobular and panlobular emphysema. *Am J Respir Crit Care Med*. (2017) 195:630–8. doi: 10.1164/rccm.201602-0278OC
 32. Bourdin A, Gamez AS, Vachier I, Crestani B. LAM is another small airway disease: lessons from microCT. *Eur Respir J*. (2020) 56:2002162. doi: 10.1183/13993003.02162-2020
 33. Katsamenis OL, Olding M, Warner JA, Chatelet DS, Jones MG, Sgalla G, et al. X-ray micro-computed tomography for nondestructive three-dimensional (3D) X-ray histology. *Am J Pathol*. (2019) 189:1608–20. doi: 10.1016/j.ajpath.2019.05.004
 34. Ackermann M, Verleden SE, Kuehnle M, Haverich A, Welte T, Laenger F, et al. Pulmonary vascular endothelialitis, thrombosis, and angiogenesis in Covid-19. *N Engl J Med*. (2020) 383:120–8. doi: 10.1056/NEJMoa2015432
 35. Wagner WL, Wuennemann F, Pacilé S, Albers J, Arfelli F, Dreossi D, et al. Towards synchrotron phase-contrast lung imaging in patients – a proof-of-concept study on porcine lungs in a human-scale chest phantom. *J Synchrotron Rad*. (2018) 25:1827–32. doi: 10.1107/S1600577518013401
 36. Soffer S, Morgenthau AS, Shimon O, Barash Y, Konen E, Glicksberg BS, et al. Artificial intelligence for interstitial lung disease analysis on chest computed tomography: a systematic review. *Acad Radiol*. (2022) 29 Suppl 2:S226–S235. doi: 10.1016/j.acra.2021.05.014

Conflict of Interest: The authors declare that the research was conducted in the absence of any commercial or financial relationships that could be construed as a potential conflict of interest.

Publisher's Note: All claims expressed in this article are solely those of the authors and do not necessarily represent those of their affiliated organizations, or those of the publisher, the editors and the reviewers. Any product that may be evaluated in this article, or claim that may be made by its manufacturer, is not guaranteed or endorsed by the publisher.

Copyright © 2022 Verleden, Braubach, Werlein, Plucinski, Kuhnel, Snoeckx, El Addouli, Welte, Haverich, Laenger, Dettmer, Pauwels, Verplancke, Van Schil, Lapperre, Kwakkel-Van-Erp, Ackermann, Hendriks and Jonigk. This is an open-access article distributed under the terms of the Creative Commons Attribution License (CC BY). The use, distribution or reproduction in other forums is permitted, provided the original author(s) and the copyright owner(s) are credited and that the original publication in this journal is cited, in accordance with accepted academic practice. No use, distribution or reproduction is permitted which does not comply with these terms.



Up-to-Date Pathologic Classification and Molecular Characteristics of Intrahepatic Cholangiocarcinoma

Taek Chung¹ and Young Nyun Park^{2*}

¹ Department of Biomedical Systems Informatics, Yonsei University College of Medicine, Seoul, South Korea, ² Department of Pathology, Graduate School of Medical Science, Brain Korea 21 Project, Yonsei University College of Medicine, Seoul, South Korea

OPEN ACCESS

Edited by:

Luca Di Tommaso,
Humanitas Research Hospital, Italy

Reviewed by:

David Kleiner,
National Cancer Institute (NIH),
United States
Mina Komuta,
International University of Health
and Welfare, Narita, Japan

*Correspondence:

Young Nyun Park
young0608@yuhs.ac

Specialty section:

This article was submitted to
Pathology,
a section of the journal
Frontiers in Medicine

Received: 18 January 2022

Accepted: 07 March 2022

Published: 31 March 2022

Citation:

Chung T and Park YN (2022)
Up-to-Date Pathologic Classification
and Molecular Characteristics
of Intrahepatic Cholangiocarcinoma.
Front. Med. 9:857140.
doi: 10.3389/fmed.2022.857140

Intrahepatic cholangiocarcinoma (iCCA) is an aggressive primary liver malignancy with an increasing incidence worldwide. Recently, histopathologic classification of small duct type and large duct type iCCA has been introduced. Both these types of tumors exhibit differences in clinicopathological features, mutational profiles, and prognosis. Small duct type iCCA is composed of non-mucin-producing cuboidal cells, whereas large duct type iCCA is composed of mucin-producing columnar cells, reflecting different cells of origin. Large duct type iCCA shows more invasive growth and poorer prognosis than small duct type iCCA. The background liver of small duct type iCCA often shows chronic liver disease related to hepatitis B or C viral infection, or alcoholic or non-alcoholic fatty liver disease/steatohepatitis, in contrast to large duct type iCCA that is often related to hepatolithiasis and liver fluke infection. Cholangiolocarcinoma is a variant of small duct type iCCA composed of naïve-looking cuboidal cells forming cords or ductule-like structures, and shows better prognosis than the conventional small duct type. Fibrous tumor stroma, one of the characteristic features of iCCA, contains activated fibroblasts intermixed with innate and adaptive immune cells. The types of stroma (mature versus immature) are related to tumor behavior and prognosis. Low tumor-infiltrating lymphocyte density, *KRAS* alteration, and chromosomal instability are related to immune-suppressive tumor microenvironments with resistance to programmed death 1/programmed death ligand 1 blockade. Data from recent large-scale exome analyses have revealed the heterogeneity in the molecular profiles of iCCA, showing that small duct type iCCA exhibit frequent *BAP1*, *IDH1/2* hotspot mutations and *FGFR2* fusion, in contrast to frequent mutations in *KRAS*, *TP53*, and *SMAD4* observed in large duct type iCCA. Multi-omics analyses have proposed several molecular classifications of iCCA, including inflammation class and proliferation class. The inflammation class is enriched in inflammatory signaling pathways and expression of cytokines, while the proliferation class has activated oncogenic growth signaling pathways. Diverse pathologic features of iCCA and its associated multi-omics characteristics are currently under active

investigation, thereby providing insights into precision therapeutics for patients with iCCA. This review provides the latest knowledge on the histopathologic classification of iCCA and its associated molecular features, ranging from tumor microenvironment to genomic and transcriptomic research.

Keywords: intrahepatic cholangiocarcinoma, pathology, small duct, large duct, tumor microenvironment, genomics, transcriptomics

INTRODUCTION

Cholangiocarcinomas (CCAs) include intrahepatic CCA (iCCA), perihilar CCA, and distal CCA (1). Anatomically, iCCA, often called as “peripheral CCA,” is defined as a tumor located in the periphery of the second-order bile ducts, ranging from segmental bile ducts to smaller branches of the intrahepatic biliary tree. Perihilar CCA, also known as Klatskin tumor, is defined as a tumor that arises at the junction where the right and left hepatic ducts meet, with the insertion site of the cystic duct as its distal limit. CCAs involving more of the distal area, such as the common bile duct, is defined as distal CCA. This review mainly focuses on iCCA.

Recent evaluation indicates that iCCA comprises approximately 10–15% of primary liver malignancies (2, 3), and its incidence worldwide has increased over the past decades (4). However, changes in the nomenclature, classification, and the disease coding system of CCA have hampered the accurate estimation of the incidence of iCCA (5). Countries with the highest incidence include South Korea (2.8 per 100,000 people/year), where *Clonorchis sinensis* infection was prevalent in the past, and Thailand (2.2 per 100,000 people/year), which still is an endemic area for infections due to *Opisthorchis viverrini* (4, 6, 7). In other countries where parasites are not endemic, the incidence of iCCA is low, usually below or around 1 per 100,000 people/year. Moreover, there are proposed risk factors such as choledochal cyst, primary sclerosing cholangitis, chronic B or C viral hepatitis, and non-alcoholic fatty liver disease caused by obesity or metabolic syndromes. However, a significant proportion of patients with iCCA have no known risk factors (4, 8). Since these patients rarely present symptoms in the early stage, they are often diagnosed with advanced disease with a dismal prognosis and 5-year overall survival rate of approximately 10% even in developed countries (9–11).

Intrahepatic cholangiocarcinoma is an epithelial neoplasm with biliary differentiation, and usually presents with abundant fibrous tumor stroma containing cancer-associated fibroblasts (CAFs), innate and adaptive immune cells, etc. Recently, iCCAs have been classified into two subtypes namely, small duct type and large duct type (3, 12). Furthermore, the molecular characteristics of iCCA are under active investigation owing

to technological advances in nucleotide sequencing and the availability of massive data sources on cancer, such as The Cancer Genome Atlas (TCGA) and cBio Cancer Genomics Portal (13, 14). The combination of histopathological and multi-omics data have provided novel insights into understanding the molecular pathology and thereby, developing therapeutic options for iCCA.

This review aims to provide the latest knowledge on the histopathologic classification of iCCA based on the fifth edition of the World Health Organization (WHO) classification of digestive system tumors. In addition, we discuss the associated molecular features based on tumor microenvironment, genomic and transcriptomic research results presented so far.

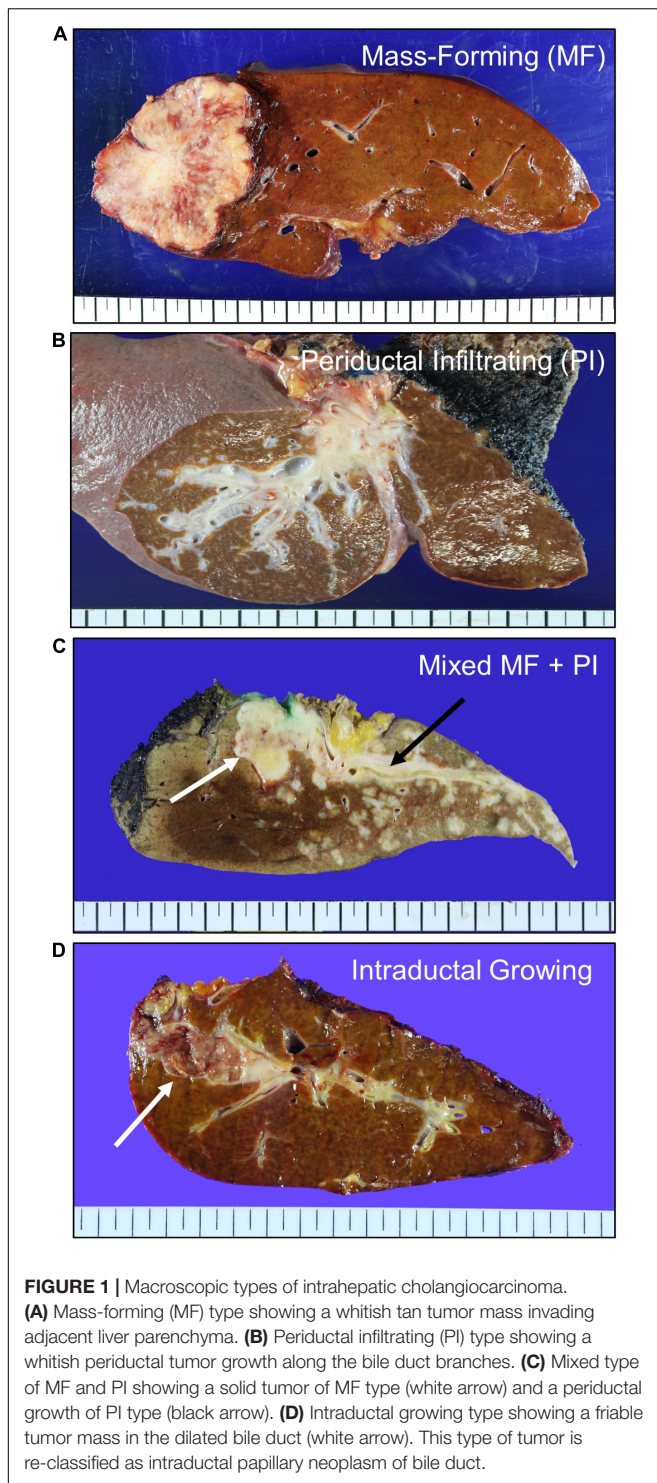
PATHOLOGICAL FEATURES OF INTRAHEPATIC CHOLANGIOCARCINOMA

Intrahepatic cholangiocarcinoma is an adenocarcinoma arising in the intrahepatic biliary tree. Fibrous tumor stroma is one of the characteristic features of iCCA, and the fibrous stroma is various in amount and distribution. The tumor center is usually more fibrotic than the tumor periphery, showing proliferating tumor cells invading into the surrounding liver. Lymphovascular and perineural invasion are often detected even at an early stage.

Gross Features of Intrahepatic Cholangiocarcinoma

Macroscopically, iCCAs can be classified into three types: mass-forming, periductal infiltrating, and intraductal growing. Based on gross appearance, the mass-forming type is most common, and often exhibits mixed features (**Figure 1**) (15). The mass-forming type shows a definite round tumor mass with invasive border. The cut surface is usually white, pale tan or yellowish in color with firm consistency due to fibrous tumor stroma. The periductal infiltrating type shows a growth pattern that extends along the bile duct, exhibiting a whitish fibrotic and thickened bile duct wall. The intraductal growing type grows into the lumen of the bile duct, forming single or multiple soft papillary masses attached to the bile duct wall. The tumor mass and resultant obstruction often dilate the bile duct and make the tumor symptomatic. Since most of the intraductal growing type iCCA cases are now being considered as malignant transformations of intraductal papillary neoplasm of the bile duct (IPNB), in the latest fifth edition of WHO classification, gross morphologic types of iCCA include mass forming, periductal infiltrating and mixed type of these two (3, 16).

Abbreviations: CCA, cholangiocarcinoma; iCCA, intrahepatic cholangiocarcinoma; CAFs, cancer-associated fibroblasts; TCGA, The Cancer Genome Atlas; WHO, World Health Organization; MUC, mucin; CRP, c-reactive protein; EBV, Epstein-Barr virus-encoded small RNA; CKs, cytokeratins; FGB, fibrinogen; B, B; CLC, cholangiolocarcinoma; HCC, hepatocellular carcinoma; DPM, ductal plate malformation; IPNB, intraductal papillary neoplasm of the bile duct; BilIN, biliary intraepithelial neoplasia; IPMN, intraductal papillary mucinous neoplasm; TAMs, tumor-associated macrophages.



Classification of Small Duct Type and Large Duct Type

Conventional iCCA can be further classified into two histopathological types according to the level or size of the affected duct. Recently, small duct type and large duct type iCCA have been introduced in the WHO classification (3).

Small duct type iCCA, which has been reported as a peripheral, ductular, and cholangiolar type, accounts for 36–84% of iCCA (12, 17–19). Small duct type iCCA shows small-sized tubular growth of cuboidal or low-columnar tumor epithelial cells. There is little or no mucin production, and occasional areas of growth exhibit a pattern resembling ductular reaction with slit-like glandular lumen (**Figures 2A,B**). Background liver of small duct type iCCA often shows chronic liver disease related to B viral hepatitis, C viral hepatitis, alcoholic hepatitis, and non-alcoholic steatohepatitis (12, 17, 20).

Large duct type iCCA, which has been reported as bile duct type or perihilar type, arises in large intrahepatic bile ducts and comprises 8–60% of iCCA cases (12, 17–19). Large duct type iCCA is composed of mucin-producing columnar cells forming irregular shaped-and-sized tubules or gland-like structures. This type usually shows a highly invasive growth pattern accompanied by a desmoplastic reaction (**Figures 2D,E**) (3). Pathological examination of the background liver of large duct type iCCA often reveals chronic bile duct injury due to hepatolithiasis, parasitic infection in bile ducts, or primary sclerosing cholangitis (8, 20).

Furthermore, histopathological features of small duct type and large duct type iCCA are related to their gross appearance. The periductal infiltrative type of iCCA is exclusively large duct type, whereas the mass-forming type is more heterogeneous, including small duct and large duct types (17, 21). Mass-forming type iCCA with small duct type histology showed better prognosis than other types (17).

Putative Cells of Origin

Small duct type iCCA occurs in smaller intrahepatic bile ducts compared to large duct type. Canals of Hering, which are histological structures that link hepatic canaliculi and the biliary tree, cuboidal cholangiocytes of bile ductules, and interlobular bile ducts are considered as the putative cells of origin (22, 23). In contrast, large duct type iCCA might be derived from columnar biliary epithelium producing mucin or peribiliary glands around them (8, 20). However, the cellular origin of iCCA is still controversial, since various lineage tracing animal studies showed mixed results indicating hepatic stem or progenitor cells, cholangiocytes or hepatocytes as the cells of origin of iCCA (24, 25). Further research is required to conclusively define the origin of small duct and large duct type iCCAs.

Immunohistochemical Markers for Small Duct Type and Large Duct Type Intrahepatic Cholangiocarcinoma

Examination of a panel of immunohistochemical (IHC) markers is useful to differentiate small duct type and large duct type. In large duct type iCCAs, high expression of mucin (MUC) core protein 5AC, MUC6, and S100 calcium-binding protein P (S100P) has been reported (26, 27), whereas neural cell adhesion molecule (NCAM, also known as CD56) and N-cadherin have been found to be highly expressed in the small duct type. NCAM and N-cadherin are normally expressed in cholangioles (28, 29). Intra- and/or extracellular mucin, detected by mucicarmine or Alcian blue staining, is abundant in the large duct type

in contrast to its scarcity or absence in the small duct type. Examining a panel of these markers, including S100P, N-cadherin, NCAM, and Alcian blue, has been reported to be more effective in differentiating small duct and large duct types (12). Additionally, c-reactive protein (CRP) was recently found to be an effective marker for the diagnosis of small duct type iCCA (30) (**Figures 2C,F**). Biliary cytokeratins (CKs) such as CK7 and CK19 are useful for confirming biliary differentiation or biliary origin. However, their ability to differentiate between small duct type and large duct type iCCA is limited (31, 32).

Histopathological features of hematoxylin and eosin-stained slides usually provide insight to distinguish small duct and large duct type iCCA. In addition, application of immunohistochemical (IHC) markers (S100P, NCAM, and N-cadherin) and special stain for mucin is useful to support the diagnosis of iCCA subtypes, especially when the tissue is limited in biopsies.

Comparison of Prognosis and Treatment Response Between Small Duct Type and Large Duct Type Intrahepatic Cholangiocarcinoma

The prognosis of small duct type iCCA is generally favorable compared to that of large duct type iCCA (12, 17, 33, 34). Accordingly, inflammation-related markers [CRP and fibrinogen (FIB)] and proliferation-related markers [extracellular signal-regulated kinases (ERK) 1/2 and Ki-67] are highly expressed in small duct type iCCA and large duct type iCCA, respectively (17). It has also been reported that the response to conventional chemotherapy is better with small duct type than with large duct type iCCA (35).

Differential Diagnosis of Intrahepatic Cholangiocarcinoma in a Biopsied Tissue

For liver primary tumors, diagnosis of iCCA requires differentiation from combined hepatocellular-cholangiocarcinoma (cHCC-CC), since both components of cHCC-CC may not clearly present due to the limitations of the biopsied tissue. Application of IHC markers for hepatocellular carcinoma (HCC) is helpful to identify portions of hepatocytic differentiation. Hepatocyte paraffin-1 (Hep Par 1) and arginase-1 (ARG1) are highly sensitive and specific (both exceeding 80%) markers, and addition of glypican-3 (GPC3) is shown to be useful for the diagnosis of poorly differentiated areas of hepatocytic differentiation with sensitivity over 80% (36).

Since an iCCA is histopathologically an adenocarcinoma, it is necessary to differentiate it from metastatic adenocarcinoma from other organs. Application of the following IHC markers is helpful. Caudal-type homeobox 2 (CDX2) is a widely used marker for the diagnosis of metastatic colorectal adenocarcinoma with sensitivity over 90%. Since its specificity is relatively low (70%) (37), combination with CK7 and CK20, which are usually negative and positive in colorectal adenocarcinoma, respectively, is recommended (32). Adenocarcinoma of the lung and ductal carcinoma of the breast, which can be differentiated by IHC staining with antibodies of thyroid transcription factor-1 (TTF-1; 75% sensitivity and specificity) (38, 39) and GATA binding protein 3 (GATA-3; over 90% sensitivity and specificity),

respectively (38, 40, 41). Paired box 8 (PAX8) is a sensitive marker for ovarian and endometrial carcinomas, as well as for renal cell carcinomas with sensitivity approaching 90% (40). Metastatic prostate adenocarcinoma is usually positive for the antibodies against prostate specific antigen (PSA) and prostate specific acid phosphatase (PSAP), with sensitivity and specificity exceeding 95% (40, 42). However, in cases of metastatic adenocarcinomas originating from organs adjacent to the liver including gallbladder, pancreas, and stomach, etc., it is difficult to differentiate iCCA from these tumors, due to the lack of specific IHC marker. Some potentially promising markers have been introduced, and filamin A was reported to show high positivity (63%) by immunohistochemistry on iCCA (43). Recently, an *in situ* hybridization assay for albumin RNA was reported to show 90% sensitivity and 100% specificity for iCCA, particularly for the differentiation of small duct type iCCA and metastatic tumors (44–46).

Variants of Intrahepatic Cholangiocarcinoma

Cholangiolocarcinoma (CLC) is a variant of iCCA that belongs to the small duct type. It is defined as an iCCA with more than 80% of the tumor area showing cholangiolocellular differentiation without hepatocellular differentiation. The prefix “cholangiolo” implies histopathological similarity to the cholangiole or canals of Hering (47). CLCs show small cuboidal cells forming cords or tubular structures with antler-like growth resembling the ductular reaction of non-tumorous liver (48). Often, the lumina of tumor cords are inconspicuous, the atypia or pleomorphism of tumor epithelial cells is minimal, and regularly spaced intervening stroma is also a characteristic feature (**Figure 3A**).

CLC is thought to arise at the bile ductule, containing hepatic stem or progenitor cells, and canals of Hering. It was previously classified as a subtype of combined hepatocellular-cholangiocarcinoma (49), however, molecular profiling studies favor the classification of CLC as part of iCCA (50). According to the current WHO classification, CLC without components of HCC or intermediate carcinoma is an iCCA and is not considered as combined hepatocellular-cholangiocarcinoma.

CLC is distinguished from conventional small duct type iCCAs based on its excellent outcome, which shows significantly higher overall and disease-free survival (49, 51). Even iCCAs with cholangiolocellular differentiation (>10% of the tumor area) were found to have a better prognosis than those without (17, 52). A transcriptomic profiling study reported that iCCA with cholangiolocellular differentiation correlated with inflammation class, while iCCA without cholangiolocellular differentiation correlated with proliferation class (the molecular classification is discussed in more detail later in the genomic-transcriptomic profiles section) (52, 53).

Intrahepatic Cholangiocarcinoma With Ductal Plate Malformation Pattern

Ductal plate malformation (DPM) refers to a developmental anomaly characterized by pathologically existing embryonic bile duct structures (“ductal plates”). The percentage of iCCAs

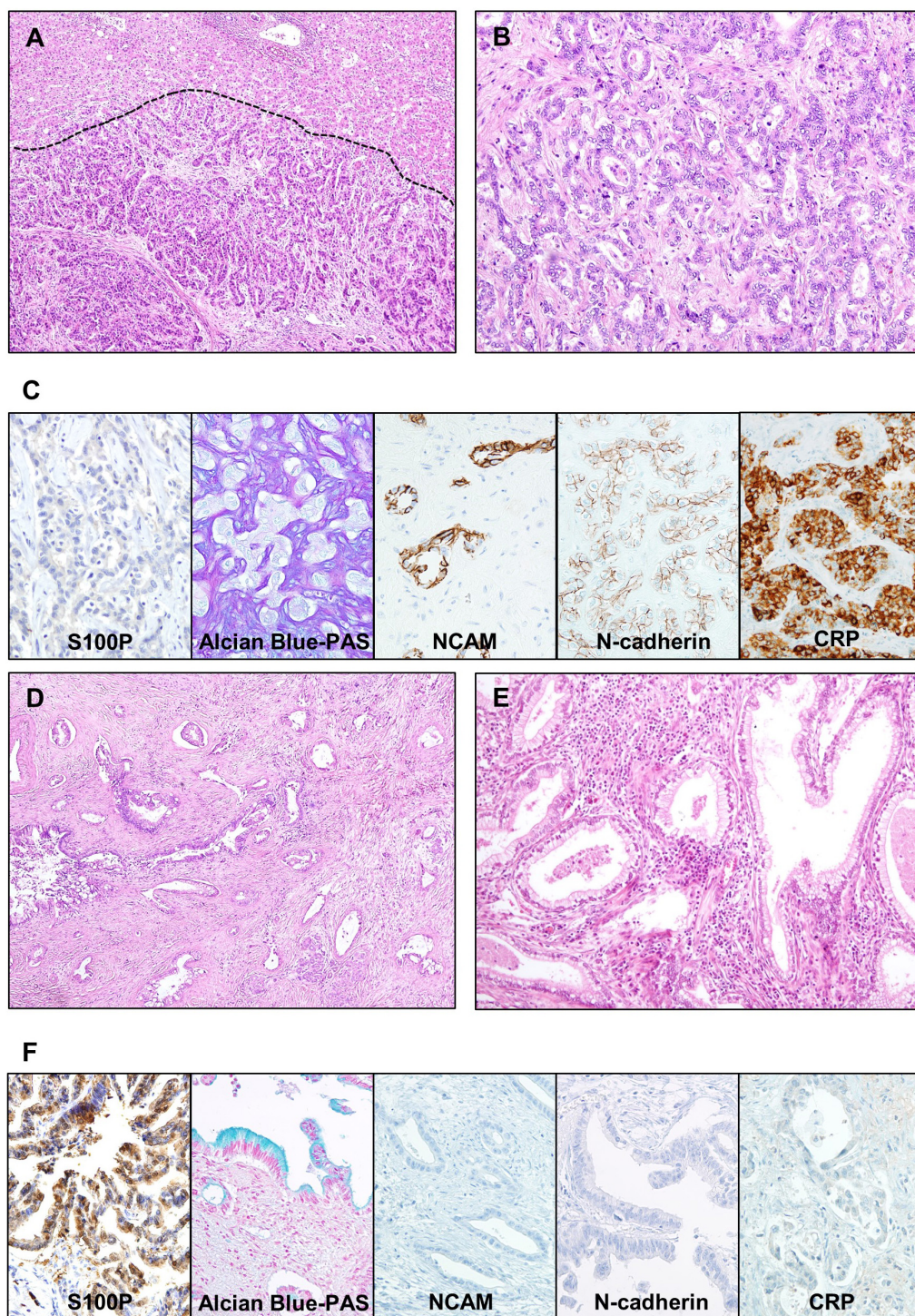


FIGURE 2 | Representative microscopic images of small duct type and large duct type intrahepatic cholangiocarcinoma (iCCA). **(A–C)** Small duct type iCCA. **(A)** A low-power view showing uniform-shaped tumor glands replacing hepatocellular trabeculae at the border (indicated by dashed line). **(B)** A higher magnification image showing the growth of cuboidal cells forming cords and small glandular structures, without intra- or extracellular mucin. **(C)** Microscopic images of special and immunohistochemical panel staining for small duct type iCCA; positive expression of NCAM, N-cadherin and CRP, negative expression of S100P, and absence of mucin in the Alcian blue staining is characteristic. **(D–F)** Large duct type iCCA. **(D)** A low magnification image shows infiltrative growth of adenocarcinoma with rich fibrous stroma. **(E)** A higher magnification image showing columnar cells with intracellular mucin forming irregular glandular spaces. **(F)** Microscopic images of special and immunohistochemical panel staining for large duct type iCCA; positive expression of S100P, presence of mucin in the Alcian blue staining, and negative expression of NCAM, N-cadherin, and CRP is characteristic. Original magnification: 40× for **(A,D)**, 100× for **(B,E)**, 200× for **(C,F)**. S100P, S100 calcium-binding protein P; NCAM, neural cell adhesion molecule; CRP, c-reactive protein; PAS, periodic acid–Schiff.

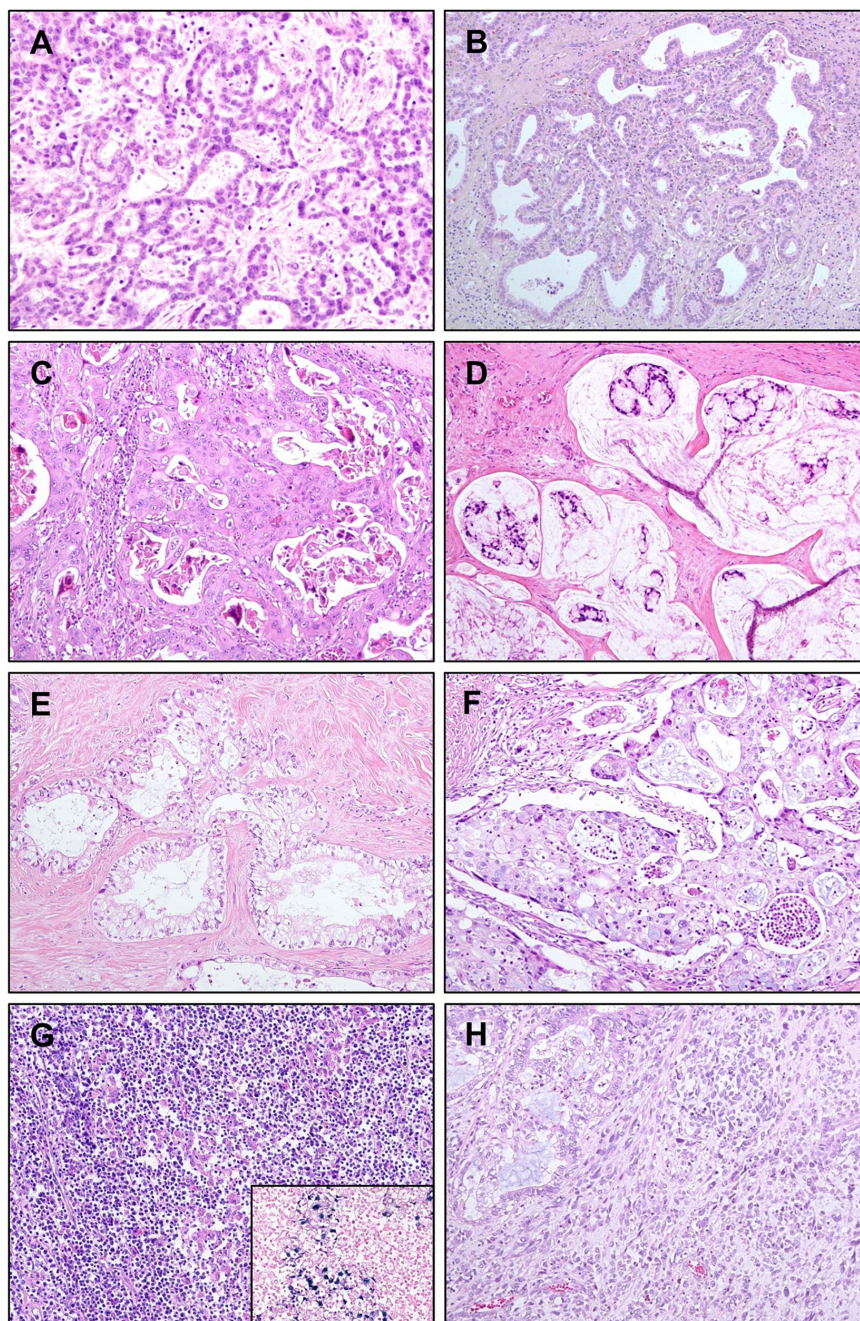


FIGURE 3 | Variants of intrahepatic cholangiocarcinoma (iCCA). **(A)** Cholangiolocarcinoma. Bland-looking small cuboidal tumor epithelial cells are forming cords or ductules, with antler-like branching pattern. **(B)** iCCA with ductal plate malformation pattern. Cuboidal tumor cells are forming irregularly dilated and coalesced spaces, resembling developmental anomaly of ductal plate. **(C)** Adenosquamous carcinoma showing both of gland-forming portion and portions with squamous differentiation. **(D)** Mucinous carcinoma. Mucin-producing tumor cell clusters are floating in mucin pools. **(E)** Clear cell carcinoma. Tumor cells have large clear cytoplasm with eccentric nuclei. **(F)** Mucoepidermoid carcinoma showing squamoid tumor cells intermixed with mucin-producing cells. **(G)** Lymphoepithelioma-like carcinoma showing marked lymphocytic infiltration into tumor epithelial component. Tumor epithelial cells are positive for Epstein-Barr virus (EBV), detected by *in situ* hybridization of EBV-encoded small RNA (inset). **(H)** Sarcomatous iCCA showing mainly pleomorphic spindle cells, with adenocarcinoma components in the upper left corner. Original magnification: 100 \times .

that are diagnosed as iCCAs with DPM pattern is very small, approximately 2.9% of cases in a cohort of 175 resected iCCAs (54). Histopathologically, the tumor epithelial cell lining is

usually benign-looking cuboidal cells without mucin production, and they form glandular structures that are elongated, tortuous, and coalesced, mimicking ductal plates (**Figure 3B**) (55). Genetic

alterations in iCCA with DPM pattern include point mutations in *FGFR2*, *PTPRT*, *ARID1A*, and *CDKN2A*, and fusion of *FGFR2* (54, 56). Patient survival seems better than that of conventional small duct type iCCAs (54).

Adenosquamous Carcinoma/Squamous Carcinoma

Adenosquamous carcinoma of the liver has both squamous epithelial and glandular components (**Figure 3C**), and its incidence is rare (57). Squamous carcinoma, showing squamous differentiation in the entire tumor is extremely rare. This type of variant iCCA is reported to be correlated with chronic cholangitis caused by liver flukes or hepatolithiasis (58). The prognosis of adenosquamous carcinoma of the liver is usually poor, with a median survival of approximately 6 months (57).

Mucinous Carcinoma/Signet Ring Cell Carcinoma

Mucinous carcinoma is a variant that belongs to large duct type iCCA. It contains an overwhelming amount of extracellular mucin in the luminal space of tumor glands, usually over 50% of the total tumor volume by convention (59), often causing tumor epithelial cells to float in the mucin pool (**Figure 3D**). This type of tumor usually occurs due to the malignant transformation of the IPNB. Signet ring cell carcinoma occasionally presents as a mucinous carcinoma with varying distribution; however, pure signet ring cell carcinoma of the liver is extremely rare. The absence of ovarian-like stroma differentiates this variant of iCCA from mucinous cystic neoplasm (60).

Clear Cell Carcinoma

Clear cell carcinoma is characterized by bulky cytoplasmic clearing and eccentrically located nuclei in most tumor epithelial cells with glandular and trabecular growth patterns (**Figure 3E**) (58, 61). Primary clear cell carcinoma of the liver can be differentiated from HCC with clear cell change, metastatic clear cell carcinoma of the kidney, and metastasis from other gastrointestinal tract tumors by IHC staining for hepatocyte paraffin 1 (HepPar-1), CD10, and CK20, respectively (62).

Mucoepidermoid Carcinoma

Primary mucoepidermoid carcinoma of the liver shows features similar to those in other organs, including the salivary glands. It reveals a more intimate mixture of epidermoid or squamous and mucin-secreting elements, compared to adenosquamous carcinoma where mucin-secreting cells and foci of squamous differentiation exist separately (**Figure 3F**) (63). There have been only a few reports, and most of them have shown a poor prognosis (64).

Lymphoepithelioma-Like Carcinoma

Lymphoepithelioma-like carcinoma is characterized by dense lymphoid stroma around the tumor epithelial cells, often forming lymphoid follicles. Tumor epithelial cells show an undifferentiated or gland-forming pattern, rarely with well-differentiated or bland-looking glands (**Figure 3G**). Almost all cases are Epstein–Barr virus-encoded small RNA (EBER) positive and usually have favorable outcomes (65, 66).

Sarcomatous Intrahepatic Cholangiocarcinoma

Sarcomatous iCCA usually shows mixed features of conventional iCCA and undifferentiated components of cells with spindle or rhabdoid features (**Figure 3H**). When a conventional iCCA component is not present, a definite diagnosis is difficult, since the sarcomatoid component is often negative for epithelial markers by IHC staining (67). Sarcomatous iCCA usually has a worse prognosis than conventional iCCAs (68).

Precursor Lesions

Biliary Intraepithelial Neoplasia

Biliary intraepithelial neoplasia (BilIN), a precursor lesion of CCA, occurs at the epithelium of intra- and extrahepatic bile ducts and in the peribiliary glands. Large duct type iCCA, but not small duct type, is often accompanied by BilIN (17, 21). BilIN is virtually invisible upon gross examination, although it may be associated with subtle changes such as mucosal thickening. Microscopically, BilIN consists of flat or micropapillary (less than 3 mm in height) epithelial lesions that are graded as low-grade or high-grade (carcinoma *in situ*) based on the highest degree of cytoarchitectural atypia (69, 70). This two-tiered classification replaces the former three-tiered classification, wherein the former BilIN-1 and BilIN-2 are now classified as low-grade, and the former BilIN-3 is now classified as high-grade.

Low-grade BilIN shows mild cytoarchitectural atypia, including flat pseudopapillary and/or micropapillary growth pattern, nuclear stratification, hyperchromatic nuclei, and increased nuclear-cytoplasmic ratio; however, nuclear polarity is preserved. High-grade BilIN is characterized by moderate to severe cytoarchitectural atypia, including more complex patterns, complete loss of polarity, marked nuclear atypia, and frequent mitosis. While IHC staining for p53 is usually negative in low-grade BilIN, it is often overexpressed in high-grade BilIN (71). The expression of p16 is relatively preserved in low-grade BilIN and decreased in high-grade BilIN (72). A notable mutation in BilIN lesions is alterations in *KRAS*, which is reported to be approximately 30% (73) (**Figures 4A,B**).

Differentiating BilIN from reactive epithelial atypia may be difficult, especially in biopsy samples. Reactive atypia shows overlapping attenuated basophilic cells with nuclei having fine and diffuse chromatin. The nucleoli are small or conspicuous. Mitotic activity may be prominent. Reactive epithelial atypia usually shows a gradual transition from uninvolved epithelium, in contrast to the abrupt change usually seen in BilIN. The IHC detection of S100P was shown to be useful, being mostly negative in reactive epithelial atypia. However, its expression increased sequentially from low-grade BilIN to high-grade BilIN and subsequently in iCCA (74).

Intraductal Papillary Neoplasm of the Bile Duct

Intraductal papillary neoplasm of the bile duct (IPNB) is defined as a grossly visible premalignant neoplasm showing intraductal papillary or villous growth of biliary-type epithelium (70). It is considered to be a counterpart of a similar tumor arising in the pancreas, the so-called intraductal papillary mucinous neoplasm (IPMN). IPNB is divided into low-grade and high-grade based on the highest degree of cytoarchitectural atypia.

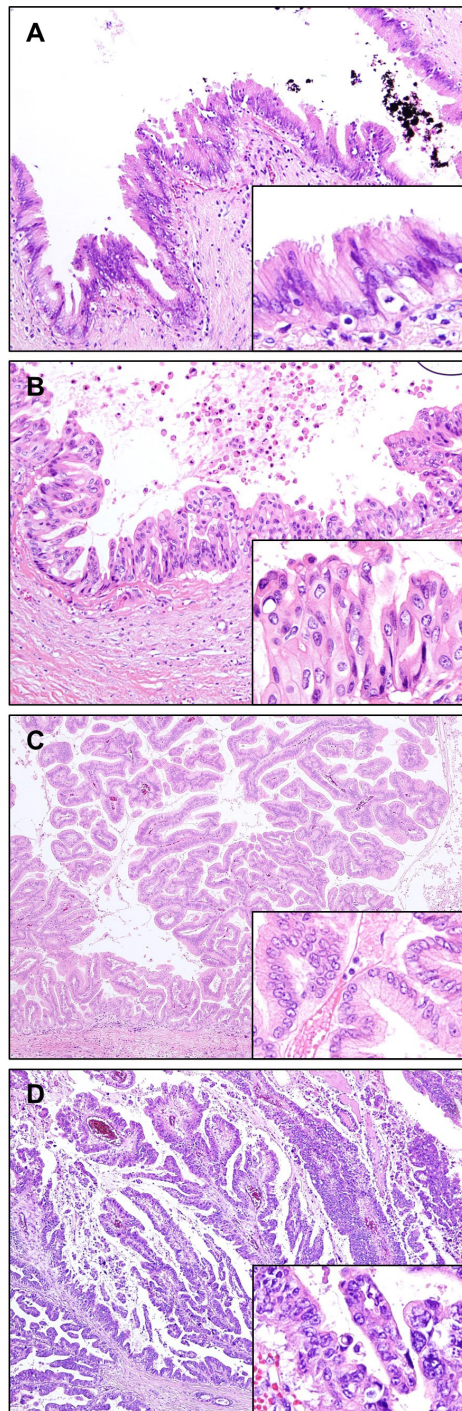


FIGURE 4 | Precursor lesions of intrahepatic cholangiocarcinoma. **(A,B)** Biliary intraepithelial neoplasia (BilIN). **(A)** Low-grade BilIN composed of columnar cells with intact nuclear polarity and minimal atypia. **(B)** High-grade BilIN showing stratification of cells with marked nuclear atypia and loss of polarity. **(C,D)** Intraductal papillary neoplasm of the bile ducts (IPNB). **(C)** Low-grade IPNB showing a papillary growth of columnar biliary type epithelial cells with mild pleomorphism and preserved nuclear polarity. **(D)** High-grade IPNB showing irregular papillary projections, composed of highly pleomorphic and stratified cells with increased nuclear-cytoplasmic ratio. Original magnification: 100× for **(A,B)**, 40× for **(C,D)**, 200× for inset images.

When invasive carcinoma develops in this lesion, it is diagnosed as IPNB with associated invasive carcinoma. High-grade IPNBs are often associated with stromal invasive carcinoma, usually consisting of tubular adenocarcinoma and occasionally mucinous carcinoma (75).

Grossly, IPNBs appear as polypoid masses with dilatation of the bile ducts. These are usually isolated papillary lesions, whereas some IPNBs appear as multiple contiguous papillary or polypoid lesions. Some IPNBs are characterized by mucus hypersecretion, forming mucin-containing fusiform dilatation or cysts, similar to those observed in IPMNs (76). Microscopically, IPNBs form papillary structures with fine fibrovascular cores (**Figures 4C,D**). Four histological subtypes are generally accepted based on cytological appearance and immunophenotype, namely, – pancreatobiliary, intestinal, gastric, and oncocytic. Immunohistochemically, MUC1 is mostly expressed in the pancreatobiliary type. Gastric type usually express MUC5AC and MUC6, and the intestinal type frequently express MUC2. CK20 is positive in the intestinal type, but not in the gastric and oncocytic types (70, 77). The presence of two or more histopathological types is common in IPNB, therefore these tumors are diagnosed based on the most prevalent histopathological type. The pancreatobiliary type is most common, with higher prevalence in western countries than in Asia. In contrast, intestinal type is more common in Asian populations than in western populations, while oncocytic and gastric types are least frequent (78). Although the clinical implications of histopathologic subtypes are still controversial, the pancreatobiliary type is reported to be linked with a higher frequency of associated invasive carcinoma, frequent lymph node metastasis, and recurrence (77).

A recent consensus has proposed a different classification for IPNBs of type 1 and type 2 (79, 80). Type 1 IPNB shows more homogeneous appearance than type 2 IPNB, and is composed of regular villous, papillary, or tubular structures usually with low-grade dysplasia, but may present with high-grade dysplasia with foci of low-grade dysplasia. Mucin overproduction is frequently observed, whereas stromal invasion is uncommon. This is most commonly found in intrahepatic bile ducts. Histological similarity with IPMN of the pancreas is also characteristic. Type 2 IPNB exhibits heterogenous appearance composed of irregular and complicated villous, papillary or tubular structures. This is usually composed of high-grade dysplasia, and foci of low-grade dysplasia are absent or minimal. Invasive carcinoma is more frequently associated with type 2 IPNB than type 1 IPNB. Mucin overproduction is not common. Type 2 IPNB arises throughout the biliary tree, including intrahepatic and extrahepatic bile ducts.

The mutational profile studies on IPNB have reported that diverse cancer driver mutations are frequently observed, including *KRAS*, *TP53*, *STK11*, *CTNNB1*, *APC*, *SMAD4*, and *GNAS*. Type 1 IPNBs show higher mutation rates of *KRAS*, *GNAS*, and *RNF43*, whereas type 2 IPNBs have higher *TP53* and *SMAD4* mutation rates (81, 82).

Although IPNBs present papillary morphology, sometimes tubular growth pattern of epithelial components with less mucin production is predominantly observed, similar to intraductal tubulopapillary neoplasm (ITPN) of the pancreas (83). Such cases have been described as intraductal tubular neoplasms

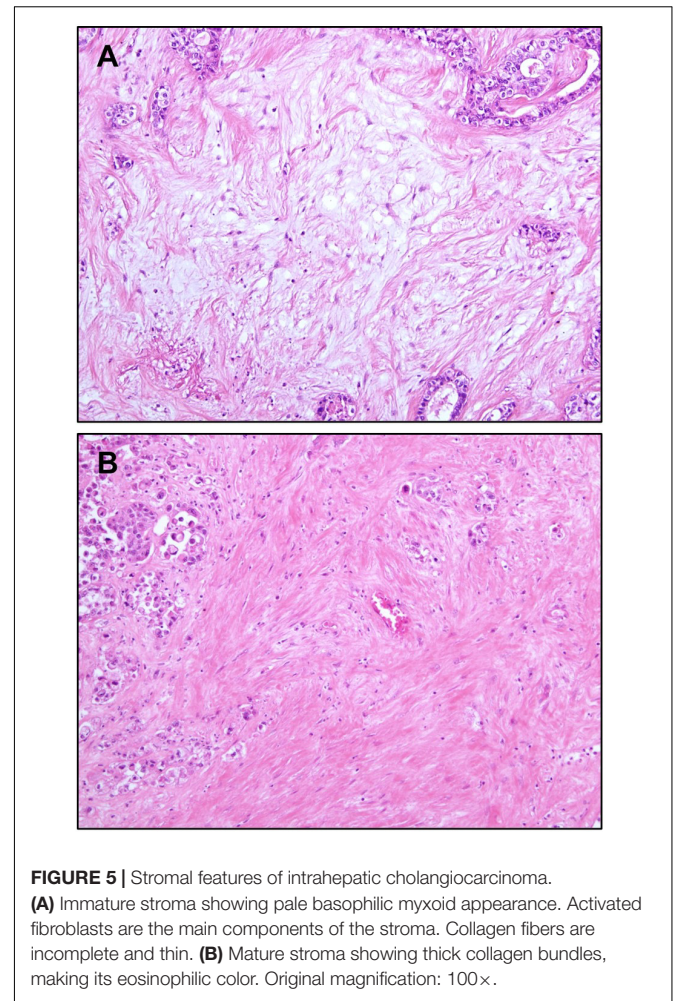
or ITPNs. Recently, ITPN has been reported to show more frequent intrahepatic occurrence in contrast to IPNB, which favors both intra- and extrahepatic locations. Furthermore, IPNB and ITPN differ in their genomic and epigenomic profiles. Recently, IPNB has been reported to share mutational profiles with extrahepatic CCA, including mutations in *TP53*, *SMAD4*, and *KRAS* and deletions on chromosomes 9q, 17p, and 18q. However, ITPN shows low overall mutational burden, and distinct DNA methylation pattern that clustered together with iCCA rather than extrahepatic CCA, suggesting that IPNB and ITPN are distinct entities (84).

TUMOR MICROENVIRONMENT OF INTRAHEPATIC CHOLANGIOCARCINOMA

One of the characteristics of iCCA is the abundance of fibrous stroma (85). The amount of fibrous stroma has been reported to be associated with poor prognosis (86). Furthermore, so-called “scirrhous type” iCCA, which is defined as iCCA having scirrhous area (where the amount of fibrous stromal component is at least equal to the area of epithelial component) more than 70% of the largest cut surface, has been reported to show worse prognosis than conventional iCCAs (87). More recently, the characteristics of immature and mature fibrous tumor stroma have been reported to be related to tumor behavior (88, 89). Immature stroma is composed of myxoid stroma with randomly oriented short keloid-like collagen bundles. In contrast, mature stroma shows multilayered mature collagen fibers (Figure 5). Accordingly, iCCAs with immature stroma have been reported to show poorer prognosis compared to iCCAs with mature stroma (88, 89).

Activated CAFs, one of the major components of the tumor microenvironment, have been demonstrated to facilitate tumor growth and progression, and promote immunosuppression in tumors (90). CAFs are thought to be recruited from hepatic stellate cells, portal fibroblasts, or circulating mesenchymal cells, but the exact source is currently unknown (91). Transforming growth factor β (TGF- β) and platelet-derived growth factor D (PDGF-D) secreted by tumor epithelial cells recruit CAFs. Recruited CAFs not only promote desmoplastic reaction by collagen and matrix metalloproteinases, but also cause tumor epithelial cells to proliferate, invade, and resist antitumor mechanisms by secreting growth factors such as PDGF-B and epidermal growth factors (92, 93). Patients with iCCA with a high proportion of activated CAFs were reported to have a shorter survival rate than patients with low CAF proportion (94).

Immune cells, including tumor-associated macrophages (TAMs) and tumor-infiltrating lymphocytes, are also main components of the tumor microenvironment. The hepatic macrophage population consists of activated macrophages derived from Kupffer cells or bone marrow-derived macrophages (95), and activated macrophages can be classified as M1 (classical) and M2 (alternative)-polarized types (96). The M2 phenotype forms the majority of TAM population in iCCA, having anti-inflammatory and pro-tumor functions mediated by



the secretion of anti-inflammatory cytokines, including IL-4, IL-10, IL-13, and TGF- β (97). These cells also promote intratumoral angiogenesis, which is vital for tumor survival and metastasis (85, 98). A high proportion of M2 TAMs in iCCA is correlated with increased invasiveness of tumor cells and poor disease-free survival (97, 99). In contrast, M1 TAMs have been reported to exert pro-inflammatory functions, including secretion of pro-inflammatory cytokines such as TNF- α , interleukin (IL)-6, and IL-1 β (99).

Tumor-infiltrating lymphocytes include B cells (CD20⁺), helper T cells (CD4⁺), cytotoxic T cells (CD8⁺), and regulatory T cells (Tregs, FOXP3⁺). The major proportion of tumor-infiltrating lymphocytes comprises T cells rather than B cells (100). The distribution and proportion of CD4⁺ and CD8⁺ T cells varies among iCCAs, and increased population of these cells is correlated with better prognosis (8, 85). In addition, iCCAs with B cell infiltration have been reported to be associated with better survival than iCCAs without B cells (101). Treg cells are a subset of CD4⁺ T cells that suppress innate and adaptive immune responses mainly by secreting IL-10 and TGF- β , which are known to promote tumor progression by inhibiting antitumor immune response. Regarding iCCA, while there are a few studies on

the clinical aspects of the presence of Treg cells, there is no sufficient evidence to draw a conclusion. Therefore, additional investigation is required (101–103).

With the advent of immune checkpoint blockade therapeutics, the expression status of cell surface proteins with immune escape mechanisms is currently under active investigation. Cytotoxic T-lymphocyte antigen-4 (CTLA-4), expressed on the surface of Treg cells, suppresses cytotoxic T cell activity by binding to CD80 of antigen-presenting cells (85). High CTLA-4 expression has been reported to be related to worse relapse-free survival of patients with CCA, raising the possibility of effective immunotherapy targeting CTLA-4 (104). Programmed death 1 (PD-1), expressed on T cells, and its ligand programmed death ligand 1 (PD-L1), on tumor epithelial cells, are other major immune checkpoints of interest. Binding of PD-L1 to PD-1 diminishes the immunological function of cytotoxic T cells. Approximately 9–30% of iCCA has been reported to be PD-L1 positive as observed by IHC staining (105–107). Recently, our group reported that *KRAS* alteration and chromosomal instability were associated with resistance to PD-1/PD-L1 blockade immunotherapy, whereas high intratumoral tumor-infiltrating lymphocyte density was associated with a favorable immunotherapy response in patients with CCA (35). Many clinical trials for iCCA using immune checkpoint inhibitors are ongoing based on the expression status of markers, including PD-1, PD-L1, and CTLA-4, with expectations of promising results in the near future (108).

MULTI-OMICS FEATURES OF INTRAHEPATIC CHOLANGIOCARCINOMA

Germline and Somatic Mutational Profile of Intrahepatic Cholangiocarcinoma

Germline Predisposition

There are a few germline predispositions for cancers, including proto-oncogenes and tumor suppressor genes, either by inheritance from parents or *de novo* mutation at the zygote level. Approximately 8–12% of iCCAs have been reported to have known pathogenic or possibly deleterious germline mutations, and the most commonly found germline-mutated genes are *BRCA1* and *BRCA2*, which are associated with DNA repair mechanism and hereditary cancer syndromes (109–112) (Table 1). Other germline variants linked with iCCA include *APC*, an antagonist of the Wnt signaling pathway, *BAP1*, which mediates deubiquitination, and mismatch repair mechanism-related genes, namely *MLH1* and *MSH2* (109, 111, 113). However, evidence regarding the association between known hereditary cancer syndromes and iCCA is currently not fully established and requires further investigation.

Somatic Short Mutations, Structural Variations, and Copy Number Aberrations

Among somatic mutations identified in iCCA, the most well-known and frequent variants are at exons 5–8 of *TP53* and

TABLE 1 | Summary of germline mutations reported in intrahepatic cholangiocarcinoma.

Gene	Frequency of occurrence (%)	References
<i>BRCA1</i>	1–3	(109–111)
<i>BRCA2</i>	1–3	(109–111)
<i>MLH1</i>	2	(109)
<i>MSH2</i>	2	(109)
<i>MUTYH</i>	2	(111)
<i>BAP1</i>	1	(111)
<i>PMS2</i>	1	(111)
<i>APC</i>	1	(111)

hotspots at codons 12/13 of *KRAS*, which are involved in cell cycle arrest/DNA repair and mitogen-activated protein kinase (MAPK) signaling pathway, respectively (114–116). Other MAPK pathway genes such as *NRAS* and *BRAF* are also frequently mutated in iCCA (117). Owing to the advancement and wide use of massive parallel sequencing techniques, many other driver gene mutations have been discovered in the last decade. Single-nucleotide variants of chromatin remodeling-related genes such as *ARID1A*, *BAP1*, and *PBRM1* have been reported with frequencies ranging from 6 to over 30% (115, 118–120). Moreover, mutations in *IDH1/2*, which acts as an epigenetic regulator, are most frequently observed, with an average incidence of approximately 15% (115, 121–124). Other somatic short mutations include Akt signaling pathway-associated genes such as *PTEN*, *PIK3CA*, and *PIK3C2A*, and *SMAD4*, a TGF- β signaling pathway gene (115, 118, 125, 126).

The most frequently found structural variation in iCCA is *FGFR* gene fusion, notably *FGFR2*, which has been reported in 6–14% of iCCAs (127, 128). The most common fusion partner is *BICC1*; however, several other genes were also found, including *AHCYL1* and *PPLN1* (128–130). Driver gene amplification was found in *ERBB2* (2–12%), *MDM2* (0–13%), *EGFR* (1–16%), and *CCND1* (10–13%). Deletion of 9p21.3, or the locus including genes *CDKN2A* and *CDKN2B* is found in 10–20% of iCCA (13, 126, 127, 131).

Microsatellite instability-high cases are usually determined by three methods namely, observing the size change in more than three out of five marker loci by polymerase chain reaction, IHC for mismatch repair proteins including, *MLH1*, *MSH2*, *MSH6*, and *PMS2*, or estimation of tumor mutation burden by NGS. Such cases are known to be rare (around 1%) in iCCA (126, 132–134). The mutational characteristics of iCCA are summarized in Table 2.

Genetic alterations are also correlated with pathological features. Hotspot mutations in *KRAS* have been reported in periductal infiltrating type, but not in mass-forming type (135). Histopathologically, small duct type has been reported to have more frequent *BAP1* and *IDH1/2* hotspot mutations and *FGFR2* fusion, and lower incidence of *KRAS* mutation than large duct type (12, 26, 51, 122, 136, 137). On the contrary, large duct type is known to have frequent mutations in *TP53*, *KRAS* and some

TABLE 2 | Major somatic variants and reported incidence in intrahepatic cholangiocarcinoma.

	Groups	Gene or locus	Frequency of occurrence (range, %)	References
Small nucleotide variants	DNA repair	<i>TP53</i>	2.5–39.3	(13, 35, 115, 120, 123, 125, 126, 131)
	Chromatin remodeling	<i>ARID1A</i>	7–36	(13, 35, 115, 120, 123, 126, 131)
		<i>BAP1</i>	6–16	(13, 35, 116, 121, 123, 126, 131)
		<i>PBRM1</i>	9–14.3	(13, 35, 116, 119, 121, 123, 126, 131)
	MAPK signaling pathway	<i>KRAS</i>	2–30.3	(13, 35, 115, 121, 123, 125, 126, 131)
		<i>NRAS</i>	3–9.3	(13, 115, 117, 119, 125, 126, 131)
		<i>BRAF</i>	3–5	(13, 35, 117, 125, 126, 131)
		<i>IDH1</i>	5–36	(13, 35, 115, 126, 131)
	Epigenetic regulator	<i>IDH2</i>	3.7–36	(13, 115, 117, 119, 121, 126, 131)
		<i>SMAD4</i>	0–9	(13, 35, 115, 126, 131)
	Akt signaling Pathway	<i>PTEN</i>	0.6–11	(13, 115, 117, 125, 126, 131)
		<i>PIK3CA</i>	3–7	(13, 35, 115, 117, 119, 120, 125, 126, 131)
		<i>PIK3C2A</i>	0–7.1	(117)
Structural variation	Translocation	<i>FGFR2</i>	6–14	(13, 127, 128, 131)
	Amplification	<i>CCND1</i>	10–13	(13, 35, 131)
		<i>EGFR</i>	1–16	(126, 131)
		<i>ERBB2</i>	2–12	(35, 126, 131)
		<i>MDM2</i>	0–13	(131)
	Deletion	9p21.3 (CDKN2A/B)	10–20	(126, 131)
Microsatellite instability			~1	(126, 131, 133)

TGF- β pathway genes, including *SMAD4*, *TGFBR2*, *FBXW7*, and *MYC* (35).

From an etiological point of view, liver fluke *O. viverrini* infection-related iCCA had a higher *TP53* mutation rate, while *BAP1* and *IDH1/2* mutations were more frequently found in non-fluke-related cases (131, 138). *TP53* mutation was also found to be significantly correlated with hepatitis B virus (HBV) infection (127, 139). Regarding patient outcome, worse overall survival of patients with mutated *TP53*, *KRAS*, and *TERT* or deleted *CDKN2A* has been reported (126).

Genomic-Transcriptomic Profiles: Molecular Classification of Intrahepatic Cholangiocarcinoma

Several multi-omics approaches have been reported in the past decade, and several molecular classifications of iCCA have been presented (Table 3).

Inflammation/Proliferation Class

Integrated gene expression and mutational analyses performed by Sia et al. revealed two classes (inflammation and proliferation) of iCCA (53). The inflammation class accounted for approximately 40% of iCCA, and it was characterized by activation of immune response-related pathways, including dendritic cell signature and cytokines such as IL-4 and IL-10. The proliferation class showed activation of several oncogenic pathways including receptor tyrosine kinase pathway genes, such as *EGF*, *RAS*, *AKT*, *MET*, and other growth factor genes. Patient outcomes were worse in the proliferation class than in the inflammation class.

Prognosis-Based Classes

Transcriptomic profiling of iCCA and perihilar CCA by Andersen et al. revealed two prognostic groups (C1 and C2) with 5-year survival rate. The group with poor prognosis (C2) indicated increased activation of *VEGF/ERBB*, *CTNNB1/MYC*, and *TNF* signaling network and *KRAS* mutation, whereas these characteristics were not seen in the group with good prognosis (C1) (140). Recently, the gene expression pattern of iCCAs with cholangiolocellular differentiation trait, having favorable prognosis, was reported to be similar to that of C1, and has a signature including upregulated expression of inflammation-related genes and downregulated expression of proliferation-related genes based on Gene Ontology terms (52, 141).

Tumor Microenvironment-Based Classes

A recent study on the classification of iCCA according to its tumor microenvironment presented four subtypes based on gene signature analysis: “immunogenic,” which shows high innate and adaptive immune cell infiltration, “myeloid-rich,” which has strong macrophage and myeloid signatures, “mesenchymal,” with strong activated fibroblast signature, and “immune-desert,” which is characterized by lowest expression of all signatures (142). The immunogenic subtype had the best outcome, whereas the mesenchymal subtype had the worst outcome, in agreement with the prognostic features of the tumor microenvironment of iCCA discussed previously.

Other Classifications

Multi-omics data from TCGA project revealed that *IDH1/2*- and *PBRM1*-mutant subgroups showed upregulation of

TABLE 3 | Notable classification of intrahepatic cholangiocarcinoma from multi-omics studies.

Base of classification	Number of cases	Molecular classification and characteristics	References
Inflammation versus proliferation signature	149	<ul style="list-style-type: none"> ● Inflammation class <ul style="list-style-type: none"> - Enriched in immune response-related pathways - Overexpression of <i>IL-4</i> and <i>IL-10</i> (Th2 marker) - Favorable prognosis ● Proliferation class <ul style="list-style-type: none"> - Enriched in oncogenic pathways including RTK and angiogenic pathways, increased expression of <i>EGF</i>, <i>RAS</i>, <i>AKT</i>, <i>MET</i>, and growth factors - Worse outcome compared to inflammation class 	Sia et al. (53)
Prognosis	104*	<ul style="list-style-type: none"> ● Cluster 1 (group with good prognosis) <ul style="list-style-type: none"> - No <i>KRAS</i> mutation - Absence or weak expression of <i>HER2</i> and <i>MET</i> ● Cluster 2 (group with poor prognosis) <ul style="list-style-type: none"> - Enriched <i>VEGF/ERBB</i>, <i>CTNNB1/MYC</i>, and TNF pathway and <i>KRAS</i> mutation 	Andersen et al. (140)
Tumor microenvironment	78	<ul style="list-style-type: none"> ● Immune desert subtype <ul style="list-style-type: none"> - Minimal expression of all TME signatures ● Immunogenic subtype <ul style="list-style-type: none"> - High innate and adaptive immune cell presence - Strong activation of fibroblasts and inflammatory and immune checkpoint pathways - Best outcome ● Myeloid-rich subtype <ul style="list-style-type: none"> - Strong monocyte-derived myeloid cell signatures - Low lymphoid signatures ● Mesenchymal subtype <ul style="list-style-type: none"> - Strong active fibroblast signatures - Worst outcome 	Job et al. (142)
TCGA project	32	<ul style="list-style-type: none"> ● <i>IDH</i>-mutant cluster <ul style="list-style-type: none"> - <i>IDH1/2</i> mutation - Enriched mitochondrial gene expression - Loss of function of <i>ARID1A</i> and <i>PBRM1</i> ● <i>CCND1</i> amplification cluster <ul style="list-style-type: none"> - Highly methylated - <i>BAP1/FGFR</i> cluster ● <i>BAP1</i> mutation or <i>FGFR2</i> fusion ● Survival difference is not significant between clusters 	Farshidfar et al. (13)
Etiologic factor-associated	69	<ul style="list-style-type: none"> ● Cluster 1 <ul style="list-style-type: none"> - Liver fluke-related - <i>ARID1A</i>, <i>BRCA1/2</i>, and <i>TP53</i> mutations - <i>ERBB2</i> amplification - CpG island hypermethylation ● Cluster 2 <ul style="list-style-type: none"> - Partly liver-fluke-related - <i>TP53</i> mutation - High expression of <i>CTNNB1</i>, <i>WNT5B</i> and <i>AKT1</i> ● Cluster 3 <ul style="list-style-type: none"> - High CNA burden - Enriched immune-related pathways ● Cluster 4 <ul style="list-style-type: none"> - Associated with viral hepatitis - <i>BAP1</i> or <i>IDH1/2</i> mutation - High expression of <i>FGFR</i> family proteins - CpG shore hypermethylation - Favorable prognosis 	Jusakul et al. (131)

*Whether only intrahepatic cholangiocarcinoma was included is not certain.

CNA, copy number aberration; HCC, hepatocellular carcinoma; IL, interleukin; RTK, receptor tyrosine kinase; TCGA-CHOL, The Cancer Genome Atlas-Cholangiocarcinoma Consortium; TME, tumor microenvironment.

mitochondrial genes and downregulation of chromatin-modifying genes such as *ARID1A* and *ARID1B* due to hypermethylation of the promoter CpG region, while cases with

FGFR2 fusion showed downregulation of mitochondrial genes (13). Furthermore, another study has proposed a classification based on the correlation of multi-omics features with etiologic

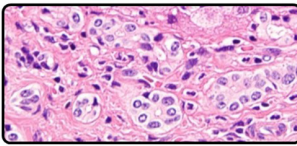
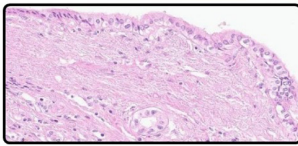
Intrahepatic Cholangiocarcinoma		
Classification	Small Duct Type	Large Duct Type
Gross Type	Mass-forming	Mixed Periductal Infiltrating
Cell of Origin		
	Canal of Hering Bile ductule	Columnar cholangiocytes Peribiliary glands
Main Etiology	Chronic hepatitis HBV / HCV Alcoholic / Metabolic	Hepatolithiasis Liver fluke PSC
Immuno-histochemistry & Mucin stain	<div> <div>NCAM N-cadherin CRP</div> <div>S100P Mucin</div> </div>	
Frequent Mutations	<i>BAP1</i> <i>IDH1/2</i> <i>FGFR2</i> fusion	<i>KRAS</i> <i>TP53</i> <i>SMAD4</i>
Suggested Molecular Classification*	<div> <div>Inflammation Class</div> <div>Proliferation Class</div> </div>	
Patient Outcome	Favorable	Poor

FIGURE 6 | Clinico-pathologic and molecular summary of intrahepatic cholangiocarcinoma (iCCA). Macro and microscopic, immunohistochemical, mutational, and clinical overview of iCCA. HBV, hepatitis B virus; HCV, hepatitis C virus; PSC, primary sclerosing cholangitis; S100P, S100 calcium-binding protein P; NCAM, neural cell adhesion molecule; CRP, c-reactive protein. *Based on the classification by Sia et al. (53).

background, showing that liver fluke-associated clusters 1 and 2, which harbor *TP53* mutation and *ERBB2* amplification in common, can be differentiated based on hypermethylated CpG island (for cluster 1). Furthermore, liver fluke-negative clusters 3 and 4 can be subdivided based on immune-related pathway enrichment (for cluster 3), and *IDH1/2* mutations, *FGFR2* fusion, and hypermethylated CpG promoter shores associated with viral hepatitis (for cluster 4) (131).

Moleculo-Pathological Correlation

The two major pathological types, small duct type and large duct type iCCA differ in their molecular characteristics. Small duct type iCCAs frequently have *BAP1*, *IDH1/2*, and *FGFR* mutations, while large duct type iCCAs more commonly show *KRAS*, *TP53*, and *SMAD4* mutations. Interestingly, iCCA with cholangiolocellular differentiation trait, which belongs to the small duct type, has been reported to be correlated with inflammation class and group with good prognosis (C1) (52, 53, 140). The pathological, clinical, and molecular characteristics of iCCA based on currently available evidence are summarized in Figure 6.

Perspectives on Targeted Therapies

Large-scale genomic analyses have identified target molecules for chemotherapy of patients with iCCA. Thus far, use of fibroblast growth factor receptor (FGFR) inhibitors and isocitrate dehydrogenase (IDH) 1 and 2 inhibitors are promising strategies against iCCA (130, 143).

Fibroblast growth factor receptor family proteins are localized on the cell membrane and transfer extracellular growth signals through intracellular tyrosine kinase domains. Pemigatinib, an oral inhibitor of FGFR1-3, has been approved by the United States Food and Drug Administration (FDA) for the treatment of patients with refractory advanced CCA with *FGFR2* fusion (130).

Isocitrate dehydrogenase 1 and 2 proteins are essential components of the tricarboxylic acid cycle, that normally generate NADPH *via* conversion of isocitrate into α -ketoglutarate. Mutant *IDH1/2* proteins accelerate this process, resulting in excess production of the byproduct, 2-hydroxyglutarate, which acts as an oncometabolite by interfering with histone and DNA methylation regulation (143). A recent phase 3 clinical trial of the *IDH1* inhibitor ivosidenib in patients

with advanced iCCA has shown promising results in increasing overall survival, and the FDA has approved its use in previously treated *IDH1*-mutated iCCA patients (143, 144).

Even though there is hope for these approved target agents, application is limited to those who harbor specific mutations, and antitumor efficacy is limited by intratumoral heterogeneity and drug resistance. Other targeted protein inhibitor molecules are in active clinical trials, including other inhibitors of FGFR family; multi-kinase inhibitors that act on epidermal growth factor receptor, vascular endothelial growth factor receptor and platelet-derived growth factor receptor; specific tyrosine kinase inhibitors targeting HER2, BRAF inhibitors, and immune checkpoint inhibitors (145, 146). To detect a variety of potential actionable mutations, the European Society for Medical Oncology has recommended routine use of NGS in patients with advanced cholangiocarcinoma (147).

CONCLUSION

Intrahepatic cholangiocarcinoma is a very heterogeneous malignancy with respect to histomorphology and molecular perspectives. The tumor microenvironment of iCCA also varies significantly depending on the type of immune cell infiltration and tumor stromal characteristics. Histopathological classification of small duct and large duct types shows differences

in etiology, molecular features, and clinical outcomes. Analyses of NGS and multi-omics studies have suggested molecular classifications of iCCA and identified *FGFR2* fusion and *IDH1/2* mutations as indications for targeted drugs. Further studies are needed for better pathological-molecular correlation and marker development for targeted therapy as well as immunotherapy to improve the treatment efficacy of patients with iCCA.

AUTHOR CONTRIBUTIONS

TC and YP contributed to the conception and design of this manuscript. TC performed the literature search, data analysis, and wrote the first draft of the manuscript. YP critically revised the manuscript. Both authors approved the submitted version.

FUNDING

This work was supported by the Basic Science Research Program through the National Research Foundation of Korea (NRF) (NRF-2020R1A2B5B01001646), and by the Bio and Medical Technology Development Program of the NRF funded by the Ministry of Science and ICT (MSIT) (NRF-2017M3A9B6061512 and NRF-2016M3A9D5A01952416).

REFERENCES

- Nagorney DM, Pawlik TM, Chun YS, Ebata T, Vauthey J-N. Perihilar bile ducts. 8th ed. In: Edge SB, American Joint Committee on Cancer editors. *AJCC Cancer Staging Manual*. New York, NY: Springer (2017).
- Massarweh NN, El-Serag HB. Epidemiology of Hepatocellular carcinoma and intrahepatic cholangiocarcinoma. *Cancer Control*. (2017) 24:1073274817729245. doi: 10.1177/1073274817729245
- Nakanuma Y, Klimstra DS, Komuta M, Zen Y. Intrahepatic cholangiocarcinoma. 5th ed. In: WHO Classification of Tumours Editorial Board editor. *Digestive System Tumours*. Lyon: International Agency for Research on Cancer (2019).
- Florio AA, Ferlay J, Znaor A, Ruggieri D, Alvarez CS, Laversanne M, et al. Global incidence of and trends in intrahepatic and extrahepatic cholangiocarcinoma from 1993 to 2012. *Cancer*. (2020) 126:2666–78. doi: 10.1002/cncr.32803
- Khan SA, Tavoroli S, Brandi G. Cholangiocarcinoma: epidemiology and risk factors. *Liver Int*. (2019) 39:19–31. doi: 10.1111/liv.14095
- Jeong Y-I, Shin H-E, Lee S-E, Cheun H-I, Ju J-W, Kim J-Y, et al. Prevalence of *Clonorchis sinensis* Infection among residents along 5 major rivers in the republic of Korea. *Korean J Parasitol*. (2016) 54:215–9. doi: 10.3347/kjp.2016.54.2.215
- Kitphati R, Watanawong O, Wongsaroj T, Nithikathkul C. National program of opisthorchiasis in Thailand; situation and policy strategy. *Int J Geoinf*. (2021) 17:61–8. doi: 10.52939/ijg.v17i2.1759
- Banales JM, Marin JJG, Lamarca A, Rodrigues PM, Khan SA, Roberts LR, et al. Cholangiocarcinoma 2020: the next horizon in mechanisms and management. *Nat Rev Gastroenterol Hepatol*. (2020) 17:557–88. doi: 10.1038/s41575-020-0310-z
- Buettner S, van Vugt JL, Jn JJ, Groot Koerkamp B. Intrahepatic cholangiocarcinoma: current perspectives. *OncoTargets Ther*. (2017) 10:1131–42. doi: 10.2147/ott.S93629
- Yu T-H, Chen X, Zhang X-H, Zhang E-C, Sun C-X. Clinicopathological characteristics and prognostic factors for intrahepatic cholangiocarcinoma: a population-based study. *Sci Rep*. (2021) 11:3990. doi: 10.1038/s41598-021-83149-5
- Lee Y-T, Wang JJ, Luu M, Nouredin M, Nissen NN, Patel TC, et al. Comparison of clinical features and outcomes between intrahepatic cholangiocarcinoma and hepatocellular carcinoma in the United States. *Hepatology*. (2021) 74:2622–32. doi: 10.1002/hep.32007
- Hayashi A, Misumi K, Shibahara J, Arita J, Sakamoto Y, Hasegawa K, et al. Distinct clinicopathologic and genetic features of 2 histologic subtypes of intrahepatic cholangiocarcinoma. *Am J Surg Pathol*. (2016) 40:1021–30. doi: 10.1097/pas.0000000000000670
- Farshidfar F, Zheng S, Gingras MC, Newton Y, Shih J, Robertson AG, et al. Integrative genomic analysis of cholangiocarcinoma identifies distinct IDH-mutant molecular profiles. *Cell Rep*. (2017) 18:2780–94. doi: 10.1016/j.celrep.2017.02.033
- Cerami E, Gao J, Dogrusoz U, Gross BE, Sumer SO, Aksoy BA, et al. The cBio cancer genomics portal: an open platform for exploring multidimensional cancer genomics data. *J Cancer Discov*. (2012) 2:401–4. doi: 10.1158/2159-8290.CD-12-0095
- Yamasaki S. Intrahepatic cholangiocarcinoma: macroscopic type and stage classification. *J Hepatobiliary Pancreat Surg*. (2003) 10:288–91. doi: 10.1007/s00534-002-0732-8
- Nakanuma Y, Miyata T, Uchida T. Latest advances in the pathological understanding of cholangiocarcinomas. *Expert Rev Gastroenterol Hepatol*. (2016) 10:113–27. doi: 10.1586/17474124.2016.1104246
- Chung T, Rhee H, Nahm JH, Jeon Y, Yoo JE, Kim Y-J, et al. Clinicopathological characteristics of intrahepatic cholangiocarcinoma according to gross morphologic type: cholangiolocellular differentiation traits and inflammation- and proliferation-phenotypes. *HPB*. (2020) 22:864–73. doi: 10.1016/j.hpb.2019.10.009
- Kim Y, Lee K, Jeong S, Wen X, Cho NY, Kang GH. DLEC1 methylation is associated with a better clinical outcome in patients with intrahepatic cholangiocarcinoma of the small duct subtype. *Virchows Arch*. (2019) 475:49–58. doi: 10.1007/s00428-018-02511-7
- Sigel CS, Dril E, Zhou Y, Basturk O, Askan G, Pak LM, et al. Intrahepatic cholangiocarcinomas have histologically and immunophenotypically distinct

- small and large duct patterns. *Am J Surg Pathol.* (2018) 42:1334–45. doi: 10.1097/pas.0000000000001118
20. Aishima S, Oda Y. Pathogenesis and classification of intrahepatic cholangiocarcinoma: different characters of perihilar large duct type versus peripheral small duct type. *J Hepatobiliary Pancreat Sci.* (2015) 22:94–100. doi: 10.1002/jhbp.154
 21. Akita M, Sofue K, Fujikura K, Otani K, Itoh T, Ajiki T, et al. Histological and molecular characterization of intrahepatic bile duct cancers suggests an expanded definition of perihilar cholangiocarcinoma. *HPB (Oxford).* (2019) 21:226–34. doi: 10.1016/j.hpb.2018.07.021
 22. Komuta M, Govaere O, Vandecaveye V, Akiba J, Van Steenberghe W, Verslype C, et al. Histological diversity in cholangiocellular carcinoma reflects the different cholangiocyte phenotypes. *Hepatology.* (2012) 55:1876–88. doi: 10.1002/hep.25595
 23. Theise ND, Saxena R, Portmann BC, Thung SN, Yee H, Chiriboga L, et al. The canals of Hering and hepatic stem cells in humans. *Hepatology.* (1999) 30:1425–33. doi: 10.1002/hep.510300614
 24. Guest RV, Boulter L, Kendall TJ, Minnis-Lyons SE, Walker R, Wigmore SJ, et al. Cell lineage tracing reveals a biliary origin of intrahepatic cholangiocarcinoma. *J Cancer Res.* (2014) 74:1005–10. doi: 10.1158/0008-5472.CAN-13-1911
 25. Moeini A, Haber PK, Sia D. Cell of origin in biliary tract cancers and clinical implications. *JHEP Rep.* (2021) 3:100226. doi: 10.1016/j.jhepr.2021.100226
 26. Tsai JH, Huang WC, Kuo KT, Yuan RH, Chen YL, Jeng YM. S100P immunostaining identifies a subset of peripheral-type intrahepatic cholangiocarcinomas with morphological and molecular features similar to those of perihilar and extrahepatic cholangiocarcinomas. *Histopathology.* (2012) 61:1106–16. doi: 10.1111/j.1365-2559.2012.04316.x
 27. Aishima S, Kuroda Y, Nishihara Y, Taguchi K, Taketomi A, Maehara Y, et al. Gastric mucin phenotype defines tumour progression and prognosis of intrahepatic cholangiocarcinoma: gastric foveolar type is associated with aggressive tumour behaviour. *Histopathology.* (2006) 49:35–44. doi: 10.1111/j.1365-2559.2006.02414.x
 28. Yu TH, Yuan RH, Chen YL, Yang WC, Hsu HC, Jeng YM. Viral hepatitis is associated with intrahepatic cholangiocarcinoma with cholangiolar differentiation and N-cadherin expression. *Mod Pathol.* (2011) 24:810–9. doi: 10.1038/modpathol.2011.41
 29. Kozaka K, Sasaki M, Fujii T, Harada K, Zen Y, Sato Y, et al. A subgroup of intrahepatic cholangiocarcinoma with an infiltrating replacement growth pattern and a resemblance to reactive proliferating bile ductules: 'bile ductular carcinoma'. *Histopathology.* (2007) 51:390–400. doi: 10.1111/j.1365-2559.2007.02735.x
 30. Akita M, Sawada R, Komatsu M, Suleman N, Itoh T, Ajiki T, et al. An immunostaining panel of C-reactive protein, N-cadherin, and S100 calcium binding protein P is useful for intrahepatic cholangiocarcinoma subtyping. *Hum Pathol.* (2021) 109:45–52. doi: 10.1016/j.humpath.2020.12.005
 31. Vijgen S, Terris B, Rubbia-Brandt L. Pathology of intrahepatic cholangiocarcinoma. *Hepatobiliary Surg Nutr.* (2017) 6:22–34. doi: 10.21037/hbsn.2016.11.04
 32. Park JH, Kim JH. Pathologic differential diagnosis of metastatic carcinoma in the liver. *Clin Mol Hepatol.* (2019) 25:12–20. doi: 10.3350/cmh.2018.0067
 33. Misumi K, Hayashi A, Shibahara J, Arita J, Sakamoto Y, Hasegawa K, et al. Intrahepatic cholangiocarcinoma frequently shows loss of BAP1 and PBRM1 expression, and demonstrates specific clinicopathological and genetic characteristics with BAP1 loss. *Histopathology.* (2017) 70:766–74. doi: 10.1111/his.13127
 34. Jeon Y, Kwon SM, Rhee H, Yoo JE, Chung T, Woo HG, et al. Molecular and radiopathologic spectrum between HCC and intrahepatic cholangiocarcinoma. *Hepatology* (2022). doi: 10.1002/hep.32397. [Epub ahead of print].
 35. Yoon JG, Kim MH, Jang M, Kim H, Hwang HK, Kang CM, et al. Molecular characterization of biliary tract cancer predicts chemotherapy and PD-1/PD-L1 blockade responses. *Hepatology.* (2021) 74:1914–31. doi: 10.1002/hep.31862
 36. Choi W-T, Ramachandran R, Kakar S. Immunohistochemical approach for the diagnosis of a liver mass on small biopsy specimens. *Hum Pathol.* (2017) 63:1–13. doi: 10.1016/j.humpath.2016.12.025
 37. Werling RW, Yaziji H, Bacchi CE, Gown AM. CDX2, a highly sensitive and specific marker of adenocarcinomas of intestinal origin: an immunohistochemical survey of 476 primary and metastatic carcinomas. *Am J Surg Pathol.* (2003) 27:303–10. doi: 10.1097/00000478-200303000-00003
 38. Stenhouse G, Fyfe N, King G, Chapman A, Kerr KM. Thyroid transcription factor 1 in pulmonary adenocarcinoma. *J Clin Pathol.* (2004) 57:383–7. doi: 10.1136/jcp.2003.007138
 39. Surrey LF, Frank R, Zhang PJ, Furth EE. TTF-1 and Napsin-A are expressed in a subset of cholangiocarcinomas arising from the gallbladder and hepatic ducts: continued caveats for utilization of immunohistochemistry panels. *Am J Surg Pathol.* (2014) 38:224–7. doi: 10.1097/pas.0000000000000138
 40. Selves J, Long-Mira E, Mathieu M-C, Rochaix P, Ilié M. Immunohistochemistry for diagnosis of metastatic carcinomas of unknown primary site. *Cancers (Basel).* (2018) 10:108. doi: 10.3390/cancers10040108
 41. Miettinen M, McCue PA, Sarlomo-Rikala M, Rys J, Czapiewski P, Wazny K, et al. GATA3: a multispecific but potentially useful marker in surgical pathology: a systematic analysis of 2500 epithelial and nonepithelial tumors. *Am J Surg Pathol.* (2014) 38:13–22. doi: 10.1097/PAS.0b013e3182a0218f
 42. Varma M, Morgan M, Jasani B, Tamboli P, Amin MB. Polyclonal anti-PSA is more sensitive but less specific than monoclonal anti-PSA: implications for diagnostic prostatic pathology. *Am J Clin Pathol.* (2002) 118:202–7. doi: 10.1309/BGWQ-P26T-7TR6-VGT3
 43. Guedj N, Zhan Q, Perigny M, Rautou PE, Degos F, Belghiti J, et al. Comparative protein expression profiles of hilar and peripheral hepatic cholangiocarcinomas. *J Hepatol.* (2009) 51:93–101. doi: 10.1016/j.jhep.2009.03.017
 44. Shahid M, Mubeen A, Tse J, Kakar S, Bateman AC, Borger D, et al. Branched chain in situ hybridization for albumin as a marker of hepatocellular differentiation: evaluation of manual and automated in situ hybridization platforms. *Am J Surg Pathol.* (2015) 39:25–34. doi: 10.1097/PAS.0000000000000343
 45. Ferrone CR, Ting DT, Shahid M, Konstantinidis IT, Sabbatino F, Goyal L, et al. The ability to diagnose intrahepatic cholangiocarcinoma definitively using novel branched DNA-enhanced albumin RNA in situ hybridization technology. *Ann Surg Oncol.* (2016) 23:290–6. doi: 10.1245/s10434-014-4247-8
 46. Collins K, Newcomb PH, Cartun RW, Ligato S. Utility and limitations of albumin mRNA in situ hybridization detection in the diagnosis of hepatobiliary lesions and metastatic carcinoma to the liver. *Appl Immunohistochem Mol Morphol.* (2021) 29:180–7. doi: 10.1097/pai.0000000000000885
 47. Banales JM, Huebert RC, Karlsen T, Strazzabosco M, LaRusso NF, Gores GJ. Cholangiocyte pathobiology. *Nat Rev Gastroenterol Hepatol.* (2019) 16:269–81. doi: 10.1038/s41575-019-0125-y
 48. Steiner PE, Higginson J. Cholangiolocellular carcinoma of the liver. *Cancer.* (1959) 12:753–9. doi: 10.1002/1097-0142(195907/08)12:4<753::aid-cnrcr2820120420>3.0.co;2-1
 49. Komuta M, Spee B, Vander Borgh T, De Vos R, Verslype C, Aerts R, et al. Clinicopathological study on cholangiolocellular carcinoma suggesting hepatic progenitor cell origin. *Hepatology.* (2008) 47:1544–56. doi: 10.1002/hep.22238
 50. Moeini A, Sia D, Zhang Z, Camprecios G, Stueck A, Dong H, et al. Mixed hepatocellular cholangiocarcinoma tumors: cholangiolocellular carcinoma is a distinct molecular entity. *J Hepatol.* (2017) 66:952–61. doi: 10.1016/j.jhep.2017.01.010
 51. Liao JY, Tsai JH, Yuan RH, Chang CN, Lee HJ, Jeng YM. Morphological subclassification of intrahepatic cholangiocarcinoma: etiological, clinicopathological, and molecular features. *Mod Pathol.* (2014) 27:1163–73. doi: 10.1038/modpathol.2013.241
 52. Rhee H, Ko JE, Chung T, Jee BA, Kwon SM, Nahm JH, et al. Transcriptomic and histopathological analysis of cholangiolocellular differentiation trait in intrahepatic cholangiocarcinoma. *Liver Int.* (2018) 38:113–24. doi: 10.1111/liv.13492
 53. Sia D, Hoshida Y, Villanueva A, Roayaie S, Ferrer J, Tabak B, et al. Integrative molecular analysis of intrahepatic cholangiocarcinoma reveals 2 classes that have different outcomes. *Gastroenterology.* (2013) 144:829–40. doi: 10.1053/j.gastro.2013.01.001

54. Chung T, Rhee H, Shim HS, Yoo JE, Choi GH, Kim H, et al. Genetic, clinicopathological, and radiological features of intrahepatic cholangiocarcinoma with ductal plate malformation pattern. *Gut Liver*. (2021). doi: 10.5009/gnl210174
55. Nakanuma Y, Sato Y, Ikeda H, Harada K, Kobayashi M, Sano K, et al. Intrahepatic cholangiocarcinoma with predominant “ductal plate malformation” pattern: a new subtype. *Am J Surg Pathol*. (2012) 36:1629–35. doi: 10.1097/PAS.0b013e31826e0249
56. Sasaki M, Sato Y, Nakanuma Y. Cholangiolocellular carcinoma with “ductal plate malformation” pattern may be characterized by ARID1A genetic alterations. *Am J Surg Pathol*. (2019) 43:352–60. doi: 10.1097/pas.0000000000001201
57. Gou Q, Fu S, Xie Y, Zhang M, Shen Y. Treatment and survival patterns of primary adenocarcinoma of the liver: a retrospective analysis. *Front Oncol*. (2021) 11:621594. doi: 10.3389/fonc.2021.621594
58. Nakanuma Y, Sato Y, Harada K, Sasaki M, Xu J, Ikeda H. Pathological classification of intrahepatic cholangiocarcinoma based on a new concept. *World J Hepatol*. (2010) 2:419–27. doi: 10.4254/wjh.v2.i12.419
59. Chi Z, Bhalla A, Saeed O, Cheng L, Curless K, Wang HL, et al. Mucinous intrahepatic cholangiocarcinoma: a distinct variant. *Hum Pathol*. (2018) 78:131–7. doi: 10.1016/j.humpath.2018.04.010
60. Sumiyoshi T, Shima Y, Okabayashi T, Ishikawa A, Matsumoto M, Iwata J, et al. Mucinous cholangiocarcinoma: clinicopathological features of the rarest type of cholangiocarcinoma. *Ann Gastroenterol Surg*. (2017) 1:114–21. doi: 10.1002/ags3.12016
61. Haas S, Gütgemann I, Wolff M, Fischer HP. Intrahepatic clear cell cholangiocarcinoma: immunohistochemical aspects in a very rare type of cholangiocarcinoma. *Am J Surg Pathol*. (2007) 31:902–6. doi: 10.1097/PAS.0b013e31802c0c8a
62. Yamamoto T, Abe T, Oshita A, Yonehara S, Katamura Y, Matsumoto N, et al. Intrahepatic cholangiocarcinoma with clear cell type following laparoscopic curative surgery. *Surg Case Rep*. (2020) 6:264. doi: 10.1186/s40792-020-01041-2
63. Guo XQ, Li B, Li Y, Tian XY, Li Z. Unusual mucoepidermoid carcinoma of the liver misdiagnosed as squamous cell carcinoma by intraoperative histological examination. *Diagn Pathol*. (2014) 9:24. doi: 10.1186/1746-1596-9-24
64. Arakawa Y, Shimada M, Ikegami T, Kubo T, Imura S, Morine Y, et al. Mucoepidermoid carcinoma of the liver: report of a rare case and review of the literature. *Hepatol Res*. (2008) 38:736–42. doi: 10.1111/j.1872-034X.2008.00335.x
65. Tsai J-H, Liao J-Y, Lee C-H, Jeng Y-M. Lymphoepithelioma-like intrahepatic cholangiocarcinoma is a distinct entity with frequent pTERT/TP53 mutations and comprises 2 subgroups based on epstein-barr virus infection. *Am J Surg Pathol*. (2021) 45:1409–18. doi: 10.1097/PAS.0000000000001716
66. Khandakar B, Liu J-R, Thung S, Li Y, Rhee H, Kagen AC, et al. Lymphoepithelioma-like neoplasm of the biliary tract with ‘probable low malignant potential’. *Histopathology*. (2022) 80:720–8. doi: 10.1111/his.14580
67. Malhotra S, Wood J, Mansy T, Singh R, Zaitoun A, Madhusudan S. Intrahepatic sarcomatoid cholangiocarcinoma. *J Oncol*. (2010) 2010:701476. doi: 10.1155/2010/701476
68. Matsukuma KE, Yeh MM. Update on the pathology of liver neoplasms. *Ann Diagn Pathol*. (2019) 38:126–37. doi: 10.1016/j.anndiagpath.2018.10.005
69. Geramizadeh B. Precursor lesions of cholangiocarcinoma: a clinicopathologic review. *Clin Pathol*. (2020) 13:2632010X20925045. doi: 10.1177/2632010X20925045
70. WHO Classification of Tumours Editorial Board. *Digestive System Tumours*. 5th ed. Lyon: International Agency for Research on Cancer (2019).
71. Nakanishi Y, Zen Y, Kondo S, Itoh T, Itatsu K, Nakanuma Y. Expression of cell cycle-related molecules in biliary premalignant lesions: biliary intraepithelial neoplasia and biliary intraductal papillary neoplasm. *Hum Pathol*. (2008) 39:1153–61. doi: 10.1016/j.humpath.2007.11.018
72. Ettel M, Eze O, Xu R. Clinical and biological significance of precursor lesions of intrahepatic cholangiocarcinoma. *World J Hepatol*. (2015) 7:2563–70. doi: 10.4254/wjh.v7.i25.2563
73. Hsu M, Sasaki M, Igarashi S, Sato Y, Nakanuma Y. KRAS and GNAS mutations and p53 overexpression in biliary intraepithelial neoplasia and intrahepatic cholangiocarcinomas. *Cancer*. (2013) 119:1669–74. doi: 10.1002/cncr.27955
74. Aishima S, Fujita N, Mano Y, Kubo Y, Tanaka Y, Taketomi A, et al. Different roles of S100P overexpression in intrahepatic cholangiocarcinoma: carcinogenesis of perihilar type and aggressive behavior of peripheral type. *Am J Surg Pathol*. (2011) 35:590–8. doi: 10.1097/PAS.0b013e31820ffdf1
75. Nakanuma Y, Kakuda Y, Uesaka K, Miyata T, Yamamoto Y, Fukumura Y, et al. Characterization of intraductal papillary neoplasm of bile duct with respect to histopathologic similarities to pancreatic intraductal papillary mucinous neoplasm. *Hum Pathol*. (2016) 51:103–13. doi: 10.1016/j.humpath.2015.12.022
76. Rocha FG, Lee H, Katabi N, DeMatteo RP, Fong Y, D’Angelica MI, et al. Intraductal papillary neoplasm of the bile duct: a biliary equivalent to intraductal papillary mucinous neoplasm of the pancreas? *Hepatology*. (2012) 56:1352–60. doi: 10.1002/hep.25786
77. Kim KM, Lee JK, Shin JU, Lee KH, Lee KT, Sung J-Y, et al. Clinicopathologic features of intraductal papillary neoplasm of the bile duct according to histologic subtype. *Am J Gastroenterol*. (2012) 107:118–25. doi: 10.1038/ajg.2011.316
78. Schlitter AM, Born D, Bettstetter M, Specht K, Kim-Fuchs C, Riener M-O, et al. Intraductal papillary neoplasms of the bile duct: stepwise progression to carcinoma involves common molecular pathways. *Mod Pathol*. (2014) 27:73–86. doi: 10.1038/modpathol.2013.112
79. Nakanuma Y, Uesaka K, Kakuda Y, Sugino T, Kubota K, Furukawa T, et al. Intraductal papillary neoplasm of bile duct: updated clinicopathological characteristics and molecular and genetic alterations. *J Clin Med*. (2020) 9:3991. doi: 10.3390/jcm9123991
80. Nakanuma Y, Uesaka K, Okamura Y, Terada T, Fukumura Y, Kakuda Y, et al. Reappraisal of pathological features of intraductal papillary neoplasm of bile duct with respect to the type 1 and 2 subclassifications. *Hum Pathol*. (2021) 111:21–35. doi: 10.1016/j.humpath.2021.01.002
81. Yang CY, Huang WJ, Tsai JH, Cheng A, Chen CC, Hsu HP, et al. Targeted next-generation sequencing identifies distinct clinicopathologic and molecular entities of intraductal papillary neoplasms of the bile duct. *Mod Pathol*. (2019) 32:1637–45. doi: 10.1038/s41379-019-0306-9
82. Aoki Y, Mizuma M, Hata T, Aoki T, Omori Y, Ono Y, et al. Intraductal papillary neoplasms of the bile duct consist of two distinct types specifically associated with clinicopathological features and molecular phenotypes. *J Pathol*. (2020) 251:38–48. doi: 10.1002/path.5398
83. Schlitter AM, Jang K-T, Klöppel G, Saka B, Hong S-M, Choi H, et al. Intraductal tubulopapillary neoplasms of the bile ducts: clinicopathologic, immunohistochemical, and molecular analysis of 20 cases. *Mod Pathol*. (2015) 28:1249–64. doi: 10.1038/modpathol.2015.61
84. Goepfert B, Stichel D, Toth R, Fritzsche S, Loeffler MA, Schlitter AM, et al. Integrative analysis reveals early and distinct genetic and epigenetic changes in intraductal papillary and tubulopapillary cholangiocarcinogenesis. *Gut*. (2022) 71:391–401. doi: 10.1136/gutjnl-2020-322983
85. Fabris L, Sato K, Alpini G, Strazzabosco M. The tumor microenvironment in cholangiocarcinoma progression. *Hepatology*. (2021) 73:75–85. doi: 10.1002/hep.31410
86. Jing C-Y, Fu Y-P, Huang J-L, Zhang M-X, Yi Y, Gan W, et al. Prognostic nomogram based on histological characteristics of fibrotic tumor stroma in patients who underwent curative resection for intrahepatic cholangiocarcinoma. *Oncologist*. (2018) 23:1482–93. doi: 10.1634/theoncologist.2017-0439
87. Kajiyama K, Maeda T, Takenaka K, Sugimachi K, Tsuneyoshi M. The significance of stromal desmoplasia in intrahepatic cholangiocarcinoma: a special reference of ‘scirrhous-type’ and ‘non-scirrhous-type’. *Growth*. (1999) 23:892. doi: 10.1097/0000478-199908000-00006
88. Zhang X-F, Dong M, Pan Y-H, Chen J-N, Huang X-Q, Jin Y, et al. Expression pattern of cancer-associated fibroblast and its clinical relevance in intrahepatic cholangiocarcinoma. *Hum Pathol*. (2017) 65:92–100. doi: 10.1016/j.humpath.2017.04.014
89. Kojima S, Hisaka T, Midorikawa R, Naito Y, Akiba J, Tanigawa M, et al. Prognostic impact of desmoplastic reaction evaluation for intrahepatic cholangiocarcinoma. *Anticancer Res*. (2020) 40:4749–54. doi: 10.21873/anticancer.14476
90. De Jaeghere EA, Denys HG, De Wever O. Fibroblasts fuel immune escape in the tumor microenvironment. *Trends Cancer*. (2019) 5:704–23. doi: 10.1016/j.trecan.2019.09.009

91. Okabe H, Beppu T, Hayashi H, Ishiko T, Masuda T, Otao R, et al. Hepatic stellate cells accelerate the malignant behavior of cholangiocarcinoma cells. *Ann Surg Oncol.* (2011) 18:1175–84. doi: 10.1245/s10434-010-1391-7
92. Clapéron A, Mergey M, Aoudjehane L, Ho-Bouldoires THN, Wendum D, Prignon A, et al. Hepatic myofibroblasts promote the progression of human cholangiocarcinoma through activation of epidermal growth factor receptor. *Hepatology.* (2013) 58:2001–11. doi: 10.1002/hep.26585
93. Fingas CD, Bronk SF, Werneburg NW, Mott JL, Guicciardi ME, Cazanave SC, et al. Myofibroblast-derived PDGF-BB promotes hedgehog survival signaling in cholangiocarcinoma cells. *Hepatology.* (2011) 54:2076–88. doi: 10.1002/hep.24588
94. Chuaysri C, Thuwajit P, Paupairoj A, Chau-In S, Suthiphongchai T, Thuwajit C. Alpha-smooth muscle actin-positive fibroblasts promote biliary cell proliferation and correlate with poor survival in cholangiocarcinoma. *Oncol Rep.* (2009) 21:957–69. doi: 10.3892/or_00000309
95. Shan Z, Ju C. Hepatic macrophages in liver injury. *Front Immunol.* (2020) 11:322. doi: 10.3389/fimmu.2020.00322
96. Sato K, Hall C, Glaser S, Francis H, Meng F, Alpini G. Pathogenesis of Kupffer cells in cholestatic liver injury. *Am J Pathol.* (2016) 186:2238–47. doi: 10.1016/j.ajpath.2016.06.003
97. Yuan H, Lin Z, Liu Y, Jiang Y, Liu K, Tu M, et al. Intrahepatic cholangiocarcinoma induced M2-polarized tumor-associated macrophages facilitate tumor growth and invasiveness. *Cancer Cell Int.* (2020) 20:586. doi: 10.1186/s12935-020-01687-w
98. Høgdall D, Lewinska M, Andersen JB. Desmoplastic tumor microenvironment and immunotherapy in cholangiocarcinoma. *Trends Cancer.* (2018) 4:239–55. doi: 10.1016/j.trecan.2018.01.007
99. Hasita H, Komohara Y, Okabe H, Masuda T, Ohnishi K, Lei XF, et al. Significance of alternatively activated macrophages in patients with intrahepatic cholangiocarcinoma. *Cancer Sci.* (2010) 101:1913–9. doi: 10.1111/j.1349-7006.2010.01614.x
100. Kasper HU, Drebbler U, Stippel DL, Dienes HP, Gillissen A. Liver tumor infiltrating lymphocytes: comparison of hepatocellular and cholangiocarcinoma. *World J Gastroenterol.* (2009) 15:5053–7. doi: 10.3748/wjg.15.5053
101. Goepfert B, Frauenschuh L, Zucknick M, Stenzinger A, Andrusis M, Klauschen F, et al. Prognostic impact of tumour-infiltrating immune cells on biliary tract cancer. *Br J Cancer.* (2013) 109:2665–74. doi: 10.1038/bjc.2013.610
102. Yugawa K, Itoh S, Yoshizumi T, Iseda N, Tomiyama T, Toshima T, et al. Prognostic impact of tumor microvessels in intrahepatic cholangiocarcinoma: association with tumor-infiltrating lymphocytes. *Mod Pathol.* (2021) 34:798–807. doi: 10.1038/s41379-020-00702-9
103. Kim H-D, Kim JH, Ryu Y-M, Kim D, Lee S, Shin J, et al. Spatial distribution and prognostic implications of tumor-infiltrating FoxP3⁺ CD4⁺ T cells in biliary tract cancer. *Cancer Res Treat.* (2021) 53:162–71. doi: 10.4143/crt.2020.704
104. Ghidini M, Cascione L, Carotenuto P, Lampis A, Trevisani F, Previdi MC, et al. Characterisation of the immune-related transcriptome in resected biliary tract cancers. *Eur J Cancer.* (2017) 86:158–65. doi: 10.1016/j.ejca.2017.09.005
105. Fontugne J, Augustin J, Pujals A, Compagnon P, Rousseau B, Luciani A, et al. PD-L1 expression in perihilar and intrahepatic cholangiocarcinoma. *Oncotarget.* (2017) 8:24644–51. doi: 10.18632/oncotarget.15602
106. Wu H, Wei Y, Jian M, Lu H, Song Q, Hao L, et al. Clinicopathological and prognostic significance of immunoscore and PD-L1 in intrahepatic cholangiocarcinoma. *OncoTargets Ther.* (2021) 14:39–51. doi: 10.2147/ott.S288982
107. Sabbatino F, Villani V, Yearley JH, Deshpande V, Cai L, Konstantinidis IT, et al. PD-L1 and HLA class I antigen expression and clinical course of the disease in intrahepatic cholangiocarcinoma. *J Clin Cancer Res.* (2016) 22:470–8. doi: 10.1158/1078-0432.CCR-15-0715
108. Rizzo A, Ricci AD, Brandi G. PD-L1, TMB, MSI, and other predictors of response to immune checkpoint inhibitors in biliary tract cancer. *Cancers (Basel).* (2021) 13:558. doi: 10.3390/cancers13030558
109. Wardell CP, Fujita M, Yamada T, Simbolo M, Fassan M, Karlic R, et al. Genomic characterization of biliary tract cancers identifies driver genes and predisposing mutations. *J Hepatol.* (2018) 68:959–69. doi: 10.1016/j.jhep.2018.01.009
110. Terashima T, Umamoto K, Takahashi H, Hosoi H, Takai E, Kondo S, et al. Germline mutations in cancer-predisposition genes in patients with biliary tract cancer. *Oncotarget.* (2019) 10:5949–57. doi: 10.18632/oncotarget.27224
111. Maynard H, Stadler ZK, Berger MF, Solit DB, Ly M, Lowery MA, et al. Germline alterations in patients with biliary tract cancers: a spectrum of significant and previously underappreciated findings. *Cancer.* (2020) 126:1995–2002. doi: 10.1002/cncr.32740
112. Golan T, Raitses-Gurevich M, Kelley RK, Bocobo AG, Borgida A, Shroff RT, et al. Overall survival and clinical characteristics of BRCA-associated cholangiocarcinoma: a multicenter retrospective study. *Oncologist.* (2017) 22:804–10. doi: 10.1634/theoncologist.2016-0415
113. Brandi G, Deserti M, Palloni A, Turchetti D, Zuntini R, Pedica F, et al. Intrahepatic cholangiocarcinoma development in a patient with a novel BAP1 germline mutation and low exposure to asbestos. *Cancer Genet.* (2020) 24:57–62. doi: 10.1016/j.cancergen.2020.10.001
114. Kiba T, Tsuda H, Hirohashi S, Inoue S, Sugimura T, Pairojkul C. Mutations of the p53 tumor suppressor gene and the ras gene family in intrahepatic cholangiocellular carcinomas in Japan and Thailand. *Mol Carcinog.* (1993) 8:312–8. doi: 10.1002/mc.2940080415
115. Ross JS, Wang K, Gay L, Al-Rohil R, Rand JV, Jones DM, et al. New routes to targeted therapy of intrahepatic cholangiocarcinomas revealed by next-generation sequencing. *Oncologist.* (2014) 19:235–42. doi: 10.1634/theoncologist.2013-0352
116. Chaisaingmongkol J, Budhu A, Dang H, Rabibhadana S, Pupacdi B, Kwon SM, et al. Common molecular subtypes among asian hepatocellular carcinoma and cholangiocarcinoma. *Cancer Cell.* (2017) 32:57–70.e3. doi: 10.1016/j.ccell.2017.05.009
117. Simbolo M, Fassan M, Ruzzenente A, Mafficini A, Wood LD, Corbo V, et al. Multigene mutational profiling of cholangiocarcinomas identifies actionable molecular subgroups. *Oncotarget.* (2014) 5:2839–52. doi: 10.18632/oncotarget.1943
118. Churi CR, Shroff R, Wang Y, Rashid A, Kang HC, Weatherly J, et al. Mutation profiling in cholangiocarcinoma: prognostic and therapeutic implications. *PLoS One.* (2014) 9:e115383. doi: 10.1371/journal.pone.0115383
119. Jiao Y, Pawlik TM, Anders RA, Selaru FM, Streppel MM, Lucas DJ, et al. Exome sequencing identifies frequent inactivating mutations in BAP1, ARID1A and PBRM1 in intrahepatic cholangiocarcinomas. *Nat Genet.* (2013) 45:1470–3. doi: 10.1038/ng.2813
120. Nakamura H, Arai Y, Totoki Y, Shirota T, Elzawahry A, Kato M, et al. Genomic spectra of biliary tract cancer. *Nat Genet.* (2015) 47:1003–10. doi: 10.1038/ng.3375
121. Fujimoto A, Furuta M, Shiraishi Y, Gotoh K, Kawakami Y, Arihiro K, et al. Whole-genome mutational landscape of liver cancers displaying biliary phenotype reveals hepatitis impact and molecular diversity. *Nat Commun.* (2015) 6:6120. doi: 10.1038/ncomms7120
122. Wang T, Drill E, Vakiani E, Pak LM, Boerner T, Askan G, et al. Distinct histomorphological features are associated with IDH1 mutation in intrahepatic cholangiocarcinoma. *Hum Pathol.* (2019) 91:19–25. doi: 10.1016/j.humpath.2019.05.002
123. Jolissaint JS, Soares KC, Seier KP, Kundra R, Gönen M, Shin PJ, et al. Intrahepatic cholangiocarcinoma with lymph node metastasis: treatment-related outcomes and the role of tumor genomics in patient selection. *Clin Cancer Res.* (2021) 27:4101–8. doi: 10.1158/1078-0432.CCR-21-0412
124. Kipp BR, Voss JS, Kerr SE, Barr Fritcher EG, Graham RP, Zhang L, et al. Isocitrate dehydrogenase 1 and 2 mutations in cholangiocarcinoma. *Hum Pathol.* (2012) 43:1552–8. doi: 10.1016/j.humpath.2011.12.007
125. Zhu AX, Borger DR, Kim Y, Cosgrove D, Ejaz A, Alexandrescu S, et al. Genomic profiling of intrahepatic cholangiocarcinoma: refining prognosis and identifying therapeutic targets. *Ann Surg Oncol.* (2014) 21:3827–34. doi: 10.1245/s10434-014-3828-x
126. Boerner T, Drill E, Pak LM, Nguyen B, Sigel CS, Doussot A, et al. Genetic determinants of outcome in intrahepatic cholangiocarcinoma. *Hepatology.* (2021) 74:1429–44. doi: 10.1002/hep.31829
127. Nepal C, O'Rourke CJ, Oliveira DVNP, Taranta A, Shema S, Gautam P, et al. Genomic perturbations reveal distinct regulatory networks in intrahepatic

- cholangiocarcinoma. *Hepatology*. (2018) 68:949–63. doi: 10.1002/hep.29764
128. Lowery MA, Ptashkin R, Jordan E, Berger MF, Zehir A, Capanu M, et al. Comprehensive molecular profiling of intrahepatic and extrahepatic cholangiocarcinomas: potential targets for intervention. *Clin Cancer Res*. (2018) 24:4154–61. doi: 10.1158/1078-0432.CCR-18-0078
 129. Borad MJ, Champion MD, Egan JB, Liang WS, Fonseca R, Bryce AH, et al. Integrated genomic characterization reveals novel, therapeutically relevant drug targets in FGFR and EGFR pathways in sporadic intrahepatic cholangiocarcinoma. *PLoS Genet*. (2014) 10:e1004135. doi: 10.1371/journal.pgen.1004135
 130. Goyal L, Kongpetch S, Crolley VE, Bridgewater J. Targeting FGFR inhibition in cholangiocarcinoma. *Cancer Treat Rev*. (2021) 95:102170. doi: 10.1016/j.ctrv.2021.102170
 131. Jusakul A, Cutcutache I, Yong CH, Lim JQ, Huang MN, Padmanabhan N, et al. Whole-genome and epigenomic landscapes of etiologically distinct subtypes of cholangiocarcinoma. *Cancer Discov*. (2017) 7:1116–35. doi: 10.1158/2159-8290.CD-17-0368
 132. Winkelmann R, Schneider M, Hartmann S, Schnitzbauer AA, Zeuzem S, Peveling-Oberhag J, et al. Microsatellite instability occurs rarely in patients with cholangiocarcinoma: a retrospective study from a German tertiary care hospital. *Int J Mol Sci*. (2018) 19:1421. doi: 10.3390/ijms19051421
 133. Goepfert B, Roessler S, Renner M, Singer S, Mehrabi A, Vogel MN, et al. Mismatch repair deficiency is a rare but putative therapeutically relevant finding in non-liver fluke associated cholangiocarcinoma. *Br J Cancer*. (2019) 120:109–14. doi: 10.1038/s41416-018-0199-2
 134. Li K, Luo H, Huang L, Luo H, Zhu X. Microsatellite instability: a review of what the oncologist should know. *Cancer Cell Int*. (2020) 20:16. doi: 10.1186/s12935-019-1091-8
 135. Ohashi K, Nakajima Y, Kanehiro H, Tsutsumi M, Taki J, Aomatsu Y, et al. Ki-ras mutations and p53 protein expressions in intrahepatic cholangiocarcinomas: relation to gross tumor morphology. *Gastroenterology*. (1995) 109:1612–7. doi: 10.1016/0016-5085(95)90650-9
 136. Goepfert B, Toth R, Singer S, Albrecht T, Lipka DB, Lutsik P, et al. Integrative analysis defines distinct prognostic subgroups of intrahepatic cholangiocarcinoma. *Hepatology*. (2019) 69:2091–106. doi: 10.1002/hep.30493
 137. Ma B, Meng H, Tian Y, Wang Y, Song T, Zhang T, et al. Distinct clinical and prognostic implication of IDH1/2 mutation and other most frequent mutations in large duct and small duct subtypes of intrahepatic cholangiocarcinoma. *BMC Cancer*. (2020) 20:318. doi: 10.1186/s12885-020-06804-6
 138. Chan-on W, Nairismägi M-L, Ong CK, Lim WK, Dima S, Pairojkul C, et al. Exome sequencing identifies distinct mutational patterns in liver fluke-related and non-infection-related bile duct cancers. *Nat Genet*. (2013) 45:1474–8. doi: 10.1038/ng.2806
 139. Zou S, Li J, Zhou H, Frech C, Jiang X, Chu JSC, et al. Mutational landscape of intrahepatic cholangiocarcinoma. *Nat Commun*. (2014) 5:5696. doi: 10.1038/ncomms6696
 140. Andersen JB, Spee B, Blechacz BR, Avital I, Komuta M, Barbour A, et al. Genomic and genetic characterization of cholangiocarcinoma identifies therapeutic targets for tyrosine kinase inhibitors. *Gastroenterology*. (2012) 142:1021–31.e15. doi: 10.1053/j.gastro.2011.12.005
 141. Ashburner M, Ball CA, Blake JA, Botstein D, Butler H, Cherry JM, et al. Gene ontology: tool for the unification of biology. *Nat Genet*. (2000) 25:25–9. doi: 10.1038/75556
 142. Job S, Rapoud D, Dos Santos A, Gonzalez P, Desterke C, Pascal G, et al. Identification of four immune subtypes characterized by distinct composition and functions of tumor microenvironment in intrahepatic cholangiocarcinoma. *Hepatology*. (2020) 72:965–81. doi: 10.1002/hep.31092
 143. Rizzo A, Ricci AD, Brandi G. IDH inhibitors in advanced cholangiocarcinoma: another arrow in the quiver? *Cancer Treat Res Commun*. (2021) 27:100356. doi: 10.1016/j.ctarc.2021.100356
 144. Zhu AX, Macarulla T, Javle MM, Kelley RK, Lubner SJ, Adeva J, et al. Final overall survival efficacy results of Ivosidenib for patients with advanced cholangiocarcinoma with IDH1 mutation: the phase 3 randomized clinical ClarIDHy trial. *JAMA Oncol*. (2021) 7:1669–77. doi: 10.1001/jamaoncol.2021.3836
 145. Acher AW, Paro A, Elfadaly A, Tsilimigras D, Pawlik TM. Intrahepatic cholangiocarcinoma: a summative review of biomarkers and targeted therapies. *Cancers (Basel)*. (2021) 13:5169. doi: 10.3390/cancers13205169
 146. Mondaca S, Razavi P, Xu C, Offin M, Myers M, Scaltriti M, et al. Genomic characterization of ERBB2-driven biliary cancer and a case of response to Ado-Trastuzumab Emtansine. *JCO Precis Oncol*. (2019) 3:1–9. doi: 10.1200/po.19.00223
 147. Mosele F, Remon J, Mateo J, Westphalen CB, Barlesi F, Lolkema MP, et al. Recommendations for the use of next-generation sequencing (NGS) for patients with metastatic cancers: a report from the ESMO precision medicine working group. *Ann Oncol*. (2020) 31:1491–505. doi: 10.1016/j.annonc.2020.07.014

Conflict of Interest: The authors declare that the research was conducted in the absence of any commercial or financial relationships that could be construed as a potential conflict of interest.

Publisher's Note: All claims expressed in this article are solely those of the authors and do not necessarily represent those of their affiliated organizations, or those of the publisher, the editors and the reviewers. Any product that may be evaluated in this article, or claim that may be made by its manufacturer, is not guaranteed or endorsed by the publisher.

Copyright © 2022 Chung and Park. This is an open-access article distributed under the terms of the Creative Commons Attribution License (CC BY). The use, distribution or reproduction in other forums is permitted, provided the original author(s) and the copyright owner(s) are credited and that the original publication in this journal is cited, in accordance with accepted academic practice. No use, distribution or reproduction is permitted which does not comply with these terms.



Senescence-Associated Molecules and Tumor-Immune-Interactions as Prognostic Biomarkers in Colorectal Cancer

Franziska Kellers¹, Aurélie Fernandez¹, Björn Konukiewitz², Mario Schindeldecker¹, Katrin E. Tagscherer¹, Achim Heintz³, Moritz Jesinghaus⁴, Wilfried Roth¹ and Sebastian Foersch^{1*}

¹ Institute of Pathology, University Medical Center Mainz, Mainz, Germany, ² Institute of Pathology, Christian-Albrecht University of Kiel, Kiel, Germany, ³ Department of General, Visceral and Vascular Surgery, Catholic Hospital Mainz, Mainz, Germany, ⁴ Department of Pathology, University Hospital Marburg, Marburg, Germany

OPEN ACCESS

Edited by:

Arndt Hartmann,
Universitätsklinikum
Erlangen, Germany

Reviewed by:

Lucia Bongiovanni,
San Raffaele Hospital (IRCCS), Italy
Antonio Palumbo Jr,
Federal University of Rio de
Janeiro, Brazil

*Correspondence:

Sebastian Foersch
sebastian.foersch@
unimedizin-mainz.de

Specialty section:

This article was submitted to
Pathology,
a section of the journal
Frontiers in Medicine

Received: 29 January 2022

Accepted: 08 March 2022

Published: 12 April 2022

Citation:

Kellers F, Fernandez A, Konukiewitz B,
Schindeldecker M, Tagscherer KE,
Heintz A, Jesinghaus M, Roth W and
Foersch S (2022)
Senescence-Associated Molecules
and Tumor-Immune-Interactions as
Prognostic Biomarkers in Colorectal
Cancer. *Front. Med.* 9:865230.
doi: 10.3389/fmed.2022.865230

Background and Aims: The initiation of cellular senescence in response to protumorigenic stimuli counteracts malignant progression in (pre)malignant cells. Besides arresting proliferation, cells entering this terminal differentiation state adopt a characteristic senescence-associated secretory phenotype (SASP) which initiates alterations to their microenvironment and effects immunosurveillance of tumorous lesions. However, some effects mediated by senescent cells contribute to disease progression. Currently, the exploration of senescent cells' impact on the tumor microenvironment and the evaluation of senescence as possible target in colorectal cancer (CRC) therapy demand reliable detection of cellular senescence *in vivo*. Therefore, specific immunohistochemical biomarkers are required. Our aim is to analyze the clinical implications of senescence detection in colorectal carcinoma and to investigate the interactions of senescent tumor cells and their immune microenvironment *in vitro* and *in vivo*.

Methods: Senescence was induced in CRC cell lines by low-dose-etoposide treatment and confirmed by Senescence-associated β -galactosidase (SA- β -GAL) staining and fluorescence activated cell sorting (FACS) analysis. Co-cultures of senescent cells and immune cells were established. Multiple cell viability assays, electron microscopy and live cell imaging were conducted. Immunohistochemical (IHC) markers of senescence and immune cell subtypes were studied in a cohort of CRC patients by analyzing a tissue micro array (TMA) and performing digital image analysis. Results were compared to disease-specific survival (DSS) and progression-free survival (PFS).

Results: Varying expression of senescence markers in tumor cells was associated with in- or decreased survival of CRC patients. Proximity analysis of p21-positive senescent tumor cells and cytotoxic T cells revealed a significantly better prognosis for patients

in which these cell types have the possibility to directly interact. *In vitro*, NK-92 cells (mimicking natural killer T cells) or TALL-104 cells (mimicking both cytotoxic T cells and natural killer T cells) led to dose-dependent specific cytotoxicity in >75 % of the senescent CRC cells but <20 % of the proliferating control CRC cells. This immune cell-mediated senolysis seems to be facilitated via direct cell-cell contact inducing apoptosis and granule exocytosis.

Conclusion: Counteracting tumorigenesis, cellular senescence is of significant relevance in CRC. We show the dual role of senescence bearing both beneficial and malignancy-promoting potential *in vivo*. Absence as well as exceeding expression of senescence markers are associated with bad prognosis in CRC. The antitumorigenic potential of senescence induction is determined by tumor microenvironment and immune cell-mediated elimination of senescent cells.

Keywords: cellular senescence, colorectal cancer, senescence-associated secretory phenotype (SASP), prognostic biomarker, senolysis

INTRODUCTION

Malignant neoplasia of colon and rectum are associated with high morbidity and mortality and account for 10 % of cancer cases and 9.4 % of cancer deaths (1). Molecular mechanisms of colorectal carcinogenesis are increasingly understood, yet the role of cellular senescence and its contribution to survival and treatment outcome of cancer patients remain unclear.

One mechanism in tumor biology that only recently started to gain more attention due to its role in carcinogenesis is cellular senescence. Cellular senescence describes a permanent cell cycle arrest following potentially protumorigenic DNA-damaging incidents in premalignant cells, thereby counteracting malignant progression (2). There is a multitude of trigger mechanisms leading to the initiation of cellular senescence. Eroded telomeres which occur after repetitive cell divisions (3) or cumulative DNA erosions due to sublethal stressful conditions such as oxidative stress (4), proliferative stress due to oncogene-induced mitogenic hyperstimulation (5–7), loss of tumor suppressors (8, 9) or the presence of DNA damaging agents can induce a DNA damage response, arresting the cell cycle of impaired cells (10). Anticancer treatment such as chemotherapeutic agents, ionizing radiation (11–15) as well as targeted therapies are capable of evoking cellular senescence (16–21). Therapy-induced senescence (TIS) has been observed in tumor cells both *in vitro* and *in vivo* (15). Apart from ceasing proliferation, senescent transformation involves characteristic morphological and metabolic changes (22). *In vitro*, senescent cells adopt a characteristic flat, enlarged “fried egg” morphology as well as nuclear alterations (23–26). Increased lysosomal activity, detected by visualization of the lysosomal enzyme Senescence-associated β -galactosidase (SA- β -GAL) at pH 6, is a widely established biomarker of senescent cells (27). While detection of SA- β -GAL may be used for identification of cellular senescence in fresh or frozen cells (28, 29), the enzyme activity-dependent assay cannot be carried out on formalin-fixed, paraffin-embedded (FFPE) tissues (29) and therefore this distinctive feature may not be used to study cellular senescence

in vivo to a large extent. Due to the irreversible proliferation arrest, the senescent state is strongly associated with an absence of proliferation markers such as Ki-67 and the expression of anti-proliferative proteins (30). The onset of the senescence program involves cell cycle suppressors such as p53, p21, and p16 (22). The extent to which these features are displayed may vary (23) and none of these characteristics are exclusively linked to cellular senescence. Consequently only a combination of markers allows for distinctive identification of senescent cells (31). Recently, there have been approaches to identify novel markers of senescence (32, 33).

Although no longer proliferating, senescent cells remain highly metabolically active and display an altered secretory and signaling activity. Apart from autocrine enforcement of the senescent state, senescent cells induce non-cell-autonomous effects via direct cell-cell contact with nearby cells, paracrine signaling, and secretion of a multitude of factors affecting angiogenesis and immune surveillance of the tissue environment. The SASP, adopted by arrested cells in the presence of DNA impairment, consists of a distinct composition of secreted molecules involving signaling factors like inflammatory cytokines, enzymes and extracellular matrix components (34). The SASP highly depends on the cell type (34) and enables senescent cells to attract immune cells such as macrophages, NK cells and T cells to the site of a tumorous lesion, activating them to specifically eliminate senescent cells and thus promoting the immunosurveillance of the tumor (35, 36). While some senescent cells remain in the tissue for years (29, 37, 38) and eventually contribute to age-related diseases (39, 40), there are settings where the SASP signaling activates an immediate immune response, resulting in the installation of a proinflammatory microenvironment and eventually the removal of the senescent cells (41, 42), termed “senolysis.” This immune cell driven clearance of senescent cells involves the innate (41, 42) as well as the adaptive immune cells (43, 44). There is evidence that senescent cells under senescence surveillance are eliminated by macrophages (45) or NK cell-mediated induction of granule exocytosis (46, 47).

Cellular senescence has been linked to colorectal carcinogenesis (40). The silencing of the senescence-regulating cell cycle suppressors p16 and p53 typically involved in cellular senescence induction (22) is a crucial step to overcome cellular senescence in colorectal carcinogenesis (48, 49). There is first evidence that measurement of cellular senescence might be a predictive parameter in CRC patients (50) but the clinical implications of the contribution of cellular senescence to colorectal carcinogenesis have not yet been studied in a large patient cohort. Since TIS occurs during various CRC therapies, the influence of this biomechanism on disease progression in CRC needs to be investigated in a clinical setting. Furthermore, it might be a promising approach in colorectal cancer therapy to use the potential of the senescence-induced immunosurveillance to counteract malignant progression (51). Evaluating the impact of cellular senescence and the potential of therapy-induced senescence in CRC demands reliable detection methods and biomarkers applicable to FFPE tissue to explore this key mechanism in colorectal carcinogenesis *in vivo*. We further explored the potential of senescence-associated molecules as prognostic and predictive biomarkers in CRC and conducted both *in vitro* and *in vivo* studies to gain a better understanding of the functional role of the interaction between senescent colorectal tumor cells and the immune system.

MATERIALS AND METHODS

Material

A list of antibodies and inhibitors used in this study can be found in **Supplementary Table 1**.

CRC Cell Culture

After preliminary experiments with various CRC cell lines, Caco-2 cells were cultivated in MEM (+15 % fetal bovine serum + 1 % pyruvate, 1 % NEAA, 1 % glutamine, 1 % penicillin, 1 % streptomycin) at 37°C and 5% CO₂ on 12-well-plates. Senescence was induced by low dose (5 μ M) Etoposide treatment. 24 h after seeding, the growth medium was replaced by medium containing 5 μ M Etoposide. Cells treated with equal volumes of Dimethyl Sulfoxide (DMSO) were used as negative control. After 48 h the medium was replaced by growth medium, and cells were allowed to recover. Analyses were performed after 72 h.

Cytoblocks of Etoposide-treated and control cells were generated after harvesting using Accutase (Sigma Aldrich) treatment, formalin (Sigma Aldrich) fixation and embedding in 1 % Agarose. For following analyses, samples were transferred to paraffin and standard sectioning (2 μ m) and subsequent staining was performed according to standard protocols used for routine pathology or as published previously (52). Furthermore, transmission electron microscopy (TEM) was performed according to protocols established for routine diagnostics at our institute (53).

Immune and CRC Cell Culture

NK-92 cells were cultivated in α -MEM + 12.5% fetal bovine serum + 12.5% horse serum + 1% penicillin + 1% streptomycin + 100–200 U/ml IL-2 (48 h) / 5 ng/ml IL-2 (every 48 h) at 37°C

and 5% CO₂. TALL-104 cells were cultivated in Iscove's Modified Dulbecco's Medium (ATCC) + 20% fetal bovine serum, 2.5 μ g /ml human albumin, 0.5 μ g/ml D-manitol + 50–100 U/ml recombinant human IL-2 (48 h) at 37°C and 5% CO₂. For co-culture experiments, Caco-2 cells were cultivated on 6-well-plates and senescence was induced as according to 3.1. After 72 h of recovery, the growth medium was replaced by immune cell growth medium containing immune cells in different target-to-effector ratios. Cells were co-cultivated for up to 180 min. Following 120 min of co-incubation, cells were washed, and non-adherent cells (immune cells and non-vital Caco-2 cells) were removed. The quantity of remaining adherent Caco-2 cells after Co-culture was measured using cell viability assays such as crystal violet (CRV) staining of the remaining adherent cells.

Senescence and Cell Viability Assays

Cellular senescence was detected by SA- β -Gal staining using the Senescence β -Galactosidase Staining kit according to the manufacturer's instructions (Cell Signaling). In addition, cells were subjected to FACS analysis using the cellular senescence live cell analysis assay (Enzo) and a Becton Dickinson FACScalibur cytometer and Cell Quest Software (BD Bioscience). For viability analysis, Caco-2 cells were treated as described. At the indicated times, cells were washed with PBS, fixed with methanol:ethanol (2:1) and stained with 0.1 % crystal violet for 30 min. The plates were washed in running tap water and air dried for 24 h. Crystal violet was solubilized using 33 % acetic acid for 30 min. The absorbance was measured at 600 nm using a microplate reader (Tecan).

Live Cell Imaging

Immune cells were added to Etoposide-treated Caco-2 cells as described above. Cells were incubated at 32°C for 180 min. Cell-cell interactions were observed using a Jenoptik GRYPHAX SUBRA camera system in 100 x magnification. Pictures of representative areas were taken with a 30 s interval.

Patient Cohort

The patient cohort consisted of up to 598 patients diagnosed with primary colorectal carcinoma at the Institute of Pathology of the University Medical Center, Mainz. These patients had not received neoadjuvant treatment prior to their surgery and were treated according to national and WHO guidelines in place at the time. Patients with a hereditary cancer syndrome or history of inflammatory bowel disease were not included in this study. Retrospective use of these and other patients' data as well as material for research purposes was approved by the ethical committee of the medical association of the State of Rhineland-Palatinate [ref. no. 837.075.16 (10394)]. All experiments were in accordance with the Declaration of Helsinki. Characteristics of the patients can be found in **Supplementary Table 2**.

Human Tissue Analyses

From each patient, FFPE tissue samples containing tissue of the primary tumor and non-cancerous tissue were obtained from routine procession of the surgery specimens. Clinical data such as age, DSS, PFS, localization and stage of the tumor

were obtained. Representative areas of tumor center, invasive margin and non-cancerous epithelium were identified by review of hematoxylin and eosin (H&E)-stained sections from each sample and cores of 1 mm in diameter were obtained using the TMArrayer (Pathology Devices, San Diego, USA) and included in the TMA. From each patient, 3 samples containing representative areas of the primary tumor were included. TMA sections were stained for various senescence-associated molecules and other cell types. Staining of the slides was carried out using an automated staining system (Agilent Technologies) and its respective reagents. IHC-stained TMA sections were digitalised using a Hamamatsu Nanozoomer Series scanner (Hamamatsu Photonics, Hamamatsu, Japan) at 20 x magnification. Slides were thoroughly annotated by a pathology expert, thereby cancerous epithelium and stroma were marked. Digital image analysis was performed using HALO (Indica Labs, Albuquerque, USA). A random forest classifier was trained to discern (cancerous) epithelium and stroma. The percentage of positive cells within the classified tumor cells was obtained. Consecutive sequential TMA sections were co-registered for additional comprehensive morphometric analyses such as distance-measurements.

Statistical Analyses

Statistical analyses were carried out using GraphPad Prism version 9. Cell viability data was compared with the control group using *t*-test or ordinary one-way ANOVA. Dunnett T3 test (statistical hypothesis testing) was used to correct for multiple testing. For each marker, the values' distribution was analyzed, and cutoff values were chosen to represent meaningful biological groups, while at the same time finding optimal cutoff values. This was done similar to the method proposed by Budczies et al. where "[t]he optimal cutoff is defined as the point with the most significant (log-rank test) split." These authors have implemented their approach as open source software named the Charité Cutoff Finder (54). Additionally, we also applied the surv_cutpoint capability of the R survminer package which functions in a similar fashion (54). Cutoff values can be found in **Supplementary Table 3**. Survival analyses were performed using Kaplan-Meier-plots, differences in survival were calculated by performing log-rank Mantel-Cox test.

RESULTS

Low dose Etoposide treatment induces senescence-related morphological changes and SA- β -Gal activity. Morphological changes commonly found in senescent cells such as enlarged size and vacuolation could be detected in cells treated with Etoposide using white light microscopy and electron microscopy (**Figure 1A**). Increased SA- β -GAL activity was observed in 71.9 % of Etoposide-treated Caco-2 cells but only 1.1 % of control cells ($p < 0.0001$) (**Figure 1B**). Senescence induced by Etoposide treatment was also confirmed by FACS analysis (**Figure 1C**).

To assess the prognostic potential of senescence-associated molecules suggested by previous studies (32, 33) in a clinical setting, we evaluated various markers in our cohort of CRC patients immunohistochemically (**Figure 2A**) and observed mixed effects. For NTAL, ARMCX3, p21, and EBP50 the

percentage of positive tumor cells showed a statistically significant prognostic effect. High expression of NTAL was linked to a better DSS and PFS (**Supplementary Figure 1**). A high expression of p21 was linked to a higher PFS (**Supplementary Figure 1**), underlining the important role of p21-mediated senescence in tumor defense. Evaluating expression of ARMCX3 and EBP50 (**Supplementary Figure 1**), we found that a high expression was associated with a decreased DSS compared to the group of patients with lower expression levels. This surprising finding led us to try a three-tier cutoff system into excessive, moderate, and low expression (**Figures 2B–F**, cutoffs on the right and in **Supplementary Table 3**). Interestingly, for all markers (including gH2AX), using this approach showed that moderate expression was associated with the best prognosis, while both low and excessive expression showed a worse prognosis. This was statistically significant for NTAL, ARMCX3, and EBP50 (**Figures 2B–E**, **Supplementary Figure 1**). Taken together, this highlights the dual role of cellular senescence, with both low and excessive expression of senescence-associated markers showing worse DSS and PFS.

In search of an explanation for this plurivalent effect we hypothesized that the negative prognosis in patients with large numbers of senescent cells might result from a defective interaction between senescent cells and the tumor microenvironment. The excessive numbers of senescent cells in patients with a negative prognosis might reflect accumulation of these cells within the tumor tissue due to an ineffective tumor immunosurveillance and a failure of the immune system to clear of senescent cells. To investigate the immunosurveillance of senescent cells in our clinical cohort and analyse immune cells targeting senescent cells, we visualized the spatial relationship of senescent cells and cytotoxic T cell as stained by CD8 (**Figure 3A**). Using digital image analysis, consecutive sections with cores of one patient stained for different molecules were co-registered and corresponding tissue areas on the different sections were identified. The average distance between these two cell populations as well as the percentage of CD8-positive cells within 100 μ m of p21-positive cells were determined (**Figure 3C**). To identify a possible impact on survival, proximity data was correlated with DSS and PFS. Interestingly, both a lower average distance between these two cell populations as well as a higher percentage of CD8-positive cells within 100 μ m of p21-positive cells were linked to a significantly increased DSS and PFS (**Figures 3B,D**). This suggests that a closer immunosurveillance of the lesion improves the prognosis of CRC patients.

To explore the senescence-induced immunosurveillance of colonic cancer cells in depth, we conducted a series of co-culture experiments. After 2 h of co-incubation, the number of adherent senescent Caco-2 cells decreased depending on the ratio of immune cells that was added. Addition of NK-92 (displaying properties of natural killer cells) or TALL-104 cells (displaying properties of both cytotoxic T cells and NKT cells) to Caco-2 cells lead to dose-dependent detaching of adherent Caco-2 cells and cell death in >75 % of senescent cells but <20 % of proliferating control cells which was confirmed by CRV staining. This dose-dependent cytotoxicity was not

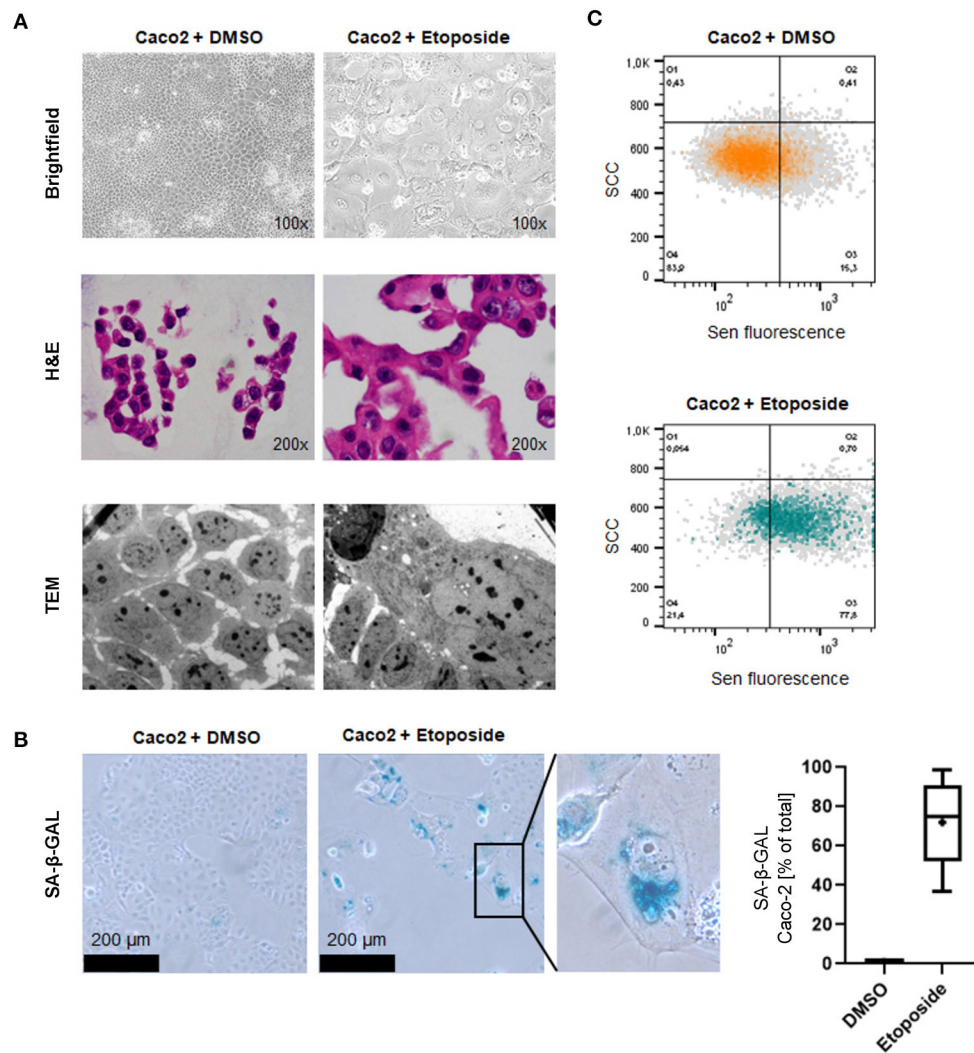


FIGURE 1 | Induction of cellular senescence *in vitro* by Etoposide treatment. **(A)** Morphological appearance of Etoposide (Eto)-treated and control (DMSO) Caco2 cells using brightfield microscopy (upper panel), normal H&E-stained sections of cytoblocks (middle panel) and TEM (lower panel). Senescent cells adopt a characteristic “fried egg” morphology, including an enlarged shape and nucleus. Cytoplasmic vacuolation is apparent. **(B)** Increased senescence SA-β-GAL staining indicates senescence induction. SA-β-GAL-positive cells were counted after DMSO and Etoposide-treatment. **(C)** FACS analysis confirms senescence induction in Etoposide-treated cells.

observed in the control group of proliferating cells that had not been exposed to Etoposide (**Figures 4A,B**). To discern whether this specific elimination of senescent cells was facilitated via factors secreted into the growth medium by the immune cells, we incubated senescent Caco-2 cells with immune cell supernatant. Importantly, addition of conditioned supernatant of TALL-104 or NK-92 cells to Etoposide-pre-treated Caco-2 cells did not decrease cell viability measured by CRV absorption (**Figures 4C,D**). To confirm the hypothesis that direct cell-cell contact with immune cells accounts for the cell death of senescent Caco-2 cells and to visualize this interaction, we conducted electron microscopy and live cell imaging during co-incubation. Live cell imaging proves directed movement of immune cells toward senescent cells followed by detaching of senescent cells.

Non-senescent cells in the environment of senescent cells were not eliminated by the immune cells to the same extent. Electron microscopy of the co-culture experiments shows direct cell-cell contact between TALL-104 cells and senescent Caco-2 cells (**Figures 4E,F, Supplementary Video 1**).

To determine how immune cells execute the elimination of senescent cells, a set of co-culture experiments was conducted under inhibition of different pathways of cell death. By adding inhibitors of apoptosis, granule exocytosis and necroptosis, the relevance of those pathways for immune cell-mediated elimination was determined. ZVAD has been demonstrated to decrease death receptor mediated cell death in senescent cells (46). Previous studies had not found an impact of caspase-dependent apoptosis on NK cell-mediated senolysis (46).

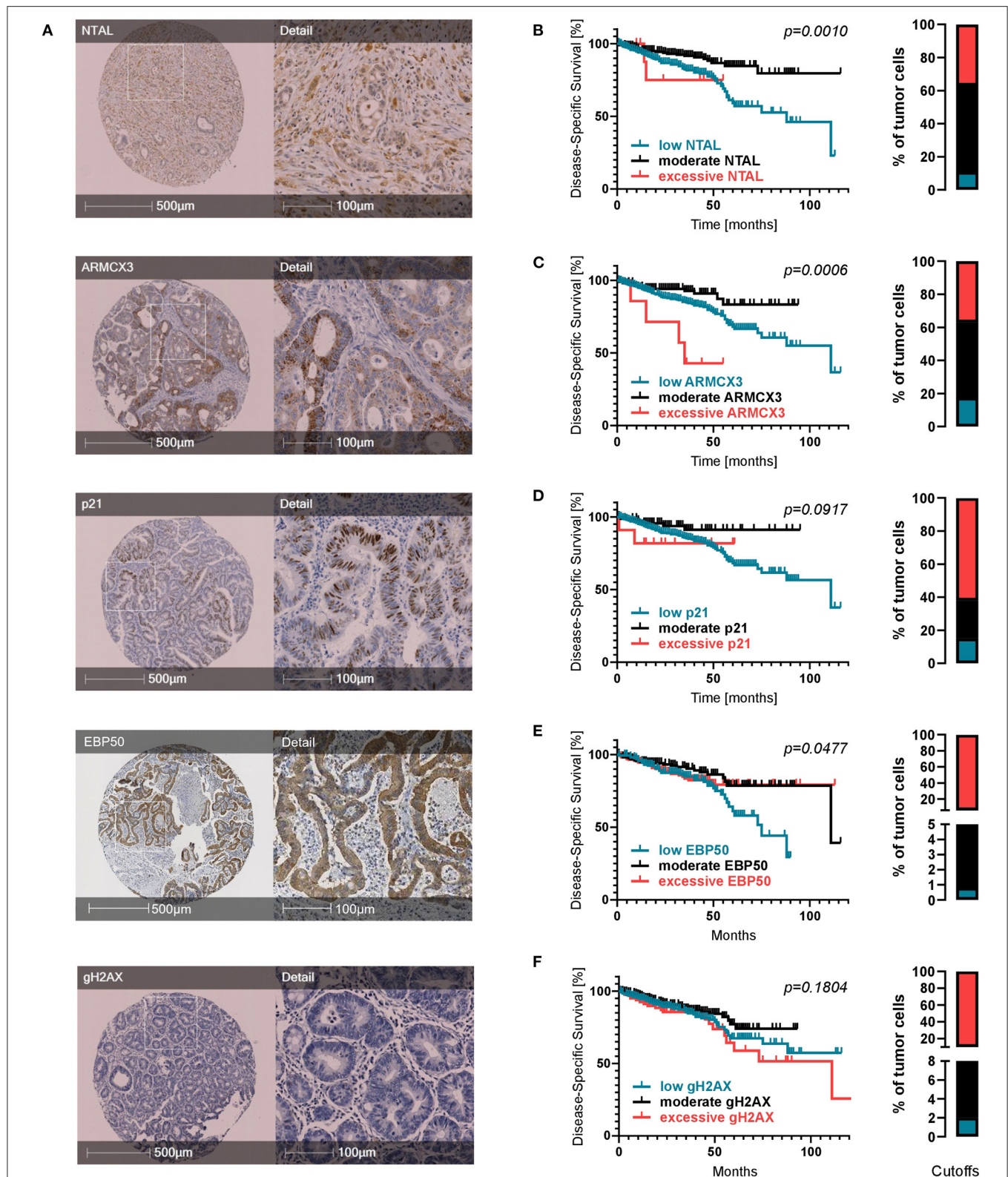
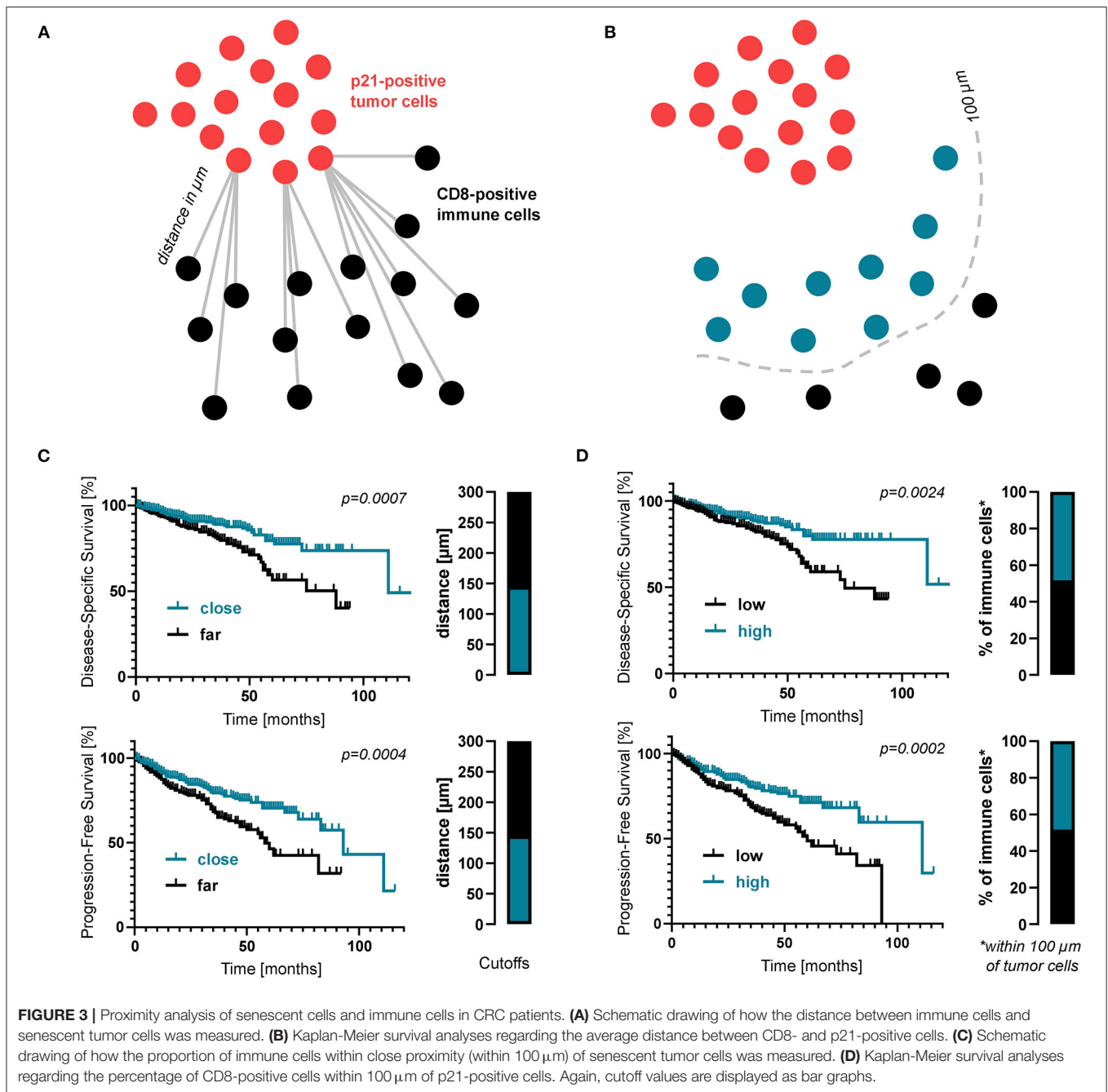
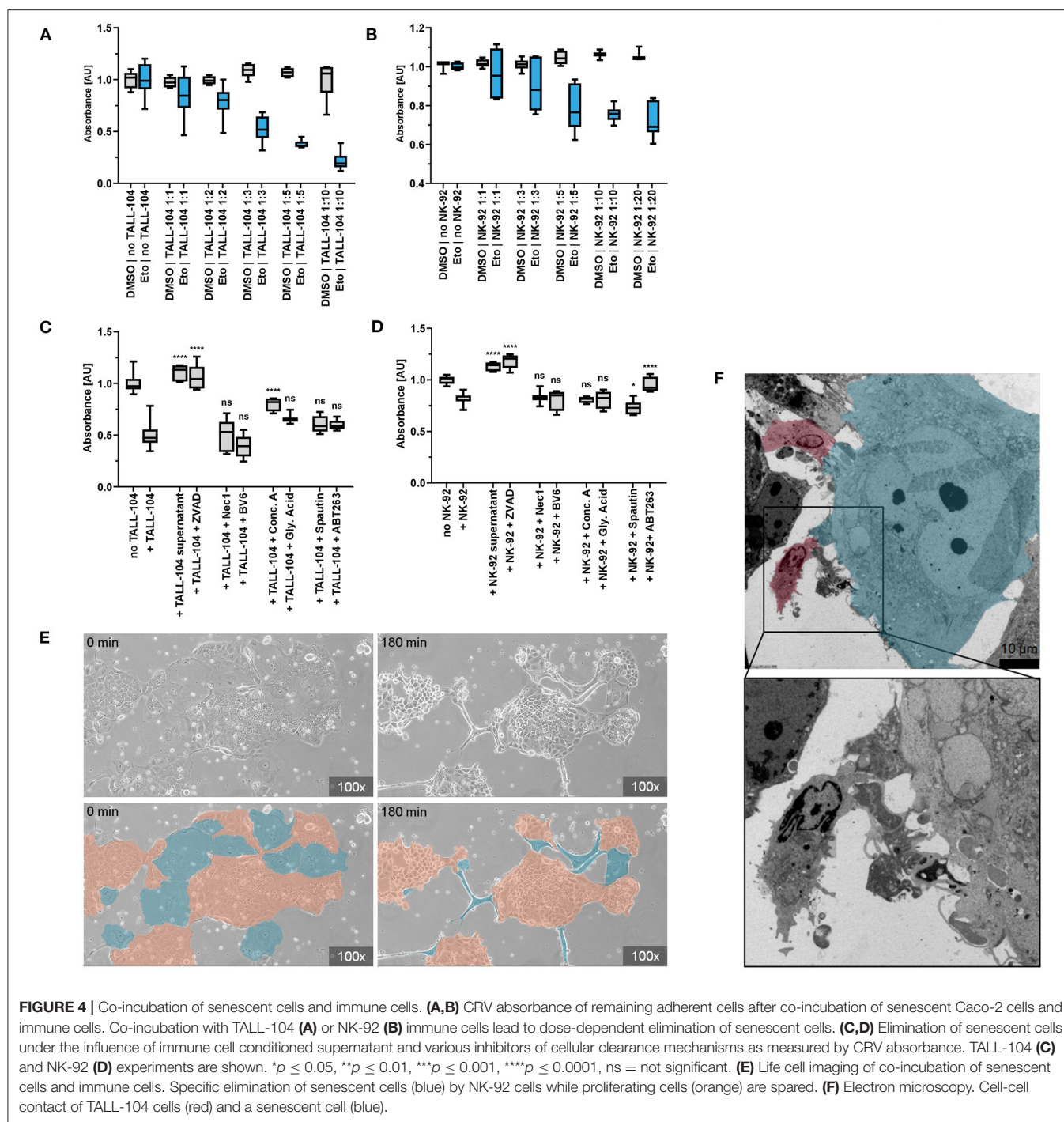


FIGURE 2 | Expression of senescence-associated molecules in CRC patients. **(A)** Representative TMA cores for each IHC marker. **(B–F)** Kaplan-Meier survival analyses regarding expression of senescence markers when divided into three subcohorts: low expression (petrol), moderate expression (black) and excessive expression (red). Cutoffs are displayed as bar graphs on the right of each curve and were calculated using a modification of the Charité Cutoff Finder from (54). Disease-specific survival is shown. Two tier subdivision, progression-free survival and detailed individual cutoff values can be found in the **Supplementary Material**.



However, we found that using pan-caspase inhibitor ZVAD to block death-receptor-mediated apoptosis resulted in significantly higher quantity of remaining adherent senescent cells after co-incubation resulting from abrogated senolysis of both NK-92 and TALL-104 cells ($p < 0.0001$). Addition of the SMAC-mimetic and apoptosis-sensitizer BV6 however did not have a measurable effect. Inhibiting the necroptosis pathway using Necrostatin-1, an allosteric inhibitor of RIP1, did not reverse the cytotoxicity of TALL-104 or NK-92 cells, suggesting a necroptosis-independent mechanism responsible for the targeted elimination of senescent

cells. To assess the role of granule exocytosis for the immune-mediated depletion of senescent cells, we conducted a set of experiments in the presence of Concanamycin A (Conc A) which inhibits perforin-based cytolytic activity by inhibition of vacuolar type H^+ -ATPase. Conc A decreased the cytotoxic effect of TALL-104 cells ($p < 0.0001$) but did not significantly prevent killing of senescent cells by NK-92 cells. HMGB1-Inhibitor glycyrrhizinic acid (Gly. Acid) was used to address HMGB1-dependent metabolic cell death. Spautin-1 ($p < 0.0230$) was used to address autophagy-associated cell death mechanisms.



ABT263 partly abrogated the cytotoxic effect of NK-92 cells ($p < 0.0001$) but did not significantly prevent killing of senescent cells by TALL-104 cells. Altogether, our co-incubation, electron microscopy and live cell imaging results indicate that direct cell-cell contact between immune cells and targeted senescent cells is a key mechanism for immune-cell-mediated senolysis. In the presence of inhibitors of apoptosis or (to some extent) granule exocytosis, immune cell-mediated elimination of senescent cells is decreased, suggesting that killing of senescent cells is mainly

facilitated via apoptosis induction and via induction of granule exocytosis (Figures 4C,D).

DISCUSSION

Arresting the cell cycle of premalignant cells as a response to oncogenic signaling and DNA impairment strongly supports the idea of senescence as a beneficial anti-cancer-mechanism (55–57). A premalignant cell's ability to senesce involves major

tumor-suppressor pathways and has been proven crucial to fight neoplastic transformation *in vivo* (6, 9, 58–60) and affects treatment outcome of cancer patients (61, 62). Recent studies point to a crucial role of cellular senescence in gastrointestinal diseases including colorectal carcinogenesis (40). Studies report that oncogene-induced senescence (OIS) prevents progression of benign KRAS-mutated sessile serrated adenomas to invasive carcinomas and provides an important barrier opposing malignancy in these early lesions. Malignant transformation to serrated adenocarcinoma requires overcoming this OIS-facilitated cell cycle arrest by downregulation of p16Ink4a (49). There is evidence to suggest that senescence detection might be of predictive value for CRC patients (50), however an extensive clinical study to evaluate the prognostic potential of senescence markers had been missing.

Our study reflects the important and complex role of cellular senescence in colorectal carcinogenesis. In many previous studies, cellular senescence has been described as a “double-edged sword” (34), referring to both the pro- and antitumorigenic effects senescent cells do have on disease progression. We demonstrate that absence of intratumoral senescence and therefore the lack of a basic antitumor defense mechanism is linked with a negative prognosis. Regarding the expression of p21, NTAL, EBP50 and ARMCX3, our results show the important role of senescence induction in tumor defense and underline the relevance of cell cycle regulator p21 and p21-mediated senescence. Moreover, we show that the occurrence of extremely high percentages of senescent cells in CRC is linked to a negative prognosis when compared to patients with moderate expression of senescence markers. These findings point to a complex role of cellular senescence in CRC, suggesting that both non-existent and extensive detection of senescent cells correlate with a negative prognosis. However, further analyses in the context of various molecular and disease subtypes are also necessary to validate our findings.

Senescent cells within the tumor do not automatically imply an effective tumor defense. An effect contributing to the negative outcome of those patients with large numbers of senescent cells might be the inflammatory micromilieu developing in close distance to senescent cells as a driver of further cell damage and therefore accelerating disease progression. While some of the factors secreted after SASP initiation contribute to maintaining the cell cycle arrest and reinforce the senescence program in premalignant cells (63–66) the SASP-driven proinflammatory alterations to the micromilieu—despite enhancing immune surveillance—do as well have malignancy-promoting effects (67).

Secreted factors may provide protumorigenic conditions and stimulate growth, dedifferentiation, and invasiveness of premalignant epithelial cells (68–70). Senescent fibroblasts signaling might contribute to growth-enabling changes to the microenvironment of dormant metastases (71). Increased VEGF expression by senescent cells increases angiogenesis in lesions at risk of malignant transformation and facilitates tumor vascularization, hereby contributing to malignant transformation (72). In CRC, VEGFR2 signaling silences the tumor-antagonizing effect of cellular senescence by actively bypassing p21 (73). There is evidence that the SASP-mediated inflammatory response

enhances immune control of senescent tumorous lesions in colorectal carcinoma and prevents malignant transformation in the presence of functional p53 but is protumorigenic in p21/p53-deficient lesions (74).

The perception of senescence as a beneficial anticancer mechanism (55–57) depends on the ability of the immune system to clear senescent cells and prevent negative effects mediated by senescent cells that remain in the tissue (39). Disruption of the tumor immunosurveillance results in accumulation of senescent cells (39), which might be the cause for the negative prognosis we observed in patients with extensive expression of senescence markers. Our study demonstrates that a dichotomous classification does not apply when describing the impact of cellular senescence detection on CRC prognosis. Senescence-associated molecules do have significant prognostic value concerning the outcome of patients with CRC. Moreover, we demonstrate that immune cells *in vitro* specifically eliminate senescent colon cancer cells while somewhat sparing proliferating cells. As Sagiv et al. showed for liver fibrosis in mice (46), we could demonstrate that NK cell-mediated clearance of senescent colorectal carcinoma cells is dependent on granule exocytosis. However, in contrast to Sagiv et al. (46) we found that suppression of the death receptor pathway by ZVAD abrogated the immune cell-mediated elimination of senescent cells in both the NK cell and the cytotoxic T cell model. Thus, our findings lead to the conclusion that induction of both apoptosis and granule exocytosis contribute to the targeted elimination of senescent cells by the immune system.

To reflect this interaction in the clinical setting, proximity analyses of the spatial relation of senescent tumor cells and immune cells are of prognostic relevance and could constitute a prognostic tool in colorectal cancer. Interestingly, we found that the spatial relation of p21-positive tumor cells and cytotoxic T cells is indicative of prognosis regarding DSS and PFS of CRC patients. There is evidence for an immune-infiltration-preventing effect of SASP signaling under certain circumstances (75). High percentage of senescent cells within the tumor—indicative of a negative prognosis as demonstrated in our study—might be the result of impeded tumor immune infiltration due to SASP signaling by senescent cells inhibiting immune cells (75). Furthermore, we showed that patients with close distance of senescent tumor cells and cytotoxic T cells do have a significant better survival which might indicate an antitumorigenic, preferable SASP signaling in these patients. How to impact SASP and induce the preferable, immunosurveillance-promoting secretory activity in senescent cells needs further evaluation and bares great potential in future therapy development. There is *in vitro* (18, 76, 77) and *in vivo* (78–80) evidence for a therapeutic approach inducing cellular senescence in cancerous lesions, evoking immune-cell mediated elimination of cancer cells and enhancing tumor surveillance (41, 44, 81). There are first therapeutic approaches of altering the senescence-induced immune response to induce an antitumorigenic microenvironment (51). Furthermore, therapeutic agents specifically eliminating senescent cells, called senolytics, have demonstrated great potential in various age-associated diseases, including cancer (82).

Taken together, cellular senescence is a key mechanism in opposing malignant transformation of impaired cells. The antitumorigenic effect of cellular senescence is dependent on an intact immune surveillance of the lesion. Therefore, the interaction of immune cells and senescent cells within the tumor microenvironment is of crucial prognostic relevance and provides targets for CRC therapy.

DATA AVAILABILITY STATEMENT

Datasets presented in this article are not readily available because of the General Data Protection Regulation regarding patient data. Requests to access the datasets should be directed to sebastian.foersch@unimedizin-mainz.de.

ETHICS STATEMENT

The studies involving human participants were reviewed and approved by the Ethical Committee of the Medical Association of the State of Rhineland-Palatinate [ref. no. 837.075.16 (10394)]. Written informed consent for participation was not required for this study in accordance with the national legislation and the institutional requirements.

AUTHOR CONTRIBUTIONS

FK and SF: conception and design. FK, SF, AF, and AH: acquisition and data. FK, SF, BK, KT, and MJ: analysis, interpretation of data, and critical revision of the manuscript. FK,

SF, and KT: drafting of the manuscript. FK, SF, and MS: statistical analysis. SF: obtaining funding, administrative, and technical, or material support. SF and WR: supervision.

FUNDING

This work was supported by the Stage-I-Program of the University Medical Center Mainz and the Mainz Research School of Translational Biomedicine (TransMed).

ACKNOWLEDGMENTS

Aspects of this work are part of the MD thesis of FK.

SUPPLEMENTARY MATERIAL

The Supplementary Material for this article can be found online at: <https://www.frontiersin.org/articles/10.3389/fmed.2022.865230/full#supplementary-material>

Supplementary Figure 1 | Additional Kaplan-Meier curves showing (A) disease-specific survival with a two-tier cutoff and (B) complementary progression-free survival. Cutoffs are displayed as bar graphs and were calculated using a modification of the Charité Cutoff Finder from (54).

Supplementary Table 1 | Antibodies and inhibitors used in this study.

Supplementary Table 2 | Clinicopathological characteristics of the patient cohort.

Supplementary Table 3 | Cutoff values for survival analysis as calculated using a modification of the Cutoff Finder from (54).

Supplementary Video 1 | Elimination of senescent Caco-2 cells by TALL-104 immune cells.

REFERENCES

- Sung H, Ferlay J, Siegel RL, Laversanne M, Soerjomataram I, Jemal A, et al. Global cancer statistics 2020: GLOBOCAN estimates of incidence and mortality worldwide for 36 cancers in 185 countries. *CA Cancer J Clin.* (2021) 71:209–49. doi: 10.3322/caac.21660
- Hayflick L. The limited *in vitro* lifetime of human diploid cell strains. *Exp Cell Res.* (1965) 37:614–36. doi: 10.1016/0014-4827(65)90211-9
- Harley CB, Futcher AB, Greider CW. Telomeres shorten during ageing of human fibroblasts. *Nature.* (1990) 345:458–60. doi: 10.1038/345458a0
- von Zglinicki T. Oxidative stress shortens telomeres. *Trends Biochem Sci.* (2002) 27:339–44. doi: 10.1016/S0968-0004(02)02110-2
- Serrano M, Lin AW, McCurrach ME, Beach D, Lowe SW. Oncogenic ras provokes premature cell senescence associated with accumulation of p53 and p16INK4a. *Cell.* (1997) 88:593–602. doi: 10.1016/S0092-8674(00)81902-9
- Bartkova J, Rezaei N, Liontos M, Karakaidos P, Kletsas D, Issaeva N, et al. Oncogene-induced senescence is part of the tumorigenesis barrier imposed by DNA damage checkpoints. *Nature.* (2006) 444:633–7. doi: 10.1038/nature05268
- Di Micco R, Fumagalli M, Cicalese A, Piccinin S, Gasparini P, Luise C, et al. Oncogene-induced senescence is a DNA damage response triggered by DNA hyper-replication. *Nature.* (2006) 444:638–42. doi: 10.1038/nature05327
- Shamma A, Takegami Y, Miki T, Kitajima S, Noda M, Obara T, et al. Rb Regulates DNA damage response and cellular senescence through E2F-dependent suppression of N-ras isoprenylation. *Cancer Cell.* (2009) 15:255–69. doi: 10.1016/j.ccr.2009.03.001
- Chen Z, Trotman LC, Shaffer D, Lin HK, Dotan ZA, Niki M, et al. Crucial role of p53-dependent cellular senescence in suppression of Pten-deficient tumorigenesis. *Nature.* (2005) 436:725–30. doi: 10.1038/nature03918
- d'Adda di Fagnana F, Reaper PM, Clay-Farrace L, Fiegler H, Carr P, Von Zglinicki T, et al. A DNA damage checkpoint response in telomere-initiated senescence. *Nature.* (2003) 426:194–8. doi: 10.1038/nature02118
- Chang BD, Broude EV, Dokmanovic M, Zhu H, Ruth A, Xuan Y, et al. A senescence-like phenotype distinguishes tumor cells that undergo terminal proliferation arrest after exposure to anticancer agents. *Cancer Res.* (1999) 59:3761–7.
- te Poele RH, Okorokov AL, Jardine L, Cummings J, Joel SP. DNA damage is able to induce senescence in tumor cells *in vitro* and *in vivo*. *Cancer Res.* (2002) 62:1876–83.
- Chang BD, Swift ME, Shen M, Fang J, Broude EV, Roninson IB. Molecular determinants of terminal growth arrest induced in tumor cells by a chemotherapeutic agent. *Proc Natl Acad Sci U S A.* (2002) 99:389–94. doi: 10.1073/pnas.012602599
- Roninson IB. Tumor cell senescence in cancer treatment. *Cancer Res.* (2003) 63:2705–15.
- Ewald JA, Desotelle JA, Wilding G, Jarrard DF. Therapy-induced senescence in cancer. *J Natl Cancer Inst.* (2010) 102:1536–46. doi: 10.1093/jnci/djq364
- Cadoo KA, Gucalp A, Traina TA. Palbociclib: an evidence-based review of its potential in the treatment of breast cancer. *Breast Cancer.* (2014) 6:123–33. doi: 10.2147/BCTT.S46725
- Yoshida A, Lee EK, Diehl JA. Induction of therapeutic senescence in vemurafenib-resistant melanoma by extended inhibition of CDK4/6. *Cancer Res.* (2016) 76:2990–3002. doi: 10.1158/0008-5472.CAN-15-2931
- Rader J, Russell MR, Hart LS, Nakazawa MS, Belcastro LT, Martinez D, et al. Dual CDK4/CDK6 inhibition induces cell-cycle arrest and senescence in neuroblastoma. *Clin Cancer Res.* (2013) 19:6173–82. doi: 10.1158/1078-0432.CCR-13-1675

19. Sherr CJ. A new cell-cycle target in cancer - inhibiting cyclin D-dependent kinases 4 and 6. *N Engl J Med.* (2016) 375:1920–3. doi: 10.1056/NEJMp1612343
20. Acosta JC, Gil J. Senescence: a new weapon for cancer therapy. *Trends Cell Biol.* (2012) 22:211–9. doi: 10.1016/j.tcb.2011.11.006
21. Dabritz JH, Yu Y, Milanovic M, Schonlein M, Rosenfeldt MT, Dorr JR, et al. CD20-targeting immunotherapy promotes cellular senescence in B-cell lymphoma. *Mol Cancer Ther.* (2016) 15:1074–81. doi: 10.1158/1535-7163.MCT-15-0627
22. von Zglinicki T, Saretzki G, Ladhoff J, d'Adda di Fagnana F, Jackson SP. Human cell senescence as a DNA damage response. *Mech Ageing Dev.* (2005) 126:111–7. doi: 10.1016/j.mad.2004.09.034
23. Matsumura T, Zerrudo Z, Hayflick L. Senescent human diploid cells in culture: survival, DNA synthesis and morphology. *J Gerontol.* (1979) 34:328–34. doi: 10.1093/geronj/34.3.328
24. Narita M, Nunez S, Heard E, Narita M, Lin AW, Hearn SA, et al. Rb-mediated heterochromatin formation and silencing of E2F target genes during cellular senescence. *Cell.* (2003) 113:703–16. doi: 10.1016/S0092-8674(03)00401-X
25. Mehta IS, Figgitt M, Clements CS, Kill IR, Bridger JM. Alterations to nuclear architecture and genome behavior in senescent cells. *Ann NY Acad Sci.* (2007) 1100:250–63. doi: 10.1196/annals.1395.027
26. Zhang R, Chen W, Adams PD. Molecular dissection of formation of senescence-associated heterochromatin foci. *Mol Cell Biol.* (2007) 27:2343–58. doi: 10.1128/MCB.02019-06
27. Kurz DJ, Decary S, Hong Y, Erusalimsky JD. Senescence-associated (beta)-galactosidase reflects an increase in lysosomal mass during replicative ageing of human endothelial cells. *J Cell Sci.* (2000) 113:3613–22. doi: 10.1242/jcs.113.20.3613
28. Itahana K, Campisi J, Dimri GP. Methods to detect biomarkers of cellular senescence: the senescence-associated beta-galactosidase assay. *Methods Mol Biol.* (2007) 371:21–31. doi: 10.1007/978-1-59745-361-5_3
29. Dimri GP, Lee X, Basile G, Acosta M, Scott G, Roskelley C, et al. A biomarker that identifies senescent human cells in culture and in aging skin in vivo. *Proc Natl Acad Sci U S A.* (1995) 92:9363–7. doi: 10.1073/pnas.92.20.9363
30. Sharpless NE, Sherr CJ. Forging a signature of in vivo senescence. *Nat Rev Cancer.* (2015) 15:397–408. doi: 10.1038/nrc3960
31. Campisi J. Aging, cellular senescence, and cancer. *Annu Rev Physiol.* (2013) 75:685–705. doi: 10.1146/annurev-physiol-030212-183653
32. Althubiti M, Lezina L, Carrera S, Jukes-Jones R, Giblett SM, Antonov A, et al. Characterization of novel markers of senescence and their prognostic potential in cancer. *Cell Death Dis.* (2014) 5:e1528. doi: 10.1038/cddis.2014.489
33. Wagner J, Damaschke N, Yang B, Truong M, Guenther C, McCormick J, et al. Overexpression of the novel senescence marker beta-galactosidase (GLB1) in prostate cancer predicts reduced PSA recurrence. *PLoS ONE.* (2015) 10:e0124366. doi: 10.1371/journal.pone.0124366
34. Coppe JP, Desprez PY, Krtolica A, Campisi J. The senescence-associated secretory phenotype: the dark side of tumor suppression. *Annu Rev Pathol.* (2010) 5:99–118. doi: 10.1146/annurev-pathol-121808-102144
35. Burton DGA, Stolzing A. Cellular senescence: immunosurveillance and future immunotherapy. *Ageing Res Rev.* (2018) 43:17–25. doi: 10.1016/j.arr.2018.02.001
36. Kuilman T, Peeper DS. Senescence-messaging secretome: SMS-ing cellular stress. *Nat Rev Cancer.* (2009) 9:81–94. doi: 10.1038/nrc2560
37. Michaloglou C, Vredeveld LC, Soengas MS, Denoyelle C, Kuilman T, van der Horst CM, et al. BRAFE600-associated senescence-like cell cycle arrest of human naevi. *Nature.* (2005) 436:720–4. doi: 10.1038/nature03890
38. Bayreuther K, Francz PI, Gogol J, Hapke C, Maier M, Meinrath HG. Differentiation of primary and secondary fibroblasts in cell culture systems. *Mutat Res.* (1991) 256:233–42. doi: 10.1016/0921-8734(91)90014-3
39. Ovadya Y, Landsberger T, Leins H, Vadai E, Gal H, Biran A, et al. Impaired immune surveillance accelerates accumulation of senescent cells and aging. *Nat Commun.* (2018) 9:5435. doi: 10.1038/s41467-018-07825-3
40. Frey N, Venturelli S, Zender L, Bitzer M. Cellular senescence in gastrointestinal diseases: from pathogenesis to therapeutics. *Nat Rev Gastroenterol Hepatol.* (2018) 15:81–95. doi: 10.1038/nrgastro.2017.146
41. Xue W, Zender L, Miething C, Dickins RA, Hernando E, Krizhanovsky V, et al. Senescence and tumour clearance is triggered by p53 restoration in murine liver carcinomas. *Nature.* (2007) 445:656–60. doi: 10.1038/nature05529
42. Iannello A, Thompson TW, Ardolino M, Lowe SW, Raulet DH. p53-dependent chemokine production by senescent tumor cells supports NKGD2D-dependent tumor elimination by natural killer cells. *J Exp Med.* (2013) 210:2057–69. doi: 10.1084/jem.20130783
43. Hoenicke L, Zender L. Immune surveillance of senescent cells—biological significance in cancer- and non-cancer pathologies. *Carcinogenesis.* (2012) 33:1123–6. doi: 10.1093/carcin/onc.2012.206
44. Kang TW, Yevsa T, Woller N, Hoenicke L, Wuestefeld T, Dauch D, et al. Senescence surveillance of pre-malignant hepatocytes limits liver cancer development. *Nature.* (2011) 479:547–51. doi: 10.1038/nature10599
45. Lujambio A, Akkari L, Simon J, Grace D, Tschaharganeh DF, Bolden JE, et al. Non-cell-autonomous tumor suppression by p53. *Cell.* (2013) 153:449–60. doi: 10.1016/j.cell.2013.03.020
46. Sagiv A, Biran A, Yon M, Simon J, Lowe SW, Krizhanovsky V. Granule exocytosis mediates immune surveillance of senescent cells. *Oncogene.* (2013) 32:1971–7. doi: 10.1038/onc.2012.206
47. Krizhanovsky V, Yon M, Dickins RA, Hearn S, Simon J, Miething C, et al. Senescence of activated stellate cells limits liver fibrosis. *Cell.* (2008) 134:657–67. doi: 10.1016/j.cell.2008.06.049
48. Leggett B, Whitehall V. Role of the serrated pathway in colorectal cancer pathogenesis. *Gastroenterology.* (2010) 138:2088–100. doi: 10.1053/j.gastro.2009.12.066
49. Carragher LA, Snell KR, Giblett SM, Aldridge VS, Patel B, Cook SJ, et al. V600EBraf induces gastrointestinal crypt senescence and promotes tumour progression through enhanced CpG methylation of p16INK4a. *EMBO Mol Med.* (2010) 2:458–71. doi: 10.1002/emmm.201000099
50. Haugstetter AM, Loddenkemper C, Lenze D, Grone J, Standfuss C, Petersen I, et al. Cellular senescence predicts treatment outcome in metastasised colorectal cancer. *Br J Cancer.* (2010) 103:505–9. doi: 10.1038/sj.bjc.6605784
51. Toso A, Revandkar A, Di Mitri D, Gucini I, Proietti M, Sarti M, et al. Enhancing chemotherapy efficacy in Pten-deficient prostate tumors by activating the senescence-associated antitumor immunity. *Cell Rep.* (2014) 9:75–89. doi: 10.1016/j.celrep.2014.08.044
52. Radspieler MM, Schindeldecker M, Stenzel P, Forsch S, Tagscherer KE, Herpel E, et al. Lamin-B1 is a senescence-associated biomarker in clear-cell renal cell carcinoma. *Oncol Lett.* (2019) 18:2654–60. doi: 10.3892/ol.2019.10593
53. Musayeva A, Manicam C, Steege A, Brochhausen C, Straub BK, Bell K, et al. Role of alpha1-adrenoceptor subtypes on corneal epithelial thickness and cell proliferation in mice. *Am J Physiol Cell Physiol.* (2018) 315:C757–65. doi: 10.1152/ajpcell.00314.2018
54. Budczies J, Klauschen F, Sinn BV, Gyorffy B, Schmitt WD, Darb-Esfahani S, et al. Cutoff Finder: a comprehensive and straightforward Web application enabling rapid biomarker cutoff optimization. *PLoS ONE.* (2012) 7:e51862. doi: 10.1371/journal.pone.0051862
55. Collado M, Serrano M. The senescent side of tumor suppression. *Cell Cycle.* (2005) 4:1722–4. doi: 10.4161/cc.4.12.2260
56. Braig M, Schmitt CA. Oncogene-induced senescence: putting the brakes on tumor development. *Cancer Res.* (2006) 66:2881–4. doi: 10.1158/0008-5472.CAN-05-4006
57. Campisi J, d'Adda di Fagnana F. Cellular senescence: when bad things happen to good cells. *Nat Rev Mol Cell Biol.* (2007) 8:729–40. doi: 10.1038/nrm2233
58. Lazzarini Denchi E, Attwooll C, Pasini D, Helin K. Deregulated E2F activity induces hyperplasia and senescence-like features in the mouse pituitary gland. *Mol Cell Biol.* (2005) 25:2660–72. doi: 10.1128/MCB.25.7.2660-2672.2005
59. Braig M, Lee S, Loddenkemper C, Rudolph C, Peters AH, Schlegelberger B, et al. Oncogene-induced senescence as an initial barrier in lymphoma development. *Nature.* (2005) 436:660–5. doi: 10.1038/nature03841
60. Collado M, Gil J, Efeyan A, Guerra C, Schuhmacher AJ, Barradas M, et al. Tumour biology: senescence in premalignant tumours. *Nature.* (2005) 436:642. doi: 10.1038/436642a
61. Childs BG, Durik M, Baker DJ, van Deursen JM. Cellular senescence in aging and age-related disease: from mechanisms to therapy. *Nat Med.* (2015) 21:1424–35. doi: 10.1038/nm.4000
62. Nardella C, Clohessy JG, Alimonti A, Pandolfi PP. Pro-senescence therapy for cancer treatment. *Nat Rev Cancer.* (2011) 11:503–11. doi: 10.1038/nrc3057

63. Acosta JC, O'Loughlen A, Banito A, Guijarro MV, Augert A, Raguz S, et al. Chemokine signaling via the CXCR2 receptor reinforces senescence. *Cell*. (2008) 133:1006–18. doi: 10.1016/j.cell.2008.03.038
64. Kuilman T, Michaloglou C, Vredeveld LC, Douma S, van Doorn R, Desmet CJ, et al. Oncogene-induced senescence relayed by an interleukin-dependent inflammatory network. *Cell*. (2008) 133:1019–31. doi: 10.1016/j.cell.2008.03.039
65. Wajapeyee N, Serra RW, Zhu X, Mahalingam M, Green MR. Oncogenic BRAF induces senescence and apoptosis through pathways mediated by the secreted protein IGFBP7. *Cell*. (2008) 132:363–74. doi: 10.1016/j.cell.2007.12.032
66. Bartek J, Hodny Z, Lukas J. Cytokine loops driving senescence. *Nat Cell Biol*. (2008) 10:887–9. doi: 10.1038/ncb0808-887
67. Campisi J. Senescent cells, tumor suppression, and organismal aging: good citizens, bad neighbors. *Cell*. (2005) 120:513–22. doi: 10.1016/j.cell.2005.02.003
68. Krtolica A, Parrinello S, Lockett S, Desprez PY, Campisi J. Senescent fibroblasts promote epithelial cell growth and tumorigenesis: a link between cancer and aging. *Proc Natl Acad Sci U S A*. (2001) 98:12072–7. doi: 10.1073/pnas.211053698
69. Parrinello S, Coppe JP, Krtolica A, Campisi J. Stromal-epithelial interactions in aging and cancer: senescent fibroblasts alter epithelial cell differentiation. *J Cell Sci*. (2005) 118:485–96. doi: 10.1242/jcs.01635
70. Coppe JP, Patil CK, Rodier F, Sun Y, Munoz DP, Goldstein J, et al. Senescence-associated secretory phenotypes reveal cell-nonautonomous functions of oncogenic RAS and the p53 tumor suppressor. *PLoS Biol*. (2008) 6:2853–68. doi: 10.1371/journal.pbio.0060301
71. Joyce JA, Pollard JW. Microenvironmental regulation of metastasis. *Nat Rev Cancer*. (2009) 9:239–52. doi: 10.1038/nrc2618
72. Coppe JP, Kauser K, Campisi J, Beausejour CM. Secretion of vascular endothelial growth factor by primary human fibroblasts at senescence. *J Biol Chem*. (2006) 281:29568–74. doi: 10.1074/jbc.M603307200
73. Foersch S, Sperka T, Lindner C, Taut A, Rudolph KL, Breier G, et al. VEGFR2 signaling prevents colorectal cancer cell senescence to promote tumorigenesis in mice with colitis. *Gastroenterology*. (2015) 149:177–89 e10. doi: 10.1053/j.gastro.2015.03.016
74. Pribluda A, Elyada E, Wiener Z, Hamza H, Goldstein RE, Biton M, et al. A senescence-inflammatory switch from cancer-inhibitory to cancer-promoting mechanism. *Cancer Cell*. (2013) 24:242–56. doi: 10.1016/j.ccr.2013.06.005
75. Choi YW, Kim YH, Oh SY, Suh KW, Kim YS, Lee GY, et al. senescent tumor cells build a cytokine shield in colorectal cancer. *Adv Sci*. (2021) 8:2002497. doi: 10.1002/advs.202002497
76. Michaud K, Solomon DA, Oermann E, Kim JS, Zhong WZ, Prados MD, et al. Pharmacologic inhibition of cyclin-dependent kinases 4 and 6 arrests the growth of glioblastoma multiforme intracranial xenografts. *Cancer Res*. (2010) 70:3228–38. doi: 10.1158/0008-5472.CAN-09-4559
77. Thangavel C, Dean JL, Ertel A, Knudsen KE, Aldaz CM, Witkiewicz AK, et al. Therapeutically activating RB: reestablishing cell cycle control in endocrine therapy-resistant breast cancer. *Endocr Relat Cancer*. (2011) 18:333–45. doi: 10.1530/ERC-10-0262
78. Leonard JP, LaCasce AS, Smith MR, Noy A, Chirieac LR, Rodig SJ, et al. Selective CDK4/6 inhibition with tumor responses by PD0332991 in patients with mantle cell lymphoma. *Blood*. (2012) 119:4597–607. doi: 10.1182/blood-2011-10-388298
79. Guha M. Blockbuster dreams for Pfizer's CDK inhibitor. *Nat Biotechnol*. (2013) 31:187. doi: 10.1038/nbt0313-187a
80. Dickson MA, Tap WD, Keohan ML, D'Angelo SP, Gounder MM, Antonescu CR, et al. Phase II trial of the CDK4 inhibitor PD0332991 in patients with advanced CDK4-amplified well-differentiated or dedifferentiated liposarcoma. *J Clin Oncol*. (2013) 31:2024–8. doi: 10.1200/JCO.2012.46.5476
81. Ventura A, Kirsch DG, McLaughlin ME, Tuveson DA, Grimm J, Lintault L, et al. Restoration of p53 function leads to tumour regression in vivo. *Nature*. (2007) 445:661–5. doi: 10.1038/nature05541
82. Wang L, Leite de Oliveira R, Wang C, Fernandes Neto JM, Mainardi S, Evers B, et al. High-throughput functional genetic and compound screens identify targets for senescence induction in cancer. *Cell Rep*. (2017) 21:773–83. doi: 10.1016/j.celrep.2017.09.085

Conflict of Interest: The authors declare that the research was conducted in the absence of any commercial or financial relationships that could be construed as a potential conflict of interest.

Publisher's Note: All claims expressed in this article are solely those of the authors and do not necessarily represent those of their affiliated organizations, or those of the publisher, the editors and the reviewers. Any product that may be evaluated in this article, or claim that may be made by its manufacturer, is not guaranteed or endorsed by the publisher.

Copyright © 2022 Kellers, Fernandez, Konukiewicz, Schindeldecker, Tagscherer, Heintz, Jesinghaus, Roth and Foersch. This is an open-access article distributed under the terms of the Creative Commons Attribution License (CC BY). The use, distribution or reproduction in other forums is permitted, provided the original author(s) and the copyright owner(s) are credited and that the original publication in this journal is cited, in accordance with accepted academic practice. No use, distribution or reproduction is permitted which does not comply with these terms.



Myxoinflammatory Fibroblastic Sarcoma of the Parotid Gland: First Case Report and Literature Review

Changhong Wei^{1,2†}, Xuejia Yang^{2†}, Pingping Guo^{3†}, Xiaoyu Chen¹, Chunjun Li¹, Jun Chen^{1*} and Sufang Zhou^{2,4*}

¹ Department of Pathology, Guangxi Medical University Cancer Hospital, Nanning, China, ² National Center for International Research of Bio-Targeting Theranostics, Guangxi Key Laboratory of Bio-Targeting Theranostics, Collaborative Innovation Center for Targeting Tumor Diagnosis and Therapy, Guangxi Medical University, Nanning, China, ³ Department of Ultrasound Imaging, Guangxi Medical University Cancer Hospital, Nanning, China, ⁴ Department of Biochemistry and Molecular Biology, School of Pre-clinical Science, Guangxi Medical University, Nanning, China

OPEN ACCESS

Edited by:

Arndt Hartmann,
Universitätsklinikum Erlangen,
Germany

Reviewed by:

Somboon Keelawat,
Chulalongkorn University, Thailand
Omar El Bounkari,
Ludwig Maximilian University
of Munich, Germany

*Correspondence:

Jun Chen
chenjun2826@163.com
Sufang Zhou
zsf200000@163.com

[†]These authors have contributed
equally to this work

Specialty section:

This article was submitted to
Pathology,
a section of the journal
Frontiers in Medicine

Received: 12 December 2021

Accepted: 22 April 2022

Published: 20 May 2022

Citation:

Wei C, Yang X, Guo P, Chen X,
Li C, Chen J and Zhou S (2022)
Myxoinflammatory Fibroblastic
Sarcoma of the Parotid Gland: First
Case Report and Literature Review.
Front. Med. 9:833822.
doi: 10.3389/fmed.2022.833822

Myxoinflammatory fibroblastic sarcoma (MIFS) is a rare, low-grade malignant soft tissue tumor. Most of the previously reported cases about this tumor were diagnosed within the soft tissues. Here, we report a unique case of MIFS of the right parotid gland in a 39-year-old Chinese male. The tumor primarily consisted of an inflammatory area and a mucus-like area in a migratory distribution. A number of lymphocytes, neutrophils, viral-like cells with large nucleoli, and eosinophilic cytoplasm or Reed-Sternberg-like cells, as well as spindle cells and epithelial-like aberrant cells, were observed within the tumor. They were found to express Vimentin and CD10 protein and no other specific immunohistochemical markers. The various cytomorphology and immunohistochemical features of this tumor were highly consistent with MIFS found in other sites. Therefore, several leading pathologists ultimately confirmed the final diagnosis of MIFS in the right parotid gland after repeated deliberation. To our knowledge, this is the first case of MIFS occurring in the parotid gland. Thus, our study provides a novel basis for identifying the biological behavior of the tumor in MIFS and also allows us to better understand the pathology of this rare tumor.

Keywords: myxoinflammatory fibroblastic sarcoma, MIFS, soft tissue tumor, Vimentin, parotid gland

INTRODUCTION

Myxoinflammatory fibroblastic sarcoma (MIFS) is a rare, slow-growing, low-grade malignant soft tissue tumor (1). It was first described by Montgomery et al. (2), and several cases have since been reported around the world (3, 4). Clinically, MIFS is considered to be a superficial tumor found within the soft tissues, and generally manifests itself as a painless subcutaneous mass in the distal limb in adults. However, in recent years, a proportion of cases have been reported in several other non-extremity sites, such as the breast, buttocks, chest wall, and thighs (3, 5, 6). However, MIFS of the parotid gland has not been reported and described previously. In this study,

we present a unique case of MIFS of the parotid gland in a Chinese patient with a characteristic histomorphology, consisting of inflammatory and mucin-like areas. It was characterized by the prominent morphological presentation of aberrant large cells, containing huge nucleoli with a typical immunophenotype (Vimentin protein positive), and other features that were consistent with the previously reported MIFS in other sites. The study was approved by the Institutional Review Board of the Cancer Hospital of Guangxi Medical University and was performed according to the principles of the “Declaration of Helsinki.” Written informed consent for this study was obtained from the patient prior to the study.

CASE PRESENTATION

Clinical Findings

A 39-year-old male patient was diagnosed with a right submandibular mass in the outpatient clinic of our hospital 2 months ago. The physical examination showed that the neck curvature and mobility were normal, no lateral curvature was noticed, and the right lower jaw could reach the size of a 2×1 -cm mass. Additionally, the mass was hard, had unclear boundary and blunt edge with poor activity, but no other abnormality was observed in other parts. After the patient was admitted to the hospital, the clinician used a fine needle for aspiration of cells from the tumor. The pathological examination further revealed that the nuclear atypical cells were visible, and the malignant possibility was not excluded. The ultrasound of the neck showed a substantial lesion of the right parotid gland, and the CT examination displayed a small

nodule below the parotid gland (**Figures 1A,B**), which was initially considered as a benign tumor or tumor-like lesion of the parotid gland. His laboratory tests for the blood routine analysis, liver function, renal function, blood sugar, and thyroid function were found to be within the normal range. His HIV, HBsAg, and HCV serology were also negative. Under the general anesthesia, the right parotid mass resection and right facial nerve anatomy were performed and, thereafter, submitted for the histopathological examination.

Pathologic Findings

Moreover, on the gross specimen, there was a gray-red, gray-yellow nodular mass within the parotid gland tissue, the size was $1.8 \times 1.5 \times 1$ cm, and there was a complete capsule. The cut surface was grayish-yellow, gray, and white, soft, mucoid, and exhibited no hemorrhagic necrosis.

Histopathological microscopy showed that the tumor consisted of the different inflammatory regions as well as mucin-like regions, and the inflammatory cells were mostly lymphocytes or neutrophils. The inflammatory regions showed large nucleoli, and the cytoplasm was eosinophilic with viral-like cells or Reed-Sternberg-like cells, and it exhibited different degrees of fibrosis. The mucus region was primarily composed of spindle cells and tissue-like or epithelial-like malformed cells. The interstitial was hyaline degeneration, and small amounts of scattered multinucleated giant cells were visible in the lesion. Transitional distribution of inflammatory and mucous areas, visible large cells of nucleoli, and mitotic figures were not commonly observed, but mildly shaped spindle cells were seen in the inflammatory area. A part of the area was characterized by mucus and fibrotic regional composition, accompanied by

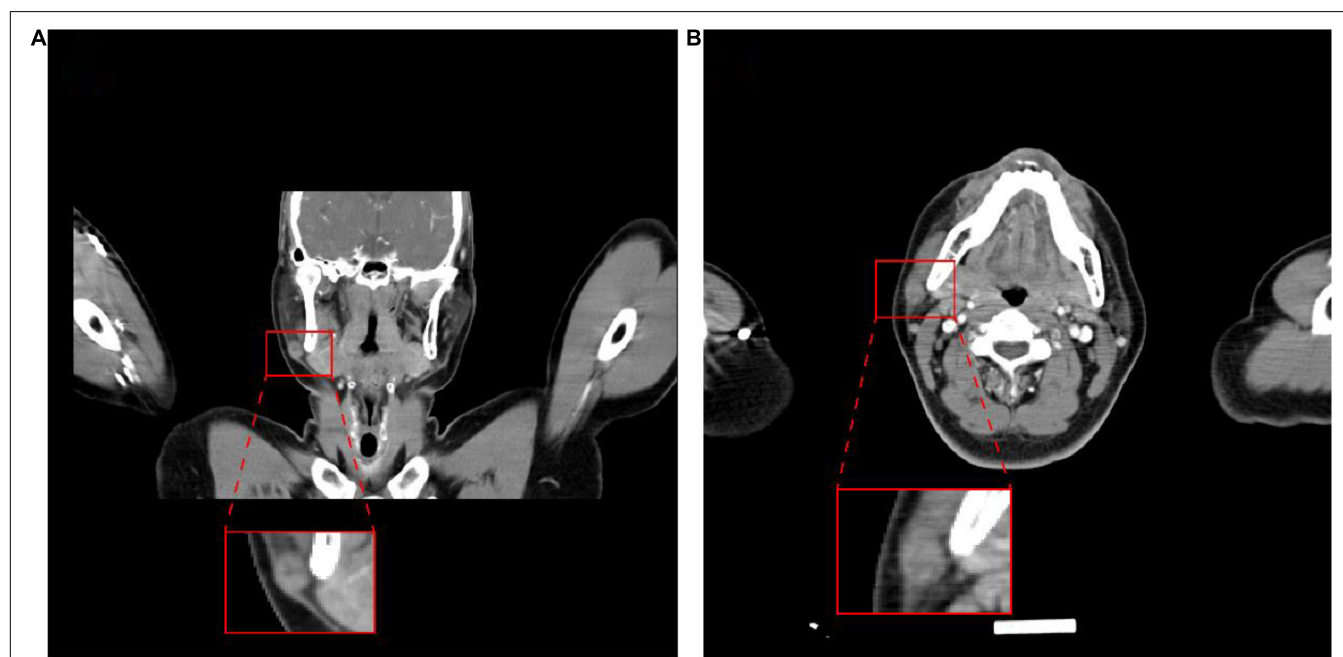


FIGURE 1 | Images of the tumor. Computed tomography showed a nodule on the lower right side of the parotid gland. **(A)** Coronal plane; **(B)** transverse plane.

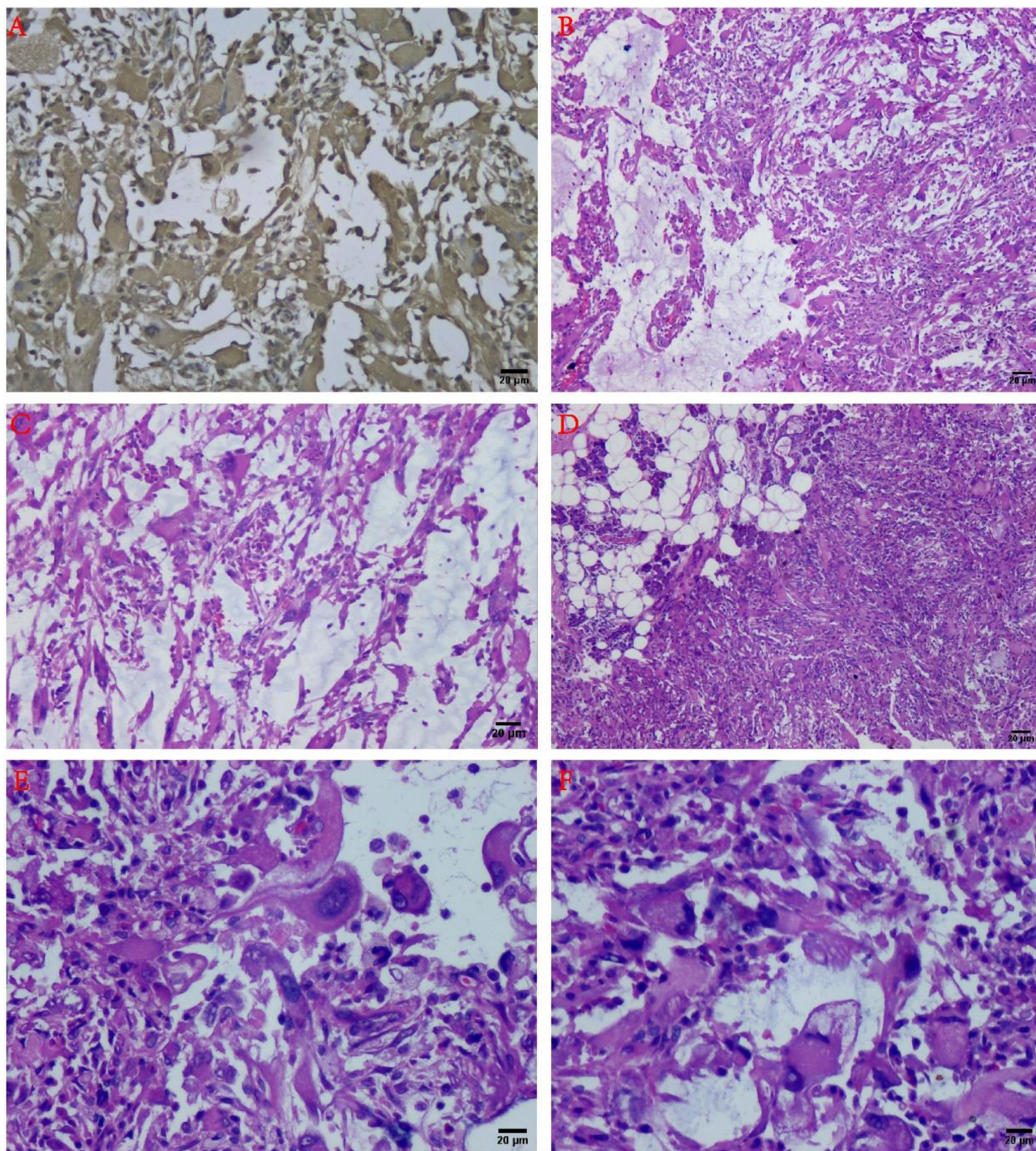


FIGURE 2 | Histology and immunohistochemistry of the tumor. **(A)** Immunohistochemical results showed Vimentin diffuse positive (+) (IHC staining, $\times 100$). **(B)** The tumor consisted of the mucous area and the fibrous area with inflammatory cell infiltration in the mucus-like area, and the various fusiform cells can be connected to each other to form a network structure (H&E staining, $\times 100$). **(C)** At the junction of the mucous area and the fiber area, inflammatory cell infiltration could be observed (H&E staining, $\times 100$). **(D)** The tumor can be infiltrated into the parotid tissue (H&E staining, $\times 100$). **(E)** Large malformed cells with large nucleoli can be noted (H&E staining, $\times 200$). **(F)** The “inclusion body” nucleolus resembling Reed-Sternberg cells has been recognized as one of the characteristics of mucinous inflammatory fibroblastic sarcoma (H&E staining, $\times 200$).

lymphocyte or neutrophil infiltration. The most characteristic morphological manifestations were the presence of the large cells with huge nucleoli, with interstitial inflammatory cell reactions.

Moreover, visible in the mucus area were the pseudo-fat cells, spindle cells involving adipose tissue, whereas the phagocytic cells can also be seen in some areas (**Figures 2B–F, 3**).

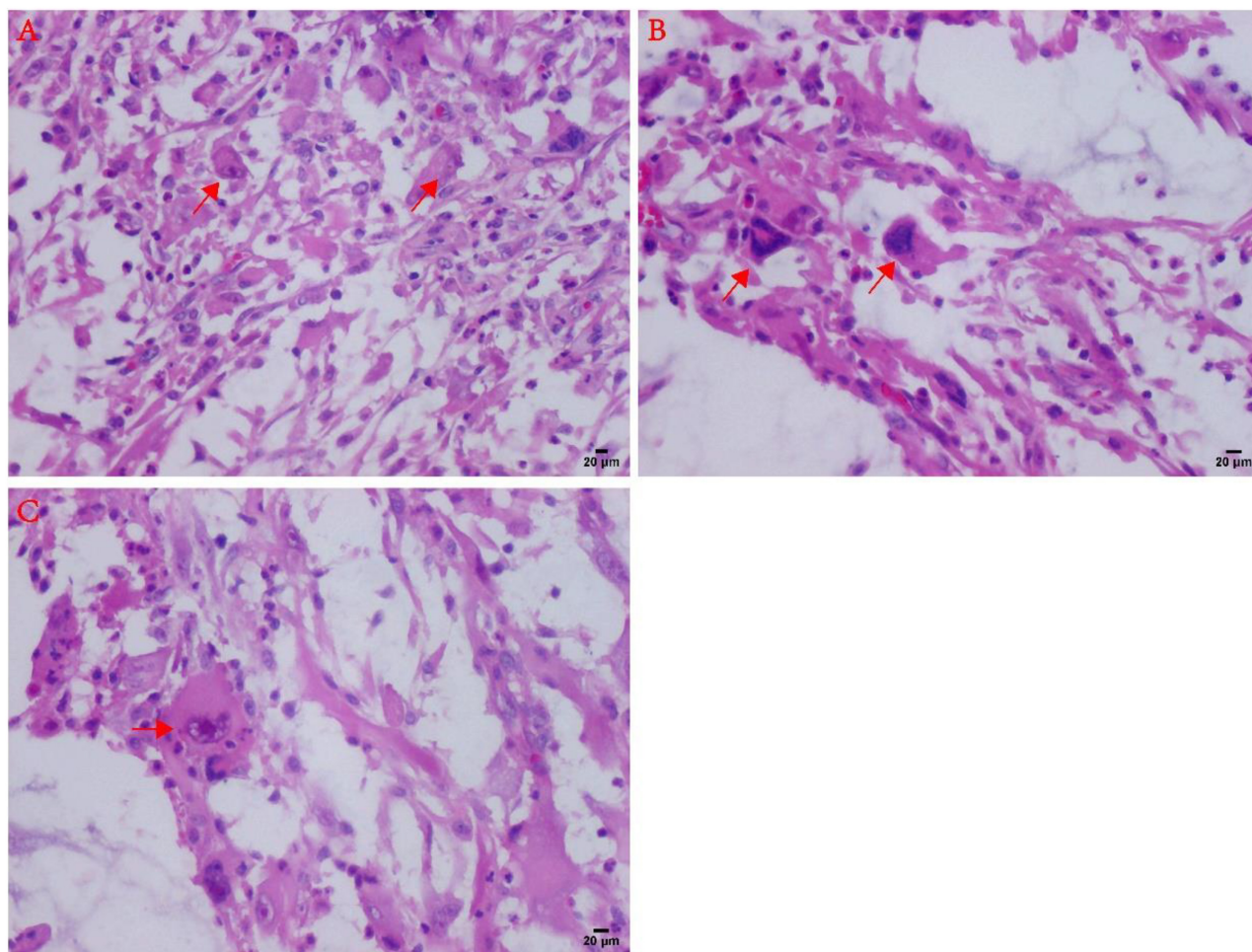


FIGURE 3 | Atypical microscopic features in MIFS. **(A)** Virus-like cells with abundant cytoplasm and nucleoli (arrows). **(B)** Large malformed cells with two enlarged nuclei shown by arrows; **(C)** R-S cell-like tumor cells with markedly large nucleoli (arrows).

Immunohistochemical Findings

Immunohistochemistry revealed that the tumor cells expressed Vimentin and CD10 (diffuse positive) (**Figures 2A, 4A**), lymphocytes expressed LCA, macrophages expressed CD163 and CD68, Ki-67 index was 10%, CK, SMA, P63, CD34, CD1a, D2-40, and S-100 were negative (**Table 1** and **Figure 4**).

According to tumor imaging, microscopic histomorphology, and comprehensive immunohistochemical analysis, the authors finally diagnosed the tumor as parotid myxoinflammatory fibroblastic sarcoma. The patient is currently in good condition and is undergoing regular follow-up in our hospital, and no recurrence or metastasis has been found.

DISCUSSION

Based on the previously published review of domestic and foreign literature, this is the first report describing the occurrence of MIFS in the parotid gland. It has been reported that MIFS usually presents as a slow-growing painless mass, mostly in adults, and

the peak age of the onset is 30–50 years old, the average age is about 40 years old. A small number of cases also occur in children or adolescents, and tumors primarily arise in the soft tissue location of the distal part of the limb (1, 7). In this study, we have summarized the clinicopathological features of MIFS reported in the literature in the rare sites (non-bone and soft tissue, since 1998) (**Table 2**) (6, 8, 9). Clinically, MIFS may be similar to benign lesions and can be often misdiagnosed as the slippery membrane inflammation, ganglion cysts, or giant cell tumor of the tendon sheath. CT or MRI usually presents as diffuse enhancement, lobulated, subcutaneous mass with non-specific magnetic resonance imaging features, thereby suggesting the presence of benign or malignant lesions (1).

The rich and diverse histological performance of MIFS is a major challenge in the diagnosis of this tumor (10). For example, the ratio of mucin-like areas, fibroinflammatory areas, and the cell area can effectively vary from case to case, and the number of cells with inclusion body-like nuclei is generally considered to be the major marker of MIFS. Another major challenge in diagnosis is the presence of severe inflammatory

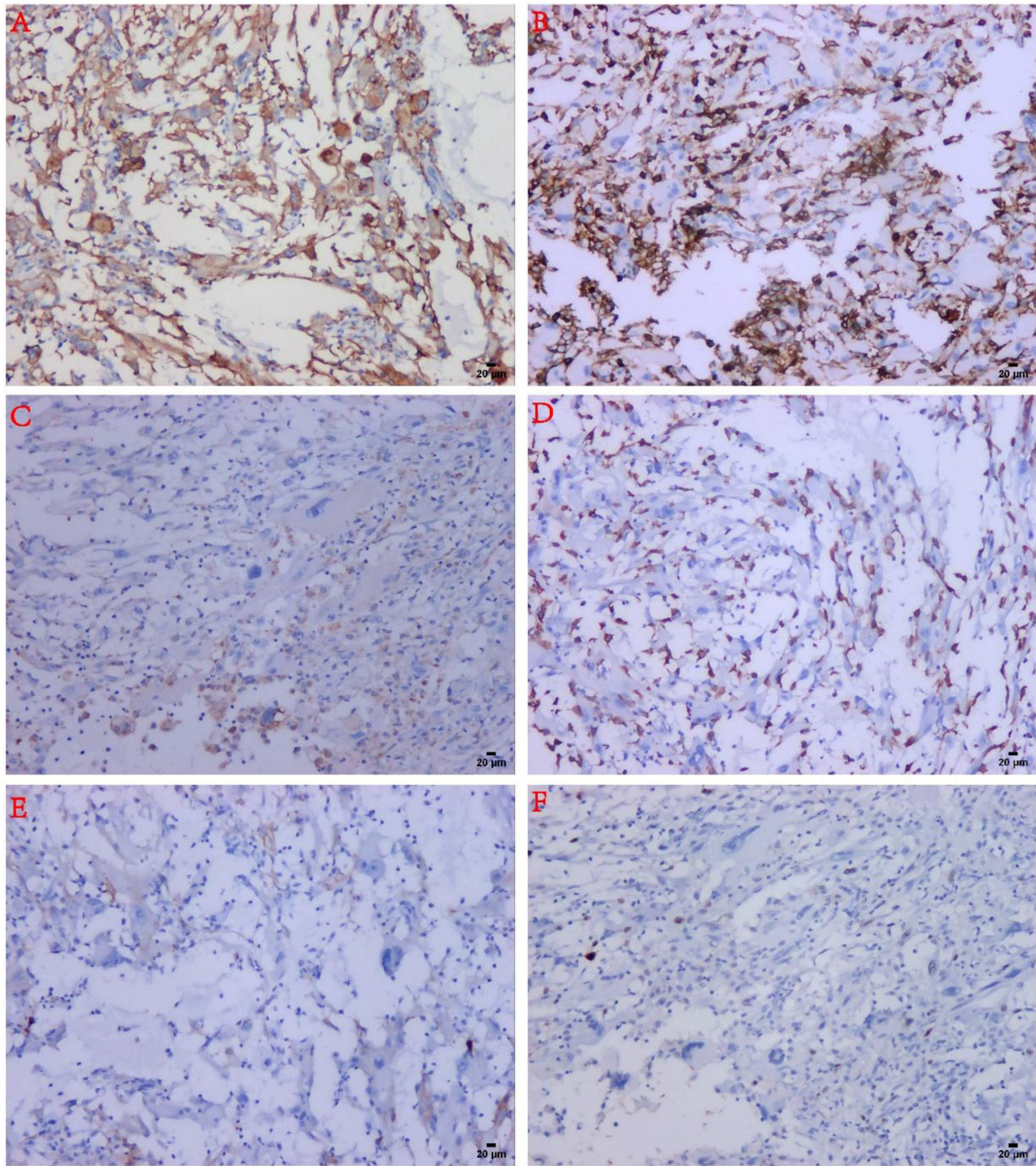


FIGURE 4 | Immunohistochemical findings in MIFS. **(A)** The tumor spindle cells and malformed cells were strongly positive for CD10. **(B)** Infiltrated inflammatory cells were strongly positive for LCA. **(C)** The reactive histiocytes were positive for CD68. **(D)** Reactive histiocytes were positive for CD163. **(E)** The tumor cells were negative for D2-40. **(F)** The tumor cells expressed low-proliferative Ki-67 (about 10%).

reactions, which are mediated primarily by the lymphocytes and lymphoid aggregates-infiltrated tumor cells. These may be mistaken for inflammatory processes or other malignant tumors, such as lymphoma mucinous fibrosarcoma (11). In the mucus background, the tumor spindle cells and epithelioid

cells are usually connected to each other to form a complex network structure, and a large number of the neutrophils, macrophages, and plasma cells can be seen, but the mitotic figures and necrosis are not commonly observed in this tumor. Immunohistochemistry has been found to play a very limited

TABLE 1 | A summary of the primary antibodies used and the results of immunohistochemistry.

Antibody	Source	Dilution	Result
CKpan	Maixin, Fuzhou, China	1:100	—
Vimentin	Maixin, Fuzhou, China	1:150	+++
LCA	Maixin, Fuzhou, China	1:100	+
CD68	Maixin, Fuzhou, China	1:100	+
Ki-67	Maixin, Fuzhou, China	1:200	+ (10%)
SMA	Maixin, Fuzhou, China	1:100	—
P63	Maixin, Fuzhou, China	1:100	—
CD34	Maixin, Fuzhou, China	1:100	—
Calponin	Maixin, Fuzhou, China	1:100	—
SMMHC	Maixin, Fuzhou, China	1:100	—
CD1a	Maixin, Fuzhou, China	1:100	—
S-100	Maixin, Fuzhou, China	1:100	—
CD163	Maixin, Fuzhou, China	1:100	+
CD10	Maixin, Fuzhou, China	1:100	+
D2-40	Maixin, Fuzhou, China	1:100	—

role in the diagnosis of MIFS because it has no specific tumor markers (12).

In the present study, the main features for the diagnosis of MIFS included areas of solid spindle cells, alternating with myxoid foci with the diffuse infiltration of inflammatory cells. Unlike other previously reported cases, a random distribution of the larger atypical cells was seen in our case, including Reed-Sternberg cells, variants of virus-like cells with inclusion-like nucleoli, and large malformed cells. Immunohistochemistry has been widely used in MIFS, but no specific immunophenotype has been found. However, differential responsiveness to the various markers has been observed in the previous studies, including Vimentin, D2-40, CD68, bcl-1, CD10, and CD163 (3, 12). In the present study, we found consistent and strong immunoreactivity for Vimentin and CD10 in the tumor cells in this case. Moreover, another novel finding of our study was the low expression of the proliferative marker Ki-67, and the most characteristic

phenomenon was that, in the large malformed cells and R-S like-cells, Ki-67 was almost absent. These pieces of evidence suggested that these atypical cells were the degenerative tumor cells that were biologically inactive.

The cytogenetic analysis of MIFS further revealed complex genetic abnormalities (13), including a circular chromosome formed on the Chromosome 3, a translocation of chromosome t (1:10) (p22: q24), rearrangement of *TGFBR3* and *MGEA5* genes (14). Some other cases showed *TGFBR3* and *MGEA5* gene rearrangement, which led to an upregulation of NPM3 and FGF8, accompanied by amplification of the *VGLL3* locus (10, 15).

Most cases of MIFS have demonstrated low malignant potential. However, 22–67% of cases can potentially recur, and only a few cases can metastasize (3), but high-grade MIFS may lead to more adverse progression (16). The best treatment for MIFS is complete surgical resection to ensure that the incisional margin is negative; however, the beneficial impact of radiotherapy and chemotherapy remains unclear (17). Our patient remained in good condition after 7 months of follow-up, and no recurrence or metastasis was observed.

CONCLUSION

In summary, we report that the first case of MIFS was detected in the parotid gland. However, due to its complex histological morphology and inflammatory background, we need to distinguish it from other similar lesions, such as inflammatory myofibroblastic sarcoma and myxofibrosarcomas, to facilitate accurate diagnosis. Although no specific immunohistochemical or molecular markers are available for the diagnosis of this tumor. In addition to describing the classical histological features in this study. Our results supported the use of a distinct panel of immunohistochemical markers, including CD10 and Vimentin, might be helpful support for MIFS diagnostics in many equivocal cases. At present, the diagnosis of MIFS is still mainly based on clinicopathological diagnosis, which needs to be combined with the appropriate clinical environment

TABLE 2 | A summary of clinicopathological features of MIFS reported in the literature from the rare sites (non-bone and soft tissue, reviewed since 1998).

Author/year	Age/gender	Location	Pathological features	Treatment	Follow-up (mo)	Outcome
Current study	39/M	Parotid gland	The tumor consisted of inflammatory regions and mucin-like regions, the inflammatory cells were mostly lymphocytes or neutrophils. The most characteristic morphological manifestations are large cells with large nucleoli, with interstitial inflammatory cell reaction.	Surgery	28	No recurrence or metastasis
Jain et al. (8)	7-month-old infant	Eyeball	A mixed cellular infiltrate composed of numerous neutrophils, larger cells appeared to be binucleate (Reed-Sternberg-like or virocyte-like)	Resection	NA	NA
Auw-Haedrich et al. (6)	27/F	Iris	Tumor contained mucinous and cellular areas with high grade of polymorphy and a large variety of cell sizes and forms	Resection	15	No recurrence
Numminen et al. (9)	51/M	Nose	The tumor was heterogeneous in composition, with myxoid, relatively acellular areas alternating with cellular areas	Surgery	48	No recurrence or metastasis

NA, not available; mo, month; F, female; M, male.

and characteristic histomorphological findings to significantly improve the treatment outcome.

DATA AVAILABILITY STATEMENT

The raw data supporting the conclusions of this article will be made available by the authors, without undue reservation.

ETHICS STATEMENT

The studies involving human participants were reviewed and approved by the Medical Ethics Committee of the Affiliated Cancer Hospital of Guangxi Medical University. The patients/participants provided their written informed consent to participate in this study. Written informed consent was obtained from the individual(s) for the publication of any potentially identifiable images or data included in this article.

REFERENCES

1. Baheti AD, Tirumani SH, Rosenthal MH, Howard SA, Shinagare AB, Ramaiya NH, et al. Myxoid soft-tissue neoplasms: comprehensive update of the taxonomy and MRI features. *AJR Am J Roentgenol.* (2015) 2:374–85. doi: 10.2214/ajr.14.12888
2. Montgomery EA, Devaney KO, Giordano TJ, Weiss SW. Inflammatory myxohyaline tumor of distal extremities with virocyte or reed-sternberg-like cells: a distinctive lesion with features simulating inflammatory conditions, Hodgkin's disease, and various sarcomas. *Mod Pathol.* (1998) 4:384–91.
3. Laskin WB, Fetsch JE, Miettinen M. Myxoinflammatory fibroblastic sarcoma: a clinicopathologic analysis of 104 cases, with emphasis on predictors of outcome. *Am J Surg Pathol.* (2014) 1:1–12. doi: 10.1097/PAS.0b013e31829f3d85
4. Patne SC, Katiyar R, Gupta SK. Intramuscular myxoinflammatory fibroblastic sarcoma of the thigh. *Pathology.* (2016) 5:527–9. doi: 10.1016/j.pathol.2016.05.003
5. Gaetke-Udager K, Yablon CM, Lucas DR, Morag Y. Myxoinflammatory fibroblastic sarcoma: spectrum of disease and imaging presentation. *Skeletal Radiol.* (2016) 3:347–56. doi: 10.1007/s00256-015-2286-2
6. Auw-Haedrich C, Mentzel T, Reinhard T. Myxoinflammatory fibroblastic sarcoma of the iris. *Pathology.* (2017) 7:794–5. doi: 10.1016/j.pathol.2017.08.016
7. Kao YC, Ranucci V, Zhang L, Sung YS, Athanasian EA, Swanson D, et al. Recurrent BRAF gene rearrangements in myxoinflammatory fibroblastic sarcomas, but not hemosiderotic fibrolipomatous tumors. *Am J Surg Pathol.* (2017) 11:1456–65. doi: 10.1097/pas.0000000000000899
8. Jain E, Kini L, Alaggio R, Ranganathan S. Myxoinflammatory fibroblastic sarcoma of eyeball in an infant: a rare presentation. *Int J Surg Pathol.* (2020) 3:306–9. doi: 10.1177/1066896919879497
9. Numminen J, Bizaki A, Kujansivu J, Huovinen S, Rautiainen M. Myxoinflammatory fibroblastic sarcoma of the nose: first reported case at an unusual location (nasal dorsum), with a review of the literature. *Ear Nose Throat J.* (2016) 3:E32–5. doi: 10.1177/014556131609500304
10. Lucas DR. Myxoinflammatory fibroblastic sarcoma: review and update. *Arch Pathol Lab Med.* (2017) 11:1503–7. doi: 10.5858/arpa.2017-0219-RA
11. Chiu HY, Chen JS, Hsiao CH, Tsai TF. Transformation of myxofibrosarcoma into myxoinflammatory fibroblastic sarcoma. *J Dermatol.* (2012) 4:422–4. doi: 10.1111/j.1346-8138.2011.01297.x

AUTHOR CONTRIBUTIONS

JC and SZ read and approved the final manuscript. CW performed the writing of the manuscript. XY and PG organized the material and helped with the analysis. XC carried out experiments. CL and JC performed the pathological analysis and diagnosed the patient. All authors wrote and revised the manuscript.

FUNDING

This study was supported by the self-funded scientific research project of Guangxi Zhuang Autonomous Region Health Commission (Z20190572 and Z20210959), Guangxi Science and Technology Research Base and Talent-specific Project (AD18126021), Key Laboratory of the Ministry of Education Project for Early Prevention, and Treatment of Regional High-risk Tumors (GKE-ZZ202007).

12. Suster D, Michal M, Huang H, Ronen S, Springborn S, Debiec-Rychter M, et al. Myxoinflammatory fibroblastic sarcoma: an immunohistochemical and molecular genetic study of 73 cases. *Mod Pathol.* (2020) 12:2520–33. doi: 10.1038/s41379-020-0580-6
13. Arbajian E, Hofvander J, Magnusson L, Mertens F. Deep sequencing of myxoinflammatory fibroblastic sarcoma. *Genes Chromosomes Cancer.* (2020) 5:309–17. doi: 10.1002/gcc.22832
14. Liu H, Sukov WR, Ro JY. The t(1;10)(p22;q24) TGFBR3/MGEA5 translocation in pleomorphic hyalinizing angiectatic tumor, myxoinflammatory fibroblastic sarcoma, and hemosiderotic fibrolipomatous tumor. *Arch Pathol Lab Med.* (2019) 2:212–21. doi: 10.5858/arpa.2017-0412-RA
15. Jeremia E, Thway K. Myxoinflammatory fibroblastic sarcoma: morphologic and genetic updates. *Arch Pathol Lab Med.* (2014) 10:1406–11. doi: 10.5858/arpa.2013-0549-RS
16. Michal M, Kazakov DV, Hadravsky L, Kinkor Z, Kuroda N, Michal M. High-grade myxoinflammatory fibroblastic sarcoma: a report of 23 cases. *Ann Diagn Pathol.* (2015) 3:157–63. doi: 10.1016/j.anndiagpath.2015.03.012
17. Tejwani A, Kobayashi W, Chen YL, Rosenberg AE, Yoon S, Raskin KA, et al. Management of acral myxoinflammatory fibroblastic sarcoma. *Cancer.* (2010) 24:5733–9. doi: 10.1002/cncr.25567

Conflict of Interest: The authors declare that the research was conducted in the absence of any commercial or financial relationships that could be construed as a potential conflict of interest.

Publisher's Note: All claims expressed in this article are solely those of the authors and do not necessarily represent those of their affiliated organizations, or those of the publisher, the editors and the reviewers. Any product that may be evaluated in this article, or claim that may be made by its manufacturer, is not guaranteed or endorsed by the publisher.

Copyright © 2022 Wei, Yang, Guo, Chen, Li, Chen and Zhou. This is an open-access article distributed under the terms of the Creative Commons Attribution License (CC BY). The use, distribution or reproduction in other forums is permitted, provided the original author(s) and the copyright owner(s) are credited and that the original publication in this journal is cited, in accordance with accepted academic practice. No use, distribution or reproduction is permitted which does not comply with these terms.



CK5/6 and GATA3 Defined Phenotypes of Muscle-Invasive Bladder Cancer: Impact in Adjuvant Chemotherapy and Molecular Subtyping of Negative Cases

Florestan J. Koll^{1,2,3*}, Alina Schwarz⁴, Jens Köllermann⁴, Severine Banek¹, Luis Kluth¹, Clarissa Wittler¹, Katrin Bankov⁴, Claudia Döring⁴, Nina Becker^{3,4}, Felix K.H. Chun¹, Peter J. Wild^{2,4,5} and Henning Reis^{4*}

OPEN ACCESS

Edited by:

Arndt Hartmann,
Universitätsklinikum Erlangen,
Germany

Reviewed by:

Takuya Koie,
Gifu University, Japan
Fumitaka Koga,
Tokyo Metropolitan Komagome
Hospital, Japan

*Correspondence:

Florestan J. Koll
florestan.johannes.koll@kgu.de
Henning Reis
Henning.reis@kgu.de

Specialty section:

This article was submitted to
Pathology,
a section of the journal
Frontiers in Medicine

Received: 13 February 2022

Accepted: 12 May 2022

Published: 16 June 2022

Citation:

Koll FJ, Schwarz A, Köllermann J, Banek S, Kluth L, Wittler C, Bankov K, Döring C, Becker N, Chun FKH, Wild PJ and Reis H (2022) CK5/6 and GATA3 Defined Phenotypes of Muscle-Invasive Bladder Cancer: Impact in Adjuvant Chemotherapy and Molecular Subtyping of Negative Cases. *Front. Med.* 9:875142. doi: 10.3389/fmed.2022.875142

¹ Department of Urology, University Hospital Frankfurt, Goethe University, Frankfurt, Germany, ² Frankfurt Cancer Institute (FCI), University Hospital, Goethe University, Frankfurt, Germany, ³ University Cancer Center (UCT) Frankfurt, University Hospital, Goethe University, Frankfurt, Germany, ⁴ Dr. Senckenberg Institute of Pathology, University Hospital Frankfurt, Frankfurt, Germany, ⁵ Frankfurt Institute for Advanced Studies, Frankfurt, Germany

Introduction and Objective: Identifying patients that benefit from cisplatin-based adjuvant chemotherapy is a major issue in the management of muscle-invasive bladder cancer (MIBC). The purpose of this study is to correlate “luminal” and “basal” type protein expression with histological subtypes, to investigate the prognostic impact on survival after adjuvant chemotherapy and to define molecular consensus subtypes of “double negative” patients (i.e., without expression of CK5/6 or GATA3).

Materials and Methods: We performed immunohistochemical (IHC) analysis of CK5/6 and GATA3 for surrogate molecular subtyping in 181 MIBC samples. The mRNA expression profiles for molecular consensus classification were determined in CK5/6 and GATA3 (double) negative cases using a transcriptome panel with 19,398 mRNA targets (HTG Molecular Diagnostics). Data of 110 patients undergoing radical cystectomy were available for survival analysis.

Results: The expression of CK5/6 correlated with squamous histological subtype (96%) and expression of GATA3 was associated with micropapillary histology (100%). In the multivariate Cox-regression model, patients receiving adjuvant chemotherapy had a significant survival benefit (hazard ratio [HR]: 0.19 95% confidence interval [CI]: 0.1–0.4, $p < 0.001$) and double-negative cases had decreased OS (HR: 4.07; 95% CI: 1.5–10.9, $p = 0.005$). Double negative cases were classified as NE-like (30%), stroma-rich (30%), and Ba/Sq (40%) consensus molecular subtypes and displaying different histological subtypes.

Conclusion: Immunohistochemical-based classification was associated with histological subtypes of urothelial MIBC. IHC markers like CK5/6 and GATA3 that are used in pathological routine could help to identify patients with basal and luminal

tumor characteristics. However, a two-sided classification system might not sufficiently reflect the heterogeneity of bladder cancer to make treatment decisions. Especially the group of IHC-double negative cases, as further analyzed by mRNA expression profiling, are a heterogeneous group with different implications for therapy.

Keywords: bladder cancer, molecular subtyping, immunohistochemistry, adjuvant chemotherapy, double negative, consensus classification

INTRODUCTION

Bladder cancer (BCa) is the second most common genitourinary malignancy with about 570,000 new cases worldwide every year (1). About 25% of patients present with the muscle-invasive disease at the time of diagnosis and >90% of cases are urothelial carcinomas. The current standard of care for muscle invasive BCa (MIBC) is radical cystectomy with pelvic lymphadenectomy. However, relapse rates after surgery are high and 5-year overall survival (OS) rates are about 43% for pT3-tumors and 25% if the tumor has spread to local lymph nodes (2, 3). Cisplatin-based adjuvant chemotherapy may prolong survival rates and should be offered to patients with pT3/4 and/or pN + tumors (4). Patient selection for adjuvant chemotherapy is based on pathological tumor stage and chemo-eligibility, but no biomarker-based selection criteria for cisplatin-based chemotherapies exist or are included in current guidelines (4). The predictive biomarker-based decisions are needed to identify potential responders to chemotherapy and those that would be unnecessarily exposed to adjuvant therapy toxicities.

In recent years, genomic sequencing techniques have advanced, leading to comprehensive genomic characterization of BCa cohorts. This led to transcriptomic-based molecular subtyping of cancers and drove our understanding of BCa biology (5–9). It has been proposed that patients with basal tumors benefit most of neoadjuvant chemotherapy (NAC), whereas luminal tumors have a better prognosis regardless of the application of NAC (10, 11). However, contradictory results have been published and different nomenclatures, definitions, numbers of molecular subtypes, and inter-/intra-tumoral heterogeneity of BCa have hindered prospective validation and clinical translation.

To facilitate the clinical implementation of subtyping into clinical routine, immunohistochemical (IHC) markers that refer to “basal” and “luminal” molecular subtypes have been proposed (12–14). Guo et al. reported that IHC-staining with GATA3 and CK5/6 can classify the BCa correctly in over 80% of the cases into luminal and basal molecular subtypes. However, it remains unclear to which molecular subtype tumors without GATA3, nor CK5/6 expression (double negative) can be assigned.

In the present study, we explore IHC markers as surrogate markers for molecular subtyping, correlations with histologic subtypes, and impact on survival with adjuvant chemotherapy in a mono-institutional cystectomy cohort of urothelial MIBC. In addition, we performed RNA-sequencing of the group of “double negative” cases (CK5/6 and GATA3 negative), which are a heterogeneous group on the molecular level.

MATERIALS AND METHODS

Cohort

Tissue/tumor samples and patient data used in this study were provided by the University Cancer Center Frankfurt (UCT). The written informed consent was obtained from all patients and the study was approved by the institutional review boards of the UCT and the ethical committee at the University Hospital Frankfurt (project-number: SUG-6-2018 and UCT-53-2021) which was conducted according to local and national regulations and according to the Declaration of Helsinki.

A total of 186 FFPE tissue samples from 181 patients with MIBC treated at the Department of Urology, University Hospital Frankfurt from 2010 to 2020 were retrieved from the archive of the Senckenberg Biobank of the Senckenberg Institute of Pathology.

Clinico-pathological and follow-up data were gathered from medical charts and records of the University Cancer Center and independently reviewed by two authors.

Histopathology of all cases was systematically re-reviewed by two experienced genitourinary pathologists according to current WHO-criteria (15). Histological subtypes were reported if at least 10% of tumor showed subtype histology including pure and mixed tumors.

Immunohistochemical Analysis

For construction of the tissue microarray (TMA), one tissue core (diameter 1 mm) of a representative tumor area was taken from a “donor” block and was arranged in a new “recipient” block using the TMA Grandmaster (3DHISTECH, Budapest, Hungary).

Hematoxylin and eosin stain slides were automatically developed on a Tissue-Tek Prisma Plus staining device (Sakura Finetek, Torrance, CA, United States). All IHC-analyses were conducted using the DAKO Omnis staining system (Agilent, Santa Clara, CA, United States) with the DAKO FLEX-Envision Kit (Agilent) according to manufacturer’s instruction. We performed staining of CK5/6 (Clone: D5/16 B4; ready-to-use kit; Dako/Agilent, Santa Clara, CA, United States) and GATA3 (Clone: L50-823; ready-to-use kit; Cell Marque, Rocklin, CA, United States). IHC “double negative” was defined as negative for expression of CK5/6 and GATA3 and “double positive” was defined as positive for expression of CK5/6 as well as GATA3.

Stained slides were scanned with the Panoramic slide scanner (3DHISTECH, Budapest, Hungary). The quantitative analysis of IHC was annotated by two genitourinary pathologists. TMA cores with either absence of representative tumor tissue or presence of staining artifacts were excluded from the analysis.

RNA Isolation and Molecular Subtype Calling

A 1 mm punch was taken from the FFPE blocks of a representative tumor area with at least 50% tumor content. RNA was isolated using the “truXTRAC FFPE total NA Kit–Column” (Covaris, Woburn, MA, United States) and RNA-concentration was measured by using the QuantiFluor RNA System (Promega, Madison, WI, United States) according to the manufacturer’s protocol. The mRNA expression of 19,398 mRNA targets was determined using the HTG Transcriptome Panel (HTG Molecular Diagnostics, Tucson, AZ, United States) on Illumina NextSeq 550 system (Illumina, San Diego, CA, United States). Gene counts were normalized using median normalization and log2-transformed for further analysis. Sequencing data have been uploaded to the Gene Expression Omnibus (GSE198607). IHC double negative samples were defined as negative for CK5/6 and GATA3 in IHC analyses and classified according to the six molecular consensus classes of MIBC using the R-based consensus MIBC classification tool and the Bioconductor-package for R (6).

Statistical Analysis

We performed descriptive statistics of all data.

For the survival analysis, only patients with radical cystectomy in “curative intent” ($n = 110$) were included to create a homogenous cohort. In total, 71 patients that did not fulfill this requirement were excluded, i.e., no radical cystectomy, with primary metastatic disease, NAC or missing follow up data. We defined the OS as main endpoint of interest, which was defined as time interval between surgery and death. Secondary endpoint was disease-free survival (DFS), defined as time interval between surgery and death due to BCa or recurrence.

Kaplan–Meier method was used to estimate and illustrate survival probabilities. We used uni- and multivariable Cox’s proportional hazards models to estimate the hazard ratio (HR) and corresponding 95% confidence interval (CI) for covariates for OS and DFS. All tests were two-tailed, and a significance level of $\alpha = 5\%$ was used. The statistical analyses were performed using the R Statistical Software (Version 4.1) and R Studio (Version 2021.09.1 + 372).

RESULTS

Patient Characteristics

Overall, we included specimen of 181 patients with MIBC on the TMA. Samples were obtained from transurethral resection of the bladder (TURB) in 86 (47.5%) cases and from cystectomy in 95 (52.5%) cases. The median age was 71 years (IQR: 62–78). A total of 140 (77%) patients were male and 41 (23%) were female. The clinico-pathological details of the cohort are summarized in Table 1.

Immunohistochemical-Classification

176 TMA-Spots were evaluable for the IHC-status of CK5/6 and GATA 3. Cases were classified into CK5/6 positive, GATA3

positive, “double negative” or “double positive” (representative images in Figure 1). CK5/6 positive cases were significantly associated with female gender (63% of tumors of female patients had CK5/6 expression vs. 37% tumors of male patients had CK5/6 expression, $p = 0.004$). CK5/6 positivity correlated with squamous histological subtype (24 of 25 cases [96%] had positive CK5/6 expression), whereas all 9 micropapillary cases were negative for the basal marker CK5/6 and positive for GATA 3 ($p < 0.0001$). All cases with neuroendocrine subtype were double negative. Twelve cases with other histological subtypes were negative for CK5/6, positive for GATA3 in 6 cases (one sarcomatoid, three plasmacytoid, one undifferentiated [giant cell], one glandular), double negative in 4 cases (one clear cell, one sarcomatoid, one undifferentiated [giant cell], one lymphoepithelial), and double positive in 2 cases (one sarcomatoid, one undifferentiated [giant cell]). Correlation of gender, tumor stage, age, and histology subtype with the two IHC markers are shown in Table 2.

Survival Analysis

We assessed survival rates of 110 patients with adequate follow up that received radical cystectomy in curative intent. Median follow-up was 66 months (IQR: 34–98 months). In this group, 35 patients received at least two cycles of adjuvant chemotherapy. Table 3 shows patients characteristics, tumor stage, and IHC markers for patients with and without adjuvant chemotherapy.

Tumor and lymph node stage as well as the application of adjuvant chemotherapy were significantly associated with OS (Figure 2 and Supplementary Figures 1, 2). The 12-month OS and DFS rates were 49% and 41 without and 77 and 62% with adjuvant chemotherapy, respectively.

In the total cohort, neither IHC markers (CK5/6, GATA3) nor the histological subtype were significantly associated with OS or DFS (Table 4 and Supplementary Figure 3). After stratification for patients receiving only the cystectomy vs. patients receiving an adjuvant chemotherapy, expression of CK5/6 had a HR of

TABLE 1 | Clinico-pathological details of 181 patients on the TMA analyzed for histological subtype of urothelial carcinoma and immunohistochemistry.

Median Age (IQR)		71 (62–78)
Gender	Male	140 (77%)
	Female	41 (23%)
Max. tumor-Stage	pT2	87 (48%)
	pT3	67 (37%)
	pT4	27 (15%)
	NOS	131 (72%)
Histological subtype on TMA spot	Squamous	25 (14%)
	Micropapillary	9 (5%)
	Neuroendocrine	4 (2%)
	Sarcomatoid	3 (2%)
	Plasmacytoid	3 (2%)
	Other (1 lymphoepithelial, 1 clear cell, 1 glandular, 3 giant cell)	6 (3%)

IQR, interquartile range; NOS, not otherwise specified; TMA, tissue micro array.

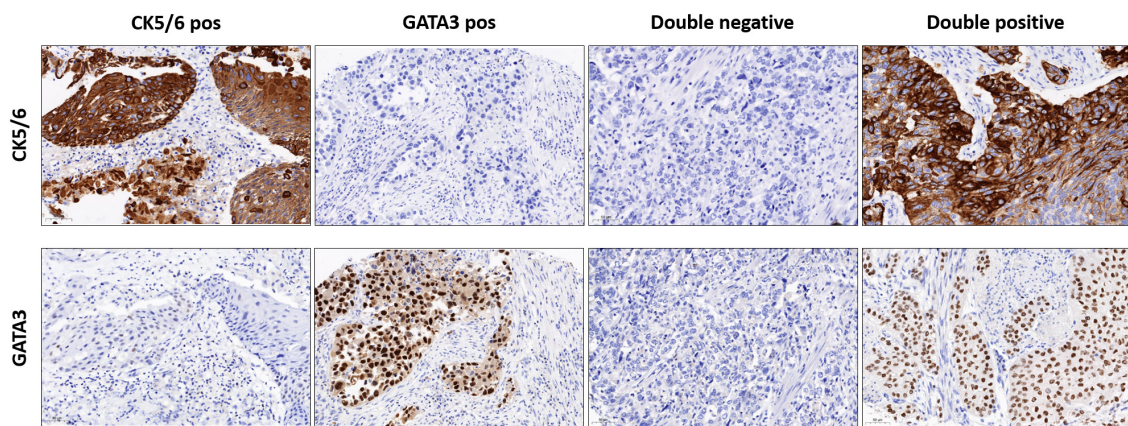


FIGURE 1 | Representative images of IHC staining of CK5/6 positive, GATA 3 positive, double negative, and double positive cases (magnification 200 ×).

TABLE 2 | Association of clinic-pathological findings with the IHC-markers CK5/6 and GATA3.

		<i>n</i> (%)	CK5/6 positive (<i>n</i> = 32)	GATA3 positive (<i>n</i> = 81)	Double negative (<i>n</i> = 17)	Double positive (<i>n</i> = 46)	<i>p</i>
Age	<70	73 (41%)	15 (47%)	29 (36%)	9 (53%)	20 (44%)	0.5
	≥70	103 (59%)	17 (53%)	52 (64%)	8 (47%)	26 (15%)	
Gender	Male	135 (77%)	23 (72%)	67 (83%)	16 (94%)	29 (63%)	0.021
	Female	41 (23%)	9 (28%)	14 (17%)	1 (6%)	17 (37%)	
Max. Tumor-Stage	pT2	83 (47%)	11 (34%)	45 (56%)	8 (47%)	19 (41%)	0.138
	pT3	66 (38%)	18 (56%)	23 (28%)	5 (29%)	20 (44%)	
	pT4	27 (15%)	3 (10%)	13 (16%)	4 (24%)	7 (15%)	
Histological subtype	NOS	127 (72%)	18 (59%)	65 (80%)	10 (59%)	34 (74%)	<0.0001
	Squamous	25 (14%)	14 (44%)	1 (1%)	0	10 (22%)	
	Micropapillary	9 (5%)	0	9 (11%)	0	0	
	Neuroendocrine	3 (2%)	0	0	3 (18%)	0	
	Sarcomatoid	3 (2%)	0	1 (1%)	1 (6%)	1 (2%)	
	Plasmacytoid	3 (2%)	0	3 (4%)	0	0	
	Undifferentiated (giant cell)	3 (2%)	0	1 (1%)	1 (6%)	1 (2%)	
	Glandular	1 (0.6%)	0	1 (1%)	0	0	
	Clear cell	1 (0.6%)	0	0	1 (6%)	0	
	Lymphoepithelial	1 (0.6%)	0	0	1 (6%)	0	

A total of 176 spots were evaluated. The *p*-values were calculated using Pearson–Chi square test. NOS, not otherwise specified. Bold values indicate significant differences with *p*-values < 0.05.

0.4 (95% CI: 0.2–1.2, *p* = 0.09) in the adjuvant chemotherapy group. A multivariate cox-regression model adjusting for tumor and lymph node (LN) stage, adjuvant chemotherapy, and IHC-staining is shown in **Figure 3**. In addition to tumor- and LN stage, the double negative cases were associated with an increased risk of death (*HR*: 4.07; 95% CI: 1.5–10.9, *p* = 0.005). Adjuvant chemotherapy was associated with the survival benefit (*HR*: 0.19; 95% CI: 0.10–0.36, *p* < 0.001). The multivariate cox-regression model for DFS is shown in the **Supplementary Material**.

Molecular Analysis of CK5/6 and GATA3 Negative Cases

Ten double negative cases were analyzed using the HTG Transcriptome Panel and molecular subtypes were determined according to the consensus classification of Kamoun et al. (6).

Three cases were classified as stroma-rich, three as NE-like and four as Ba/Sq. **Table 5** shows molecular subtypes with histological subtype and pathological stage. The Ba/Sq cases showed heterogeneous histology with lymphoepithelial, undifferentiated (giant cell) and sarcomatoid subtypes. According to the UNC classification system, all cases were classified as basal (8). And according to the TCGA classification system, cases were classified as basal-squamous and neuronal (5). Representative HE-stained pictures of histological subtype and their molecular subtype are shown in **Figure 4**.

DISCUSSION

This study shows a high concordance of an IHC-subclassification based on the two markers CK5/6 and GATA3 with histological

TABLE 3 | Characteristics of patients with and without adjuvant chemotherapy.

		CE only <i>n</i> = 75	Adjuvant Chemotherapy <i>n</i> = 35	<i>p</i>
Age (IQR)		72 (64.25–76.75)	60 (52.75–71)	
Age	<71	32 (43%)	26 (74%)	0.002
	≥71	43 (57%)	9 (26%)	
Gender	Male	59 (79%)	28 (80%)	1.0
	Female	16 (21%)	7 (20%)	
Stage Max.	pT2	23 (31%)	5 (14%)	0.12
	pT3	37 (49%)	24 (69%)	
	pT4	15 (20%)	6 (17%)	
Lymph node status	pN0	42 (56%)	13 (37%)	0.084
	pN1 + pNx	33 (44%)	22 (63%)	
R-Status	R0	60 (80%)	28 (80%)	1.0
	R1/R2/Rx	15 (20%)	7 (20%)	
Histological subtype	NOS	57 (77%)	23 (66%)	0.39
	Squamous	8 (11%)	4 (11%)	
	Micropapillary	5 (7%)	2 (6%)	
	Neuroendocrine	1 (1%)	2 (6%)	
	Other	3 (4%)	4 (11%)	
Type of chemotherapy	Gem/Cis		28 (80%)	
	Gem/Carbo		4 (11%)	
	Platin/Etoposid		2 (6%)	
	other		1 (3%)	
Recurrence	No	54 (72%)	18 (51%)	0.058
	Yes	21 (28%)	17 (49%)	
CK5/6 + GATA3	CK5/6 pos	14 (19%)	5 (15%)	0.45
	GATA 3 pos	36 (48%)	13 (38%)	
	Double neg	7 (9%)	6 (18%)	
	Double pos	18 (24%)	10 (29%)	

CE, cystectomy; NOS, not otherwise specified; Gem/Cis, gemcitabine/cisplatin; Gem/Carbo, gemcitabine/carboplatin; R-Status, resection status. Bold values indicate significant differences with *p*-values < 0.05.

subtypes in MIBC. Double negative patients without expression of CK5/6 nor GATA3 had decreased OS rates. Subtyping of double negative cases revealed a histological and molecular heterogeneous subgroup. Strengths of our study are the

pathological re-review of all cases, evaluation of standardized IHC-staining, the use of a broad transcriptome panel for molecular phenotyping, and the analysis of adjuvant chemotherapy in a clinically well-annotated cohort of patients with MIBC.

The use of molecular subtyping to guide the selection of systemic therapies has been proposed for NAC and immune checkpoint inhibitors (7, 10, 16). However, contradictory results published in the past years and the diversity of molecular subtype taxonomy until the publication of the consensus classification have hindered the use and clinical translation (6, 17–19). Data to provide guidance to select patients for adjuvant chemotherapy based on molecular subtypes are sparse.

It has been suggested that CK5/6 and GATA3 expression can identify basal and luminal molecular subtypes in 80–90% of cases which could be a useful tool in routine pathological assessments to identify the basic molecular subtypes of BCa (12). Other studies using more markers confirmed a good correlation of IHC-based subtyping with gene expression-based subtypes (determined by targeted NanoString panels), but still with a risk of differing classification in about 15–20% of cases (13, 20).

Our results show that CK5/6 expression was associated with squamous histological subtype and female gender, which

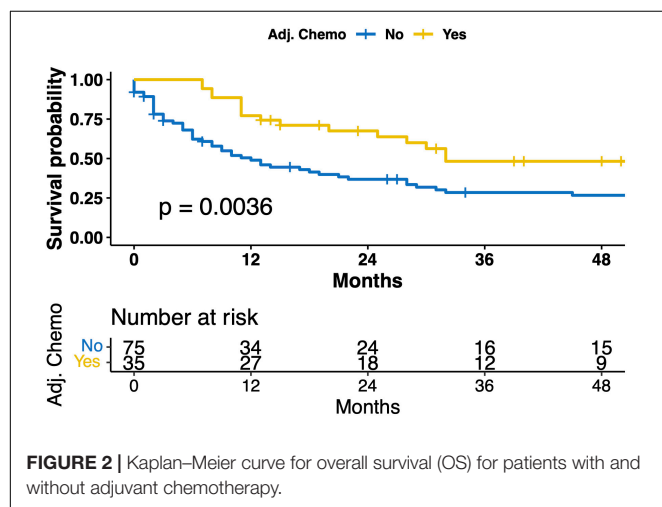
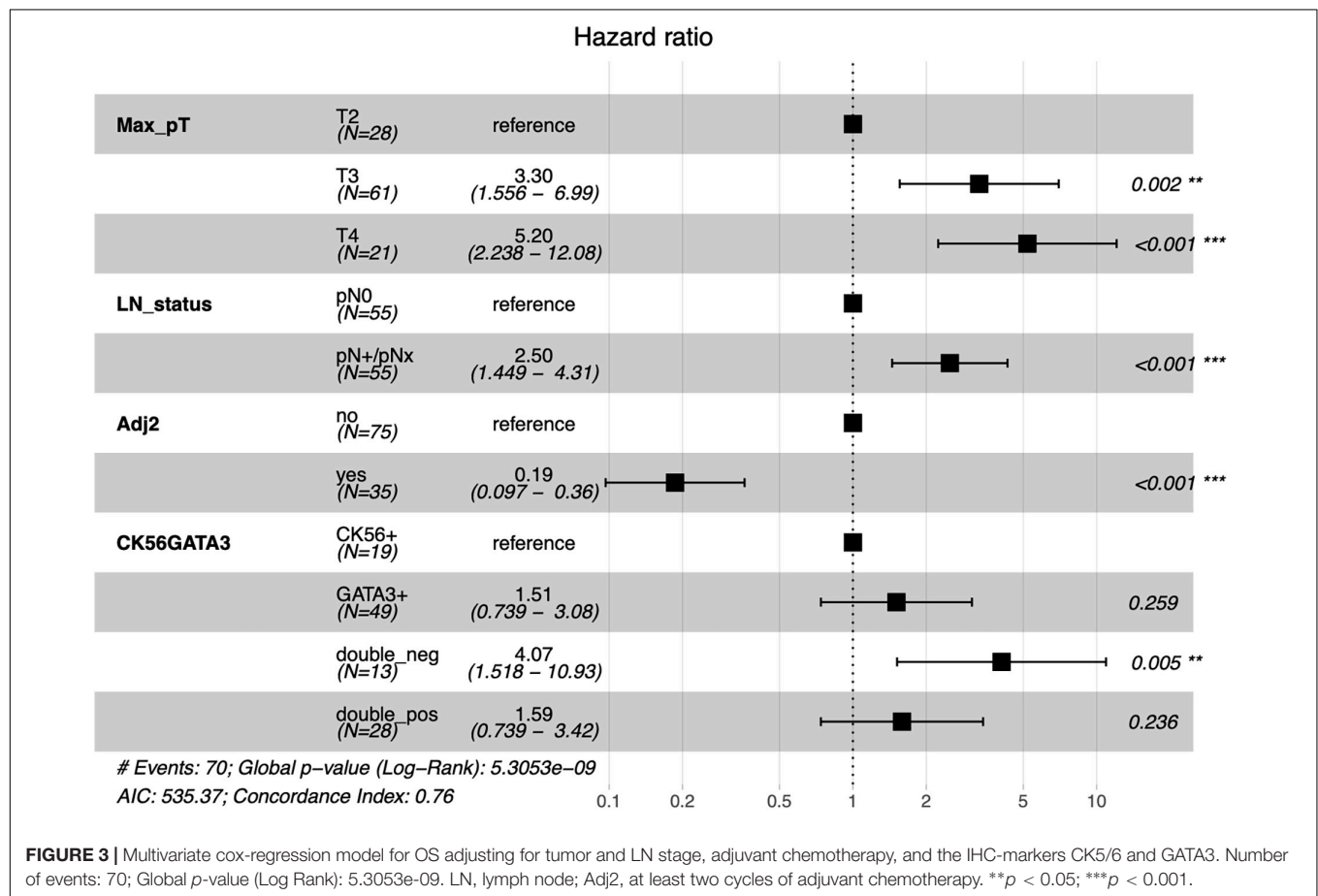


TABLE 4 | Univariate cox-regression model for histological subtype and IHC-markers CK5/6 and GATA3 stratified for patients with and without adjuvant chemotherapy.

		Total cohort (n = 110)	p	Adjuvant chemotherapy (n = 35)	p	CE only (n = 75)	p
Histological subtype on TMA	NOS	Reference		Reference		Reference	
	Squamous	0.8 (0.3–1.7)	0.5	0.4 (0.06–3.4)	0.6	0.9 (0.4–2.2)	0.9
	Micropapillary	1.2 (0.5–3.1)	0.7	2.9 (0.6–13.1)	0.2	0.89 (0.3–2.9)	0.9
	Neuroendocrine	0.9 (0.2–4.1)	0.9	1.8 (0.2–14.1)	0.6	NA	
	Other	0.7 (0.3–1.9)	0.5	0.9 (0.2–4.2)	0.9	0.8 (0.2–3.5)	0.8
CK56	Pos	0.9 (0.5–1.4)	0.5	0.4 (0.2–1.2)	0.09	1.1 (0.7–1.9)	0.7
GATA3	Pos	0.8 (0.5–1.3)	0.3	0.7 (0.3–1.8)	0.4	0.8 (0.4–1.4)	0.4
CK56 + GATA3	CK56 pos	Reference		Reference			
	GATA3 pos	1.0 (0.5–2.0)	0.9	1.9 (0.4–8.8)	0.4	0.9 (0.4–1.8)	0.71
	Double neg	1.6 (0.7–3.7)	0.3	0.3 (0.5–16.7)	0.2	1.7 (0.6–4.7)	0.31
	Double pos	1.0 (0.5–2.1)	1.0	1.1 (0.1–5.0)	0.8	1.3 (0.6–2.8)	0.59

CE, cystectomy; NOS, not otherwise specified.

**FIGURE 3 |** Multivariate cox-regression model for OS adjusting for tumor and LN stage, adjuvant chemotherapy, and the IHC-markers CK5/6 and GATA3. Number of events: 70; Global p-value (Log Rank): 5.3053e-09. LN, lymph node; Adj2, at least two cycles of adjuvant chemotherapy. ** $p < 0.05$; *** $p < 0.001$.

is in concordance with published data (6, 13). The same applies to the positive correlation between GATA3-expression and micropapillary histological subtype. Four cases with neuroendocrine histological subtype were double negative in IHC-analyses.

To test the two-marker-based IHC-classification for its predictive value of chemotherapy efficacy, we performed analyses in the cohort of adjuvant-treated patients. We are aware, that our survival analyses, which demonstrated a significant

benefit for patients receiving adjuvant chemotherapy, hold the risk of selection bias since patients receiving chemotherapy were younger and kidney function or comorbidities were not considered. However, when analyzing only patients receiving chemotherapy, none of the markers predicted survival, but cases expressing the basal marker CK5/6 tend to have improved survival with adjuvant chemotherapy, with the level of significance missed (HR 0.42 95% KI 0.15–1.2, $p = 0.09$). These results are in line with the available data for NAC

TABLE 5 | Description of double negative cases analyzed for mRNA expression profiles, including histological subtypes on TMA and whole slide, and molecular subtypes according to the consensus, UNC, and TCGA (5) classifier.

Patient	Age at surgery	Gender	Max. pT stage	LN metastases	Predominant histological subtype on TMA	Histological subtype on whole slide	Adjuvant chemotherapy	Consensus class	UNC subtype	TCGA subtype
001_069	68	m	3b	Yes	Lymphoepithelial	Lymphoepithelial	Yes	Ba/Sq	Basal	Basal_squamous
001_004	71	m	4a	No	Undifferentiated/Giant cell	Undifferentiated/Giant cell	No	Ba/Sq	Basal	Basal_squamous
001_033	71	m	3b	Yes	NOS	NOS + Squamous	No	Ba/Sq	Basal	Basal_squamous
001_039	60	m	2b	Yes	Sarcomatoid	Sarcomatoid	Yes	Ba/Sq	Basal	Basal_squamous
001_012	57	m	4b	Yes	NOS	NOS	Yes	Stroma-rich	Basal	Basal_squamous
001_040	78	m	4a	Yes	NOS	NOS	Yes	Stroma-rich	Basal	Basal_squamous
001_065	70	m	4a	No	NOS	NOS + Pseudoglandular	No	Stroma-rich	Basal	Basal_squamous
001_021	62	m	3b	No	NOS	Neuroendocrine	Yes	NE-like	Basal	Neuronal
001_050	62	m	3b	Yes	Neuroendocrine	Neuroendocrine	Yes	NE-like	Basal	Neuronal
001_071	67	m	2b	No	Neuroendocrine	Neuroendocrine	No	NE-like	Basal	Neuronal

Ba/Sq, basal/squamous; m, male; NE, neuroendocrine; NOS, not otherwise specified; UNC, University of North Carolina; TCGA, the cancer genome atlas.

proposing that patients with basal-like tumors respond better to chemotherapy, whereas luminal-like tumors have an inferior response to chemotherapy.

For the neoadjuvant setting, Seiler and colleagues developed a single-sample genomic subtyping classifier to subdivide patients into four groups revealing that patients with basal tumors had the most improvement in OS with NAC compared with surgery alone (10). More recent studies showed similar results for non-luminal tumors (11, 20). Contrary results from Sjö Dahl and colleagues as well as Taber and colleagues, however, indicated that basal tumors less frequently respond to NAC and according to Kamoun and colleagues, the consensus molecular subtypes do not correlate with response to NAC (6, 17, 18). Therefore, further research will have to clarify the role of molecular subtypes as predictive markers of chemotherapy efficacy.

In addition to the findings in cases with IHC expression of at least one marker, we detected a subgroup of double negative cases without expression of CK5/6 or GATA3. The cohort seems to be of biological significance, as patients in this group had an increased risk of death in multivariate analysis. This finding has recently been described also by other groups (13, 14). However, no detailed molecular analyses were reported, as no full transcriptomic analyses were performed (12, 13). We, therefore, conducted further molecular analyses of the double negative group using an mRNA transcriptome panel covering approximately 19,300 targets, thus enabling us to call consensus class molecular subtypes.

Double negative cases tended to be molecularly basal-like according to the UNC classifier but are more heterogeneous than a two-tailed-classification can represent. Three molecular subtypes (Ba/Sq, stroma-rich, neuronal) and five histological subtypes (NOS, neuroendocrine, sarcomatoid, undifferentiated/giant cell, lymphoepithelioma-like) were present in this group. This highlights the heterogeneity of double negative cases and implicates that a more complex system than a two-tailed classification might be needed for more individualized treatment decisions. For example, the (molecular and histological) neuroendocrine subtype is known to have a poor prognosis and thus should be treated aggressively with upfront chemotherapy and might be responsive to immune checkpoint inhibition (4, 16). On the other hand, the lymphoepithelioma-like subtype of urothelial carcinoma is associated with a more favorable prognosis and might be more responsive to immune checkpoint inhibition as proposed by the results of the PURE-1 trial (21, 22). The well-known fact of intra-tumoral heterogeneity in urothelial BCa adds to these facts.

The limitations of our study are the retrospective design and the low number of molecular analyses. Due to low numbers, we did not include patients receiving NAC in our survival analysis. Selecting patients for NAC, which is the recommended treatment for MIBC, might be of higher clinical relevance than for adjuvant chemotherapy. In addition, we performed two IHC-marker analyses only to surrogate basal and luminal molecular subtypes. However, this was intentionally done to create comparability with the literature. Other studies using more markers for protein-based subtyping reported similar

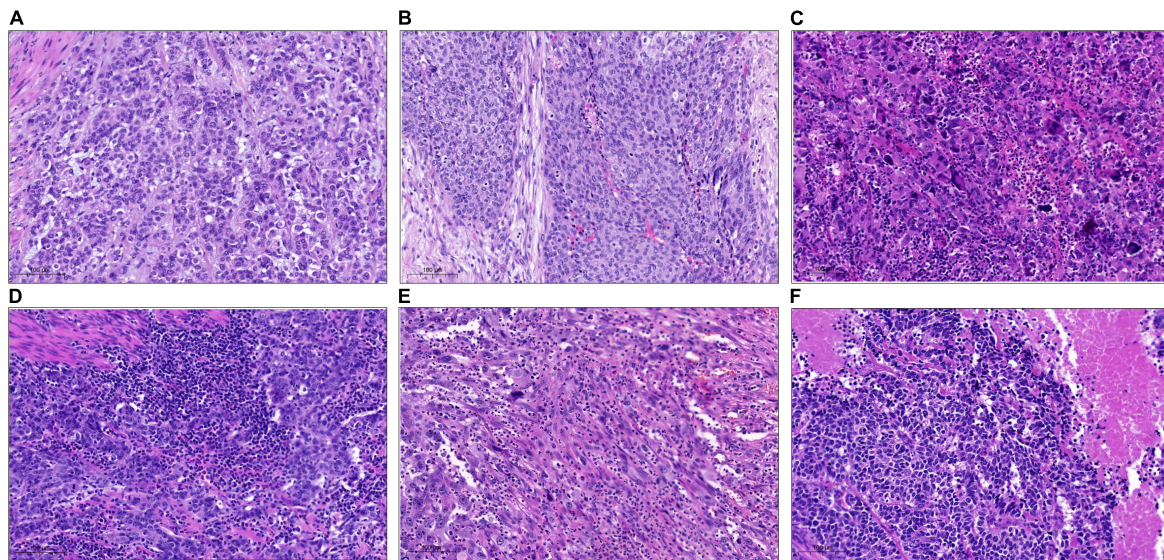


FIGURE 4 | Representative pictures of different histological subtypes on the whole slides classified as double negative in tissue micro array (TMA)-analysis and their molecular consensus subtypes. **(A)** Histological subtype: NOS; molecular Subtype: Stroma-rich. **(B)** Histological subtype: NOS (+ squamous on whole slide); molecular subtype: Ba/Sq. **(C)** Histological subtype: poorly differentiated/giant cell; molecular subtype: Ba/Sq. **(D)** Histological subtype: lymphoepithelial; molecular subtype: Ba/Sq. **(E)** Histological subtype: sarcomatoid; molecular subtype: Ba/Sq. **(F)** Histological subtype: neuroendocrine; molecular subtype: NE-like. Ba/Sq, basal/squamous; NE, neuroendocrine; NOS, not otherwise specified.

results with high concordance of histological subtypes and IHC, but also demonstrated that protein-based subtyping did not predict survival in population-based cystectomy cohorts (13, 19). Thus, the question remains if a limited protein-based assessment of surrogate markers for molecular subtypes can serve as a predictor for chemotherapy response or if mRNA-expression profiles are necessary for adequate determination of molecular subtypes or other markers like immune cell infiltration are necessary for patient selection (18). So far, the histopathological staging remains the most important prognostic factor (23). However, efforts to bring the results of the large transcriptomic studies into a clinical routine are underway (24).

In conclusion, we demonstrated that an IHC-based classification was associated with histological subtypes of urothelial MIBC. Although IHC markers used in pathological routine might help to identify patients with basal and luminal tumor characteristics, a two-sided classification system might not sufficiently reflect the heterogeneity of BCa to guide treatment decisions. Especially the group of IHC-double negative cases is a heterogeneous group with different implications for therapy.

DATA AVAILABILITY STATEMENT

The datasets presented in this study can be found in online repositories. The names of the repository/repositories and accession number(s) can be found below: The gene expression omnibus (GEO) with accession GSE198607 (<https://www.ncbi.nlm.nih.gov/geo/query/acc.cgi?acc=GSE198607>).

ETHICS STATEMENT

Written informed consent was obtained from all patients, and the study was approved by the Institutional Review Boards of the UCT and the Ethical Committee at the University Hospital Frankfurt (project numbers: SUG-6-2018 and UCT-53-2021).

AUTHOR CONTRIBUTIONS

FK, HR, and PW contributed to conception and design of the study. FK, LK, SB, CW, AS, and KB organized the database and samples. AS, NB, KB, JK, HR, and PW performed data curation and formal analysis. FK and CD performed the statistical analysis and analysis of sequencing data. AS, NB, and KB performed IHC. FK wrote the first draft of the manuscript. HR, PW, and FC performed review and editing of the manuscript and supervision. All authors contributed to manuscript revision, read, and approved the submitted version.

FUNDING

Florestan Koll was funded by the Mildred Scheel Career Center Frankfurt (Deutsche Krebsstiftung).

SUPPLEMENTARY MATERIAL

The Supplementary Material for this article can be found online at: <https://www.frontiersin.org/articles/10.3389/fmed.2022.875142/full#supplementary-material>

REFERENCES

- Sung H, Ferlay J, Siegel RL, Laversanne M, Soerjomataram I, Jemal A, et al. Global cancer statistics 2020: GLOBOCAN estimates of incidence and mortality worldwide for 36 cancers in 185 countries. *CA*. (2021) 71:209–49. doi: 10.3322/caac.21660
- Hautmann RE, Gschwend JE, de Petriconi RC, Kron M, Volkmer BG. Cystectomy for transitional cell carcinoma of the bladder: results of a surgery only series in the neobladder era. *J Urol*. (2006) 176:486–92.
- Stein JP, Lieskovsky G, Cote R, Groshen S, Feng AC, Boyd S, et al. Radical cystectomy in the treatment of invasive bladder cancer: long-term results in 1,054 patients. *J Clin Oncol*. (2001) 19:666–75. doi: 10.1200/JCO.2001.19.3.666
- Witjes JA, Bruins HM, Cathomas R, Comperat EM, Cowan NC, Gakis G, et al. European association of urology guidelines on muscle-invasive and metastatic bladder cancer: summary of the 2020 guidelines. *Eur Urol*. (2021) 79:82–104.
- Robertson AG, Kim J, Al-Ahmadie H, Bellmunt J, Guo G, Cherniack AD, et al. Comprehensive molecular characterization of muscle-invasive bladder cancer. *Cell*. (2017) 171:540–56.e25.
- Kamoun A, de Reynies A, Allory Y, Sjodahl G, Robertson AG, Seiler R, et al. A consensus molecular classification of muscle-invasive bladder cancer. *Eur Urol*. (2019) 77:420–33.
- Choi W, Porten S, Kim S, Willis D, Plimack ER, Hoffman-Censits J, et al. Identification of distinct basal and luminal subtypes of muscle-invasive bladder cancer with different sensitivities to frontline chemotherapy. *Cancer Cell*. (2014) 25:152–65. doi: 10.1016/j.ccr.2014.01.009
- Damrauer JS, Hoadley KA, Chism DD, Fan C, Tiganelli CJ, Wobker SE, et al. Intrinsic subtypes of high-grade bladder cancer reflect the hallmarks of breast cancer biology. *Proc Natl Acad Sci USA*. (2014) 111:3110–5. doi: 10.1073/pnas.1318376111
- Sjodahl G, Lauss M, Lovgren K, Chebil G, Gudjonsson S, Veerla S, et al. A molecular taxonomy for urothelial carcinoma. *Clin Cancer Res*. (2012) 18:3377–86. doi: 10.1158/1078-0432.CCR-12-0077-T
- Seiler R, Ashab HAD, Erho N, van Rhijn BWG, Winters B, Douglas J, et al. Impact of molecular subtypes in muscle-invasive bladder cancer on predicting response and survival after neoadjuvant chemotherapy. *Eur Urol*. (2017) 72:544–54. doi: 10.1016/j.eururo.2017.03.030
- Lotan Y, de Jong JJ, Liu VYT, Bismar TA, Boorjian SA, Huang HC, et al. Patients with muscle-invasive bladder cancer with nonluminal subtype derive greatest benefit from platinum based neoadjuvant chemotherapy. *J Urol*. (2021) 207:541–50. doi: 10.1097/JU.0000000000002261
- Guo CC, Bondaruk J, Yao H, Wang Z, Zhang L, Lee S, et al. Assessment of luminal and basal phenotypes in bladder cancer. *Sci Rep*. (2020) 10:9743. doi: 10.1038/s41598-020-66747-7
- Weyerer V, Stoehr R, Bertz S, Lange F, Geppert CI, Wach S, et al. Prognostic impact of molecular muscle-invasive bladder cancer subtyping approaches and correlations with variant histology in a population-based mono-institutional cystectomy cohort. *World J Urol*. (2021) 39:4011–9. doi: 10.1007/s00345-021-03788-1
- Bejrananda T, Kanjanapradit K, Saetang J, Sangkhathat S. Impact of immunohistochemistry-based subtyping of GATA3, CK20, CK5/6, and CK14 expression on survival after radical cystectomy for muscle-invasive bladder cancer. *Sci Rep*. (2021) 11:21186. doi: 10.1038/s41598-021-00628-5
- Moch H, Ulbright TM, Reuter VE. *WHO Classification of Tumours of the Urinary System and Male Genital Organs*. Lyon: International Agency for Research on Cancer (2016).
- Kim J, Kwiatkowski D, McConkey DJ, Meeks JJ, Freeman SS, Bellmunt J, et al. The cancer genome atlas expression subtypes stratify response to checkpoint inhibition in advanced urothelial cancer and identify a subset of patients with high survival probability. *Eur Urol*. (2019) 75:961–4. doi: 10.1016/j.eururo.2019.02.017
- Sjodahl G, Abrahamsson J, Holmsten K, Bernardo C, Chebil G, Eriksson P, et al. Different responses to neoadjuvant chemotherapy in urothelial carcinoma molecular subtypes. *Eur Urol*. (2021) 81:523–32.
- Taber A, Christensen E, Lamy P, Nordentoft I, Prip F, Lindskrog SV, et al. Molecular correlates of cisplatin-based chemotherapy response in muscle invasive bladder cancer by integrated multi-omics analysis. *Nat Commun*. (2020) 11:4858.
- Kollberg P, Chebil G, Eriksson P, Sjodahl G, Liedberg F. Molecular subtypes applied to a population-based modern cystectomy series do not predict cancer-specific survival. *Urol Oncol*. (2019) 37:791–9. doi: 10.1016/j.urolonc.2019.04.010
- Font A, Domenech M, Benitez R, Rava M, Marques M, Ramirez JL, et al. Immunohistochemistry-based taxonomical classification of bladder cancer predicts response to neoadjuvant chemotherapy. *Cancers (Basel)*. (2020) 12:1784. doi: 10.3390/cancers12071784
- Amin MB. Histological variants of urothelial carcinoma: diagnostic, therapeutic and prognostic implications. *Mod Pathol*. (2009) 22(Suppl. 2):S96–118. doi: 10.1038/modpathol.2009.26
- Necchi A, Raggi D, Gallina A, Madison R, Colecchia M, Luciano R, et al. Updated results of PURE-01 with preliminary activity of neoadjuvant pembrolizumab in patients with muscle-invasive bladder carcinoma with variant histologies. *Eur Urol*. (2020) 77:439–46. doi: 10.1016/j.eururo.2019.10.026
- Morera DS, Hasanali SL, Belew D, Ghosh S, Klaassen Z, Jordan AR, et al. Clinical parameters outperform molecular subtypes for predicting outcome in bladder cancer: results from multiple cohorts including TCGA. *J Urol*. (2020) 203:62–72. doi: 10.1097/JU.0000000000000351
- Olah C, Hahnen C, Nagy N, Musial J, Varadi M, Nyiro G, et al. A quantitative polymerase chain reaction based method for molecular subtype classification of urinary bladder cancer-Stromal gene expressions show higher prognostic values than intrinsic tumor genes. *Int J Cancer*. (2021) 150:856–67. doi: 10.1002/ijc.33809

Conflict of Interest: Sequencing was performed as part of a collaboration agreement with HTG Molecular Diagnostics.

The authors declare that the research was conducted in the absence of any commercial or financial relationships that could be construed as a potential conflict of interest.

Publisher's Note: All claims expressed in this article are solely those of the authors and do not necessarily represent those of their affiliated organizations, or those of the publisher, the editors and the reviewers. Any product that may be evaluated in this article, or claim that may be made by its manufacturer, is not guaranteed or endorsed by the publisher.

Copyright © 2022 Koll, Schwarz, Köllermann, Banek, Kluth, Wittler, Bankov, Döring, Becker, Chun, Wild and Reis. This is an open-access article distributed under the terms of the Creative Commons Attribution License (CC BY). The use, distribution or reproduction in other forums is permitted, provided the original author(s) and the copyright owner(s) are credited and that the original publication in this journal is cited, in accordance with accepted academic practice. No use, distribution or reproduction is permitted which does not comply with these terms.



The Role of Chronic Liver Diseases in the Emergence and Recurrence of Hepatocellular Carcinoma: An Omics Perspective

Sofia Zanutti^{1†}, Gina F. Boot^{2†}, Mairene Coto-Llerena^{2,3}, John Gallon², Gabriel F. Hess⁴, Savas D. Soysal⁴, Otto Kollmar⁴, Charlotte K. Y. Ng^{5,6,7} and Salvatore Piscuoglio^{2,3*}

¹Anatomic Pathology Unit, IRCCS Humanitas University Research Hospital, Milan, Italy, ²Visceral Surgery and Precision Medicine Research Laboratory, Department of Biomedicine, University of Basel, Basel, Switzerland, ³Institute of Medical Genetics and Pathology, University Hospital Basel, Basel, Switzerland, ⁴Clarunis, University Center for Gastrointestinal and Liver Diseases, St. Clara Hospital and University Hospital Basel, Basel, Switzerland, ⁵Department for BioMedical Research, University of Bern, Bern, Switzerland, ⁶Swiss Institute of Bioinformatics, Lausanne, Switzerland, ⁷Bern Center for Precision Medicine, Bern, Switzerland

OPEN ACCESS

Edited by:

Arndt Hartmann,
Universitätsklinikum
Erlangen, Germany

Reviewed by:

Antonio Sica,
University of Eastern Piedmont, Italy
Stefano Caruso,
Université Paris-Est Créteil Val de
Marne, France

*Correspondence:

Salvatore Piscuoglio
s.piscuoglio@unibas.ch

[†]These authors have contributed
equally to this work

Specialty section:

This article was submitted to
Pathology,
a section of the journal
Frontiers in Medicine

Received: 03 March 2022

Accepted: 23 May 2022

Published: 24 June 2022

Citation:

Zanutti S, Boot GF, Coto-Llerena M,
Gallon J, Hess GF, Soysal SD,
Kollmar O, Ng CKY and Piscuoglio S
(2022) The Role of Chronic Liver
Diseases in the Emergence and
Recurrence of Hepatocellular
Carcinoma: An Omics Perspective.
Front. Med. 9:888850.
doi: 10.3389/fmed.2022.888850

Hepatocellular carcinoma (HCC) typically develops from a background of cirrhosis resulting from chronic inflammation. This inflammation is frequently associated with chronic liver diseases (CLD). The advent of next generation sequencing has enabled extensive analyses of molecular aberrations in HCC. However, less attention has been directed to the chronically inflamed background of the liver, prior to HCC emergence and during recurrence following surgery. Hepatocytes within chronically inflamed liver tissues present highly activated inflammatory signaling pathways and accumulation of a complex mutational landscape. In this altered environment, cells may transform in a stepwise manner toward tumorigenesis. Similarly, the chronically inflamed environment which persists after resection may impact the timing of HCC recurrence. Advances in research are allowing an extensive epigenomic, transcriptomic and proteomic characterization of CLD which define the emergence of HCC or its recurrence. The amount of data generated will enable the understanding of oncogenic mechanisms in HCC from the CLD perspective and provide the possibility to identify robust biomarkers or novel therapeutic targets for the treatment of primary and recurrent HCC. Importantly, biomarkers defined by the analysis of CLD tissue may permit the early detection or prevention of HCC emergence and recurrence. In this review, we compile the current omics based evidence of the contribution of CLD tissues to the emergence and recurrence of HCC.

Keywords: hepatocellular carcinoma, chronic liver disease, genomics, epigenetics, transcriptomics, proteomics, metabolomics

INTRODUCTION

Despite the extensive characterization of the molecular landscape of hepatocellular carcinoma (HCC), the mechanisms through which the liver tissue drives the emergence and recurrence of HCC remain poorly understood. The most common etiologies of chronic liver disease (CLD) are chronic hepatitis B or C viral infection (HBV and HCV, respectively), alcohol-related liver disease (ALD), and non-alcoholic fatty liver disease (NAFLD) (1, 2). The unresolved

inflammation associated with CLD often leads to fibrosis and subsequent cirrhosis, characterized by a buildup of scar tissue in the liver. Moreover, the resulting oxidative stress, through generation of reactive oxygen and nitrogen species in proliferating hepatocytes, as well as inflammatory cells responding to molecules released by damaged hepatocytes, promotes an environment that accelerates malignant transformation and survival of hepatocytes (3).

Despite surgical treatment in HCC yielding high survival outcomes at 5 years, the incidence of intrahepatic recurrence after curative resection remains unsatisfactory at 70% (1). Whereas, early recurrences (<2 years) typically arise from micrometastases following resection, late recurrences (>2 years) are consistent with a phenomenon known as the “field effect,” where *de novo* tumors arise due to an inflammatory carcinogenic microenvironment (4). In recent years, the focus of next generation sequencing profiling has shifted from delineating genomic biomarkers in tumoral tissue to acquiring a multi-omic overview of the tumor microenvironment (TME) and the characterization of the contribution of CLD tissue to HCC development. This review summarizes the current omics knowledge about HCC emergence and recurrence by investigating the putative involvement of CLD tissues.

THE ROLE OF CHRONIC LIVER DISEASE IN HCC EMERGENCE

The Role of the Genetic Landscape in CLD in HCC Emergence

Several monogenic diseases trigger the development of cirrhosis and increase the risk for CLD-HCC initiation. These diseases are characterized by germline mutations of genes including *HFE1* (encoding MHC-I like molecules (5), *ATP7B* liver copper homeostasis (6), *FAH* [required during the tyrosine catabolic pathway (7), *UROD* essential for heme biosynthesis (8)], glucose-6-phosphatase (G6Pase) (9, 10) and *SERPINA1* [cofactor for TTR expression (11, 12)]. In addition, numerous single-nucleotide polymorphisms (SNPs) have been reported to be associated with HCC development (13). HCC-associated SNPs are not by themselves pathogenic *per se*, but require an additional cause of CLD. For example, the interplay between aflatoxin B1, HBV and SNPs of *GSTM1* and *GSTT1* (null alleles) increases the risk of HCC emergence (14). While SNP of *PNPLA3* (rs738409) is strongly associated with CLD (ALD and NAFLD) related HCC (15–17), its contribution is minor in HCC promoted by HCV infection (18, 19). Interestingly, in the context of hepatic fibrosis, cells overexpressing *PNPLA3* promoted immune cells chemotaxis (monocytes and macrophages) as compared to their wild type *PNPLA3* carriers (20). In addition to SNP of *PNPLA3* (rs738409), SNPs in *TM6SF2* (rs58542926), and *HSD17B13* (rs72613567) increase and decrease the risk of alcohol-related cirrhosis HCC, respectively (21). Whereas, SNPs in *WNT3A-WNT9A* (rs708113) were found to exert a protective role in hepatocarcinogenesis (22).

The higher mutational burden found in CLDs compared to the normal liver suggests positive selection shapes the

genomic landscape during HCC emergence (23–27). Analysis of somatic mutations across healthy, ALD- and NAFLD-livers revealed that somatic mutations in *FOXO1*, *CIDEA*, and *GPAM* detected in CLD tissue showed convergent evolution. Of note, mutations in metabolism genes were observed in both ALD and NAFLD but less frequently in HCC (28). Ng et al. identified 7 significantly mutated genes across 122 HCC biopsies and showed 7% of samples harbored *GPAM* mutations (7 of 9 were frameshift mutations), which were more frequent than mutations in cancer-related genes such as *ARID2* and *RB1* (29). Mutations were identified in CLD tissues with allelic frequencies suggesting clonal expansion in CLD (26). Some non-driver mutations may become an advantageous asset for the liver's ability to not only withstand injuries but also to regenerate. In this study, genes involved in the control of liver regeneration were the most recurrently mutated within cirrhotic nodules, including driver mutations in cancer-related gene *ARID1A*, which controls gene expression associated with emergence of injury-induced liver progenitor-like cells (30). Recently, the relationship between *ARID1A* expression and immune cells that infiltrate tumors was clarified, whereby *ARID1A* expression in hepatocytes was positively associated with activated eosinophils, T helper cells, central memory T and Th2 cells (31). Frequent and cancer-promoting mutations in *ARID1A* and *TP53* were also acquired in subpopulations of hepatocytes in cirrhotic regenerating nodules, where an increase in clonal size was primarily observed in CLD but rarely in HCC cases (24). It is now well-established that alterations in *TP53* signaling pathways affect the TME at all stages of HCC development from initiation to metastasis, i.e., *via* hepatocytes, hepatic stellate cells (HSCs), immune cells, as well as cancer stem cells (32, 33). In one of the studies exploring the role of p53 in the immune response arising from embryonic liver progenitor cells, mutual *H-Ras* expression and *TP53* downregulation resulted in HCC development. The data indicated that p53 exerted a cytostatic effect by blocking proliferation and triggering cellular senescence, rendering cancer cells susceptible to recognition by the immune system (34). Cancer removal was affected by immune cells, including macrophages, neutrophils and NK cells (34–36). Non-hepatocyte tumor suppressive effects of *TP53* were mediated by its activity in HSCs. Lujambio et al. tested the conditional inactivation of p53 in HSCs during liver fibrosis. Depletion of p53 resulted in increased fibrosis and excessive extracellular matrix production, which eventually led to tumor occurrence and liver failure. It was shown that the formation of HCC did not directly evolve from p53-depleted HSCs, rather its deletion in these cells created a niche for hepatocytes malignant transformation (36). In addition, p53 expression levels (high or depleted) of HSCs were shown to modulate the different tumor-inhibiting phenotype of macrophages (M1 or M2, respectively) (36). It is important to stress that the previously mentioned experiments were performed in immunologically-compromised mice, thereby without an appropriate immune response. Nevertheless, these results support a model whereby physiological p53 activity in hepatocytes and HSCs facilitate tumor clearance. Liver injury also affects p53 in HSCs. For instance, following liver injury, the increase of p53 levels trigger

senescence of HSCs, thus promoting clearance of the scar tissue by immune cells. This response can be viewed as a balancing factor between regeneration and malignant transformation: p53 signaling protects from transformation while activating progenitor cells for compensatory liver repopulation (36, 37).

Mutational signatures in cirrhotic liver are conserved in HCC (27), including aging-associated single base substitution and indel mutational signatures in CLD, relating to increased proliferation after tissue regeneration (38). Together with senescence, a state of permanent cell cycle arrest, short telomeres in hepatocytes are hallmarks of cirrhosis (39), where shortening occurs more quickly than through aging alone. *TERT* promoter mutations occur predominantly at two hotspots of chromosome 5 (40) and one of the key mechanisms involved in malignant transformation of cirrhotic hepatocytes is the reactivation of telomerase by mutations in its promoter such as the well-characterized -124 and -146 C>T transitions. In line with these observations, the *TERT* promoter is frequently mutated in premalignant cirrhotic nodules early during hepatocarcinogenesis (23). Recently, hotspot mutations in the *TERT* promoter were found to be altered in a focal nodular hyperplasia lesion and clonally related HCC lesions (41). In contrast to other studies, Kim et al. found that *TERT* promoter mutations were only detectable in HCC, yet not in the cirrhotic nodules (24). These findings suggest that *TERT* promoter mutations can frequently act as a gatekeeper event during the transformation sequence, but are not always necessary for HCC emergence. Importantly, mutations arising in regenerating nodules of CLD tissues suggest an early carcinogenic event depicting clonal expansion in the stepwise malignant transformation from CLD to HCC (Figure 1).

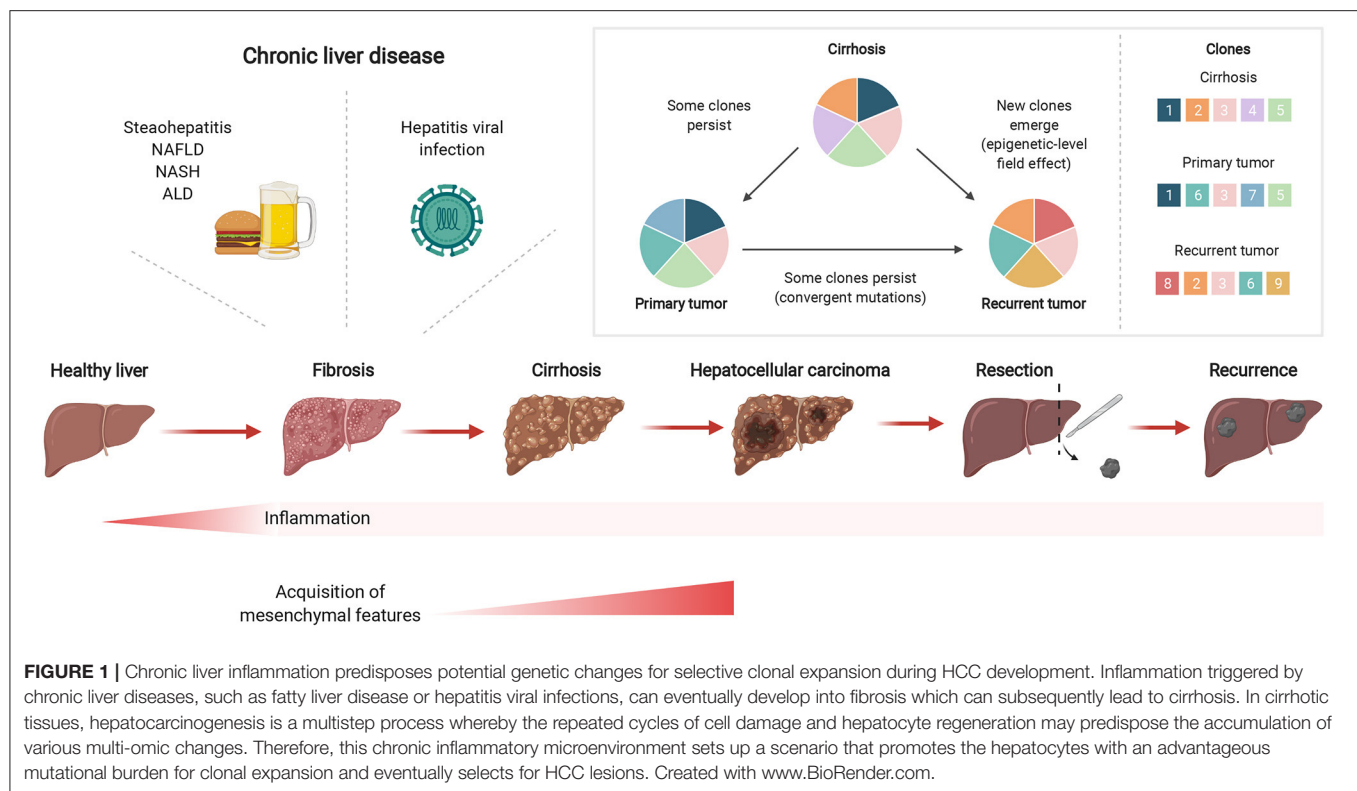
Epigenetic Alterations Predispose Cells to Tumorigenesis

CLDs trigger mechanisms that lead not only to the accumulation of genetic mutations but also of various cooperative epigenetic changes. Epigenetic silencing plays a key role in HCC emergence, where promoter methylation of tumor suppressor genes such as *RASSF1A* are noted at high frequency during the progression from cirrhosis to HCC (42). Okamoto et al. reported that hepatitis infections trigger an innate immune response dependent on natural killer (NK) cells to elicit DNA methylation, including methylation of *RASSF1A* (43). Comparison of promoter methylation profiles in the CLD tissue from HCC patients (cirrhotic vs. non-cirrhotic) identified aberrant promoter methylation of *UGT1A7* and *PLG*, genes which function in fibrogenesis and detoxification of carcinogens, respectively (44). These results highlight the importance of elucidating the underlying mechanisms of CLD beyond the genomic level to better understand the evolution of HCC. In line with this, our group recently demonstrated that CLDs trigger the formation of an epigenetic niche that predisposes cells to oncogenic alteration (45). We developed a CLD-associated DNA methylation score with prognostic value in HCC. High CLD methylation score was associated with higher levels of *TP53* somatic alterations in HCC, a poor prognostic

marker (46). Additionally, we showed that despite not harboring genetic alterations observed in HCC, CLD samples showed hypomethylation of genes such as *HDAC11*, which is highly expressed in immune cells (47), *UBD* (*FAT10*), involved in the inflammatory response and immune cell infiltration (47, 48), and *TAGLN2* that controls liver cancer cell motility (47–49). These genes are reported to be upregulated in HCC and in certain cases also to promote tumor progression (50–52). In this way, epigenetic changes during CLD influence the emergence of HCC by epigenetic regulation of gene expression, and could also create a permissive environment for the acquisition of genetic alterations that influence HCC prognosis.

Transcriptomic Dysregulation in CLD Contributes to Emergence of HCC

Gene expression in CLD patients is associated with HCC outcomes, suggesting that the environment in which HCC develops exerts an influence on tumor development (12, 45, 53, 54). One study investigated gene expression in non-tumoral liver tissues in patients with early-stage HCC and in liver tissue from patients with cirrhosis without HCC (55). They identified an immune-regulatory gene expression signature which is associated with risk of HCC development in cirrhotic patients (median follow up, 10 years). Our group observed increased expression of immune gene sets in CLD but not HCC samples, in line with the shift toward a suppressive immune environment in HCC to allow tumor growth (45, 56). The overexpression of *CTNNB1*, associated with mutations in this gene, occurred in both cirrhotic tissues and tumors and correlated with higher expression of Wnt pathway target genes involved in apoptosis and proliferation, such as *c-Myc* (57). Interestingly, missense mutations in exon-3 of *CTNNB1* do not promote *CTNNB1* overexpression but cause an aberrant activation of the Wnt signaling pathway by preventing phosphorylation and the degradation of β -catenin. The subset of cases with exon-3 mutations shows a more aggressive phenotype of HCC (58). Of note, *Wnt/CTNNB1* mutations correlate with a significant reduction of activated immune cells and immune activation pathways with an increase of M2-type macrophages in HCC patients (58–61). Although often driven by mutation affecting its promoter, *TERT* overexpression was shown to be associated with macrophage activation in patients with ALD. The study unveiled the cross-talk of *TERT* with the NF- κ B pathway during macrophage polarization (62). Transcriptomic analysis of premalignant cirrhotic nodules and early HCCs also suggests that the MYC transcription signature may play a role in malignant transformation (63). Indeed, E2F and MYC-targets gene sets were also found to be upregulated compared to normal liver in a progressive manner from CLD to HCC (45). In addition, current data indicates a significant link between hepatic inflammation mediators and *c-Myc* in CLDs. The relationship between *c-Myc* and aberrant expression of inflammatory mediators play a central role in fibrosis, cirrhosis, and liver cancer. For example, *c-Myc* upregulates IL-8, IL-10, TNF- α , and TGF- β , while its expression is promoted by IL-1, IL-2, IL-4, TNF- α , and TGF- β (64). Cancer-related pathways,



including epithelial-to-mesenchymal-transition (EMT), were identified to be transcriptionally dysregulated in precancerous lesions, independent of genetic alterations (45). The process of EMT in fibrogenic disorders includes phenotypic plasticity, where epithelial cells may dedifferentiate to a mesenchymal-like state in the hostile inflammatory environment, and acquire features such as increased motility (65, 66). Overall, these data highlight how dysregulation of transcriptional programmes may already be activated in CLD and contribute to tumorigenesis.

Tumors occur in a liver microenvironment comprising endothelial, immune and hepatic stellate cells, which contributes to the development of HCC through a complex network of intercellular interactions. Single cell RNA-sequencing (scRNA-seq) enables the study of this heterogeneous environment at the level of individual cells and captures the mutual regulatory mechanisms within a tissue. The transcriptomic profiles of individual cell populations in the liver microenvironment from 4 patients with healthy liver tissues, 3 patients with cirrhosis and 16 cases of HBV-related HCC tissues have been investigated using scRNA-seq and demonstrated the increasing immune cell involvement in each tissue from normal to HCC, relating to inflammatory damage from cirrhosis and the immune response (54). From eight identified genes whose expression in endothelial and stellate cells (liver-resident fibroblasts activated in CLD to support the tumor-promoting microenvironment) correlated with survival in HCC patients (54), four were potential oncogenes with high expression in HCC (*CKS2*, *HSP90AB1*, *RPL12*, *S100A6*) and two were potential tumor-suppressor genes (*CCL14* and *CD5L*) with low expression. The importance of

these genes has been corroborated in other studies, for example the silencing of *CKS2* has indeed been shown to inhibit cancer cell proliferation in HCC cells (67). Xing et al. reported that *CD5L* was decreased in liver tissues (54), however *CD5L* has also been found to be upregulated in HCC and liver cirrhosis (68–72) with a functional involvement in cellular proliferation promotion and antiapoptotic responses by binding to *HSPA5* (73). *CD5L* further emerges as a key player in fibrosis in the setting of CLD as it exerts a protective effect on fibrosis by a combination of mechanisms, including protection from damage, prevention from fibrosis and immune cell infiltration (74). Indeed, *CD5L* prevents neutrophil and monocyte-derived macrophage infiltration in the inflamed liver (74). Zhang et al. performed scRNAseq on healthy liver, cirrhosis and HCC patients to reveal the landscape of cirrhosis-associated immune cell infiltration in HCC (75). By looking both at differential genes in the B cell developmental trajectory from healthy liver to CLD to HCC and the tumor-associated genes between cirrhotic and malignant hepatocytes, the authors identified enrichment for the humoral immune response pathway and response to oxidative stress (75). In the hepatocytes, they identified key prognostic genes (*FTCD*, *MARCKSL1*, *CXCL3*, *RGS5*, *KNG1*, and *S100A16*) and *JUN* transcription factor was suggested to play a role in malignant transformation. In a study investigating tumor-infiltration in HCC at the multi-omics level, *SPP1* was indicated as an immune-related predictor of poor survival and mediator of macrophage-HCC cell interactions (76). Dong et al. used scRNA-seq to compare gene expression between tumor and inflammatory para-tumor tissue, inferring *MLXIPL* as an

important transcription factor in the route from normal liver cells to HCC subclones (77). Profiling gene expression in single cell populations in CLD is an expanding area and has the potential to reveal the role of individual cell types in HCC emergence, thus far revealing expression of genes in hepatocytes, and also endothelial cells, stellate cells and B cells, for regulating tumor proliferation and the immune response in the damaged CLD microenvironment.

Elucidating the Role of CLD in HCC Emergence Through Proteomics and Metabolomics Profiling

Proteomic- and metabolomic-based profiling adds valuable layers of information to the molecular landscape, since proteins and interactions between them are fundamental to cellular behavior. Functional proteomic analysis with regard to three major pathways in the liver (metabolism, complement and coagulation cascades) revealed a division of labor and complementarity among the different liver cell types. Upon mapping liver-disease-related genes to the healthy liver cell types, a high degree of enrichment was noted in the non-parenchymal cells (HSCs, Kupffer cells, liver sinusoidal endothelial cells and immune cells around the hepatocytes (78), highlighting the important regulative role of these cells in immunologic responses and disease development (79). During the progression of chronic liver injury toward fibrosis, the local interaction between Kupffer cells and resident liver macrophages is initiated, triggering the release of cytokines and chemokines (80, 81). The activation and proliferation of HSCs produce Extracellular matrix (ECM) proteins that subsequently form a fibrous scar (82–84). A further comprehensive serum proteomic analysis evaluated changes in protein levels between cirrhosis patients with and without HCC and discovered 21 novel diagnostic biomarkers for HCC enriched for the complement and coagulation cascade pathway (85). Proteins found differentially expressed in cirrhotic samples, FGFR4, TPM4, TPM2, LAALS3BP, and APOA1, were identified as the center of respective protein-protein interaction networks in CLD (86). Pathway enrichment of these networks suggest key roles for these proteins not only in the pathology of cirrhosis but potentially in HCC progression. Aberrant expression of FGFR4 has been reported to contribute to HCC progression (87), and proteins in the corresponding network were enriched for the MAPK cascade, which plays a pivotal role in HCC development due to activation by upstream growth factors (88), whereas APOA1 is prognostic for survival in HCC patients and predictive of early recurrence. Further research is required in following CLD cases to identify predictive biomarkers and to assert the role of CLD in shaping the proteome in HCC development, as large proteogenomics studies have thus far focused on characterizing the tumoral tissue in HCC (89, 90).

Metabolomics provides holistic information on dynamic metabolic responses resulting from perturbations caused by CLD. Metabolites related to ammonia recycling, the urea cycle, and amino acid metabolism were found to discriminate between HCC and cirrhosis. A panel of metabolites including methionine, proline, ornithine, pimelylcarnitine, and octanoylcarnitine

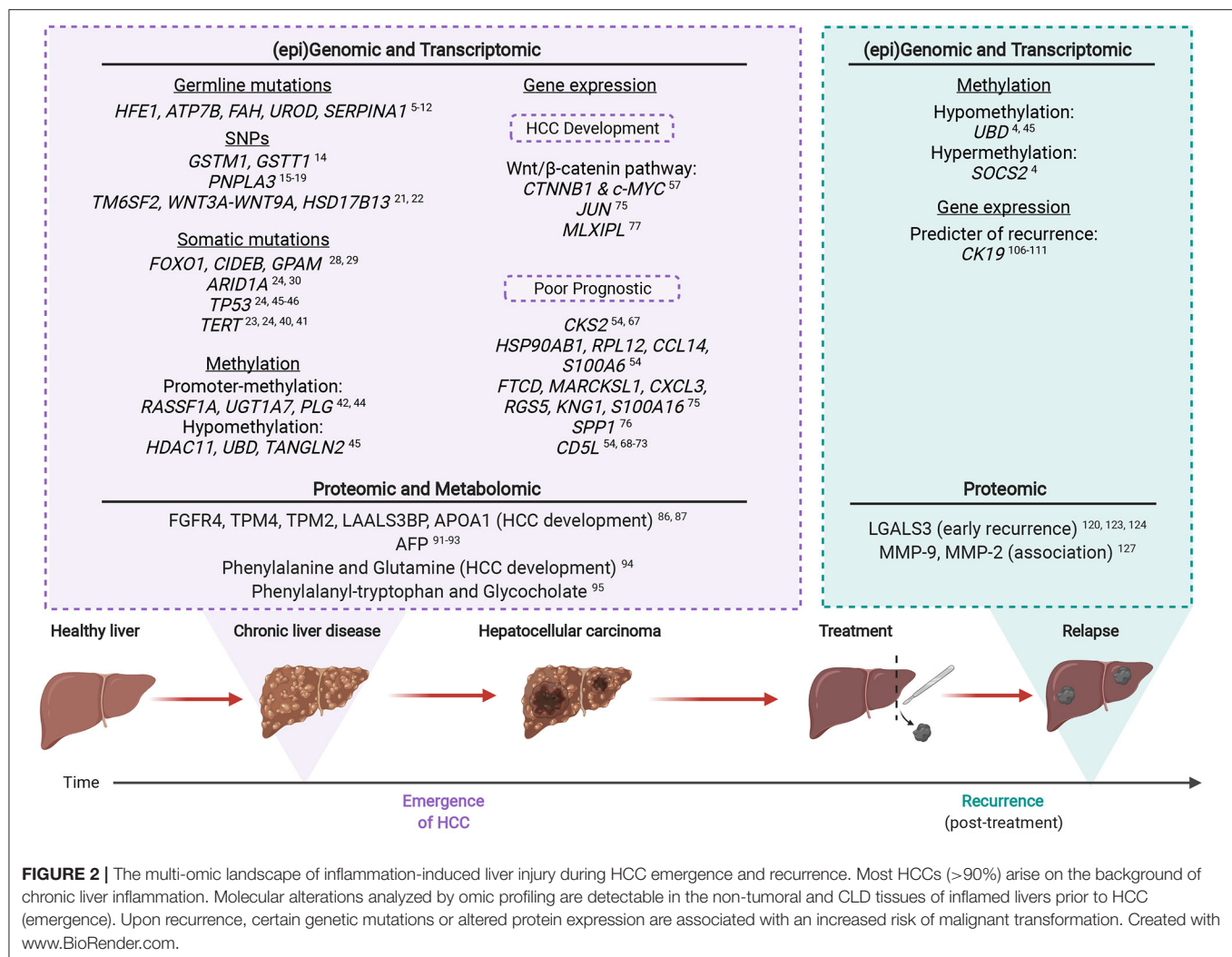
demonstrated higher diagnostic accuracy compared to alpha-fetoprotein (AFP) alone and was validated in another cohort (91). Nevertheless, AFP plays an important role in the development and progression of HCC as it activates the PI3K/AKT/mTOR pathway to promote expression of oncogenes such as Ras, Src, and CXCR4. It also leads to immune evasion by inducing apoptosis in antigen-presenting cells and inhibiting proliferation of infiltrating immune cells (92, 93). In an exploratory research, phenylalanine and glutamine were associated with development of HCC in patients with cirrhosis (94) while a larger multicentre study, analyzing a panel of metabolites, identified and phenylalanyl-tryptophan and glycocholate and validated these in an independent cohort. The panel showed a reliable HCC diagnosis in high-risk cirrhosis which, in combination with AFP, improved the panel's sensitivity (95). Metabolomics results indicate the utility of identifying perturbed metabolic pathways for determining biomarkers for cirrhotic patients that are at high risk of developing HCC, but metabolomic profiles of cirrhotic patients differ depending on the underlying etiology (96). There have been a number of studies on the metabolome of cirrhotic patients, as listed by Khan et al. (96), or in studies that discriminate HCC from cirrhotic background (97) which may explain altered pathways during hepato-carcinogenesis. However, there is not a uniform consensus regarding shift of metabolite expression in the emergence of HCC from CLD. This is in part due to the technical limitations including large numbers of metabolites exceeding analysis capabilities, too few metabolites in the database to garner true positive results, or challenges in experimental reproducibility, as well as differences in clinical characteristics in the HCC cohorts between studies.

MOLECULAR ALTERATIONS IN NON-RESOLVED LIVER INFLAMMATION PREDICT HCC RECURRENCE

Recurrence of HCC after therapy or resection represents an important clinical issue as it affects up to 70% of patients within 5 years (1, 2), with risk of late recurrence doubling upon the presence of liver cirrhosis (98). Current evidence suggests that inflammatory signals might increase tumor fitness and reduce expression of “stress ligands” on cancer cells (99–101) thereby allowing the outgrowth of malignant clones (102). This is especially evident in HCC where inflammation-induced tissue injury in CLD, cell death and liver regeneration following resection potentiate tumor outgrowth.

The Epigenetic Predisposition of CLD Tissues for HCC Recurrence

Recurrent tumors have been shown to harbor distinct genomic profiles and more aggressive phenotypes compared to primary tumors in HCC, suggesting an intracellular reprogramming during tumor recurrence (103). The carcinogenic environment of CLD may foster tumor recurrence through selective pressures for clonal outgrowth as micrometastases, or by formation of multiple *de novo* tumors, with the latter clinically defined as recurrence despite being genetically independent from the



primary. Recently, Ding et al. profiled matched initial/recurring tumors and neighboring cirrhotic/fibrotic liver in 133 HCC patients at the genetic and epigenetic (DNA methylation) levels (4). In this study, whole genome sequencing identified a patient with independent multifocal tumors originating from different clones. By contrast, aberrant methylation patterns were maintained from cirrhosis to both tumors, suggesting epigenetic alterations already existed in the CLD tissue. Many early methylation changes linking CLD to HCC were shown to target genes involved in inflammation-associated tumorigenesis, including *SOCS2* hypermethylation and *UBD* hypomethylation, the latter of which was also found hypomethylated in CLD samples by Gallon et al. (45). Interestingly, *SOCS2* has a critical role during tumor-immune surveillance (104) and in restraining deleterious immune responses upon severe liver injury (105).

Overall, aberrant methylation patterns and epigenetic alterations in HCC reflect their corresponding cirrhotic/fibrotic livers in the majority of cases, including both initial and recurring tumors. Therefore, these underlying mechanisms that exist in the liver before carcinogenesis highly influence the risk of

carcinogenesis from liver diseases to HCC and evidence the relevance of the epigenetic-level field effect.

Expression of Inflammatory Pathway Genes in CLD Tissues Associate With HCC Recurrence

Persistent liver damage and concomitant non-resolved inflammation is known to alter the genomic landscape of the liver. As discussed above, this specific genetic background subsequently promotes the transformation of hepatocytes into progenitor cells. However, the switch from a normal to a malignant setting has been shown to be marked by the expression of cytokeratin *CK19* in hepatocytes in the presence of inflammation or other stimuli (106). A large number of studies showed that *CK19* also is aberrantly expressed in HCC and gene signatures of this progenitor marker were independent predictors of HCC recurrence after liver transplant (107–111). Despite a lack of association between gene expression profiles in tumor tissues and HCC recurrence in a cohort of 106 patients,

a gene-expression signature in the non-tumoral adjacent liver tissues was found to be predictive of late recurrence and overall survival (53). In this study, the genes found to be indicative of poor prognosis were not only enriched for the NF- κ B inflammatory response but also for oxidative stress and IL-6 growth signaling pathways. The gene set was further validated in non-tumor tissues with varying etiology, indicating the robustness of the late recurrence signature. Interestingly, death of hepatocytes is known to trigger expression of IL-6 and other growth factors to promote survival and growth of neighboring mutated hepatocytes (112). IL-6 signaling mediated by tumor-associated macrophages was found to promote a cancer stem cell phenotype in HCC, which due to the self-renewal and tumor-initiating capacity of stem cells, is involved in recurrence and metastasis. NF- κ B (activated by IL-6) and STAT3 pathways are key orchestrators connecting non-resolving inflammation with HCC, which control the expression of genes involved in cell proliferation and immune functions (3). Transcriptional studies also demonstrate enhanced expression of distinct inflammatory cytokines and chemokines in primary tumors and metastatic lesions (113, 114). In line with this, intrahepatic metastasis in HBV-related HCC was found to be associated with a Th2-dominant cytokine gene expression profile in non-cancerous hepatic tissues from metastatic HCC patients (115). Chronic hepatitis infections result in the production of a cirrhotic liver which can promote the formation of *de novo* tumors, leading to late recurrence. In an effort to identify gene signatures related to HCC recurrence, Okamoto et al. profiled the gene expression of liver tissue of HCV patients and created a prediction score which could stratify the risk of patients of multicentric HCC recurrence (116). To understand gene expression signatures in HCV patients, Tsuchiya and colleagues profiled the tumor and non-tumor tissues of HCV-positive HCC patients. The resulting gene set successfully separated patients with and without HCC recurrence and further analysis revealed that hepatic nuclear factor 4- α and interferon gamma were the two main networks involved during HCC recurrence (117). Overall, these results demonstrate that non-tumoral transcriptional profiles can predict HCC recurrence independent of expression in the tumors, pointing toward the tumor microenvironment as being implicated in recurrence after resection. Furthermore, non-resolved inflammation and activation of inflammatory pathways are key in HCC late recurrence and disease progression.

Proteomics-Level Evidence of Immune Cell Involvement in HCC Recurrence

Tumor-promoting inflammation closely resembles inflammatory mechanisms typically found during immune responses. Hence, the study of the proteome within the inflamed non-tumoral background of HCC provides a framework for analyzing cellular networks and a reference for altered communication associated with pathology. The control of liver inflammation and regeneration is mainly orchestrated by infiltrating inflammatory cells. Upon hepatic injury, resident Kupffer cells, circulating monocytes, macrophages, dendritic cells and neutrophils interact to maintain the liver tissue architecture. Interestingly, studies

have shown that upon inflammation triggered by CLDs or surgery, myeloid cells can act in a dual mode, that is by promoting regeneration or, on the contrary, driving inflammatory processes that could aid tumor recurrence (118). In healthy tissues, myeloid cells play a vital role in tissue repair, as well as protective immunity through cytokine secretion and phagocytosis. However, in the underlying environment of non-resolving inflammation in HCC, myeloid cells are shifted toward immunosuppressive and tumor-promoting states such as tumor-associated macrophages and myeloid-derived suppressor cells (119). Between patients with recurrent and non-recurrent HCC, most differentially expressed proteins also belonged to immune system pathways (120). This included LGALS3, which was associated with early recurrence and ability of tumors to suppress the immune system. LGALS3 secreted by the cells of the TME alters immune cell function by inhibiting the expression of T cell receptors and preventing NK cell receptor binding to antigen (121, 122). Interestingly, this lectin was previously found to be expressed in HCC and focal regenerating nodules of cirrhotic tissue, despite being absent in normal hepatocytes (123, 124), possibly representing an early neoplastic event. Autophagy is a fundamental pathway that has multiple effects on immunity and inflammation, by influencing the development, homeostasis and survival of both immune and inflammatory cells. Of note, low concentration of the autophagy-related marker LC3 on HCC and adjacent liver microenvironment can be a significant predictor of both early and late HCC recurrence (125). Interestingly, autophagy proteins in the myeloid cells of the TME contribute to immune suppression of T lymphocytes by effecting LC3-associated phagocytosis. Altered LC3-associated phagocytosis in the myeloid compartment, subsequently induces control of tumor growth by tumor-associated macrophages upon phagocytosis of dying tumor cells (126). An additional class of enzymes involved in HCC recurrence which are typically expressed by the “pro-restorative” macrophage infiltrate (118) are matrix metalloproteinases (MMPs). MMPs are a family of proteolytic enzymes that perform multiple roles in the normal immune response to infection. MMP-9 overexpression by tumor-associated macrophages is associated with higher invasive potential of HCC (118). Interestingly, MMP-9 and MMP-2 positive staining in stromal tissue adjacent to tumors is associated with HCC recurrence in patients with underlying cirrhosis (127). Taken together, these results highlight the key roles of cells in the inflamed tumor microenvironment in cancer development and recurrence.

The key omic factors involved in CLD-HCC are summarized in **Figure 2**, from studies which indicate that HCC emergence and recurrence highly depend on the genomic, transcriptomic, proteomic and metabolomic background of CLD tissues.

CONCLUSION

The molecular mechanisms underlying HCC tumorigenesis from a background of CLD are gradually being unveiled through recent sequencing efforts. Omics based studies facilitate the study of global changes in biomolecules in a high

throughput manner, and hence are well-poised to reveal the complex changes which lead to HCC emergence and recurrence. Convergent mutations underlie clonal expansion from CLD, indicating selective pressure from the damaged environment, with aberrant methylation patterns from CLD persisting in HCC. In the emergence of HCC from CLD, *TERT* promoter mutations aid hepatocyte fitness and there is evidence of hypomethylation associated with upregulation of tumor-promoting genes, as well as epigenetic silencing of tumor suppressor genes. Current studies support the “epigenetic priming” model, whereby epigenetic changes induced by a prolonged chronic state sensitize cells to genetic mutations and altered transcriptional landscape, triggering tumorigenic progression and recurrence. Further implicated in the emergence of HCC are transcriptional dysregulation of genes involved in the WNT/b-catenin pathway and enrichment of the humoral response pathway, whereas pathways implicated in recurrent HCC include IL-6 growth signaling, NF- κ B, IFN- γ and HNF4a pathways. During both emergence and recurrence, evidence from multi-omic studies predominantly highlights members of the inflammatory response, underlying the key role of a chronically inflamed microenvironment as the molecular link between CLD and HCC. We are only now starting to appreciate the dynamicity, heterogeneity and complexity

of the initial steps required to predispose CLD tissues to full blown HCC. Overall, the expansion of ongoing analysis of non-tumoral tissue and CLD will have a major impact in the management of HCC, thus supporting the necessary development and refinement of preventive therapeutic strategies that reflect the molecular dysregulations associated with the CLD background.

AUTHOR CONTRIBUTIONS

SP, MC-L, and JG: conceptualization. SZ and GB: literature research and preparation of the first draft of the manuscript. SZ: figure design. SP, CN, MC-L, GH, SS, OK, JG, and GB: critical revision and editing. All authors have read and agreed to the published version of the manuscript.

FUNDING

CN and SP were supported by the Swiss Cancer Research foundation (KFS-4543-08-2018, KFS-4988-02-2020-R, respectively); SZ was supported by AIRC grant number IG 2019 Id.23615; SP was supported by the Professor Dr. Max Cloëtta Foundation; JG was supported by the University of Basel (Research Fund Junior Researchers).

REFERENCES

- Llovet JM, Kelley RK, Villanueva A, Singal AG, Pikarsky E, Roayaie S, et al. Hepatocellular carcinoma. *Nat Rev Dis Primers*. (2021) 7:6. doi: 10.1038/s41572-020-00240-3
- Llovet JM, Schwartz M, Mazzaferro V. Resection and liver transplantation for hepatocellular carcinoma. *Semin Liver Dis*. (2005) 25:181–200. doi: 10.1055/s-2005-871198
- Yu L-X, Ling Y, Wang H-Y. Role of nonresolving inflammation in hepatocellular carcinoma development and progression. *NPJ Precis Oncol*. (2018) 2:6. doi: 10.1038/s41698-018-0048-z
- Ding X, He M, Chan AWH, Song QX, Sze SC, Chen H, et al. Genomic and epigenomic features of primary and recurrent hepatocellular carcinomas. *Gastroenterology*. (2020) 1630–1645.e6. doi: 10.1053/j.gastro.2019.09.056
- Barton JC, Edwards CQ, Acton RT. HFE gene: structure, function, mutations, and associated iron abnormalities. *Gene*. (2015) 574:179–92. doi: 10.1016/j.gene.2015.10.009
- Lutsenko S. Human copper homeostasis: a network of interconnected pathways. *Curr Opin Chem Biol*. (2010) 14:211–7. doi: 10.1016/j.cbpa.2010.01.003
- Zhang L, Shao Y, Li L, Tian F, Cen J, Chen X, et al. Efficient liver repopulation of transplanted hepatocyte prevents cirrhosis in a rat model of hereditary tyrosinemia type I. *Sci Rep*. (2016) 6:31460. doi: 10.1038/srep31460
- Adapa SR, Hunter GA, Amin NE, Marinescu C, Borsky A, Sagatys EM, et al. Heme overdrive rewires pan-cancer cell metabolism. *bioRxiv*. (2022). doi: 10.1101/2022.02.18.481061
- Franco LM, Krishnamurthy V, Bali D, Weinstein DA, Arn P, Clary B, et al. Hepatocellular carcinoma in glycogen storage disease type Ia: a case series. *J Inherit Metab Dis*. (2005) 28:153–62. doi: 10.1007/s10545-005-7500-2
- Bianchi L. Glycogen storage disease I and hepatocellular tumours. *Eur J Pediatr*. (1993) 152(Suppl. 1):S63–70. doi: 10.1007/BF02072092
- Niemietz C, Bezerra F, Almeida MR, Guo S, Monia BP, Saraiva MJ, et al. SERPINA1 modulates expression of amyloidogenic transthyretin. *Exp Cell Res*. (2020) 395:112217. doi: 10.1016/j.yexcr.2020.112217
- Zucman-Rossi J, Villanueva A, Nault J-C, Llovet JM. Genetic landscape and biomarkers of hepatocellular carcinoma. *Gastroenterology*. (2015) 149:1226–39.e4. doi: 10.1053/j.gastro.2015.05.061
- Nahon P, Zucman-Rossi J. Single nucleotide polymorphisms and risk of hepatocellular carcinoma in cirrhosis. *J Hepatol*. (2012) 57:663–74. doi: 10.1016/j.jhep.2012.02.035
- Wang B, Huang G, Wang D, Li A, Xu Z, Dong R, et al. Null genotypes of GSTM1 and GSTT1 contribute to hepatocellular carcinoma risk: evidence from an updated meta-analysis. *J Hepatol*. (2010) 53:508–18. doi: 10.1016/j.jhep.2010.03.026
- Romeo S, Kozlitina J, Xing C, Pertsemlidis A, Cox D, Pennacchio LA, et al. Genetic variation in PNPLA3 confers susceptibility to nonalcoholic fatty liver disease. *Nat Genet*. (2008) 40:1461–5. doi: 10.1038/ng.257
- Liu Y-L, Patman GL, Leathart JBS, Piguet A-C, Burt AD, Dufour J-F, et al. Carriage of the PNPLA3 rs738409C >G polymorphism confers an increased risk of non-alcoholic fatty liver disease associated hepatocellular carcinoma. *J Hepatol*. (2014) 61:75–81. doi: 10.1016/j.jhep.2014.02.030
- Trépo E, Nahon P, Bontempi G, Valenti L, Falletti E, Nischalke H-D, et al. Association between the PNPLA3 (rs738409 C>G) variant and hepatocellular carcinoma: evidence from a meta-analysis of individual participant data. *Hepatology*. (2014) 59:2170–7. doi: 10.1002/hep.26767
- Singal AG, Manjunath H, Yopp AC, Beg MS, Marrero JA, Gopal P, et al. The effect of PNPLA3 on fibrosis progression and development of hepatocellular carcinoma: a meta-analysis. *Am J Gastroenterol*. (2014) 109:325–34. doi: 10.1038/ajg.2013.476
- Guyot E, Sutton A, Rufat P, Laguillier C, Mansouri A, Moreau R, et al. PNPLA3 rs738409, hepatocellular carcinoma occurrence and risk model prediction in patients with cirrhosis. *J Hepatol*. (2013) 58:312–8. doi: 10.1016/j.jhep.2012.09.036
- Bruschi FV, Claudel T, Tardelli M, Caligiuri A, Stulnig TM, Marra F, et al. The PNPLA3 I148M variant modulates the fibrogenic phenotype of human hepatic stellate cells. *Hepatology*. (2017) 65:1875–90. doi: 10.1002/hep.29041
- Stickel F, Hampe J. Rs708113 in WNT3A-WNT9A and hepatocellular carcinoma risk. *Lancet Oncol*. (2022) 23:14–16. doi: 10.1016/S1470-2045(21)00663-X

22. Trépo E, Caruso S, Yang J, Imbeaud S, Couchy G, Bayard Q, et al. Common genetic variation in alcohol-related hepatocellular carcinoma: a case-control genome-wide association study. *Lancet Oncol.* (2022) 23:161–71. doi: 10.1016/S1470-2045(21)00603-3
23. Nault JC, Calderaro J, Di Tommaso L, Balabaud C, Zafrani ES, Bioulac-Sage P, et al. Telomerase reverse transcriptase promoter mutation is an early somatic genetic alteration in the transformation of premalignant nodules in hepatocellular carcinoma on cirrhosis. *Hepatology.* (2014) 60:1983–92. doi: 10.1002/hep.27372
24. Kim SK, Takeda H, Takai A, Matsumoto T, Kakiuchi N, Yokoyama A, et al. Comprehensive analysis of genetic aberrations linked to tumorigenesis in regenerative nodules of liver cirrhosis. *J Gastroenterol.* (2019) 54:628–40. doi: 10.1007/s00535-019-01555-z
25. Torrecilla S, Sia D, Harrington AN, Zhang Z, Cabellos L, Cornella H, et al. Trunk mutational events present minimal intra- and inter-tumoral heterogeneity in hepatocellular carcinoma. *J Hepatol.* (2017) 67:1222–31. doi: 10.1016/j.jhep.2017.08.013
26. Zhu M, Lu T, Jia Y, Luo X, Gopal P, Li L, et al. Somatic mutations increase hepatic clonal fitness and regeneration in chronic liver disease. *Cell.* (2019) 177:608–21.e12. doi: 10.1016/j.cell.2019.03.026
27. Brunner SF, Roberts ND, Wylie LA, Moore L, Aitken SJ, Davies SE, et al. Somatic mutations and clonal dynamics in healthy and cirrhotic human liver. *Nature.* (2019) 574:538–42. doi: 10.1038/s41586-019-1670-9
28. Ng SWK, Rouhani FJ, Brunner SF, Brzozowska N, Aitken SJ, Yang M, et al. Convergent somatic mutations in metabolism genes in chronic liver disease. *Nature.* (2021) 598:473–8. doi: 10.1038/s41586-021-03974-6
29. Ng CKY, Dazert E, Boldanova T, Coto-Llerena M, Nuciforo S, Ercan C, et al. Integrative proteogenomic characterization of hepatocellular carcinoma across etiologies and stages. *Nat Commun.* (2022) 13:2436. doi: 10.1038/s41467-022-29960-8
30. Li W, Yang L, He Q, Hu C, Zhu L, Ma X, et al. A homeostatic Arid1a-dependent permissive chromatin state licenses hepatocyte responsiveness to liver-injury-associated YAP signaling. *Cell Stem Cell.* (2019) 25:54–68.e5. doi: 10.1016/j.stem.2019.06.008
31. Feng Y, Tang X, Li C, Su Y, Wang X, Li N, et al. ARID1A is a prognostic biomarker and associated with immune infiltrates in hepatocellular carcinoma. *Can J Gastroenterol Hepatol.* (2022) 2022:3163955. doi: 10.1155/2022/3163955
32. Llovet JM, Zucman-Rossi J, Pikarsky E, Sangro B, Schwartz M, Sherman M, et al. Hepatocellular carcinoma. *Nat Rev Dis Primers.* (2016) 2:16018. doi: 10.1038/nrdp.2016.18
33. Gillet R, Grimmer G, Bennoun M, Caron de Fromentel C, Briand P, Joulin V. The consequence of p53 overexpression for liver tumor development and the response of transformed murine hepatocytes to genotoxic agents. *Oncogene.* (2000) 19:3498–507. doi: 10.1038/sj.onc.1203671
34. Xue W, Zender L, Miething C, Dickins RA, Hernando E, Krizhanovsky V, et al. Senescence and tumour clearance is triggered by p53 restoration in murine liver carcinomas. *Nature.* (2007) 445:656–60. doi: 10.1038/nature05529
35. Iannello A, Thompson TW, Ardolino M, Lowe SW, Raulet DH. p53-dependent chemokine production by senescent tumor cells supports NKG2D-dependent tumor elimination by natural killer cells. *J Exp Med.* (2013) 210:2057–69. doi: 10.1084/jem.20130783
36. Lujambio A, Akkari L, Simon J, Grace D, Tschaharganeh DF, Bolden JE, et al. Non-cell-autonomous tumor suppression by p53. *Cell.* (2013) 153:449–60. doi: 10.1016/j.cell.2013.03.020
37. Krizhanovsky V, Yon M, Dickins RA, Hearn S, Simon J, Miething C, et al. Senescence of activated stellate cells limits liver fibrosis. *Cell.* (2008) 134:657–67. doi: 10.1016/j.cell.2008.06.049
38. Nguyen L, Jager M, Lieshout R, de Ruiter PE, Locati MD, Besselink N, et al. Precancerous liver diseases do not cause increased mutagenesis in liver stem cells. *Commun Biol.* (2021) 4:1301. doi: 10.1038/s42003-021-02839-y
39. Hoare M, Das T, Alexander G. Ageing, telomeres, senescence, and liver injury. *J Hepatol.* (2010) 53:950–61. doi: 10.1016/j.jhep.2010.06.009
40. Yuan X, Larsson C, Xu D. Mechanisms underlying the activation of TERT transcription and telomerase activity in human cancer: old actors and new players. *Oncogene.* (2019) 38:6172–83. doi: 10.1038/s41388-019-0872-9
41. Ercan C, Coto-Llerena M, Gallon J, Fourie L, Marinucci M, Hess GF, et al. Genomic analysis of focal nodular hyperplasia with associated hepatocellular carcinoma unveils its malignant potential: a case report. *Commun Med.* (2022) 2:1–8. doi: 10.1038/s43856-022-00074-y
42. Um T-H, Kim H, Oh B-K, Kim MS, Kim KS, Jung G, et al. Aberrant CpG island hypermethylation in dysplastic nodules and early HCC of hepatitis B virus-related human multistep hepatocarcinogenesis. *J Hepatol.* (2011) 54:939–47. doi: 10.1016/j.jhep.2010.08.021
43. Okamoto Y, Shinjo K, Shimizu Y, Sano T, Yamao K, Gao W, et al. Hepatitis virus infection affects DNA methylation in mice with humanized livers. *Gastroenterology.* (2014) 146:562–72. doi: 10.1053/j.gastro.2013.10.056
44. Hernandez-Vargas H, Lambert M-P, Le Calvez-Kelm F, Gouysse G, McKay-Chopin S, Tavtigian SV, et al. Hepatocellular carcinoma displays distinct DNA methylation signatures with potential as clinical predictors. *PLoS ONE.* (2010) 5:e9749. doi: 10.1371/journal.pone.0009749
45. Gallon J, Coto-Llerena M, Ercan C, Bianco G, Paradiso V, Nuciforo S, et al. Epigenetic priming in chronic liver disease impacts the transcriptional and genetic landscapes of hepatocellular carcinoma. *Mol Oncol.* (2021) 16:665–82. doi: 10.1002/1878-0261.13154
46. Kancherla V, Abdullazade S, Matter MS, Lanzafame M, Quagliata L, Roma G, et al. Genomic analysis revealed new oncogenic signatures in TP53-mutant hepatocellular carcinoma. *Front Genet.* (2018) 9:2. doi: 10.3389/fgene.2018.00002
47. Villagra A, Cheng F, Wang HW, Suarez I, Glozak M, Maurin M, et al. The histone deacetylase HDAC11 regulates the expression of interleukin 10 and immune tolerance. *Nat Immunol.* (2009) 10:349–62. doi: 10.1038/ni0609-665c
48. Aiche M, Groettrup M. The ubiquitin-like modifier FAT10 in cancer development. *Int J Biochem Cell Biol.* (2016) 79:451–61. doi: 10.1016/j.biocel.2016.07.001
49. Leung WK, Ching AK, Chan AW, Poon TC, Mian H, Wong AS, et al. A novel interplay between oncogenic PFTK1 protein kinase and tumor suppressor TAGLN2 in the control of liver cancer cell motility. *Oncogene.* (2011) 30:4464–75. doi: 10.1038/nc.2011.161
50. Lee CGL, Ren J, Cheong ISY, Ban KHK, Ooi LLPJ, Yong Tan S, et al. Expression of the FAT10 gene is highly upregulated in hepatocellular carcinoma and other gastrointestinal and gynecological cancers. *Oncogene.* (2003) 22:2592–603. doi: 10.1038/sj.onc.1206337
51. Wurmbach E, Chen Y-B, Khitrov G, Zhang W, Roayaie S, Schwartz M, et al. Genome-wide molecular profiles of HCV-induced dysplasia and hepatocellular carcinoma. *Hepatology.* (2007) 45:938–47. doi: 10.1002/hep.21622
52. Shi J, Ren M, She X, Zhang Z, Zhao Y, Han Y, et al. Transgelin-2 contributes to proliferation and progression of hepatocellular carcinoma via regulating Annexin A2. *Biochem Biophys Res Commun.* (2020) 523:632–8. doi: 10.1016/j.bbrc.2020.01.028
53. Hoshida Y, Villanueva A, Kobayashi M, Peix J, Chiang DY, Camargo A, et al. Gene expression in fixed tissues and outcome in hepatocellular carcinoma. *N Engl J Med.* (2008) 359:1995–2004. doi: 10.1056/NEJMoa0804525
54. Xing X, Song J. Identification of the different gene expression characteristics from liver cirrhosis to hepatocellular carcinoma using single-cell sequencing analyses. *J Immunol Res.* (2021) 2021:6619302. doi: 10.1155/2021/6619302
55. Moeini A, Torrecilla S, Tovar V, Montironi C, Andreu-Oller C, Peix J, et al. An immune gene expression signature associated with development of human hepatocellular carcinoma identifies mice that respond to chemopreventive agents. *Gastroenterology.* (2019) 157:1383–97.e11. doi: 10.1053/j.gastro.2019.07.028
56. Albillos A, Lario M, Álvarez-Mon M. Cirrhosis-associated immune dysfunction: distinctive features and clinical relevance. *J Hepatol.* (2014) 61:1385–96. doi: 10.1016/j.jhep.2014.08.010
57. Javanmard D, Najafi M, Babaei MR, Karbalaie Niya MH, Esghaei M, Panahi M, et al. Investigation of gene mutations and expression in hepatocellular carcinoma and cirrhosis in association with hepatitis B virus infection. *Infect Agent Cancer.* (2020) 15:37. doi: 10.1186/s13027-020-00297-5
58. Cieply B, Zeng G, Proverbs-Singh T, Geller DA, Monga SPS. Unique phenotype of hepatocellular cancers with exon-3 mutations in beta-catenin gene. *Hepatology.* (2009) 49:821. doi: 10.1002/hep.22695

59. Pinyol R, Sia D, Llovet JM. Immune exclusion-Wnt/CTNNB1 class predicts resistance to immunotherapies in HCC. *Clin Cancer Res.* (2019) 25:2021–23. doi: 10.1158/1078-0432.CCR-18-3778
60. Chen L, Zhou Q, Liu J, Zhang W. CTNNB1 alternation is a potential biomarker for immunotherapy prognosis in patients with hepatocellular carcinoma. *Front Immunol.* (2021) 12:759565. doi: 10.3389/fimmu.2021.759565
61. Mo Z, Wang Y, Cao Z, Li P, Zhang S. An integrative analysis reveals the underlying association between CTNNB1 mutation and immunotherapy in hepatocellular carcinoma. *Front Oncol.* (2020) 10:853. doi: 10.3389/fonc.2020.00853
62. Wu X-Q, Yang Y, Li W-X, Cheng Y-H, Li X-F, Huang C, et al. Telomerase reverse transcriptase acts in a feedback loop with NF- κ B pathway to regulate macrophage polarization in alcoholic liver disease. *Sci Rep.* (2016) 6:1–14. doi: 10.1038/srep18685
63. Kaposi-Novak P, Libbrecht L, Woo HG, Lee Y-H, Sears NC, Conner EA, et al. Central role of c-Myc during malignant conversion in human hepatocarcinogenesis. *Cancer Res.* (2009) 69:2775–82. doi: 10.1158/0008-5472.CAN-08-3357
64. Liu T, Zhou Y, Ko KS, Yang H. Interactions between Myc and mediators of inflammation in chronic liver diseases. *Mediat Inflamm.* (2015) 2015:276850. doi: 10.1155/2015/276850
65. Pinzani M. Epithelial-mesenchymal transition in chronic liver disease: fibrogenesis or escape from death? *J Hepatol.* (2011) 55:459–65. doi: 10.1016/j.jhep.2011.02.001
66. van Zijl F, Zulehner G, Petz M, Schneller D, Kornauth C, Hau M, et al. Epithelial-mesenchymal transition in hepatocellular carcinoma. *Future Oncol.* (2009) 5:1169–79. doi: 10.2217/fon.09.91
67. Ji X, Xue Y, Wu Y, Feng F, Gao X. High-expressed CKS2 is associated with hepatocellular carcinoma cell proliferation through down-regulating PTEN. *Pathol Res Pract.* (2018) 214:436–41. doi: 10.1016/j.prp.2017.12.006
68. Gangadharan B, Antrobus R, Dwek RA, Zitzmann N. Novel serum biomarker candidates for liver fibrosis in hepatitis C patients. *Clin Chem.* (2007) 53:1792–9. doi: 10.1373/clinchem.2007.089144
69. Sarvari J, Mojtahedi Z, Taghavi SAR, Kuramitsu Y, Shahrabadi MS, Ghaderi A, et al. Differentially expressed proteins in chronic active hepatitis, cirrhosis, and HCC related to HCV infection in comparison with HBV infection: a proteomics study. *Hepat Mon.* (2013) 13:e8351. doi: 10.5812/hepatmon.8351
70. Mera K, Uto H, Mawatari S, Ido A, Yoshimine Y, Nosaki T, et al. Serum levels of apoptosis inhibitor of macrophage are associated with hepatic fibrosis in patients with chronic hepatitis C. *BMC Gastroenterol.* (2014) 14:1–10. doi: 10.1186/1471-230X-14-27
71. Gray J, Chattopadhyay D, Beale GS, Patman GL, Miele L, King BP, et al. A proteomic strategy to identify novel serum biomarkers for liver cirrhosis and hepatocellular cancer in individuals with fatty liver disease. *BMC Cancer.* (2009) 9:1–11. doi: 10.1186/1471-2407-9-271
72. Yamazaki T, Mori M, Arai S, Tateishi R, Abe M, Ban M, et al. Circulating AIM as an indicator of liver damage and hepatocellular carcinoma in humans. *PLoS ONE.* (2014) 9:e109123. doi: 10.1371/journal.pone.0109123
73. Aran G, Sanjurjo L, Bárcena C, Simon-Coma M, Téllez É, Vázquez-Vitali M, et al. CD5L is upregulated in hepatocellular carcinoma and promotes liver cancer cell proliferation and antiapoptotic responses by binding to HSPA5 (GRP78). *FASEB J.* (2018) 32:3878–91. doi: 10.1096/fj.201700941RR
74. Bárcena C, Aran G, Perea L, Sanjurjo L, Téllez É, Oncins A, et al. CD5L is a pleiotropic player in liver fibrosis controlling damage, fibrosis and immune cell content. *EBioMedicine.* (2019) 43:513–24. doi: 10.1016/j.ebiom.2019.04.052
75. Zhang S, Liu Z, Wu D, Chen L, Xie L. Single-cell RNA-seq analysis reveals microenvironmental infiltration of plasma cells and hepatocytic prognostic markers in HCC with cirrhosis. *Front Oncol.* (2020) 10:596318. doi: 10.3389/fonc.2020.596318
76. Liu L, Zhang R, Deng J, Dai X, Zhu X, Fu Q, et al. Construction of TME and identification of crosstalk between malignant cells and macrophages by SPP1 in hepatocellular carcinoma. *Cancer Immunol Immunother.* (2022) 71:121–36. doi: 10.1007/s00262-021-02967-8
77. Dong X, Wang F, Liu C, Ling J, Jia X, Shen F, et al. Single-cell analysis reveals the intra-tumor heterogeneity and identifies MLXIPL as a biomarker in the cellular trajectory of hepatocellular carcinoma. *Cell Death Discov.* (2021) 7:1–13. doi: 10.1038/s41420-021-00403-5
78. Marrone G, Shah VH, Gracia-Sancho J. Sinusoidal communication in liver fibrosis and regeneration. *J Hepatol.* (2016) 65:608–17. doi: 10.1016/j.jhep.2016.04.018
79. Ding C, Li Y, Guo F, Jiang Y, Ying W, Li D, et al. A cell-type-resolved liver proteome. *Mol Cell Proteomics.* (2016) 15:3190–202. doi: 10.1074/mcp.M116.060145
80. Dixon LJ, Barnes M, Tang H, Pritchard MT, Nagy LE. Kupffer cells in the liver. *Compr Physiol.* (2013) 3:785–97. doi: 10.1002/cphy.c120026
81. van der Heide D, Weiskirchen R, Bansal R. Therapeutic targeting of hepatic macrophages for the treatment of liver diseases. *Front Immunol.* (2019) 10:2852. doi: 10.3389/fimmu.2019.02852
82. Ying HZ, Chen Q, Zhang WY, Zhang HH, Ma Y, Zhang SZ, et al. PDGF signaling pathway in hepatic fibrosis pathogenesis and therapeutics (Review). *Mol Med Rep.* (2017) 16:7879–89. doi: 10.3892/mmr.2017.7641
83. Dewidar B, Meyer C, Dooley S, Meindl-Beinker AN. TGF- β in hepatic stellate cell activation and liver fibrogenesis-updated 2019. *Cells.* (2019) 8:1419. doi: 10.3390/cells8111419
84. Marcher A-B, Bendixen SM, Terkelsen MK, Hohmann SS, Hansen MH, Larsen BD, et al. Transcriptional regulation of hepatic stellate cell activation in NASH. *Sci Rep.* (2019) 9:1–13. doi: 10.1038/s41598-019-39112-6
85. Tsai T-H, Song E, Zhu R, Di Poto C, Wang M, Luo Y, et al. LC-MS/MS-based serum proteomics for identification of candidate biomarkers for hepatocellular carcinoma. *Proteomics.* (2015) 15:2369–81. doi: 10.1002/pmic.201400364
86. Safaei A, Rezaei TM, Arefi OA, Zamanian AM, Mohebbi SR, Nikzamir AR. Protein-protein interaction network analysis of cirrhosis liver disease. *Gastroenterol Hepatol Bed Bench.* (2016) 9:114–23.
87. Raja A, Park I, Haq F, Ahn S-M. FGF19-FGFR4 signaling in hepatocellular carcinoma. *Cells.* (2019) 8:536. doi: 10.3390/cells8060536
88. Moon H, Ro SW. MAPK/ERK signaling pathway in hepatocellular carcinoma. *Cancers.* (2021) 13:3026. doi: 10.3390/cancers13123026
89. Gao Q, Zhu H, Dong L, Shi W, Chen R, Song Z, et al. Integrated proteogenomic characterization of HBV-related hepatocellular carcinoma. *Cell.* (2019) 179:561–77.e22. doi: 10.1016/j.cell.2019.08.052
90. Jiang Y, Sun A, Zhao Y, Ying W, Sun H, Yang X, et al. Proteomics identifies new therapeutic targets of early-stage hepatocellular carcinoma. *Nature.* (2019) 567:257–61. doi: 10.1038/s41586-019-0987-8
91. Kim DJ, Cho EJ, Yu KS, Jang JJ, Yoon JH, Park T, et al. Comprehensive metabolomic search for biomarkers to differentiate early stage hepatocellular carcinoma from cirrhosis. *Cancers.* (2019) 11:1497. doi: 10.3390/cancers11101497
92. Zhu M, Lu Y, Li W, Guo J, Dong X, Lin B, et al. Hepatitis B virus X protein driven alpha fetoprotein expression to promote malignant behaviors of normal liver cells and hepatoma cells. *J Cancer.* (2016) 7:935–46. doi: 10.7150/jca.13628
93. Meng W, Bai B, Bai Z, Li Y, Yue P, Li X, et al. The immunosuppression role of alpha-fetoprotein in human hepatocellular carcinoma. *Discov Med.* (2016) 21:489–94.
94. Liang K-H, Cheng M-L, Lo C-J, Lin Y-H, Lai M-W, Lin W-R, et al. Plasma phenylalanine and glutamine concentrations correlate with subsequent hepatocellular carcinoma occurrence in liver cirrhosis patients: an exploratory study. *Sci Rep.* (2020) 10:1–7. doi: 10.1038/s41598-020-67971-x
95. Luo P, Yin P, Hua R, Tan Y, Li Z, Qiu G, et al. A Large-scale, multicenter serum metabolite biomarker identification study for the early detection of hepatocellular carcinoma. *Hepatology.* (2018) 67:662–75. doi: 10.1002/hep.29561
96. Khan V, Putluri N, Sreekumar A, Mindikoglu AL. Current applications of metabolomics in cirrhosis. *Metabolites.* (2018) 8:67. doi: 10.3390/metabo8040067
97. Guo W, Tan HY, Wang N, Wang X, Feng Y. Deciphering hepatocellular carcinoma through metabolomics: from biomarker discovery to therapy evaluation. *Cancer Manag Res.* (2018) 10:715–34. doi: 10.2147/CMAR.S156837
98. Poon RT, Fan ST, Ng IO, Lo CM, Liu CL, Wong J. Different risk factors and prognosis for early and late intrahepatic recurrence after resection of hepatocellular carcinoma. *Cancer.* (2000) 89:500–7. doi: 10.1002/1097-0142(20000801)89:3<500:AID-CNCR4>3.0.CO;2-O

99. Alexandre Iannello DHR. Immunosurveillance of senescent cancer cells by natural killer cells. *Oncoimmunology*. (2014) 3:e27616. doi: 10.4161/onci.27616
100. Lam AR, Bert NL, Ho SS, Shen YJ, Tang LF, Xiong GM, et al. RAE1 ligands for the NKG2D receptor are regulated by STING-dependent DNA sensor pathways in lymphoma. *Cancer Res*. (2014) 74:2193–203. doi: 10.1158/0008-5472.CAN-13-1703
101. Shifrin N, Raulet DH, Ardolino M. NK cell self tolerance, responsiveness and missing self recognition. *Semin Immunol*. (2014) 26:138–44. doi: 10.1016/j.smim.2014.02.007
102. Kuraishy A, Karin M, Grivennikov SI. Tumor promotion via injury- and death-induced inflammation. *Immunity*. (2011) 35:467–77. doi: 10.1016/j.immuni.2011.09.006
103. Choi J-H, Kim MJ, Park YK, Im J-Y, Kwon SM, Kim HC, et al. Mutations acquired by hepatocellular carcinoma recurrence give rise to an aggressive phenotype. *Oncotarget*. (2016) 8:22903–16. doi: 10.18632/oncotarget.14248
104. Nirschl CJ, Suárez-Fariñas M, Izar B, Prakadan S, Dannenfels R, Tirosch I, et al. IFN γ -Dependent tissue-immune homeostasis is co-opted in the tumor microenvironment. *Cell*. (2017) 170:127–41.e15. doi: 10.1016/j.cell.2017.06.016
105. Monti-Rocha R, Cramer A, Leite PG, Antunes MM, Pereira RVS, Barroso A, et al. SOCS2 is critical for the balancing of immune response and oxidative stress protecting against acetaminophen-induced acute liver injury. *Front Immunol*. (2018) 9:3134. doi: 10.3389/fimmu.2018.03134
106. Zhuo J-Y, Lu D, Tan W-Y, Zheng S-S, Shen Y-Q, Xu X. CK19-positive hepatocellular carcinoma is a characteristic subtype. *J Cancer*. (2020) 11:5069–77. doi: 10.7150/jca.44697
107. Durnez A, Verslype C, Nevens F, Fevery J, Aerts R, Pirenne J, et al. The clinicopathological and prognostic relevance of cytokeratin 7 and 19 expression in hepatocellular carcinoma. A possible progenitor cell origin. *Histopathology*. (2006) 49:138–51. doi: 10.1111/j.1365-2559.2006.02468.x
108. Lee JJ, Lee J-W, Kim JM, Kim JK, Chung HJ, Kim YS. Prognosis of hepatocellular carcinoma expressing cytokeratin 19: comparison with other liver cancers. *World J Gastroenterol*. (2012) 18:4751–7. doi: 10.3748/wjg.v18.i34.4751
109. Wu PC, Fang JW, Lau VK, Lai CL, Lo CK, Lau JY. Classification of hepatocellular carcinoma according to hepatocellular and biliary differentiation markers. Clinical and biological implications. *Am J Pathol*. (1996) 149:1167–75.
110. Govaere O, Komuta M, Berkens J, Spee B, Janssen C, de Luca F, et al. Keratin 19: a key role player in the invasion of human hepatocellular carcinomas. *Gut*. (2014) 63:674–85. doi: 10.1136/gutjnl-2012-304351
111. Miltiadous O, Sia D, Hoshida Y, Fiel MI, Harrington AN, Thung SN, et al. Progenitor cell markers predict outcome of patients with hepatocellular carcinoma beyond Milan criteria undergoing liver transplantation. *J Hepatol*. (2015) 63:1368–77. doi: 10.1016/j.jhep.2015.07.025
112. Sakurai T, He G, Matsuzawa A, Yu GY, Maeda S, Hardiman G, et al. Hepatocyte necrosis induced by oxidative stress and IL-1 α release mediate carcinogen-induced compensatory proliferation and liver tumorigenesis. *Cancer Cell*. (2008) 14:156–65. doi: 10.1016/j.ccr.2008.06.016
113. Binnewies M, Roberts EW, Kersten K, Chan V, Fearon DE, Merad M, et al. Understanding the tumor immune microenvironment (TIME) for effective therapy. *Nat Med*. (2018) 24:541–50. doi: 10.1038/s41591-018-0014-x
114. Puram SV, Tirosch I, Parikh AS, Patel AP, Yizhak K, Gillespie S, et al. Single-Cell transcriptomic analysis of primary and metastatic tumor ecosystems in head and neck cancer. *Cell*. (2017) 171:1611–24.e24. doi: 10.1016/j.cell.2017.10.044
115. Budhu A, Forgues M, Ye QH, Jia HL, He P, Zanetti KA, et al. Prediction of venous metastases, recurrence, and prognosis in hepatocellular carcinoma based on a unique immune response signature of the liver microenvironment. *Cancer Cell*. (2006) 10:99–111. doi: 10.1016/j.ccr.2006.06.016
116. Okamoto M, Utsunomiya T, Wakiyama S, Hashimoto M, Fukuzawa K, Ezaki T, et al. Specific gene-expression profiles of noncancerous liver tissue predict the risk for multicentric occurrence of hepatocellular carcinoma in hepatitis C virus-positive patients. *Ann Surg Oncol*. (2006) 13:947–54. doi: 10.1245/ASO.2006.07.018
117. Tsuchiya M, Parker JS, Kono H, Matsuda M, Fujii H, Rusyn I. Gene expression in nontumoral liver tissue and recurrence-free survival in hepatitis C virus-positive hepatocellular carcinoma. *Mol Cancer*. (2010) 9:1–11. doi: 10.1186/1476-4598-9-74
118. Weston CJ, Zimmermann HW, Adams DH. The role of myeloid-derived cells in the progression of liver disease. *Front Immunol*. (2019) 10:893. doi: 10.3389/fimmu.2019.00893
119. Wan S, Kuo N, Kryczek I, Zou W, Welling TH. Myeloid cells in hepatocellular carcinoma. *Hepatology*. (2015) 62:1304. doi: 10.1002/hep.27867
120. Bhat M, Clotet-Freixas S, Baciu C, Pasini E, Hammad A, Ivanics T, et al. Combined proteomic/transcriptomic signature of recurrence post-liver transplantation for hepatocellular carcinoma beyond Milan. *Clin Proteomics*. (2021) 18:27. doi: 10.1186/s12014-021-09333-x
121. Ruvolo PP. Galectin 3 as a guardian of the tumor microenvironment. *Biochim Biophys Acta*. (2016) 1863:427–37. doi: 10.1016/j.bbamcr.2015.08.008
122. Ruvolo PP. Galectins as regulators of cell survival in the leukemia niche. *Adv Biol Regul*. (2019) 71:41–54. doi: 10.1016/j.jbior.2018.09.003
123. Jiang S-S, Weng D-S, Wang Q-J, Pan K, Zhang Y-J, Li Y-Q, et al. Galectin-3 is associated with a poor prognosis in primary hepatocellular carcinoma. *J Transl Med*. (2014) 12:1–14. doi: 10.1186/s12967-014-0273-3
124. Hsu DK, Dowling CA, Jeng KC, Chen JT, Yang RY, Liu FT. Galectin-3 expression is induced in cirrhotic liver and hepatocellular carcinoma. *Int J Cancer*. (1999) 81:519–26.
125. Lin CW, Chen YS, Lin CC, Lee PH, Lo GH, Hsu CC, et al. Autophagy-related gene LC3 expression in tumor and liver microenvironments significantly predicts recurrence of hepatocellular carcinoma after surgical resection. *Clin Transl Gastroenterol*. (2018) 9:166. doi: 10.1038/s41424-018-0033-4
126. Cunha LD, Yang M, Carter R, Guy C, Harris L, Crawford JC, et al. LC3-Associated phagocytosis in myeloid cells promotes tumor immune tolerance. *Cell*. (2018) 175:429–41.e16. doi: 10.1016/j.cell.2018.08.061
127. Zhang Q, Chen X, Zhou J, Zhang L, Zhao Q, Chen G, et al. CD147, MMP-2, MMP-9 and MVD-CD34 are significant predictors of recurrence after liver transplantation in hepatocellular carcinoma patients. *Cancer Biol Ther*. (2006) 5:808–14. doi: 10.4161/cbt.5.7.2754

Conflict of Interest: The authors declare that the research was conducted in the absence of any commercial or financial relationships that could be construed as a potential conflict of interest.

Publisher's Note: All claims expressed in this article are solely those of the authors and do not necessarily represent those of their affiliated organizations, or those of the publisher, the editors and the reviewers. Any product that may be evaluated in this article, or claim that may be made by its manufacturer, is not guaranteed or endorsed by the publisher.

Copyright © 2022 Zanotti, Boot, Coto-Llerena, Gallon, Hess, Soysal, Kollmar, Ng and Piscuoglio. This is an open-access article distributed under the terms of the Creative Commons Attribution License (CC BY). The use, distribution or reproduction in other forums is permitted, provided the original author(s) and the copyright owner(s) are credited and that the original publication in this journal is cited, in accordance with accepted academic practice. No use, distribution or reproduction is permitted which does not comply with these terms.



Investigation of Functional Synergism of CENPF and FOXM1 Identifies POLD1 as Downstream Target in Hepatocellular Carcinoma

Daniel Wai-Hung Ho[†], Wai-Ling Macrina Lam[†], Lo-Kong Chan[†] and Irene Oi-Lin Ng^{*}

Department of Pathology and State Key Laboratory of Liver Research, University of Hong Kong, Hong Kong, Hong Kong SAR, China

OPEN ACCESS

Edited by:

Luigi M. Terracciano,
University of Basel, Switzerland

Reviewed by:

Haeryoung Kim,
Seoul National University Hospital,
South Korea
Luca Di Tommaso,
Humanitas Research Hospital, Italy

*Correspondence:

Irene Oi-Lin Ng
iolng@hku.hk

[†]These authors have contributed
equally to this work

Specialty section:

This article was submitted to
Pathology,
a section of the journal
Frontiers in Medicine

Received: 22 January 2022

Accepted: 17 June 2022

Published: 05 July 2022

Citation:

Ho DW, Lam WM, Chan LK and
Ng IO (2022) Investigation
of Functional Synergism of CENPF
and FOXM1 Identifies POLD1 as
Downstream Target in Hepatocellular
Carcinoma. *Front. Med.* 9:860395.
doi: 10.3389/fmed.2022.860395

Background: Lines of evidence implicate CENPF and FOXM1 may have novel co-operative roles in driving hepatocellular carcinoma (HCC).

Objective: We investigated the clinicopathological correlation, functional characterization, molecular mechanism and translational significance of CENPF and FOXM1.

Methods: We carried out integrative studies investigating functional synergism of CENPF and FOXM1 in HCC and its metastasis. Human HCC samples, HCC cell lines and mouse model were used in the studies. Stable knockdown, q-PCR, Western blotting, whole-transcriptomic sequencing (RNA-seq), as well as cell and mouse assays were performed.

Results: Upon clinicopathological correlation, we found that co-overexpression of CENPF and FOXM1 in human HCCs was associated with more aggressive tumor behavior including presence of venous invasion, tumor microsatellite formation, and absence of tumor encapsulation. Moreover, co-silencing FOXM1 and CENPF using shRNA approach in HCC cell lines resulted in significantly reduced cell proliferation. Furthermore, our RNA-seq and differential gene expression analysis delineated that CENPF and FOXM1 co-regulated a specific set of target genes in various metabolic processes and oncogenic signaling pathways. Among them, POLD1, which encodes the catalytic subunit of DNA polymerase δ , was ranked as the top downstream target co-regulated by CENPF and FOXM1. POLD1 expression was positively correlated with that of FOXM1 and CENPF in HCCs. In addition, POLD1 expression was significantly upregulated in HCC tumors. Functionally, *in vivo* orthotopic injection model showed that stable knockdown of POLD1 in HCC cells suppressed tumor incidence and tumorigenicity and had a trend of diminished lung metastasis.

Conclusion: Taken together, our data suggest that CENPF and FOXM1 could synergistically support hepatocarcinogenesis via the regulation of POLD1. CENPF and FOXM1 may represent new vulnerabilities to novel drug-based therapy in HCC.

Keywords: CENPF, FOXM1, POLD1, liver cancer, HCC, functional synergism

INTRODUCTION

Hepatocellular carcinoma (HCC) is one of the leading causes of cancer death worldwide (1, 2) and the second and third commonest cancer, respectively, in China and Hong Kong. Indeed, 55% of all new liver cancers worldwide each year occur in China including Hong Kong, due to a high prevalence of hepatitis B viral (HBV) infection (3, 4). It has a poor prognosis and only few effective treatment options are available. Despite years of efforts in studying the molecular mechanism of HCC carcinogenesis, current understanding on this lethal disease is still limited. In a recent study of our group (5), we have utilized whole-transcriptome sequencing technology to perform a differential gene expression (DGE) analysis using the dataset of 50 pairs (tumor and the corresponding non-tumorous liver tissue) of HCC cases from The Cancer Genome Atlas (TCGA). By comparing the gene expression in HCC tumors and their corresponding non-tumorous liver tissues, differentially expressed genes in HCC were identified. Among the 734 differentially expressed genes, CENPF and FOXM1 were listed as the first and third most upregulated genes respectively in HCC. Both FOXM1 and CENPF are crucial for cell-cycle progression, especially in the G2/M phase.

In a study on mitosis regulation and aging, CENPF was demonstrated to be a direct target of the cell cycle master regulator FOXM1 (6). Hence, it is traditionally believed that CENPF is a downstream target of FOXM1 and under the regulation by FOXM1. Interestingly, CENPF and FOXM1 were predicted to be master regulators of prostate cancer malignancy in a cross-species computational analysis by comparing interactomes of human and mice (7), and experimental validation demonstrated that they function synergistically to promote tumor growth by regulating prostate cancer-associated target gene expression profiles. Knockdown of CENPF and FOXM1 synergistically reduced the proliferation of cancer cells and tumor growth in cell-line-derived xenografts. It was further demonstrated that knockdown of CENPF expression reduced the binding of FOXM1 to its targets, suggesting CENPF is required for appropriate genomic binding by FOXM1. Additional data showed that they were co-localized in nucleus and their subcellular co-localization was mutually dependent.

Taken together, multiple lines of evidence imply CENPF and FOXM1 may have novel cooperative roles in regulating the expression of shared target genes. Hence, we postulate that they may have functional synergism in driving hepatocarcinogenesis.

MATERIALS AND METHODS

Quantitative Real-Time Polymerase Chain Reaction

RNA was extracted by Trizol (Thermo Fisher Scientific, Waltham, MA, United States) and cDNA was synthesized by a reverse transcription kit (Thermo Fisher Scientific, Waltham, MA, United States). Quantitative real-time polymerase chain reaction (qRT-PCR) was performed with target-specific TaqMan probes (Thermo Fisher Scientific, Waltham, MA, United States)

listed in **Supplementary Table 1**. The mRNA expression was normalized by the expression of the housekeeping gene *HPRT*.

Clinical Specimens and Clinicopathological Correlation Analysis

The primary HCC specimens and their corresponding non-tumorous liver tissues of randomly selected 118 human HCC cases were surgically resected from HCC patients in Queen Mary Hospital of Hong Kong between year 1991 and 2017. None of the patients had received therapies before hepatic tumor resection. Total RNA of these 118 pairs clinical specimens were isolated for subsequent qRT-PCR and clinicopathological correlation analysis using SPSS24.0 software, as previously described (8). We did not differentiate into micro- or macrovascular invasion. However, although the venous invasion included both microvascular and macrovascular invasion, mostly it was microvascular invasion. The tumor microsatellites were defined as microscopic or small tumor nodules less than 1 cm in diameter and in close proximity to the main tumor. Direct liver invasion was defined as invasion of the tumor cells into the non-tumorous liver parenchyma without separation by tumor capsule or fibrous layer (9). The use of clinical specimens was approved by the Institutional Review Board of the University of Hong Kong and the Hospital Authority.

Cell Lines and Culture Conditions

Hepatocellular carcinoma cell line Hep3B (HB-8064) was obtained from the American Type Culture Collection (ATCC) and HCC cell line Huh7 (JCRB0403) was obtained from JCRB Cell Bank. MHCC97L was a gift from Liver Cancer Institute, Fudan University. Hep3B cells were cultured in Minimum Essential Medium (MEM) supplemented with 1mM sodium pyruvate (NaPy). MHCC97L cells were cultured in Dulbecco's modified Eagle minimal high glucose essential medium (DMEM-HG) supplemented with 1mM NaPy. Huh7 cells were cultured in DMEM-HG media. All cell culture media mentioned above were further supplemented with 10% fetal bovine serum (FBS), 1% penicillin, and 1% streptomycin unless otherwise specified. Cell line cultures were maintained in 37°C and 5% CO₂ incubator.

Authentication of HCC cell lines used in this study was performed by short tandem repeat (STR) DNA Profiling in March 2018 and no cellular cross-contamination was detected. STR result for MHCC97L is provided in **Supplementary Figure 1**. Cell cultures were tested negative for Mycoplasma contamination. "Xenome," utilizing RNA-seq data, estimated a negligible 0.04–0.42% ($n = 3$) for MHCC97L, while 0.15–0.40% for clinical human NTL and HCC samples ($n = 6$) with mouse contamination, thus indicating our MHCC97L cells do not contain cells of murine origin (10). Furthermore, MHCC97L used in this study contains HBV integration in the TERT locus of the genome (8).

Stable Lentiviral-Based Short-Hairpin RNA Knockdown Cell Models

FOXM1, CENPF, and POLD1 were stably knocked down in MHCC97L HCC cells by the lentiviral-based short-hairpin

RNA (shRNA) approach as previously described (11, 12). The oligonucleotide sequences encoding non-targeted control (shNTCC) shRNA and shRNAs that specifically target FOXM1 (shFOXM1), CENPF (shCENPF), and POLD1 (shPOLD1) (Integrated DNA Technologies, Coralville, IA, United States) were summarized in **Supplementary Table 2**. The forward and reverse oligonucleotides were reannealed to generate shRNA cassettes and each of them was individually cloned into pLKO.1-Puro plasmid with puromycin resistance gene as selection marker. For lentiviral packaging, individual shRNA plasmid was co-transfected with the packaging mix into 293FT cells by lipofectamine 2000 transfection reagent (Invitrogen) at a plasmid to lipofectamine ratio ($\mu\text{g}:\mu\text{L}$) of 1:2. The viral supernatants were harvested 48 h post-transfection and used to transduce MHCC97L cells. About 1 $\mu\text{g}/\text{mL}$ puromycin was applied to the viral-transduced cells for at least 4 days to select for stable knockdown clones. The knockdown efficiencies of FOXM1 and CENPF were examined by RT-qPCR and western blot.

Western Blot Analysis

Cells were lysed by 6X protein sample buffer (0.35 M Tris-HCl, pH 6.8, 30% glycerol, 20% SDS, 9.3% DTT and 0.05% bromophenol blue) and resolved by SDS-polyacrylamide gel electrophoresis. Immunoblots were incubated with primary antibody rabbit anti-human FOXM1 (D12D5) XP (Cell Signaling Technology, Danvers, MA, United States), rabbit anti-human CENPF (D6X4L) (Cell Signaling Technology, Danvers, MA, United States) and mouse anti-human β -actin (Sigma Aldrich, St. Louis, MO, United States) at 4°C overnight, followed by horseradish peroxidase-labeled anti-rabbit or anti-mouse secondary antibodies (Sigma Aldrich, St. Louis, MO, United States) at room temperature for 2 h. The chemiluminescence signal was detected with the ECL detection system (GE Healthcare, Lafayette, CO, United States).

Cell Proliferation Assay by Direct Cell Counting

About 2×10^4 cells of each cell line were seeded into each well of multiple 24-well culture plates in triplicates and incubated in a 37°C humidified incubator with 5% CO₂. Cell growth was assessed by determining the number of cells in each well every 24 h for 4 consecutive days. Direct cell counting was performed using COULTER COUNTER Z1 Cell and Particle Counter (Beckman Coulter).

Cell Growth Inhibition Assay by XTT Assay

Cell Proliferation II Kit (XTT) (Roche, Basel, Switzerland) was used to determine the percentage of cell growth inhibition according to the manufacturer's instructions.

Animal Studies

All animal studies were approved by the Animals (Control of Experiments) Ordinance of Hong Kong and the Committee on the Use of Live Animals in Teaching and Research (CULATR) of the University of Hong Kong (CULATR number: 3848-15), and

strictly following the institutional regulations and guidelines. All animal studies were performed on 4 to 6 weeks old BALB/c-nu/nu (nude) athymic male mice, which were provided by the Centre for Comparative Medicine Research of the University of Hong Kong.

In vivo Orthotopic Liver Injection Model

POLD1 was knocked down in luciferase-labeled MHCC97L (MHCC97L-Luc) HCC cells by shRNA approach. The orthotopic liver injection was performed on 4 to 6 weeks old BALB/c-nu/nu (nude) athymic male mice to assess the metastatic potential of the injected HCC cells as previously described (13). About 1×10^6 of MHCC97L-luc stable cells were resuspended in 15 μL of Matrigel Basement Membrane Matrix (Corning) diluted with serum-free cell culture medium in a 1:1 ratio and then injected into the left lobe of the livers of mice by a 29-gauge needle (Hamilton, Reno, NV, United States). The abdominal wound was sutured after the injection. At 6-week post-injection, bioluminescence imaging of the xenografts was performed. Mice were anesthetized with Pentobarbital at 80 mg/kg, followed by injection of D-luciferin at 100 mg/kg (Perkin-Elmer, Waltham, MA, United States) into the tumor-bearing mice intraperitoneally. Bioluminescence images were acquired by IVIS Spectrum *in vivo* imaging system (Perkin-Elmer, Waltham, MA, United States) to measure the total flux of the bioluminescent signals emitted from the dissected liver tumor xenografts and the distant lung metastases.

Identification of FOXM1 and CENPF Co-regulated Genes by RNA-Sequencing

RNA-sequencing (RNA-seq) was performed to identify downstream target genes that were co-regulated by FOXM1 and CENPF. FOXM1 and CENPF were either individually silenced or co-silenced in Huh7, Hep3B and MHCC97L using small-interfering RNA (siRNA) approach and subjected to RNA-seq subsequently. Before transfection, 1.5×10^5 per well of cells were seeded onto a 6-well plate (for RNA extraction) and 3.5×10^5 per well of cells were seeded onto a 60-mm plate (for protein extraction) and were incubated in a 37°C humidified incubator with 5% CO₂ overnight. The siRNAs of the non-target control (NTC), FOXM1 and/or CENPF (Dharmacon, GE Healthcare, Lafayette, CO, United States) listed in **Supplementary Table 3** were transfected into the HCC cells with DharmaFECT 1 transfection reagent (Dharmacon, GE Healthcare, Lafayette, CO, United States). The cells were incubated for further 72 h and then subjected to RNA and protein extraction. Real-time PCR and western blot analysis were performed to confirm the knockdown efficiencies of FOXM1 and CENPF. Successful individual and co-knockdown cells were subjected to bioanalyzer analysis (Agilent) for RNA sample quality control followed by RNA-seq analysis (polyA and mRNA) at the Center for PanorOmic Sciences of the University of Hong Kong. The RNA-seq data has been deposited to NCBI SRA (PRJNA800214).

The DGE profiles of FOXM1 and/or CENPF knockdown HCC cell lines were analyzed by edgeR. Furthermore, additional filters were applied to confine the candidate gene list co-regulated

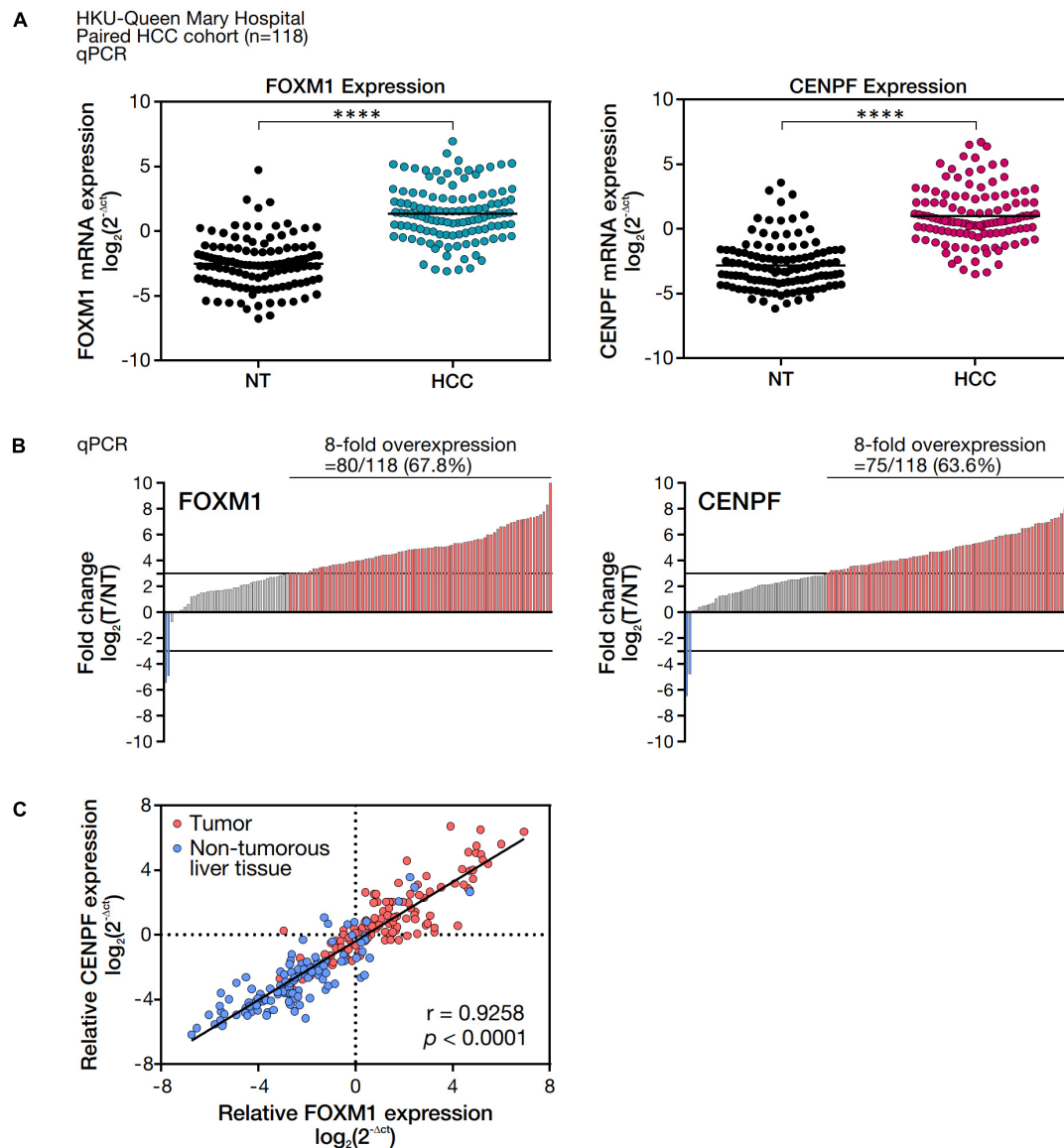


FIGURE 1 | FOXM1 and CENPF mRNA expression level and correlation analysis in HCC tumor and the corresponding non-tumorous liver tissues. **(A)** mRNA expression levels of FOXM1 and CENPF in 118 pairs of HCC and NT samples. mRNA expressions were normalized by housekeeping gene, *HPRT*. **(B)** Waterfall plot showing overall distribution of the fold change of FOXM1 and CENPF mRNA expression in 118 HCC clinical paired samples. **(C)** Pearson correlation analysis between FOXM1 and CENPF relative mRNA expression. Statistical significance was calculated by one-sample *t*-test (**** $p < 0.001$).

by FOXM1 and CENPF based on four criteria: (i) they were differentially expressed with a *p*-value less than 0.05; (ii) with log CPM (counts per million) greater than 1; (iii) with an absolute log fold change greater than 1; and (iv) they were commonly differentially expressed in all 3 HCC cell lines with co-knockdown of FOXM1 and CENPF. Criteria (i)–(iii) applied to DGE analysis using both TCGA and our in-house whole-transcriptome sequencing of HCC clinical cases. To validate with DGE analysis results from the knockdown cell lines, correlation analysis between the candidate genes and FOXM1 and/or CENPF was performed using the TCGA and our in-house whole-transcriptome sequencing cohort of HCC clinical cases (14). The

activated and repressed candidate genes that were potentially co-regulated by FOXM1 and CENPF were also subjected to gene set enrichment analysis (15).

RESULTS

Expression and Clinical Relevance of FOXM1 and CENPF in Human HCCs

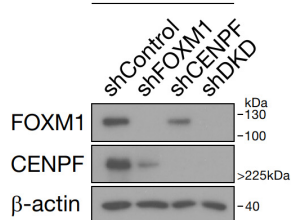
To validate FOXM1 and CENPF expression in our cohort of HCC patients, we examined the abundance of mRNA expression of FOXM1 and CENPF in 118 randomly selected pairs of HCC

TABLE 1 | Clinicopathological correlation analysis of FOXM1 and CENPF.

Clinical parameters		FOXM1 expression(T/NT)			CENPF expression(T/NT)			FOXM1 and CENPF expression (T/NT)		
		≥8-Fold	<8-Fold	p-Value	≥8-Fold	<8-Fold	p-Value	≥8-Fold	<8-Fold	p-Value
Gender	Male	63	28	0.348	60	31	0.223	54	37	0.446
	Female	17	10		15	12		15	12	
Venous invasion	Yes	48	19	0.204	49	18	0.011*	45	22	0.022*
	No	32	19		26	25		24	27	
Tumor encapsulation	Yes	23	15	0.146	20	18	0.057	18	20	0.059
	No	57	22		55	24		51	28	
Tumor microsatellite formation	Yes	48	16	0.045*	47	17	0.010*	44	20	0.009*
	No	31	22		27	26		24	29	
Direct liver invasion	Yes	32	10	0.123	29	13	0.254	27	15	0.225
	No	44	25		42	27		38	31	
Tumor size	>5 cm	53	22	0.221	50	25	0.204	46	29	0.228
	≤5 cm	26	16		24	18		22	20	
Cirrhosis	Yes	35	23	0.066	36	22	0.445	31	27	0.183
	No	45	15		39	21		38	22	
Chronic liver disease	Yes	73	37	0.205	68	42	0.140	62	48	0.084
	No	7	1		7	1		7	1	
Cellular differentiation (Edmonson's grading)	I-II	34	18	0.403	33	19	0.560	31	21	0.459
	III-IV	45	20		41	24		37	28	
Tumor stage	I/II	25	16	0.195	22	19	0.093	21	20	0.195
	III/IV	53	22		51	24		46	29	

Clinicopathological correlation analysis between the indicated clinical parameters and the individual and co-expression of FOXM1 and CENPF in human HCC (n = 118) at an 8-fold difference cut-off. Statistical analyses were done by SPSS software 24.0. Asterisks (*) indicate statistically significant ($p < 0.05$). T; HCC tumorous tissue; NT; corresponding non-tumorous liver tissue. P values are shown in bold to emphasize they are < 0.05 .

A MHCC97L-luciferase



B Cell proliferation assay MHCC97L-luciferase

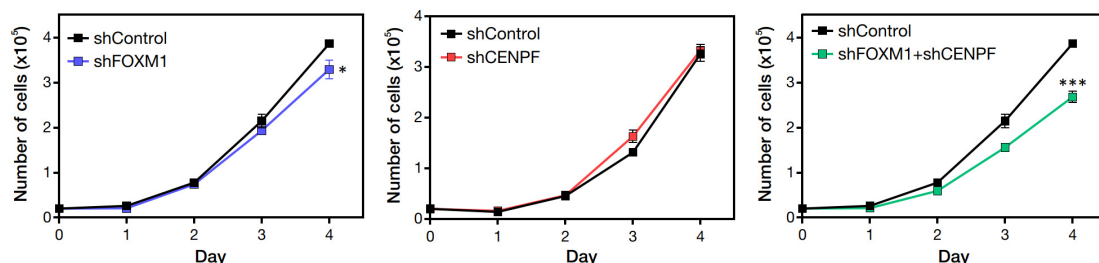
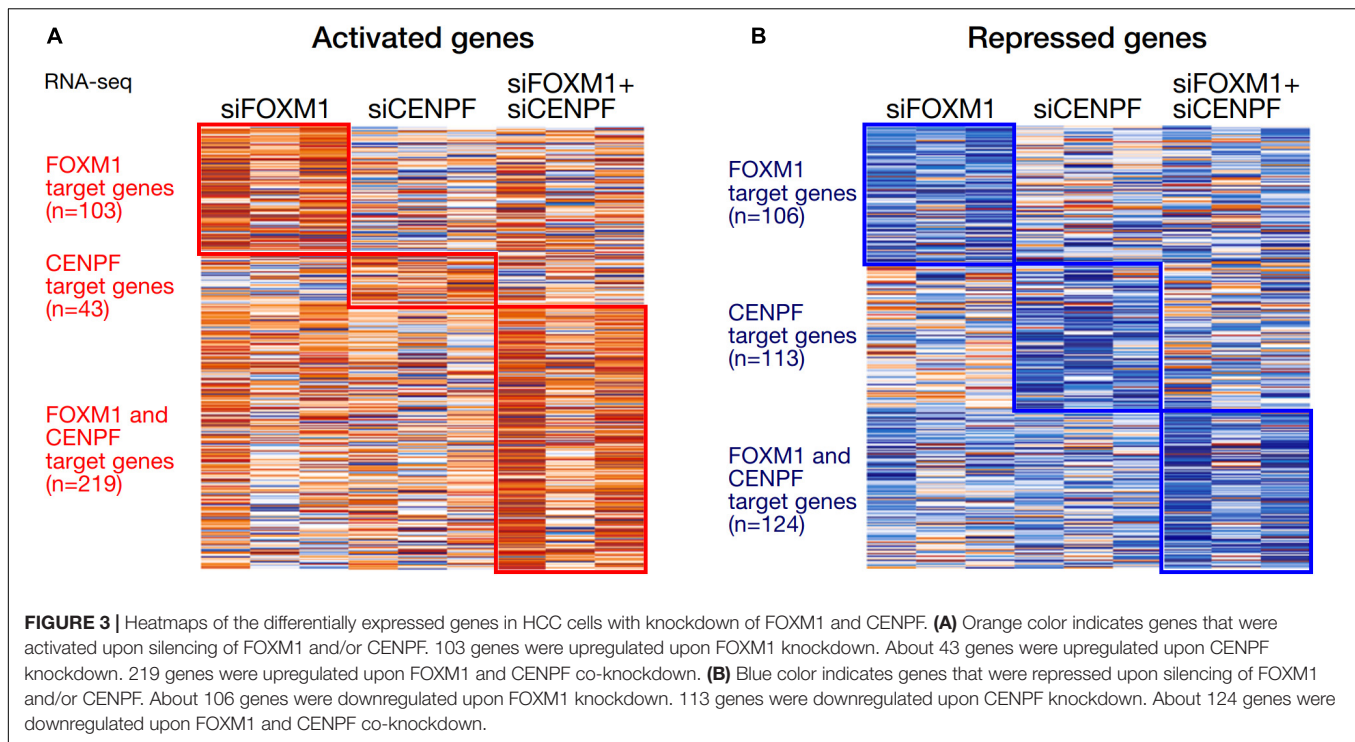


FIGURE 2 | Pro-proliferative role of FOXM1 and CENPF. **(A)** Western blot analysis showing single and double knockdown efficiencies of FOXM1 and CENPF in MHCC97L-Luc cells. **(B)** Representative cell proliferation assay showing the growth curves of HCC cells with single and co-knockdown of FOXM1 and CENPF for four consecutive days. Statistical significance was calculated by one-sample *t*-test (* $p < 0.05$; *** $p < 0.001$). shDKD, shRNA double knockdown of FOXM1 and CENPF cells.



clinical samples (tumor, HCC, and corresponding non-tumorous liver tissues, NT) by real-time RT-PCR analysis. By comparing the mRNA expression levels between the HCC and NT samples, both FOXM1 and CENPF were shown to be significantly upregulated ($****p < 0.0001$), respectively (**Figure 1A**). The overall distribution of FOXM1 and CENPF expression in our cohort was displayed in the waterfall plot (**Figure 1B**). Using a cut-off at 8-fold difference between HCC and NT, 80 of the 118 HCC cases (67.8%) showed an overexpression of FOXM1, and 75 of the 118 HCC cases (63.6%) showed an overexpression of CENPF, whereas only 2 HCC cases (1.69%) had under-expression of either FOXM1 or CENPF. Interestingly, when we compared the relative expression of FOXM1 and CENPF in HCC and NT, respectively, we observed that they were positively correlated with each other ($r = 0.9258$, $p < 0.0001$), and substantially higher expressions in the tumor samples (**Figure 1C**).

To examine the clinical relevance of FOXM1 and CENPF, either in terms of their expression alone or co-expression, clinicopathological correlation analysis was performed. Using a threshold of 8-fold difference between T and NT, we showed that the overexpression of FOXM1 was positively correlated with the presence of tumor microsatellite formation ($p = 0.045$), whereas the overexpression of CENPF was positively correlated with the presence of venous invasion ($p = 0.011$) and the presence of tumor microsatellite ($p = 0.010$). Remarkably, co-overexpression of FOXM1 and CENPF were positively correlated with the presence of venous invasion ($p = 0.022$) and the presence of tumor microsatellite formation ($p = 0.009$), while the absence of tumor encapsulation ($p = 0.059$) was also suggested but did not reach statistical significance (**Table 1**).

FOXM1 and CENPF Were Critical for Cell Proliferation

FOXM1 and CENPF were individually silenced and co-silenced in MHCC97L-Luc HCC cell line by shRNA approach. We confirmed the successful knockdown by Western blot analysis (**Figure 2A**). To investigate the role of FOXM1 and CENPF in cell proliferation *in vitro*, the established stable knockdown cell lines were analyzed by anchorage-dependent cell proliferation assay. Co-knockdown of FOXM1 and CENPF cells showed the most significantly reduced proliferation rate ($p < 0.05$) (**Figure 2B**).

Identification of Commonly Regulated Genes by FOXM1 and CENPF Using RNA-Seq

To investigate the potential synergistic underlying mechanism of FOXM1 and CENPF in HCC, we have established single and co-knockdown FOXM1 and CENPF cell lines using small-interfering RNA (siRNA) transient knockdown approach for subsequent RNA-seq. siRNA knockdown cell lines were established in Huh7, Hep3B and MHCC97L HCC cells. The knockdown efficiencies were confirmed by real-time RT-PCR and western blot analysis (**Supplementary Figure 2**). Among all, siFOXM1-6, siCENPF-10 and siFOXM1-6/siCENPF-10 exhibited strongest knockdown efficiencies consistently in all 3 HCC cell lines. Thus, they were used for RNA-seq, together with the siRNA control cells.

We analyzed the expression profiles from the HCC cell lines in which they were individually silenced or co-silenced by DGE analysis. From the DGE analysis across all 3 sets of knockdown cell lines, we have identified 209 genes that

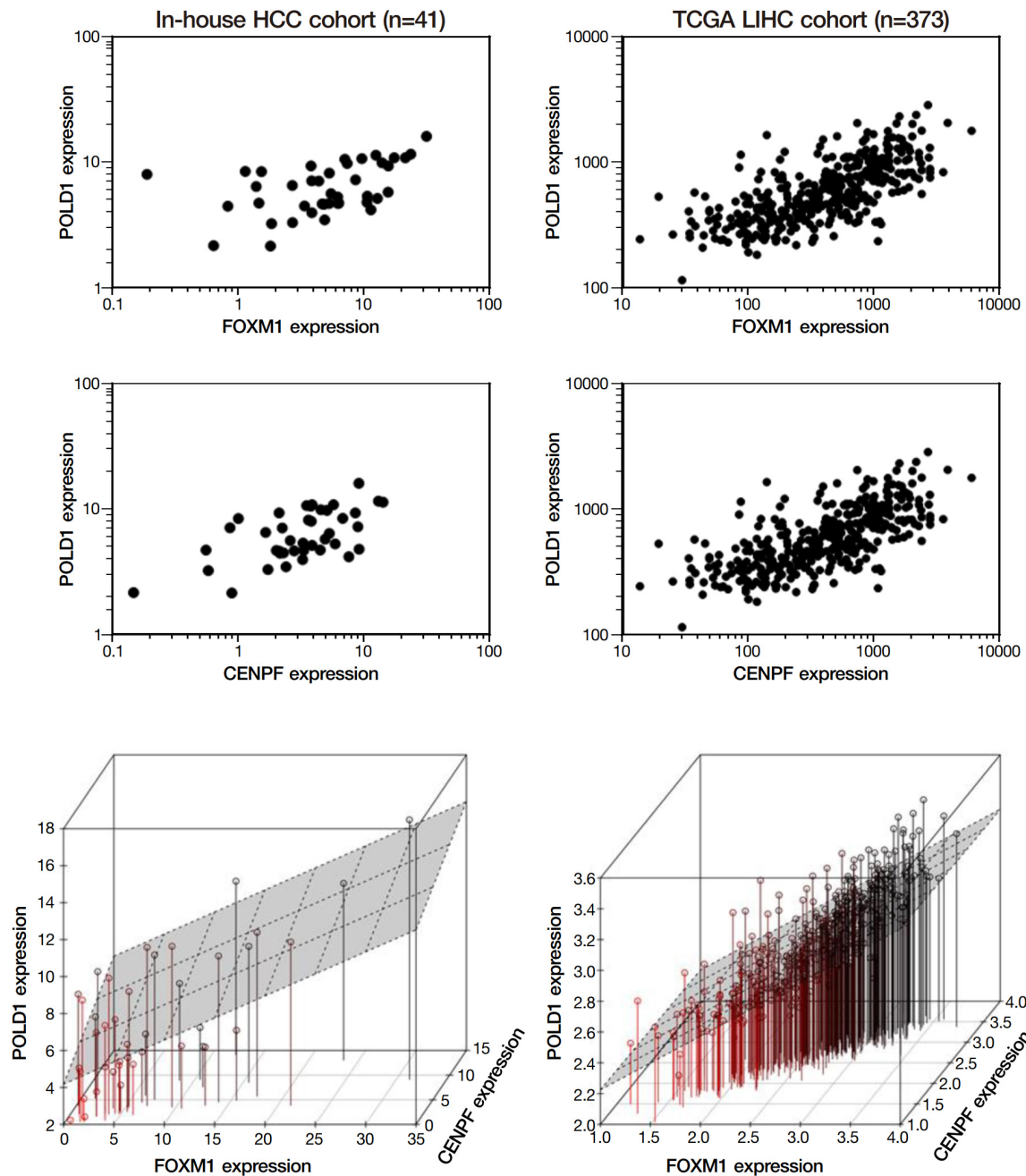
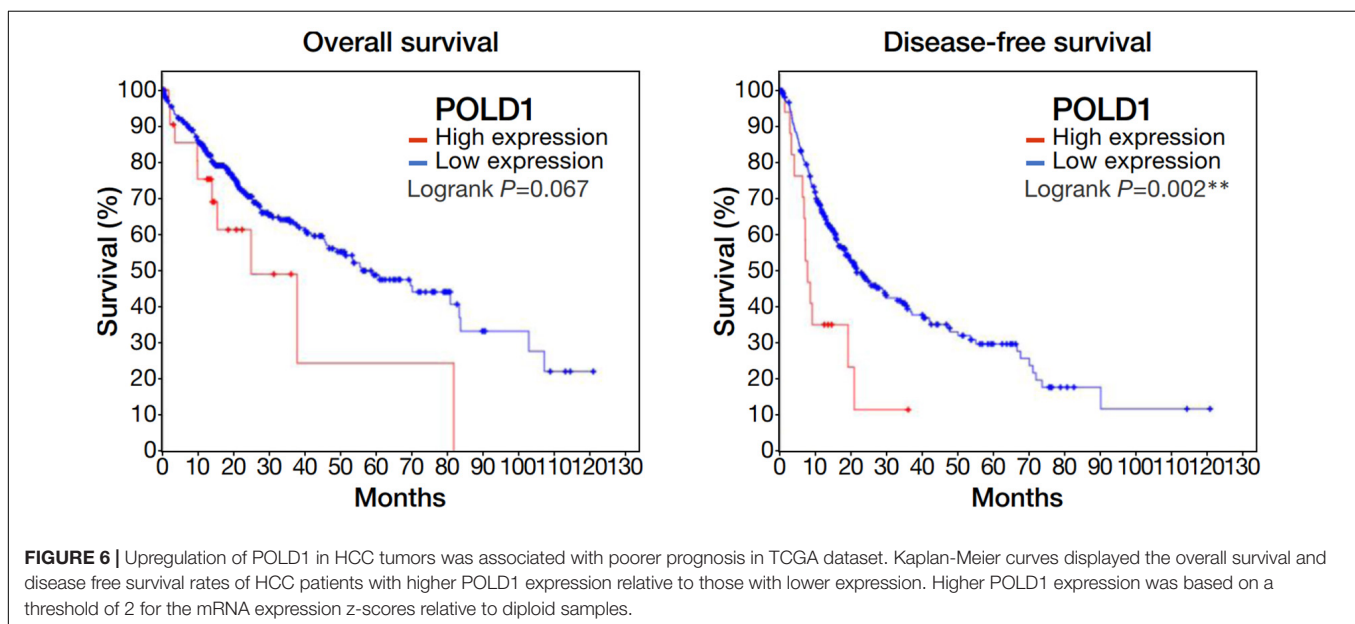
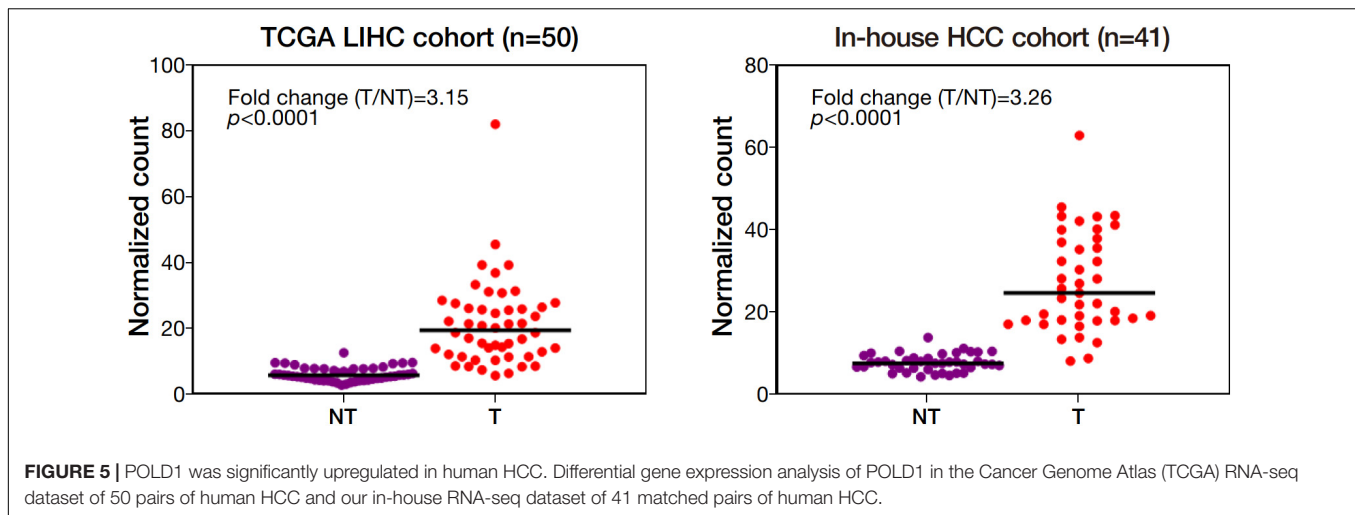


FIGURE 4 | POLD1 was positively correlated with FOXM1 and CENPF. Correlation analysis among the list of repressed candidate genes using our in-house RNA-seq dataset and the TCGA RNA-seq dataset. Both analyses indicated POLD1 was significantly correlated to both FOXM1 and CENPF ($p < 0.05$). Three-dimensional plot showed the correlation between the expressions of FOXM1, CENPF and POLD1 in both datasets.

were regulated by FOXM1, with 103 being activated and 106 being repressed upon FOXM1 knockdown; 156 genes that were regulated by CENPF, with 43 being activated and 113 being repressed upon CENPF knockdown; and 343 genes that were co-regulated by FOXM1 and CENPF, with 219 being activated and 124 being repressed upon co-knockdown of FOXM1 and CENPF (Figure 3). Among 343 candidate genes that were potentially being co-regulated by FOXM1 and CENPF, we further filtered

out 29 genes that were activated and 4 genes that were repressed upon co-knockdown of FOXM1 and CENPF in HCC cells (Supplementary Figure 3).

To elucidate the molecular pathways underlying the synergistic interaction of FOXM1 and CENPF, we subjected the list of activated and repressed candidate genes for gene set enrichment analysis using two databases, including Gene Ontology (biological process) and Reactome Pathway. We found



that the differentially expressed genes were mainly enriched in biological pathways associated with various metabolic processes and biological signaling pathways. Notably, these genes were also enriched in several signaling pathways that are associated with tumorigenesis, including insulin growth factor (IGF) and platelet-derived growth factor (PDGF) signaling pathways (Supplementary Figure 4).

Among the 4 repressed gene candidates (Supplementary Figure 3), correlation analysis was performed using our in-house RNA-seq and the TCGA dataset. We found that *POLD1* (DNA Polymerase Delta 1) is positively correlated with both FOXM1 and CENPF, respectively and concurrently, in both RNA-seq datasets (Figure 4). In addition, *POLD1* expression was significantly upregulated in HCC tumor when compared with the corresponding liver tissue in TCGA RNA-seq dataset (fold change = 3.15, $p < 0.0001$) and in our in-house RNA-seq dataset (fold change = 3.26,

$p < 0.0001$) (Figure 5). Furthermore, we found that HCC patients with higher expression of *POLD1* had shorter overall survival and disease-free survival rates from the TCGA data analysis (Figure 6).

Effect of Knockdown of POLD1 in Tumorigenicity and Lung Metastasis in HCC

We knockdown *POLD1* (shPOLD1) in MHCC97L HCC cells by shRNA approach and performed *in vivo* liver orthotopic injection assay to assess the functional role of *POLD1* in liver tumorigenicity and lung metastasis. We showed that shPOLD1 strongly reduced tumor incidence. The tumor sizes (measured by total flux signal) were significantly reduced in mice injected with shPOLD1 HCC cells. We also observed a trend of diminished lung metastasis upon knockdown

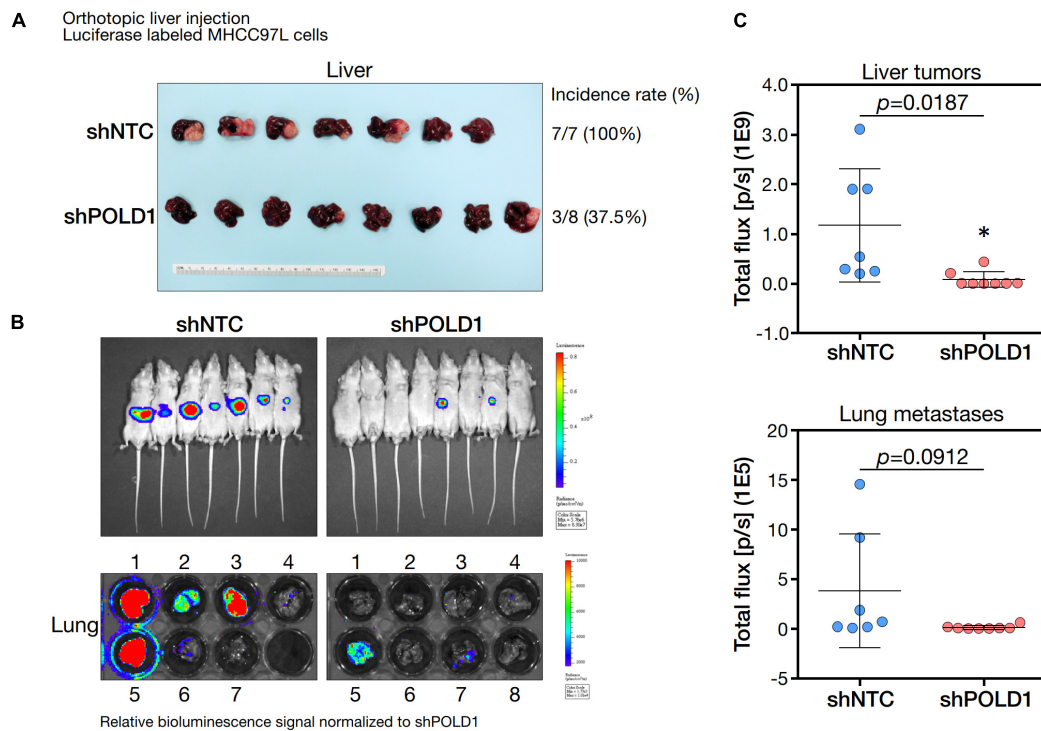


FIGURE 7 | Knockdown of POLD1 in MHCC97L-luc cells reduced tumor incidence, tumor sizes and lung metastases in orthotopic liver injection model. The *in vivo* functional role of POLD1 knockdown was evaluated as compared to the non-target control (NTC). Comparison was based on **(A)** tumorigenicity and **(B,C)** tumor size and lung metastasis.

of POLD1, but the difference could not reach statistical significance (Figure 7).

DISCUSSION

Development of HCC is a multistep process results from accumulation of mutational events in cancer driver genes. The alterations in driver genes promote oncogenic functions, such as proliferation, survival, cell motility and immune evasion. Moreover, accumulation of genetic and epigenetic alterations could contribute to tumor initiation, progression, metastasis and resistance to therapy (16). The malignant phenotype of cancer entails the dysregulation of cell cycle machinery, which serves as a convergence point for cellular transformation (17).

In this study, we demonstrated the significant roles of FOXM1 and CENPF in hepatocarcinogenesis. First, we found the co-overexpression of FOXM1 and CENPF in HCC was associated with aggressive tumor behavior, including the presence of venous invasion, tumor microsatellite formation, and the absence of tumor encapsulation by clinicopathological correlation analysis. Second, we demonstrated that FOXM1 and CENPF are important for cell growth. Third, our RNA-seq study further delineated that FOXM1 and CENPF co-regulated a set of genes that play essential roles in various metabolic processes and oncogenic signaling pathways. Among all differentially expressed genes between the wild-type HCC cells and FOXM1 and/or

CENPF knockdown cell lines, *POLD1*, which encodes for the catalytic subunit of DNA polymerase δ , was ranked as the top downstream target co-regulated by FOXM1 and CENPF.

In addition to the delineation of underlying mechanism of FOXM1 and CENPF in HCC, we have also been able to demonstrate their therapeutic implications in HCC using *in vitro* models. Despite the efficacy of existing molecularly targeted drugs, e.g., sorafenib and regorafenib, there is still an unmet medical need for patients with advanced HCC. With the successful advent of immune checkpoint inhibitors (ICIs), the combo of atezolizumab and bevacizumab has become the standard of care. However, although early clinical outcomes are impressive, a significant proportion of patients do not respond to this regimen. Uncontrolled cell growth is one of the characteristics of cancer, which entails aberrant activities of cell cycle proteins. Upregulation of FOXM1 and CENPF were shown to be crucial for the deregulated cell proliferation in HCC in this study. HCC may be uniquely dependent on FOXM1 and CENPF for cell growth; thus, we speculated that targeting these two cell cycle regulators offer considerable potentials in treating HCC. Thiostrepton is a potential inhibitor of FOXM1 (18, 19) while zoledronic acid is a potential inhibitor of CENPF (20–22). Indeed, we observed thiostrepton and zoledronic acid inhibited HCC cells selectively, as compared to the normal liver cells (Supplementary Figure 5). Further studies are awaited to confirm their potential usage in HCC treatment. It would also be interesting to test these inhibitors in the presence of ICI

treatment, for instance in immunocompetent mouse models.

Taken together, our study provided new insight into the underlying synergistic mechanism of FOXM1 and CENPF via the regulation of POLD1, which plays a significant role in HCC progression. Moreover, FOXM1 and CENPF also represent new vulnerabilities to novel drug-based therapy in HCC.

DATA AVAILABILITY STATEMENT

The datasets presented in this study can be found in online repositories. The names of the repository/repositories and accession number(s) can be found in <https://www.ncbi.nlm.nih.gov/bioproject/>, PRJNA800214.

ETHICS STATEMENT

The studies involving human participants were reviewed and approved by Institutional Review Board of the University of Hong Kong/Hospital Authority Hong Kong West Cluster. The patients/participants provided their written informed consent to participate in this study. The animal study was reviewed and approved by Committee on the Use of Live Animals in Teaching and Research (CULATR) of the University of Hong Kong.

AUTHOR CONTRIBUTIONS

DH and IN: study concept and design. DH, W-LL, L-KC, and IN: acquisition of data, analysis and interpretation of data, and drafting of the manuscript. IN: acquisition of clinical samples. All authors reviewed and approved the final draft of the manuscript.

FUNDING

The study was supported by the National Natural Science Foundation of China (81872222), Health and Medical Research

Fund (03142836 and 07182546), General Research Fund (17100021 and 17117019), Hong Kong Research Grants Council Theme-based Research Scheme (T12-704/16-R), and Innovation and Technology Commission grant for State Key Laboratory of Liver Research. IN is Loke Yew Professor in Pathology.

ACKNOWLEDGMENTS

We thank the Center for PanorOmic Sciences of The University of Hong Kong for the RNA-seq service.

SUPPLEMENTARY MATERIAL

The Supplementary Material for this article can be found online at: <https://www.frontiersin.org/articles/10.3389/fmed.2022.860395/full#supplementary-material>

Supplementary Figure 1 | Short tandem repeat (STR) DNA profiling of MHCC97L.

Supplementary Figure 2 | Transient knockdown efficiencies of FOXM1 and CENPF in Huh7, Hep3B and MHCC97L. **(A)** mRNA expression and **(B)** protein expression of FOXM1 and CENPF upon siRNA transfection.

Supplementary Figure 3 | Candidate genes that were co-regulated by FOXM1 and CENPF. Additional filters (differential expression with $p < 0.05$; $\log\text{CPM} > 1$; and $|\log\text{FC}| > 1$) were used to narrow down the list of candidate genes. Among all, there were 29 genes being activated and 4 being repressed upon co-silencing of FOXM1 and CENPF across Huh7, Hep3B and MHCC97L.

Supplementary Figure 4 | Gene set enrichment analysis of the candidate genes co-regulated by FOXM1 and CENPF. The analysis was performed using Gene Ontology (GO) biological processes and Reactome Pathway.

Supplementary Figure 5 | Half-maximal inhibitory concentration (IC_{50}) of thiostrepton and zoledronic acid in HCC cell and non-tumorigenic liver cells. The percent growth inhibition curve showed the response of the Huh7 HCC cell line and two non-tumorigenic liver cell lines, including MIHA and LO2, to thiostrepton or zoledronic acid treatments at varying dosage. Thio, thiostrepton; ZOL, zoledronic acid.

REFERENCES

1. Sung H, Ferlay J, Siegel RL, Laversanne M, Soerjomataram I, Jemal A, et al. Global cancer statistics 2020: globocan estimates of incidence and mortality worldwide for 36 cancers in 185 countries. *CA Cancer J Clin.* (2021) 71:209–49. doi: 10.3322/caac.21660
2. Llovet JM, Kelley RK, Villanueva A, Singal AG, Pikarsky E, Roayaie S, et al. Hepatocellular carcinoma. *Nat Rev Dis Primers.* (2021) 7:6. doi: 10.1038/s41572-020-00240-3
3. Ho DW, Lo RC, Chan LK, Ng IO. Molecular pathogenesis of hepatocellular carcinoma. *Liver Cancer.* (2016) 5:290–302. doi: 10.1159/000449340
4. Ho DW, Lyu X, Ng IO. Viral integration detection strategies and a technical update on virus-clip. *BioCell.* (2021) 45:1495–500. doi: 10.32604/biotech.2021.017227
5. Ho DW, Kai AK, Ng IO. TCGA whole-transcriptome sequencing data reveals significantly dysregulated genes and signaling pathways in hepatocellular carcinoma. *Front Med.* (2015) 9:322–30. doi: 10.1007/s11684-015-0408-9
6. Laoukili J, Kooistra MR, Bras A, Kaur J, Kerkhoven RM, Morrison A, et al. FoxM1 is required for execution of the mitotic programme and chromosome stability. *Nat Cell Biol.* (2005) 7:126–36. doi: 10.1038/ncb1217
7. Aytes A, Mitrofanova A, Lefebvre C, Alvarez MJ, Castillo-Martin M, Zheng T, et al. Cross-species regulatory network analysis identifies a synergistic interaction between FOXM1 and CENPF that drives prostate cancer malignancy. *Cancer Cell.* (2014) 25:638–51. doi: 10.1016/j.ccr.2014.03.017
8. Sze KM, Ho DW, Chiu YT, Tsui YM, Chan LK, Lee JM, et al. Hepatitis B virus-telomerase reverse transcriptase promoter integration harnesses host ELF4, resulting in telomerase reverse transcriptase gene transcription in hepatocellular carcinoma. *Hepatology.* (2021) 73:23–40. doi: 10.1002/hep.31231
9. Ng IO, Lai EC, Ng MM, Fan ST. Tumor encapsulation in hepatocellular carcinoma. A pathologic study of 189 cases. *Cancer.* (1992) 70:45–9. doi: 10.1002/1097-0142(19920701)70:1<45::aid-cnrcr2820700108>3.0.co;2-7
10. Conway T, Wazny J, Bromage A, Tymms M, Sooraj D, Williams ED, et al. Xenome—a tool for classifying reads from xenograft samples. *Bioinformatics.* (2012) 28:i172–8. doi: 10.1093/bioinformatics/bts236
11. Ho DWH, Chan LK, Chiu YT, Xu IMJ, Poon RTP, Cheung TT, et al. TSC1/2 mutations define a molecular subset of HCC with aggressive behaviour and treatment implication. *Gut.* (2017) 66:1496–506. doi: 10.1136/gutjnl-2016-312734

12. Ho DW, Tsui YM, Sze KM, Chan LK, Cheung TT, Lee E, et al. Single-cell transcriptomics reveals the landscape of intra-tumoral heterogeneity and stemness-related subpopulations in liver cancer. *Cancer Lett.* (2019) 459:176–85. doi: 10.1016/j.canlet.2019.06.002
13. Ma W, Ho DW, Sze KM, Tsui YM, Chan LK, Lee JM, et al. APOBEC3B promotes hepatocarcinogenesis and metastasis through novel deaminase-independent activity. *Mol Carcinog.* (2019) 58:643–53. doi: 10.1002/mc.22956
14. Ho DW, Tsui YM, Chan LK, Sze KM, Zhang X, Cheu JW, et al. Single-cell RNA sequencing shows the immunosuppressive landscape and tumor heterogeneity of HBV-associated hepatocellular carcinoma. *Nat Commun.* (2021) 12:3684. doi: 10.1038/s41467-021-24010-1
15. Ho DW, Ng IO. uGPA: unified gene pathway analyzer package for high-throughput genome-wide screening data provides mechanistic overview on human diseases. *Clin Chim Acta.* (2015) 441:105–8.
16. Llovet JM, Zucman-Rossi J, Pikarsky E, Sangro B, Schwartz M, Sherman M, et al. Hepatocellular carcinoma. *Nat Rev Dis Primers.* (2016) 2:16018. doi: 10.1038/nrdp.2016.18
17. Williams GH, Stoeber K. The cell cycle and cancer. *J Pathol.* (2012) 226:352–64.
18. Hegde NS, Sanders DA, Rodriguez R, Balasubramanian S. The transcription factor FOXM1 is a cellular target of the natural product thiostrepton. *Nat Chem.* (2011) 3:725–31. doi: 10.1038/nchem.1114
19. Kwok JM, Myatt SS, Marson CM, Coombes RC, Constantinidou D, Lam EW. Thiostrepton selectively targets breast cancer cells through inhibition of forkhead box M1 expression. *Mol Cancer Ther.* (2008) 7:2022–32. doi: 10.1158/1535-7163.MCT-08-0188
20. Brown HK, Ottewill PD, Coleman RE, Hoken I. The kinetochore protein Cenp-F is a potential novel target for zoledronic acid in breast cancer cells. *J Cell Mol Med.* (2011) 15:501–13. doi: 10.1111/j.1582-4934.2009.00955.x
21. Mi YJ, Gao J, Xie JD, Cao JY, Cui SX, Gao HJ, et al. Prognostic relevance and therapeutic implications of centromere protein F expression in patients with esophageal squamous cell carcinoma. *Dis Esophagus.* (2013) 26:636–43. doi: 10.1111/dote.12002
22. Cao JY, Liu L, Chen SP, Zhang X, Mi YJ, Liu ZG, et al. Prognostic significance and therapeutic implications of centromere protein F expression in human nasopharyngeal carcinoma. *Mol Cancer.* (2010) 9:237. doi: 10.1186/1476-4598-9-237

Conflict of Interest: The authors declare that the research was conducted in the absence of any commercial or financial relationships that could be construed as a potential conflict of interest.

Publisher's Note: All claims expressed in this article are solely those of the authors and do not necessarily represent those of their affiliated organizations, or those of the publisher, the editors and the reviewers. Any product that may be evaluated in this article, or claim that may be made by its manufacturer, is not guaranteed or endorsed by the publisher.

Copyright © 2022 Ho, Lam, Chan and Ng. This is an open-access article distributed under the terms of the Creative Commons Attribution License (CC BY). The use, distribution or reproduction in other forums is permitted, provided the original author(s) and the copyright owner(s) are credited and that the original publication in this journal is cited, in accordance with accepted academic practice. No use, distribution or reproduction is permitted which does not comply with these terms.



Ferroptosis in Intrahepatic Cholangiocarcinoma: *IDH1*^{105GGT} Single Nucleotide Polymorphism Is Associated With Its Activation and Better Prognosis

Samantha Sarcognato^{1*}, Diana Sacchi¹, Luca Fabris², Giacomo Zanus^{3,4}, Enrico Gringeri⁴, Monia Niero¹, Giovanna Gallina¹ and Maria Guido^{1,5}

¹ Department of Pathology, Azienda ULSS2 Marca Trevigiana, Treviso, Italy, ² Department of Molecular Medicine – DMM, University of Padova, Padova, Italy, ³ 4th Surgery Unit, Azienda ULSS2 Marca Trevigiana, Treviso, Italy, ⁴ Department of Surgery, Oncology and Gastroenterology – DISCOG, University of Padova, Padova, Italy, ⁵ Department of Medicine – DIMED, University of Padova, Padova, Italy

OPEN ACCESS

Edited by:

Arndt Hartmann,
Universitätsklinikum Erlangen,
Germany

Reviewed by:

Henning Reis,
Goethe University Frankfurt, Germany
Hwajeong Lee,
Albany Medical College, United States

*Correspondence:

Samantha Sarcognato
samantha.sarcognato@
aulss2.veneto.it

Specialty section:

This article was submitted to
Pathology,
a section of the journal
Frontiers in Medicine

Received: 28 February 2022

Accepted: 21 June 2022

Published: 08 July 2022

Citation:

Sarcognato S, Sacchi D, Fabris L,
Zanus G, Gringeri E, Niero M,
Gallina G and Guido M (2022)
Ferroptosis in Intrahepatic
Cholangiocarcinoma: *IDH1*^{105GGT}
Single Nucleotide Polymorphism Is
Associated With Its Activation
and Better Prognosis.
Front. Med. 9:886229.
doi: 10.3389/fmed.2022.886229

Objectives: Intrahepatic cholangiocarcinoma (ICC) has a dismal prognosis and often demonstrates an anti-apoptotic landscape, which is a key step to chemotherapy resistance. Isocitrate dehydrogenase 1 or 2 (*IDH1-2*)-mutated ICCs have been described and associated with better prognosis. Ferroptosis is a regulated iron-mediated cell death induced by glutathione peroxidase 4 (GPX4) inhibition, and may be triggered pharmacologically. GPX4 is overexpressed in aggressive cancers, while its expression is inhibited by *IDH1*^{R132C} mutation in cell lines. We investigated tissue expression of ferroptosis activation markers in ICC and its correlation with clinical-pathological features and *IDH1-2* status.

Materials and Methods: We enrolled 112 patients who underwent hepatic resection or diagnostic liver biopsy for ICC. Immunostaining for transferrin-receptor 1 and GPX4, and Pearls' stain for iron deposits were performed to evaluate ferroptosis activation. Immunostaining for STAT3 was performed to study pro-inflammatory and anti-apoptotic landscape. Main *IDH1-2* mutations were investigated in 90 cases by real-time polymerase chain reaction.

Results: GPX4 overexpression was seen in 79.5% of cases and related to poor histological prognostic factors (grading and perineural and vascular invasion; $p < 0.005$ for all) and worse prognosis (OS $p = 0.03$; DFS $p = 0.01$). STAT3 was expressed in 95.5% of cases, confirming the inflammation-related anti-apoptotic milieu in ICC, and directly related to GPX4 expression ($p < 0.0001$). A high STAT3 expression correlated to a worse prognosis (OS $p = 0.02$; DFS $p = 0.001$). Nearly 12% of cases showed *IDH1*^{105GGT} single nucleotide polymorphism, which was never described in ICC up to now, and was related to lower tumor grade ($p < 0.0001$), longer overall survival ($p = 0.04$), and lower GPX4 levels ($p = 0.001$).

Conclusion: Our study demonstrates for the first time that in most inflammatory ICCs ferroptosis is not active, and its triggering is related to *IDH1-2* status. This supports the possible therapeutic role of ferroptosis-inducer drugs in ICC patients, especially in drug-resistant cases.

Keywords: intrahepatic cholangiocarcinoma, ferroptosis, *IDH1*^{105GGT} single nucleotide polymorphism, STAT3, GPX4

INTRODUCTION

Intrahepatic cholangiocarcinoma (ICC) is the second most common primary liver tumor, whose incidence and mortality have increased worldwide over the last decades (1–6). Because of a frequent diagnosis at an advanced stage, ICC prognosis remains dismal. Surgical resection is the only potentially curative treatment option, but recurrence rates remain high. Patients with metastatic or unresectable disease undergo palliative non-curative systemic therapies, with only modest increases in overall survival and frequent development of chemoresistance, often due to an escape from drug-induced apoptosis by cancer cells (1, 3–5, 7, 8).

Advances have been made in the last decade regarding ICC molecular background. In particular, Sia et al. identified two molecular subclasses, named the proliferative and the inflammation-related classes (9). The latter is defined by the triggering of pro-inflammatory signaling pathways *via* different interleukins and the signal transducer and activator of transcription 3 (STAT3) protein (4, 9). STAT3 is involved in several cellular processes, inhibits apoptosis, and it is known to play a role in many cancer types, being associated with a worse prognosis (4, 10–13).

A subgroup of ICCs showing missense mutations in the isocitrate dehydrogenase 1 and 2 (*IDH1-2*) genes has also been described (14, 15). *IDH*-mutated ICCs exhibit high expression of mitochondrial genes and low expression of chromatin modifier genes and were demonstrated to have a better prognosis than cases with wild type *IDH1-2* (3, 4, 14–17).

Ferroptosis is a newly described form of regulated iron-mediated cell death type, whose activation requires high intracytoplasmic iron concentrations and the inhibition of the reduced glutathione (GSH)-dependent enzyme glutathione peroxidase 4 (GPX4) (18, 19). GPX4 overexpression has been described in many aggressive cancers, making it a potential therapeutic target able to promote death in drug-tolerant tumor cells. Many molecules currently exist that are able to trigger the ferroptotic cascade, known as ferroptosis inducers, either by decreasing GSH levels, such as erastin, or by directly inhibiting GPX4 activity, such as RSL3. Some of them are currently under investigation in clinical trials for cancer treatment (19, 20). So far, no data are reported in the literature regarding the possible role of ferroptosis and ferroptosis inducers in ICC.

An *in vitro* study by Wang et al. (21) conducted on different cell lines firstly demonstrated that tumor-derived *IDH1*^{R132C} mutation sensitizes cells to ferroptosis, by reducing

GPX4 levels through the production of the oncometabolite 2-hydroxyglutarate (2-HG). In their work, mutated cells were able to undergo ferroptosis in response to erastin but not to RSL3, which acts in a concentration-dependent manner, implying that 2-HG acts directly on GPX4 expression (21).

Basing on this background, the aim of our study was to investigate tissue expression of ferroptosis activation markers in ICC cases, and to correlate it with clinical-pathological features, STAT3 expression, and *IDH1-2* status.

MATERIALS AND METHODS

Case Selection

We retrospectively collected a total of 112 consecutive patients with a diagnosis of ICC. Among them, 90 patients underwent laparoscopic hepatic resection with curative intent from January 2006 to May 2021. The remaining 22 patients were patients with liver mass who underwent diagnostic liver biopsy, eventually diagnosed as ICC, who subsequently underwent surgery in a different hospital. Thirty patients included in our cohort were already investigated before, as part of a previous study (22). Exclusion criteria were (i) the administration of any systemic or loco-regional therapy prior to surgery/biopsy, (ii) a survival of less than 3 months after surgery (for patients who underwent resection), to exclude deaths due to surgical complications, and (iii) the absence of available residual tumor tissue for immunohistochemical (IHC) stains and molecular tests. Only surgical specimens were considered for molecular analyzes. The study complies with the ethical guidelines of the 1975 Declaration of Helsinki and obtained the approval from the local Ethics Committee (Ethics Committee for Clinical Research—University Hospital of Padova, Italy; protocol #: 0038038/17). All of the patients gave their appropriate informed consent to any procedure.

Clinical Data

Patients' relevant clinical and laboratory data were retrieved from medical records, including sex, age, serum ferritin levels, the presence of any underlying chronic hepatic or biliary disease, the presence of cirrhosis, and the administration of adjuvant chemotherapy. We also reported whether lymphadenectomy was performed during surgery or not.

All patients who underwent surgery were clinically followed-up, and regularly subjected to ultrasonography and computed tomography to detect any recurrence of the disease. Overall and disease-free survival time was obtained from medical charts.

Histological Study

All of the cases were blindly and contemporarily reviewed by an experienced (MG) and two trainee (SS and DS) liver pathologists, and relevant histological features were recorded, including macroscopic tumor type, histotype, grade of differentiation, T stage (according to the revised 8th edition of the UICC staging system) (23), margin status (for surgical resections), and the presence of vascular and perineural invasion and lymph node metastasis.

Immunohistochemical Study

Tissue microarrays (TMAs) made of formalin-fixed paraffin-embedded ICC tissue cores (with a diameter of 2 mm) were obtained by selecting two or three representative tumor areas from each liver resection case, depending on tumor dimension. All of the samples were processed by using the TMA Master platform (3DHistech, Budapest, Hungary), a semi-automatic and computer-assisted TMA platform.

Immunostains were performed on TMA and liver biopsy sections by using the following antibodies: anti-STAT3 (clone F-2; Santa Cruz Biotechnology, Dallas, TX, United States; dilution 1:200; mouse monoclonal), anti-GPX4 (clone E-12; Santa Cruz Biotechnology, Dallas, TX, United States; dilution 1:400; mouse monoclonal), and anti-transferrin receptor 1 (TFR1; also known as CD71) (clone 10F11; Leica Biosystems, Newcastle upon Tyne, United Kingdom; dilution 1:100; mouse monoclonal). All IHC stains were conducted according to standard protocols by using the Dako Omnis autostainer (Dako, Glostrup, Denmark), and all of the slides were counterstained with hematoxylin. Appropriate positive and negative controls were used for each run. In evaluating the expression of all markers, only cytoplasmic staining was considered. STAT3 and GPX4 expression was semi-quantitatively scored from 0 to 2+, as follows: 0 = negative; 1+ = expression in $\leq 50\%$ of tumor cells (TCs); 2+ = expression in $> 50\%$ of TCs (Figure 1). Finally, TFR1 positivity was evaluated as follows: 0 = negative or positive in $\leq 10\%$ of TCs; 1+ = expression in 11–50% of TCs; 2+ = expression in $> 50\%$ of TCs (Figure 2).

In every case, we also performed histochemical Perls' stain (Artisan Iron Stain Kit, Dako, Glostrup, Denmark) to detect intratumoral iron deposits, which were recorded as absent/present (Figure 3).

Molecular Study

As reported above, only surgical specimens (90 cases) were considered for molecular tests. For each case, DNA extraction was performed on selected representative areas of formalin-fixed paraffin-embedded ICC tissue, with Qiasymphony DSP DNA Mini Kit (Qiagen, Hilden, Germany). DNA quantity was measured spectrophotometrically by using NanoDrop ND 100 Spectrophotometer (Thermo Fisher Scientific, Waltham, MA, United States). Detection of the main *IDH1* (codons 105 and 132) and *IDH2* (codons 140 and 172) gene mutations was performed by real-time polymerase chain reaction (PCR) analysis (Easy PGX ready IDH1-2, Easy PGX platform, Diatech Pharmacogenetics, Jesi, Italy), according to the manufacturer's

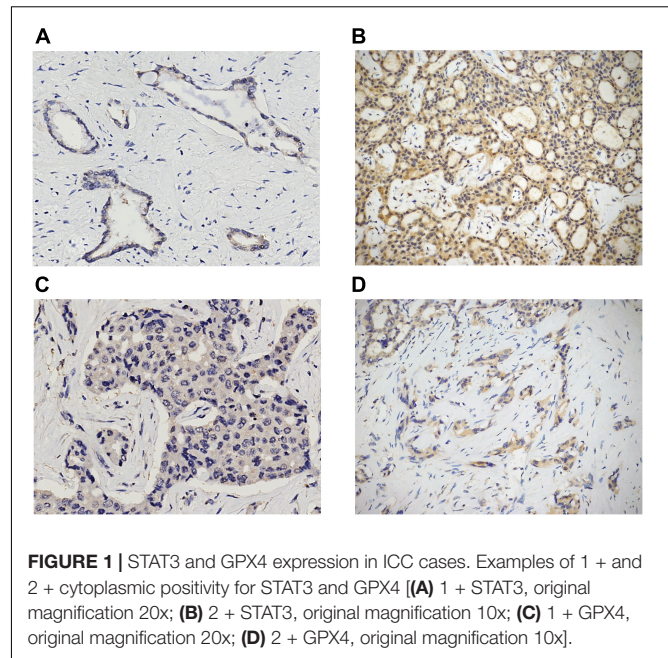


FIGURE 1 | STAT3 and GPX4 expression in ICC cases. Examples of 1+ and 2+ cytoplasmic positivity for STAT3 and GPX4 [(A) 1+ STAT3, original magnification 20x; (B) 2+ STAT3, original magnification 10x; (C) 1+ GPX4, original magnification 20x; (D) 2+ GPX4, original magnification 10x].

instructions. When necessary, the identified mutations were confirmed by PCR analysis and Sanger sequencing, by using the ABI PRISM 3500 Genetic Analyzer (Applied Biosystems, Waltham, MA, United States).

Statistical Analysis

Continuous variables were expressed as median (range) while categorical variables as frequency and percentage. For clinical-pathological correlations, appropriated tests were used, including Student's *t*-test, one-way ANOVA test, Spearman rank correlation test and Fisher exact probability test. The Kaplan–Meier method was used to create survival curves, which were compared by using both the log-rank and the Breslow (generalized Wilcoxon) tests. Multivariate Cox backward stepwise regression analyzes were performed including all of the variables identified as significant on univariate Cox regression analyzes. Hazard ratios (HRs) and their 95% confidence intervals (CIs) were calculated. *p* values < 0.05 were considered statistically significant. Data analyzes were performed by applying Statistical Package for the Social Science (SPSS, version 25, IBM SPSS Statistics, Chicago, IL, United States) and GraphPad (version 6, GraphPad Software, San Diego, CA, United States) statistical software.

RESULTS

Clinical Features

Overall, in our cohort of 112 patients there were 58 males (51.8%) and 54 females (48.2%), with a median age of 68 years (range 34–92 years). Seventeen patients (15.2%) had a cirrhotic liver, and 36 patients (32.1%) received adjuvant chemotherapy after resection/biopsy. Patients had a median follow-up of 1.7 years (range 0.3–8.8 years). Lymphadenectomy was performed in 33/90 patients who underwent surgery. Clinical and laboratory

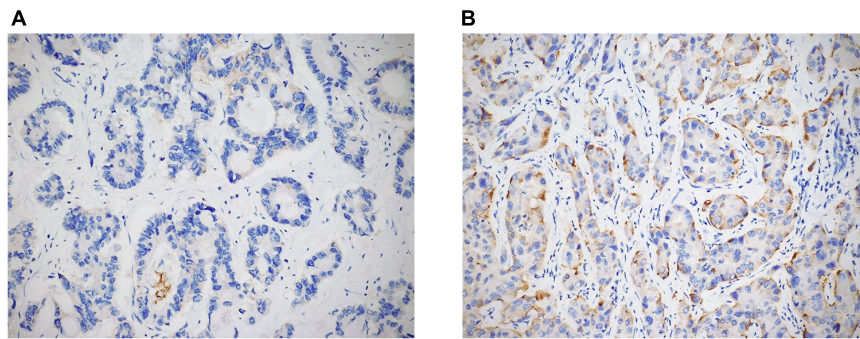


FIGURE 2 | TFR1 expression in ICC cases was semi-quantitatively evaluated as negative, 1 + [(A) original magnification 20x], and 2 + [(B) original magnification 20x].

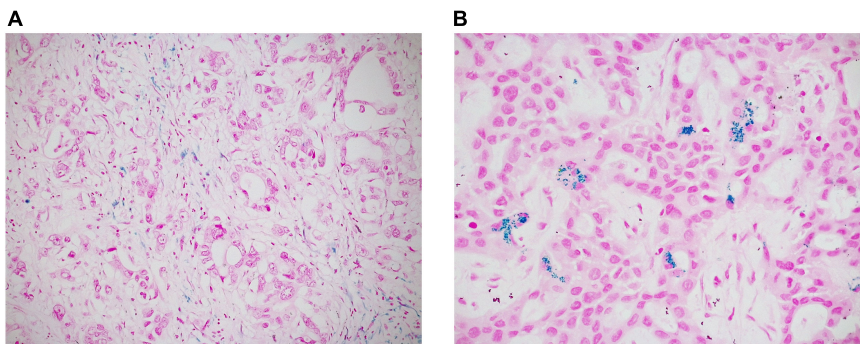


FIGURE 3 | Intratumoral iron deposits in ICC were evaluated as absent/present. Negative cases often showed iron deposition in peri-tumoral macrophages, but not in neoplastic cells [(A) original magnification 20x]; in positive cases, iron deposits appear as intracytoplasmic blue granules in tumor cells [(B) original magnification 40x].

features of all the patients are summarized in **Table 1**. Age, sex, the presence of underlying chronic liver diseases, and the administration of adjuvant chemotherapy were not related to patients' prognosis. Furthermore, overall and disease-free survivals were not different between patients with or without cirrhosis, probably because of the low number of cirrhotic patients in our cohort.

Histological Features and Clinical-Pathological Correlations

Macroscopically, all cases were mass forming, while, histologically, there were 82 cases (73.2%) of small duct type ICC and 30 cases (26.8%) of large duct type ICC. We observed vascular invasion in 78 out of 112 patients (69.6%), while perineural invasion was present in 50/112 cases (44.6%), as reported in **Table 2**. Among the 33 patients who underwent lymphadenectomy, 15 had lymph node metastases. Forty-seven patients out of the 90 who underwent surgery (52.2%) had a complete surgical excision of the tumor (R0 cases), while the remaining 43 patients (47.8%) showed a microscopic neoplastic infiltration of the resection margin (R1 cases).

As expected, grading and the presence of perineural and vascular neoplastic invasion were all related to worse overall

($p = 0.009$, $p < 0.0001$, and $p = 0.004$, respectively) and disease-free survivals ($p = 0.01$, $p = 0.002$, and $p = 0.001$, respectively). An advanced T stage (i.e., T stage 3 and 4) was related to a reduced overall survival ($p = 0.06$). We failed to find any correlation between patients' prognosis and histotype or resection margin status. We did not observe differences in survival times between cases with or without lymph node metastases.

Immunohistochemical Features and Clinical-Pathological Correlations

In our cohort, most of the cases showed GPX4 expression, either 1 + (43/112; 38.4%) or 2 + (46/112; 41.1%), while only 23 cases (20.5%) were completely negative. Twenty-two patients out of 112 (19.6%) showed 1 + TFR1 expression, while 7 cases showed a 2 + TFR1 positivity (6.3%). Intratumoral iron deposits were observed in only 2 cases (1.8%); among them, one showed a focal and one a diffuse deposition. Interestingly, the case that showed diffuse iron deposits had both a strong TFR1 expression and a completely negative GPX4 stain (**Supplementary Figure 1**). Taken together, these findings suggest an inhibition of the ferroptotic cascade in ICC. Most of our cases showed either a 1 + (56/112; 50%) or 2 + (51/112; 45.5%) STAT3 expression, with only 5 cases (4.5%) showing a completely negative reaction, suggesting an activation of the inflammatory pathway in our ICC

TABLE 1 | Clinical and laboratory features of the patients.

Feature	N = 112
Age [years]	
Median (range)	68 (34 – 92)
Sex N (%)	
Males	58 (51.8)
Females	54 (48.2)
Ferritin [ng/ml]	
Median (range)	260.5 (53 – 943.5)
Underlying diseases N (%)	
HBV hepatitis	6 (5.4)
HCV hepatitis	11 (9.8)
Alcoholic hepatitis	6 (5.4)
NAFLD/NASH	6 (5.4)
Cryptogenic cirrhosis	1 (0.9)
Cirrhosis N (%)	17 (15.2)
Adjuvant chemotherapy N (%)	36 (32.1)
Recurrence N (%)	60 (53.6)
Exitus N (%)	73 (65.2)

HBV, hepatitis B virus; HCV, hepatitis C virus; NAFLD, non-alcoholic fatty liver disease; NASH, non-alcoholic steatohepatitis.

TABLE 2 | Histological features of the patients.

Feature	N = 112
Histotype	
N (%)	
Small duct type	82 (73.2)
Large duct type	30 (26.8)
Grade	
N (%)	
G1	15 (13.4)
G2	49 (43.8)
G3	48 (42.8)
T stage [N = 90]	
N (%)	
T1a	13 (14.4)
T1b	11 (12.2)
T2	46 (51.1)
T3	13 (14.4)
T4	7 (7.9)
Vascular invasion N (%)	78 (69.6)
Perineural invasion N (%)	50 (44.6)
Lymph node metastasis [N = 33] N (%)	15 (45.5)
Resection margin status [N = 90]	
N (%)	
R0	47 (52.2)
R1	43 (47.8)

cohort. Histochemical and immunohistochemical expressions of the different markers are summarized in **Table 3**.

Statistical analyzes showed a direct correlation between GPX4 expression and the presence of poor prognostic histological parameters, that is grading ($p < 0.0001$) and perineural ($p = 0.03$) and vascular invasion ($p < 0.0001$). We also found a direct

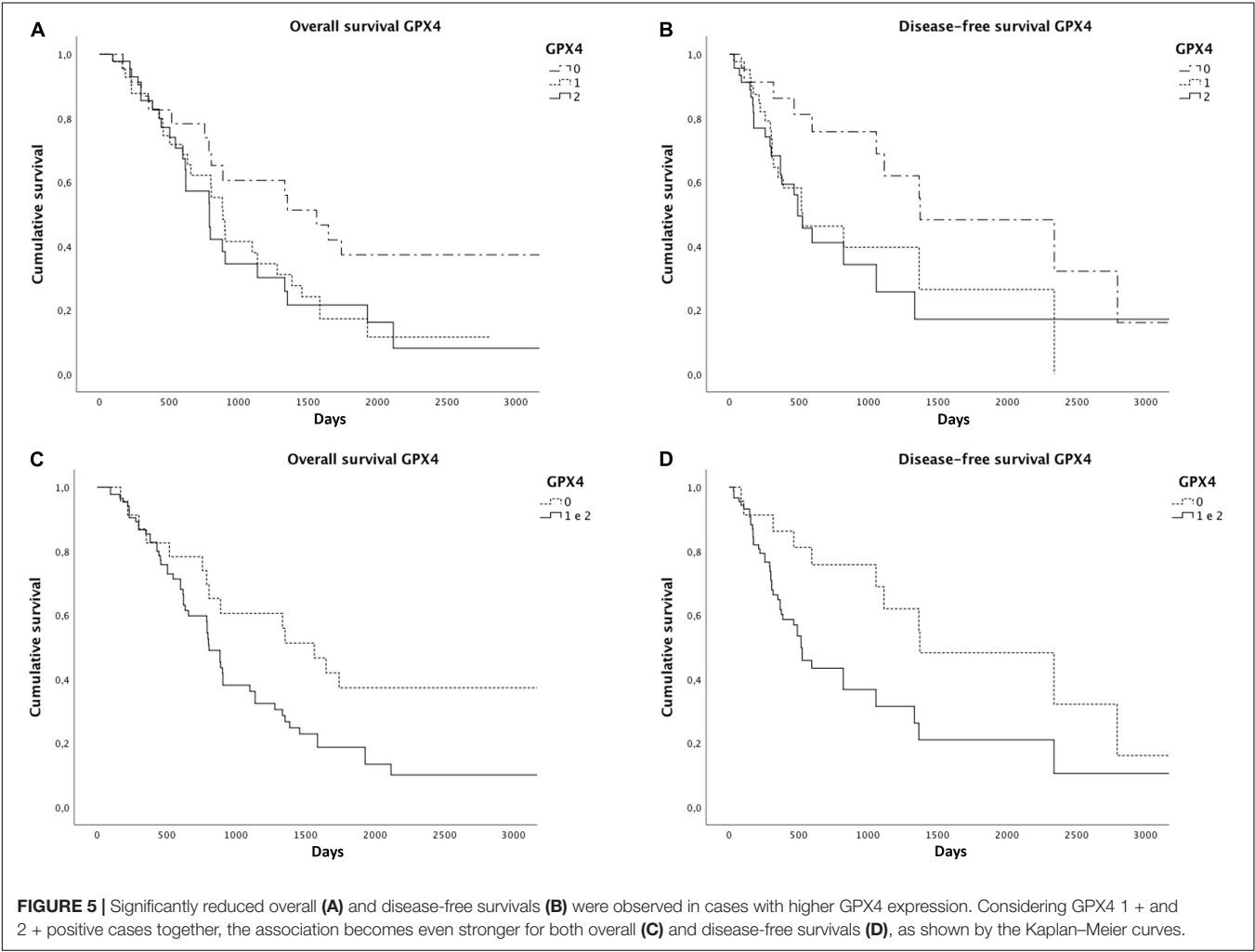
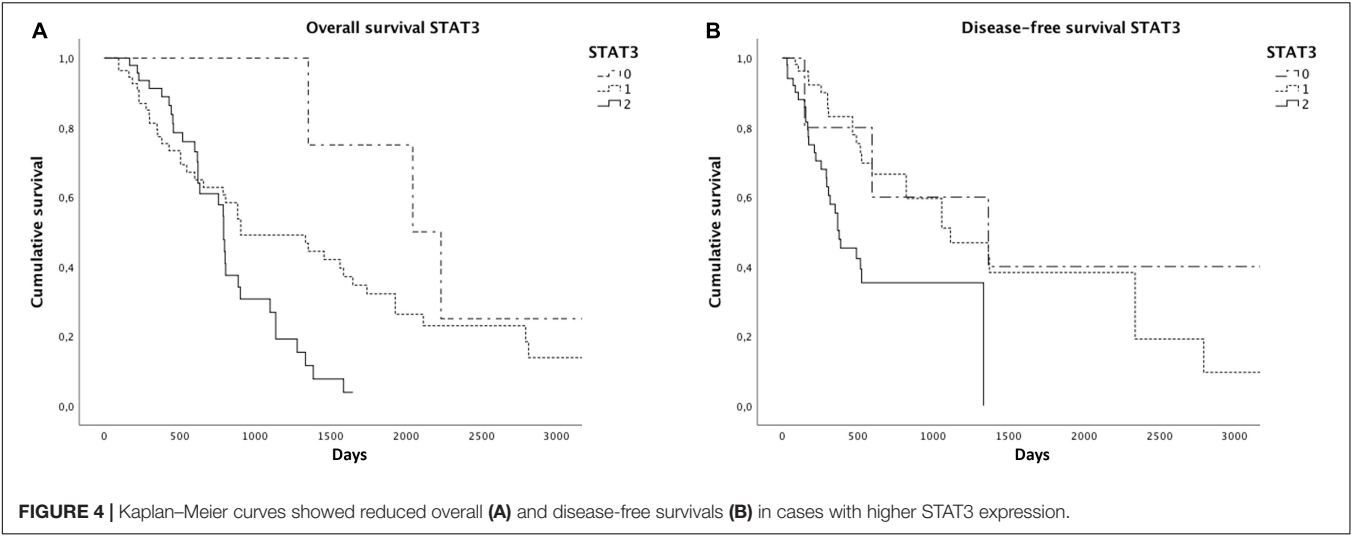
TABLE 3 | Histochemical and immunohistochemical expression of the different markers in ICC cases.

Marker	N = 112
GPX4	
N (%)	
0	23 (20.5)
1 +	43 (38.4)
2 +	46 (41.1)
TFR1	
N (%)	
0	83 (74.1)
1 +	22 (19.6)
2 +	7 (6.3)
Intratymoral iron deposits	
N (%)	
Absent	110 (98.2)
Present	2 (1.8)
STAT3	
N (%)	
0	5 (4.5)
1 +	56 (50)
2 +	51 (45.5)

association between the presence of the same unfavorable histological factors and STAT3 expression ($p = 0.001$, $p = 0.04$, and $p = 0.07$ for grading, perineural invasion, and vascular invasion, respectively), confirming what previously reported (4, 10). No associations were found between the same histological features and TFR1 expression, neither between them and the presence of iron deposits. No correlations were found between marker expression (and iron deposits) and tumor T stage. We observed a direct association between STAT3 and GPX4 expression ($p < 0.0001$) (**Supplementary Figure 2**), suggesting inhibition of ferroptosis in ICCs with an inflammatory background. Accordingly, we found an inverse correlation between STAT3 and TFR1 expression ($p = 0.04$). We failed to find any correlation between TFR1 and GPX4 expression, as well as between ferroptosis markers and STAT3 expression and the presence of intratumoral iron deposits.

Age, sex, the presence of any underlying chronic liver disease, the presence of cirrhosis, ferritin levels, tumor histotype, and the presence of nodal metastases were not related to the expression of any of the markers, neither to the presence of iron deposits.

As already reported in the literature, STAT3 expression was related to a worse overall ($p = 0.02$) and disease-free survival ($p = 0.001$) (**Figure 4**). We found significantly reduced overall ($p = 0.06$) and disease-free survivals ($p = 0.04$) in cases with a higher GPX4 expression, as shown by the Kaplan-Meier curves (**Figure 5**). Considering GPX4 1 + and 2 + positive cases together, the association becomes even stronger for both overall and disease-free survival ($p = 0.03$ and $p = 0.01$, respectively) (**Figure 5**), suggesting that mild GPX4 presence is enough to inhibit ferroptosis and reduce survival times. TFR1 expression and the presence of iron deposits were not related to survival times.



Molecular Features and Clinical-Pathological Correlations

Molecular analysis results are reported in **Table 4**. As shown, they revealed *IDH1* point mutations in 15 out of 76 tested cases (19.7%), of which 14 involving codon 132 and one involving codon 105. Only one case showed a point mutation in *IDH2* codon 172 (1.3%). In 9 cases (11.8%) molecular tests described a single nucleotide polymorphism (SNP) in codon 105 of the *IDH1* gene, causing a change in the nucleotide sequence from GGC [Gly] to GGT [Gly] (C > T). Among them, two cases showed both a point mutation in *IDH1* (codon 132) and the *IDH1*^{105GGT} SNP. No relationships were found between the presence of *IDH1* point mutations and the presence of the *IDH1*^{105GGT} SNP.

Statistical analyzes showed an inverse correlation between the presence of *IDH1*^{105GGT} SNP and tumor grading ($p < 0.0001$). On the contrary, a direct relationship was found between tumor grading and the wild type status of *IDH1-2* genes ($p = 0.004$). No associations between tumor grading and the presence of point mutations in *IDH1-2* genes were observed. We also failed to find any correlation between *IDH1-2* status and age, sex, the presence of any underlying chronic liver disease, the presence of cirrhosis, ferritin levels, tumor histotype, the presence of perineural and vascular invasion, T stage and the presence of nodal metastases.

Furthermore, GPX4 expression was inversely correlated to the presence of *IDH1*^{105GGT} SNP ($p = 0.001$) (**Supplementary Figure 3**), while it was directly related to the presence of an *IDH1-2* point mutation ($p = 0.06$) or wild type *IDH1-2* ($p = 0.04$). No associations were found between *IDH1-2* status and STAT3 and TFR1 expression, neither between *IDH1-2* status and intratumoral iron deposits.

Finally, cases with *IDH1*^{105GGT} SNP showed a better overall survival than cases with wild type *IDH1-2* (1,648 days vs. 887 days; $p = 0.04$) and cases with *IDH1-2* point mutations (1,648 days vs. 1,333 days; $p = 0.09$) (**Figure 6**). We did not find any relationship between *IDH1-2* status and disease-free survival times. The multivariate Cox regression analysis, including

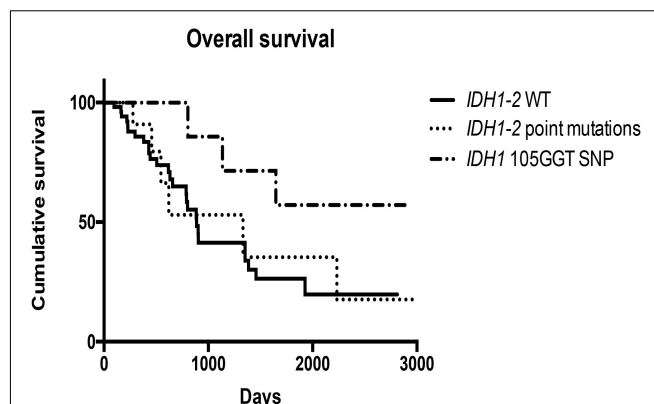


FIGURE 6 | Kaplan-Meier curves showed different overall survivals in cases bearing *IDH1*^{105GGT} SNP, *IDH1-2* point mutations and wild type *IDH1-2*.

variables that were identified as significant on univariate survival analyzes (grading, perineural and vascular neoplastic invasion, T stage, STAT3 and GPX4 expression, and *IDH1*^{105GGT} SNP) showed that only the presence of perineural invasion is an independent predictor of a worse overall survival [$p < 0.0001$, HR = 3.64 (95% CI: 1.86–7.11)], while the multivariate Cox regression analysis including grading, perineural and vascular neoplastic invasion, and STAT3 and GPX4 expression found that STAT3 expression and vascular invasion are independent predictors of a reduced disease-free survival [$p = 0.03$, HR = 1.81 (95% CI: 1.05–3.14), and $p = 0.05$, HR = 1.97 (95% CI: 1.02–3.84), respectively] (**Supplementary Table 1**).

DISCUSSION

In this study, we describe for the first time that in most inflammatory ICCs ferroptosis seems to be not active, and that its activation may depend on *IDH1-2* status. In our cohort, GPX4 was overexpressed in almost 80% of the cases, suggesting an inhibition of the ferroptotic cascade in most of our patients. GPX4 expression was found to be related to the presence of histological poor prognostic features, namely high grade and vascular and perineural invasion, and to reduced overall and disease-free survivals, implying that ferroptosis inhibition confers a worse prognosis, as expected.

We also observed that STAT3 was overexpressed in more than 90% of cases, indicating that they can be classified as inflammation-related ICC, according to the molecular classification proposed by Sia et al. (9). We confirm the poor prognostic role of STAT3 already reported in the literature (4, 10). In fact, we found a correlation between its expression and the presence of histological poor prognostic features, and worse overall and disease-free survivals in cases with higher STAT3 expression. Since this subclass of ICC is characterized by a pro-inflammatory and anti-apoptotic molecular milieu, and that pro-apoptotic drugs demonstrated only mild improvements in patients' prognosis and a frequent development of chemoresistance (4, 7, 11), the induction of other

TABLE 4 | *IDH1* and *IDH2* gene status in ICC cases.

Adequacy	N = 90
Inadequate samples	14/90 (15.6%)
Adequate samples	76/90 (84.4%)
Molecular alterations	N = 76
<i>IDH1</i> point mutations*	15/76 (19.7%)
Arg132Cys	6/76 (7.9%)
Arg132His	2/76 (2.6%)
Arg132Val	1/76 (1.3%)
Arg132Ser	1/76 (1.3%)
Arg132X	4/76 (5.2%)
Gly105Asn	1/76 (1.3%)
<i>IDH1</i>^{105GGT} SNP*	9/76 (11.8%)
<i>IDH2</i> Arg172X	1/76 (1.3%)
<i>IDH1-2</i> WT	53/76 (69.7%)

*2 cases showed both an *IDH1* point mutation in codon 132 (Arg132Cys and Arg132His) and *IDH1*^{105GGT} SNP. SNP, single nucleotide polymorphism; WT, wild type.

different cell death types, including ferroptosis, is a possible alternative way to kill resistant tumor cells. In line with this hypothesis, the high GPX4 levels found in our patients suggest that ferroptosis could be pharmacologically induced, by acting directly on GPX4 inhibition.

Molecular analyses on our cohort demonstrated *IDH1* (codon 132 or 105) or *IDH2* (codon 172) point mutations in nearly 20% of the cases, in line with the literature (3, 4, 14–17). Surprisingly, we found a SNP on codon 105 of the *IDH1* gene in 12% of our cases, which was never reported in ICC before. Patients bearing this molecular feature had a good histological profile, namely low histological tumor grade, and longer overall survival times. Synonymous SNPs are point mutations that cause a nucleotide change, which do not alter the amino acid sequence of the protein. However, sometimes they may lead to a protein defect and have functional consequences (24). The *IDH1*^{105GGT} SNP we described in our cohort was previously reported in acute myeloid leukemia, gliomas, and thyroid tumors, and have a poorly understood role in tumorigenesis (24–27). Indeed, it was linked to an adverse prognosis in acute myeloid leukemia and glioblastomas, while it seemed to confer longer survivals in patients with grade II or III gliomas (28, 29), in line with our results. The explanation of this finding is not clear, since the biologic consequences of this SNP remain speculative. It has been hypothesized that *IDH1*^{105GGT} SNP may alter *IDH1* mRNA stability or increase mRNA levels, leading to altered NADPH production (24, 28, 30), but further studies are needed to elucidate this issue. In line with previously reports (24, 28, 30), in two of our cases we described the concomitant presence of the *IDH1*^{105GGT} SNP and a point mutation in *IDH1* (codon 132). It is known that, even if *IDH1*^{105GGT} SNP is very close to codon 132, no correlation between the two molecular alterations exists (24, 30), as we confirm in our cohort.

The inverse correlation we observed between the presence of *IDH1*^{105GGT} SNP and GPX4 levels may suggest an activation of the ferroptotic cascade in ICCs bearing this molecular feature, and eventually explains the longer overall survivals observed in these patients. On the other side, we failed to confirm the association between *IDH1*^{R132C} mutation and reduced GPX4 levels reported by Wang et al. (21), but this might be explained by the different experimental conditions we worked under (cell lines versus ICC tissue and *in vitro* versus *in vivo*). Considering our survival data, it is possible that both *IDH1*^{105GGT} SNP and *IDH1*^{R132C} mutation act on GPX4 in different ways or with different intensity, since *IDH1*^{R132C} mutation-bearing cases showed overall survival times shorter than those seen in *IDH1*^{105GGT} SNP cases, but longer than those of patients with wild type *IDH1*-2. However, molecular mechanisms explaining how *IDH1*^{105GGT} SNP act on GPX4 level reduction are unknown and impossible to infer basing on our data. So additional *in vitro* studies are indispensable to address this key issue. Moreover, the number of patients overall bearing the *IDH1*^{105GGT} SNP in our cohort is low, and this limits the strength of our data, so additional studies based on larger cohorts may be of help to confirm our results. It is of interest to note that patients bearing *IDH1*^{105GGT} SNP are not expected to respond to GPX4-inhibitor drugs, such as RSL3, since GPX4 levels are already

very low in these cases. However, as Wang et al. reported on *IDH1*^{R132C}-mutated cell lines (21), *IDH1*^{105GGT} SNP-bearing ICCs may respond to ferroptosis-inducers acting on GSH levels, such as erastin. Therefore, knowing the molecular background in ICC patients is fundamental to choose the appropriate pharmacological therapy to induce tumor cell death, particularly in cases developing drug-resistance.

In conclusion, our study demonstrates for the first time that in most inflammatory ICCs ferroptosis seems to be not active, and that its triggering may be related to some molecular features of the tumor. *IDH1*-2 status is essential to determine whether (and which type of) ferroptosis-inducer drugs might be useful in ICC patient treatment, especially in drug-resistant cases.

DATA AVAILABILITY STATEMENT

The original contributions presented in this study are included in the article/**Supplementary Material**, further inquiries can be directed to the corresponding author.

ETHICS STATEMENT

The studies involving human participants were reviewed and approved by Ethics Committee for Clinical Research—University Hospital of Padova, Italy. Written informed consent for participation was not required for this study in accordance with the national legislation and the institutional requirements.

AUTHOR CONTRIBUTIONS

SS contributed to conception and design, acquisition of data, analysis and interpretation of data, writing and revision of the manuscript. DS contributed to conception and design, acquisition of data, analysis and interpretation of data, and revision of the manuscript. LF, GZ, and EG contributed to revision of the manuscript. MN contributed to development of methodology and technical and material support. GG contributed to development of methodology, analysis and interpretation of data, and technical and material support. MG contributed to conception and design, interpretation of data, revision of the manuscript, and study supervision. All authors contributed to the article and approved the submitted version.

ACKNOWLEDGMENTS

We thank Roberta Pozzobon, Irene Sarcinelli, and Ylenia Barbanera for the technical support.

SUPPLEMENTARY MATERIAL

The Supplementary Material for this article can be found online at: <https://www.frontiersin.org/articles/10.3389/fmed.2022.886229/full#supplementary-material>

REFERENCES

- Mejia JC, Pasko J. Primary liver cancers: intrahepatic cholangiocarcinoma and hepatocellular carcinoma. *Surg Clin North Am.* (2020) 100:535–49. doi: 10.1016/j.suc.2020.02.013
- Sarcognato S, Sacchi D, Fassan M, Fabris L, Cadamuro M, Guido M, et al. Cholangiocarcinoma. *Pathologica.* (2021) 113:158–69. doi: 10.32074/1591-951X-252
- Sirica AE, Gores GJ, Groopman JD, Selaru FM, Strazzabosco M, Zhu AX, et al. Intrahepatic cholangiocarcinoma: continuing challenges and translational advances. *Hepatology.* (2019) 69:1803–15. doi: 10.1002/hep.30289
- Acher AW, Paro A, Elfadaly A, Tsilimigras D, Pawlik TM. Intrahepatic cholangiocarcinoma: a summative review of biomarkers and targeted therapies. *Cancers (Basel).* (2021) 13:5169. doi: 10.3390/cancers13205169
- El-Diwany R, Pawlik TM, Ejaz A. Intrahepatic cholangiocarcinoma. *Surg Oncol Clin N Am.* (2019) 28:587–99. doi: 10.1016/j.soc.2019.06.002
- Sung H, Ferlay J, Siegel RL, Laversanne M, Soerjomataram I, Freddie Bray F, et al. Global cancer statistics 2020: GLOBOCAN estimates of incidence and mortality worldwide for 36 cancers in 185 countries. *CA Cancer J Clin.* (2021) 71:209–49. doi: 10.3322/caac.21660
- Cadamuro M, Brivio S, Spirli C, Joplin RE, Strazzabosco M, Fabris L. Autocrine and paracrine mechanisms promoting chemoresistance in cholangiocarcinoma. *Int J Mol Sci.* (2017) 18:149. doi: 10.3390/ijms18010149
- Morton SD, Cadamuro M, Brivio S, Vismara M, Stecca T, Strazzabosco M, et al. Leukemia inhibitory factor protects cholangiocarcinoma cells from drug-induced apoptosis via a PI3K/AKT-dependent Mcl-1 activation. *Oncotarget.* (2015) 6:26052–64. doi: 10.18632/oncotarget.4482
- Sia D, Hoshida Y, Villanueva A, Roayaie S, Ferrer J, Llovet JM, et al. Integrative molecular analysis of intrahepatic cholangiocarcinoma reveals 2 classes that have different outcomes. *Gastroenterology.* (2013) 144:829–40. doi: 10.1053/j.gastro.2013.01.001
- Johnston P, Grandis JR. STAT3 SIGNALING: anticancer strategies and challenges. *Mol Interv.* (2011) 11:18–26. doi: 10.1124/mi.11.1.4
- Jin K, Li T, Sánchez-Duffhues G, Zhou F, Zhang L. Involvement of inflammation and its related microRNAs in hepatocellular carcinoma. *Oncotarget.* (2017) 8:22145–65. doi: 10.18632/oncotarget.13530
- Yu H, Lee H, Herrmann A, Buettner R, Jove R. Revisiting STAT3 signalling in cancer: new and unexpected biological functions. *Nat Rev Cancer.* (2014) 14:736–46. doi: 10.1038/nrc3818
- Darnell J, Kerr I, Stark G. Jak-STAT pathways and transcriptional activation in response to IFNs and other extracellular signaling proteins. *Science.* (1994) 264:1415–21. doi: 10.1126/science.8197455
- Farshidfar F, Zheng S, Gingras M, Newton Y, Shih J, Kleiner DE, et al. Integrative genomic analysis of cholangiocarcinoma identifies distinct IDH-mutant molecular profiles. *Cell Rep.* (2017) 19:2878–80. doi: 10.1016/j.celrep.2017.06.008
- Borger DR, Tanabe KK, Fan KC, Lopez HU, Fantin VR, Iafrate AJ, et al. Frequent mutation of isocitrate dehydrogenase (IDH)1 and IDH2 in cholangiocarcinoma identified through broad-based tumor genotyping. *Oncologist.* (2012) 17:72–9. doi: 10.1634/theoncologist.2011-0386
- Haber PK, Sia D. Translating cancer genomics for precision oncology in biliary tract cancers. *Discov Med.* (2019) 28:255–65.
- Moeini A, Sia D, Bardeesy N, Mazzaferro V, Llovet JM. Molecular pathogenesis and targeted therapies for intrahepatic cholangiocarcinoma. *Clin Cancer Res.* (2016) 22:291–300. doi: 10.1158/1078-0432.CCR-14-3296
- Galluzzi L, Vitale I, Aaronson SA, Abrams JM, Adam D, Agostinis P, et al. Molecular mechanisms of cell death: recommendations of the nomenclature committee on cell death 2018. *Cell Death Differ.* (2018) 25:486–541. doi: 10.1038/s41418-017-0012-4
- Xu T, Ding W, Ji X, Ao X, Liu Y, Yu W, et al. Molecular mechanisms of ferroptosis and its role in cancer therapy. *J Cell Mol Med.* (2019) 23:4900–12. doi: 10.1111/jcmm.14511
- Wang H, Lin D, Yu Q, Li Z, Lenahan C, Shao A, et al. A promising future of ferroptosis in tumor therapy. *Front Cell Dev Biol.* (2021) 9:629150. doi: 10.3389/fcell.2021.629150
- Wang T, Liang J, Zhang C, Xiong Y, Guan K, Yuan H. The oncometabolite 2-hydroxyglutarate produced by mutant IDH1 sensitizes cells to ferroptosis. *Cell Death Dis.* (2019) 10:755. doi: 10.1038/s41419-019-1984-4
- Sarcognato S, Gringeri E, Fassan M, Di Giunta M, Cillo U, Guido M, et al. Prognostic role of BAP-1 and PBRM-1 expression in intrahepatic cholangiocarcinoma. *Virchows Arch.* (2019) 474:29–37. doi: 10.1007/s00428-018-2478-y
- Brierley J, Gospodarowicz MK, Wittekind C. *TNM Classification of Malignant Tumours*. Eighth ed. Hoboken, NJ: John Wiley & Sons, Inc (2017).
- Acquaviva G, Visani M, de Biase D, Marucci G, Franceschi E, Tallini G, et al. Prevalence of the single-nucleotide polymorphism rs11554137 (IDH1 105GGT) in brain tumors of a cohort of Italian patients. *Sci Rep.* (2018) 8:4459. doi: 10.1038/s41598-018-22222-y
- Ho PA, Kopecky KJ, Alonzo TA, Gerbing RB, Miller KL, Kuhn J, et al. Prognostic implications of the IDH1 synonymous SNP rs11554137 in pediatric and adult AML: a report from the Children's Oncology Group and SWOG. *Blood.* (2011) 118:4561–6. doi: 10.1182/blood-2011-04-348888
- Hemerly JP, Bastos AU, Cerutti JM. Identification of several novel non-p.R132 IDH1 variants in thyroid carcinomas. *Eur J Endocrinol.* (2010) 163:747–55. doi: 10.1530/EJE-10-0473
- Murugan AK, Bojdani E, Xing M. Identification and functional characterization of isocitrate dehydrogenase 1 (IDH1) mutations in thyroid cancer. *Biochem Biophys Res Commun.* (2010) 393:555–9. doi: 10.1016/j.bbrc.2010.02.095
- Wang X, Boisselier B, Rossetto M, Marie Y, Idbaih A, Sanson M, et al. Prognostic impact of the isocitrate dehydrogenase 1 single-nucleotide polymorphism rs11554137 in malignant gliomas. *Cancer.* (2013) 119:806–13. doi: 10.1002/cncr.27798
- Franceschi E, De Biase D, Di Nunno V, Pession A, Tosoni A, Brandes AA, et al. IDH1 105GGT single nucleotide polymorphism improves progression free survival in patients with IDH mutated grade II and III gliomas. *Pathol Res Pract.* (2021) 221:153445. doi: 10.1016/j.prp.2021.153445
- Wagner K, Damm F, Göhring G, Görlich K, Heuser M, Schäfer I, et al. Impact of IDH1 R132 mutations and an IDH1 single nucleotide polymorphism in cytogenetically normal acute myeloid leukemia: SNP rs11554137 is an adverse prognostic factor. *J Clin Oncol.* (2010) 28:2356–64. doi: 10.1200/JCO.2009.27.6899

Conflict of Interest: The authors declare that the research was conducted in the absence of any commercial or financial relationships that could be construed as a potential conflict of interest.

Publisher's Note: All claims expressed in this article are solely those of the authors and do not necessarily represent those of their affiliated organizations, or those of the publisher, the editors and the reviewers. Any product that may be evaluated in this article, or claim that may be made by its manufacturer, is not guaranteed or endorsed by the publisher.

Copyright © 2022 Sarcognato, Sacchi, Fabris, Zanusi, Gringeri, Niero, Gallina and Guido. This is an open-access article distributed under the terms of the Creative Commons Attribution License (CC BY). The use, distribution or reproduction in other forums is permitted, provided the original author(s) and the copyright owner(s) are credited and that the original publication in this journal is cited, in accordance with accepted academic practice. No use, distribution or reproduction is permitted which does not comply with these terms.



OPEN ACCESS

EDITED BY

Luca Di Tommaso,
Humanitas Research Hospital, Italy

REVIEWED BY

Ralf Huss,
Augsburg University Hospital, Germany
Jakob Nikolas Kather,
University Hospital RWTH Aachen,
Germany

*CORRESPONDENCE

Heather Dawson
heather.dawson@unibe.ch

SPECIALTY SECTION

This article was submitted to
Pathology,
a section of the journal
Frontiers in Medicine

RECEIVED 03 March 2022

ACCEPTED 28 June 2022

PUBLISHED 22 July 2022

CITATION

Dawson H (2022) Digital pathology –
Rising to the challenge.
Front. Med. 9:888896.
doi: 10.3389/fmed.2022.888896

COPYRIGHT

© 2022 Dawson. This is an
open-access article distributed under
the terms of the [Creative Commons
Attribution License \(CC BY\)](#). The use,
distribution or reproduction in other
forums is permitted, provided the
original author(s) and the copyright
owner(s) are credited and that the
original publication in this journal is
cited, in accordance with accepted
academic practice. No use, distribution
or reproduction is permitted which
does not comply with these terms.

Digital pathology – Rising to the challenge

Heather Dawson*

Institute of Pathology, University of Bern, Bern, Switzerland

Digital pathology has gone through considerable technical advances during the past few years and certain aspects of digital diagnostics have been widely and swiftly adopted in many centers, catalyzed by the COVID-19 pandemic. However, analysis of requirements, careful planning, and structured implementation should to be considered in order to reap the full benefits of a digital workflow. The aim of this review is to provide a practical, concise and hands-on summary of issues relevant to implementing and developing digital diagnostics in the pathology laboratory. These include important initial considerations, possible approaches to overcome common challenges, potential diagnostic pitfalls, validation and regulatory issues and an introduction to the emerging field of image analysis in routine.

KEYWORDS

digital pathology, scanner acquisition, validation, image analysis, artificial intelligence

Introduction

In many parts of the world, at least part of pathologists' work has become "digital," i.e., conventional routine replaced by digital images. However, many pathology institutes that pursue the path to digital pathology realize that this is not always as straightforward as it seems. As technical aspects and possibilities advance at nearly dizzying speed, it must be emphasized that a digital approach will affect many fundamental aspects of daily routine in a pathology lab. Careful planning and certain practical considerations can be paramount for a smooth transition to an efficient digital workflow. The objective of this article is to provide a broad overview of digital pathology for the general pathologist and address real-world issues which may be underrepresented in the literature. Select review articles, white papers and consensus guidelines are recommended for further in-depth reading (1–5).

What constitutes digital pathology? Broadly interpreted, this can entail any sort of work involving a digital image. For instance, digital photography to capture and store macroscopic images can be considered one of the first widespread aspects of digital pathology. Real-time sharing of pathology images with a common viewer (telepathology) has been favored for some time by hospital systems with multiple sites

and increasingly implemented during the COVID-19 pandemic (6). The most complex application is the digitization and storage of whole slides images (WSI), either for use in diagnostic routine or for educational or research purposes.

Advantages and challenges of digital pathology

There are various potential advantages of digital pathology, including:

- Patient safety-related: Provided storage is reliable and data secure, a scanned slide cannot be lost or broken. Most viewer programs also have annotation functions, which enable the documentation of exact measurements (for instance, the exact infiltration depth of a tumor or distance to resection margins).
- Access to slides: One of the most obvious drivers of digital pathology in the past 2 years has been pandemic-related to enable remote work. The retrieval of archived slides can also be considerably simplified and does not require staff assistance. Depending on the laboratory setup, scanned cases can also improve workflow by reducing physical slide distribution.
- Sharing cases: Digitized scans can be easily shared for second opinions, interdisciplinary tumor conferences and educating students and residents.
- Research: Established archives of scanned WSI or tissue microarrays can be mined for research projects and enables centralized, standardized repositories of research data (including patient data, tissue-related data etc.).
- Implementation of automated algorithms: WSI are prerequisite for the vast possibilities of additional image analysis software for diagnostic assistance (see below).
- What are system requirements and IT resources? How can storage space be ensured and how much is needed? How can graphics processing units/central processing units (GPUs/CPU) be accessed? This will highly depend on the planned scope of application. For instance, assuming a biopsy slide output of 1,600/day and an average of 2 GB/slide, 1 PB/year should be calculated if all scans are to be archived.
- System compatibility: How is the interface with the laboratory information system (LIS) and how compatible is the scanner with barcodes from different manufacturers?
- Requirements for access to scans and image management system (IMS): Should scans be available *via* web browser? How can slides be shared? What are requirements for annotation and measurement tools? How can patient metadata from the LIS be integrated to the IMS?
- Workflow integration: How does scanning harmonize with other lab processes? Is continuous loading/unloading possible?
- Openness of system for application of plugin software: Does the scan and proposed IMS enable the use of desired third party software?
- Regional differences in regulatory issues: Is FDA or equivalent approval required for a scanner to be used in a diagnostic setting?
- Financial aspects: Transitioning to a digital pathology workflow requires considerable short-term investments and additional personnel. However, well-planned implementation may result in increased productivity in the long-term, and potentially counteract shortages in trained pathologists who are faced with an increased case load (5, 7). The business case and potential financial gains of a particular pathology institute highly depend on the scope of the project and pre-existing efficiency of the laboratory setup (7).

Initial considerations

The benefits of digital are certainly met with their share of challenges, both from a technical and organizational point of view. First, it should be clear that there is no “one-size-fits-all” solution and that needs of individual institutions will differ. Prior to making large investments, current system requirements should be specified and future ones anticipated. Important considerations may be:

- Scope of application: Is the aim to go fully digital or only scan a certain amount of slides? The amount of expected slides to be scanned and the scanning speed will influence the type and number of scanners to purchase.
- Some points can only be adequately addressed in a trial period. At the beginning, scanner acquisition is typically one of the first large investments in implementing digital pathology. For instance, a possible approach would be to test several scanners and submit them to a performance test (Table 1), including (8):
- Technical aspects: Speed, file size, interruptions, rescan rates, focus and tissue identification issues; what is the proportion of poor quality scans (blurriness, incomplete scans).
- Workflow-related aspects: Handling and user-friendliness, continuous scanning, LIS integration, openness of file format.
- Medical aspects: How do MDs rate the quality of scans including special stains and the usability of the viewer? What is the general impression among different scanners?

Getting started

The implementation of digital pathology is complex and interdisciplinary. Key players include IT, laboratory staff, MDs and institute management. Although the strategic decision to use digital pathology is traditionally made at the management level, it is important to involve all units at an early stage of development. Our digital pathology team includes a project manager, 2 pathologists, a specialized technician, an IT specialist responsible for our LIS and a LEAN specialist, and meets regularly with the head of the pathology lab and representatives of our LIS and IMS providers. The digital pathology group also works closely with our computational pathology researchers. However, the main goal is the continuous development of digital pathology for diagnostic routine in the department.

Our histology lab is organized according to Lean principles (9). As many processes in the lab including the physical transfer of histology slides already revolve around a Lean workflow we were faced with the challenge of integrating an additional step. Since scanning needs to match the batch-based

distribution of slides, continuous scanning is necessary to keep our workflow running. Also, space restrictions and an ideal position of the scanner need to be taken into consideration (Figure 1). However, a Lean approach to digitizing cases is not just limited to the scanner itself. Automated processes starting with accession can help to minimize waste and save time. For instance, if correctly identified, a particular case can be processed so that slides are scanned and algorithms already run before the scan reaches the pathologist. In addition, standardized sampling and measurements of gross specimens enable the automated labeling of scanned slides and necessary elements directly transferred to synoptic reports.

Some practical aspects of tissue processing will influence digitizing slides. For example, small biopsies very close to the edges of the slide may not be identified by the scanner, which can lead to relevant patient safety issues (see discussion on quality control). Therefore, this must be taken into account at the microtome. Also, some scanners will accept racks directly from some stainers, but it must be ensured that slides are dry, as slides with wet mounting medium tend to stick to the rack and will not be scanned. The use of barcodes for specimen labeling is

TABLE 1 Example performance test for scanners under consideration for purchase.

Technical aspects

File size	File sizes can vary considerably (up to over fourfold) among different scanners and will therefore have a major impact on the storage space needed.
Scan time at 40× magnification and for dayload	The scanning speed can be a bottleneck in the diagnostic workflow depending on the number of slides, the type of specimen (biopsies vs. resections) and the number of pathologists to be signing out cases digitally. In our experience, scan times may vary up to a minute per slide on different scanners at the same magnification.
Interruptions	The vulnerability to interruptions is one of the most important aspects of scanner performance and can have an especially profound impact on overnight scanning. Software, hardware and slide-related issues may all contribute to interruptions.
Rescan rate	After quality control check, establish the proportion of slides that need to be rescanned (e.g., due to focus issues and missing tissue).
Focus	Tissue can be either entirely or only partially out of focus. The technology of continuous autofocus can result in different areas of the slide being out of focus but lower rates of WSI completely out of focus in comparison to scanners using focus points.
Tissue identification	Scanners use their own algorithms to detect tissue on a slide and therefore variability in tissue detection may be seen among different scanners. For patient safety reasons it is crucial that all tissue is scanned and this must be ensured for each slide. Faintly stained tissue (e.g., myxoid substance or fat) can be missed and only partially scanned by some scanners.
Openness of file format	The scan format should ideally be open for the integration for an independent choice of image analysis tools and convertible into other formats.

Workflow-related aspects

User friendliness	The laboratory staff should be involved in evaluating the usability of scanner software and hardware.
Loading of racks	There are several possibilities: manual loading of slides one by one, overturning of racks from staining machines in one step and direct loading of racks from stainers. However, slides with wet mounting medium tend to stick to the rack and will not be scanned.
Continuous scanning	Some scanners stop to open, others continue with the process even if opened to reload, which can have a considerable effect on case distribution depending on the workflow.
LIS integration	This is crucial, especially for work in the remote setting in terms of work lists and case management. Cooperation with LIS providers is important to ensure that the requirements of the institute are met.

MD-related aspects

IMS	The IMS may be from a different provider than the scanner itself, but is essential for digital sign-out and should be considered during scanner testing. Pathologists should feel comfortable using the IMS, which should provide certain tools (measurement, area calculation, regions of interest, snapshot etc.).
Pathologist evaluation	Pathologists should compare their impression of WSI in terms of quality of the scans and their level of diagnostic confidence. A case set should including potentially difficult cases (e.g., special stains containing microorganisms). Side by side comparisons of WSI from different can be especially helpful in the decision making process.

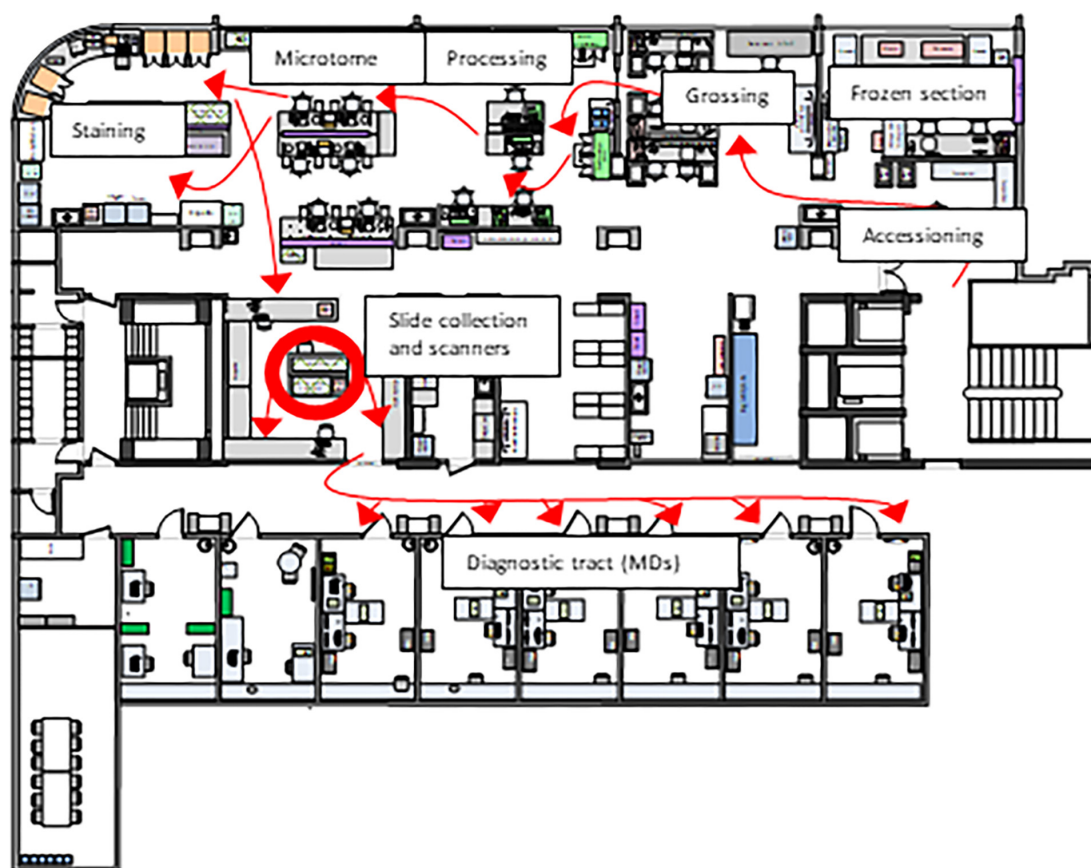


FIGURE 1

Layout of our histology laboratory according to Lean principles. The red arrows that represent the path taken by a specimen from acquisition to the MD are unidirectional ("LEAN biopsy/resection street"). Therefore, the Lean solution was to place scanners in the slide sorting area (red circle), which minimizes waste both for a hybrid solution (digital and conventional sign-out) and fully digital sign-out.

used in many laboratories and is required for a digital workflow. Regardless of whether slides are scanned or not, barcodes are the basis of a digital tracking system, which can drastically improve patient safety and also be used as a management tool (e.g., measurement of turnaround times and performance indicators). Robust barcode reading is also essential for the scanning process and there are several types of barcode printers which vary in terms of price, print quality and scanner readability (10). The highest quality barcodes are produced by thermal printers which are more expensive than other types of printers, but may save time and effort by drastically reducing failure rates in barcode reading. Alternatively, training laboratory staff to recognize poor quality barcodes may also yield acceptable barcode scanning rates.

The MD team

Prior to routine scanning in our department (also before the COVID-19 pandemic), MDs were involved in rating of several

tested scanners in terms of handling issues, comparison of side by side scans and scan quality and asked about their general attitude toward digital pathology in general. Most pathologists were open to the digital future, for instance 75% felt they would be able to make diagnoses on scanned images (8). This is in concordance to a national survey performed in Switzerland in 2019, where the majority of pathologists (66%) also reported feeling comfortable rendering primary diagnoses on scanned slides (11). Inevitably, the importance of digital pathology has risen significantly, leading to increased use digital pathology in daily routine. Unsurprisingly, a more recent poll of Swiss pathologists at the height of the pandemic revealed the use of digital pathology for primary routine diagnostics had more than doubled since onset of the pandemic (30 vs. 13.5%) (12).

In the midst of the rise in digital pathology, it cannot be forgotten that currently, the vast majority of pathologists have completed their training and accumulated years if not decades of experience using conventional light microscopy. Therefore, most pathologists still currently consider conventional microscopy as gold standard not only when it comes to

diagnostic confidence, but also speed and efficiency in routine. In our experience, when faced with a high diagnostic workload and the option between digital and conventional work, many pathologists will still prefer to work with glass slides. The optimization of digital pathology in this regard is truly challenging on many levels and should not be underestimated. Even if performance issues as frequently encountered in the setting of remote work can be eliminated, each extra mouse click will add up to a considerable and noticeable amount of extra time spent on sign-out over the course of a busy workday. Investing time to achieve optimal user interface in the LIS and IMS are especially important and require close cooperation between the MDs and technical team.

The perceived ease of digital pathology is an important factor for everyday use in diagnostic routine. Speed, accuracy, ease of use and ergonomics should all be taken into consideration. However, although crucial from a practical point of view, reports in the literature on such aspects of digital sign-out are rare. Certain input devices such as a conventional mouse may be straining, especially when using the wheel for zooming over a prolonged period of time. Here, other types of devices may be preferred, especially in terms of comfort (13).

Although several studies have demonstrated that digital pathology is non-inferior to conventional light microscopy in a wide spectrum of diseases and organ systems (14, 15), there are still some potential issues to be aware of. For instance, the detection of microorganisms and subtle morphological features such as nuclear details, including mitotic figures and chromatin patterns on scanned slides can be challenging. This can be due to several reasons. For instance, poor quality of scans can be a major source of uncertainty and discrepancies from glass slide diagnoses, in which case rescanning at a higher magnification or Z-stacking may increase diagnostic confidence (Figure 2) (14). However, it has also been suggested that many discrepancies are not due to limitations of diagnosis on WSI as a process but other factors, such as naturally occurring interobserver variability, inadequate tissue processing or lack of experience of the pathologist (16).

Validation

As digital diagnostics represents a technique that significantly differs from conventional light microscopy, validation tests must encompass the entire digital system to ensure necessary standards are met. This includes the scanning process, the LIS and IMS interface and archiving of WSI. Good practice statements and recommendations of the College of American pathologists (CAP) (3) from which general principles have been adapted by most societies are summarized in Table 2.

Pathologists themselves are a crucial part of the validation process, especially since not all pathologists may be confident with working in a digital process and should be given the

possibility to acquire skills outside live reporting. There are several published recommendations for pathologist validation which are more or less extensive (3, 17, 18) but share the following principles:

- Training and validation cases should reflect real life work and include all types of stains used in diagnostic routine (including special stains and immunohistochemistry).
- Validation should include a comparison between diagnoses made by the same pathologist on glass slides and WSI after a washout period to minimize recall bias and eliminate interobserver variability. All pathologists using digital diagnostics in routine must complete the validation study.
- Documentation of the validation protocol including concordance and discordance of cases. The level of concordance between diagnoses on glass slides and WSI is generally expected to be over 95%.

In addition to diagnostic routine on WSI, all image analysis tools must be validated by each institution prior to clinical use, irrespectively of FDA- (or equivalent) approval status. As specific guidelines for validation studies and acceptance criteria for such tools are lacking, the approval of a validation study design is left up to the discretion of the medical director. However, the basic aspects as mentioned above should be applied: the validation study should be applicable to the intended clinical use in which the tool will be employed and encompass the spectrum and complexity expected to be encountered in diagnostic routine. Important considerations for in-house algorithm validation study design are listed in Table 3.

Quality control of whole slides images

Suboptimal WSI can be due either to issues in tissue handling (e.g., folds, tears, poor staining, thick cuts etc.) or the scanning process (focus issues, tissue recognition, etc.). Quality control of WSI is important for troubleshooting and fixing the root of the cause. If left up to the pathologist to identify poor images, important time is lost in which the underlying problem could already have been solved. Therefore, quality control should ideally be performed in the pathology laboratory. Quality control of glass slides may be acceptable on random samples and certain issues picked up by the naked eye of experienced technicians, but quality control of WSI may require opening each scan, which is quite time-consuming and not feasible for many laboratories – especially considering the amount of extra work scanning may entail. Therefore, automated quality control tools are highly desirable to relieve the laboratory staff of this process. Several automated tools have been proposed, some of which merely identify focus quality (19, 20). However, a more comprehensive solution which addresses both laboratory- and

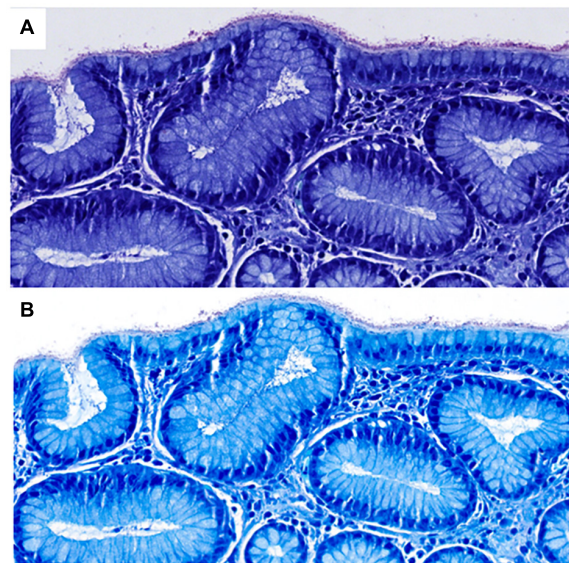


FIGURE 2

Scanned Giemsa stains from two different scanners (A,B) used in diagnostic routine at our institute in a case of *H. pylori* gastritis (both at 40 \times , images courtesy of Ursina Begré). Note the differences in color and brightness between scanners. In a survey of our MDs, scanner B provided a higher level of diagnostic security on Giemsa scans of gastric biopsies but both scanners performed similarly at 40 \times . Therefore, Giemsa stains for gastric biopsies are scanned at higher magnification per default.

TABLE 2 Summary of good practice statements (GPS) of the College of American pathologists (3).

GPS 1: All pathology laboratories implementing digital pathology for diagnostic purposes should carry out their own validation studies.

GPS 2: Validation should be appropriate for and applicable to the intended clinical use and clinical setting of the particular application. Validation of WSI systems should involve specimen preparation types relevant to intended use. If a new application for WSI is desired and differs materially from the previously validated use, a separate validation for the new application should be performed.

GPS 3: Validation should closely simulate the real-world clinical environment in which the technology will be used.

GPS 4: Validation should encompass the entire WSI system. However, it is not necessary to validate each individual component (i.e., computer hardware, monitor, network, scanner) of the system or the individual steps of the digital imaging process.

GPS 5: Laboratories should have procedures in place to address changes to the digitized system that could impact clinical results.

GPS 6: Pathologists adequately trained to use the WSI system must be involved in the validation process.

GPS 7: The validation process should confirm all material on a glass slide to be scanned is included in the digital image.

GPS 8: Documentation should be maintained recording the method, measurements, and final approval of validation for the WSI system to be used in the laboratory.

GPS 9: Pathologists should review slides in a validation set in random order. This applies both to the review modality (glass slides or digital) and the order in which slides are reviewed within each modality.

scan-related quality control issues would be ideal, especially in a workflow where all slides are digitized. In 2019, the free open-source software HistoQC was introduced as potential tool for automated quality control (21). Although more of a prototype in its initial form, hampered by its complex configuration and limitations in interpreting calculated metrics (22), further developments may be expected for this tool to be used as a ready-to-use program for clinical application in the future.

Image analysis – friend or foe?

One of the most obvious advantages of digital pathology is the implementation of automated algorithms to assist in

diagnostics. Most tools rely on artificial intelligence, which is an umbrella term that encompasses machine learning and deep learning. Machine learning is a term for computer systems that learn and adapt without following explicit instructions by using algorithms and statistical models to analyze and draw inferences from patterns with data. Deep learning is a type of machine learning based on artificial neural networks, which are inspired by the understanding of biological neural networks (23). Image analysis tasks cover a wide range of potential applications. Basic tasks that might already be in use include quantitative analyses such as a count of objects (e.g., mitoses, tumor-infiltrating lymphocytes, immunohistochemical biomarkers like Ki-67 in breast cancer etc.) that are traditionally perceived as repetitive

TABLE 3 Considerations for validation study design for image analysis tools.

Ground truth definition	<p>The algorithm output must be compared to a ground truth to establish precision and recall (precision addresses the proportion of positive identifications that was actually correct, i.e., a model with no false positives has a precision of 1.0; recall addresses the proportion of actual positives that were correctly identified, i.e., a model with no false negatives has a recall of 1.0) This can be done in several ways:</p> <ol style="list-style-type: none"> 1. Manual annotation: most exact method for comparison to algorithm output but time-consuming 2. Eyeballing (if applicable): Region of interest can be pre-set, replicates real-life diagnostic setting 3. Comparison with previously reported values (derived from LIS): Least exact method, region of interest not standardized, but least time-consuming
Case selection	There are no published guidelines on the number of cases that should be included but the case mix should reflect the real life setting in terms of morphological heterogeneity and complexity (e.g., different histological variants/subtypes)
Acceptable range of output values	Define acceptable range of deviation to ground truth. This may depend on clinically relevant cutoffs that determine therapy (e.g., PD-L1, Ki67)
Possible confounding effects	If several scanners are used to run the algorithm on check whether the scanner has an effect on algorithm output
Identify discrepant cases and analyze reasons for discrepancy	Output values outside the defined acceptable range are discrepant to the ground truth. Can systematic reasons be identified (for example threshold of color detection, falsely identified tumor cells etc.)? Are the ground truth values really correct? In the case of substantial discrepancies, support of the provider may be warranted.

and time-consuming in routine and may be prone to inter- and intraobserver variability (24).

Other applications may focus on evaluating diagnostic features, such as distinguishing diseased from normal tissue, grading cancers or differentiating between different cancer types. Some systems appear highly successful in tumor detection with reported near perfect accuracy rates (25). There are currently two approaches to implementing cancer-detection algorithms, either as a “first read,” in which slides are analyzed prior to the pathologist, highlighting suspicious areas with the aim to improve diagnostic efficiency. In the “second read” approach, slides are evaluated in parallel to the pathologist and notifies in case of clinically relevant discrepancies (for instance a missed focus of cancer tissue) with the intention to minimize error rates. At present, FDA-approval for use in primary diagnostics is limited to only very few products (26) but will certainly be expanded in the near future.

More advanced applications include predictions that might not be evident to the human eye. Comprehensive image analysis for complex aspects such as different cell types in the tumor microenvironment or tumor heterogeneity is simply not feasible without some kind of computational method. Clinically relevant information such as survival, molecular classifications or response to therapy can possibly be predicted by a WSI. For instance, a published algorithm reported predicting HER2 amplification in breast cancer with an AUC of 0.70 (95% CI 0.63–0.77) and more favorable survival in trastuzumab-treated patients according to the automated prediction status (ERBB2 score) (27). In addition, a high ERBB2 score in CISH-HER2 negative patients was associated with unfavorable survival, indicating that the algorithm picked up HER2-cancer-like morphological features linked to poorer outcomes. Another potential tool aiming for a one-stop-shop workflow for pan-cancer image-based detection of clinically actionable genetic alterations based on H&E stained slides was able to significantly predict mutational status of at least some oncogenic genes in

14/14 cancer types, whereas the highest accuracy was achieved for lung, colorectal and breast cancer (AUC 0.60–0.78; 0.65–0.76 and 0.66–0.78, respectively) (28). Evidently, such tools are still of exploratory nature, but it can be assumed that they too will be used in the clinical setting at some point. However, several issues concerning validation in algorithms that could directly influence clinical decision-making will need to be addressed – especially if artificial intelligence (AI)-tools are considered to replace the current gold standard of molecular-based assays - underlining the need for investigation in randomized clinical trials.

Although many studies report high accuracy rates of AI algorithms, this does not necessarily translate to usability in routine (29). Algorithms themselves should undergo rigorous validation on multiple levels according to good practice guidelines (23), ensuring exposure to a wide variety of data sources (including external validation sets, different scanners etc.). However, even if all measures are taken to meet these standards, real-life data will still typically have many more sources of nuances and variation than the datasets used for training and validation. Additionally, it must be emphasized that algorithms are far from replacing the work of pathologists, which is to take an integrative approach incorporating medical knowledge, diagnostic experience and the particular circumstances of a certain case to either make a final diagnosis or decide if further work-up is needed. Therefore, for the foreseeable future a constructive strategy could be to view AI tools as a way of increasing efficiency and enhancing the quality of diagnoses in routine (30).

Globally relevant issues

Clearly, digital pathology requires significant financial investments that might be affordable for high-income countries but exorbitant for many low- and middle-income countries. Although listed prices vary greatly depending on the product,

a single high-throughput scanner will cost between \$100'000 to \$400'000 (7). Further costs include hardware (high-resolution display screens and high-performance computers), additional software, IT infrastructure and personnel. In addition to financial issues, low-and middle-income countries tend to suffer from a general shortage of pathologists which often prefer to practice in urban agglomerations, whereas a large proportion of the population lives in rural areas (31). Therefore, unfortunately, the wealth of a particular region will influence potential applications of digital pathology. For instance, especially developing countries can benefit from educational aspects of digital pathology with increasing availability of virtual or hybrid courses, eliminating travel costs. Also, telepathology can aid in seeking second opinions from colleagues, increasing diagnostic quality. Algorithm-assisted diagnostics can also potentially be used to provide some relief to a high workload. Although traditionally, all of these aspects require some financial investment in terms of scanning machines, recent efforts have been made to develop a cost-efficient real-time microscope-based solution for deploying AI tools, eliminating the need for WSI (32).

Conclusion

Digital pathology is a complex endeavor which requires careful planning in advance. The preparation phase should include detailed analysis of the requirements, starting point and goals of a particular institute as there is no one-size-fits-all solution. In our experience, it is important to assemble a team from the beginning consisting of key players involving all areas which will be affected by digital pathology (including MDs, lab technicians, researchers, etc.). Test phases with structured performance analysis are recommended prior to purchasing large equipment such as scanners. To ensure equivalent diagnostic quality to conventional routine diagnostics, validation studies on the process of digital pathology as a whole and add-ons such as image analysis tools must be performed by each laboratory according to guidelines or good practice standards. Acceptance of digital

pathology generally appears to be high, although affinity for digital work can vary among pathologists. Providing a user friendly, simple and ergonomic digital workspace requires effort but can ease the transition to routine digital diagnostics. At the moment, AI algorithms can be viewed as a possibility to aid and enhance certain aspects of routine diagnostic work rather than replacing the pathologist. Combining forces of human experience, research and AI is bound to help advance an efficient workflow and personalized healthcare treatment.

Author contributions

The author confirms being the sole contributor of this work and has approved it for publication.

Acknowledgments

The author thank Inti Zlobec, Caroline Hammer, and Linda Studer from the Institute of Pathology, University of Bern for providing material and their valuable insights for the preparation of this manuscript.

Conflict of interest

The author declares that the research was conducted in the absence of any commercial or financial relationships that could be construed as a potential conflict of interest.

Publisher's note

All claims expressed in this article are solely those of the authors and do not necessarily represent those of their affiliated organizations, or those of the publisher, the editors and the reviewers. Any product that may be evaluated in this article, or claim that may be made by its manufacturer, is not guaranteed or endorsed by the publisher.

References

1. Zarella MD, Bowman D, Aeffner F, Farahani N, Xthona A, Absar SE, et al. A practical guide to whole slide imaging: a white paper from the digital pathology association. *Arch Pathol Lab Med.* (2019) 143:222–34.
2. Fraggetta F, L'Imperio V, Ameisen D, Carvalho R, Leh S, Kiehl TR, et al. Best practice recommendations for the implementation of a digital pathology workflow in the anatomic pathology laboratory by the European society of digital and integrative pathology (ESDIP). *Diagnostics.* (2021) 11:2167. doi: 10.3390/diagnostics11112167
3. Evans AJ, Brown RW, Bui MM, Chlipala EA, Lacchetti C, Milner DA, et al. Validating whole slide imaging systems for diagnostic purposes in pathology. *Arch Pathol Lab Med.* (2021) 146:440–50. doi: 10.5858/arpa.2020-0723-CP
4. Baxi V, Edwards R, Montalto M, Saha S. Digital pathology and artificial intelligence in translational medicine and clinical practice. *Mod Pathol.* (2022) 35:23–32.
5. Hanna MG, Ardon O, Reuter VE, Sirintrapun SJ, England C, Klimstra DS, et al. Integrating digital pathology into clinical practice. *Mod Pathol.* (2022) 35:152–64.
6. Lujan GM, Savage J, Shana'ah A, Yearsley M, Thomas D, Allenby P, et al. Digital pathology initiatives and experience of a large academic institution during the coronavirus disease 2019 (COVID-19) pandemic. *Arch Pathol Lab Med.* (2021) 145:1051–61. doi: 10.5858/arpa.2020-0715-SA
7. Lujan G, Quigley JC, Hartman D, Parwani A, Roehmholdt B, Meter BV, et al. Dissecting the business case for adoption and implementation of digital pathology:

- a white paper from the digital pathology association. *J Pathol Inform.* (2021) 12:17. doi: 10.4103/jpi.jpi_67_20
8. University of Bern. *J. U. Digitalisation of Diagnostic Histopathology Slides - A Comparative Study*. Bern: University of Bern (2018).
9. Blank A, Dawson H, Hammer C, Perren A, Lugli A. Lean management in the pathology laboratory. *Pathologe.* (2017) 38:540–4.
10. Hanna MG, Pantanowitz L. Bar coding and tracking in pathology. *Clin Lab Med.* (2016) 36:13–30.
11. Unternaehrer J, Grobholz R, Janowczyk A, Zlobec I, Swiss Digital Pathology Consortium [SDPC]. Current opinion, status and future development of digital pathology in Switzerland. *J Clin Pathol.* (2020) 73:341–6.
12. Koelzer VH, Grobholz R, Zlobec I, Janowczyk A, Swiss Digital Pathology Consortium [SDPC]. Update on the current opinion, status and future development of digital pathology in Switzerland in light of COVID-19. *J Clin Pathol.* (2021). [Epub ahead of print]. doi: 10.1136/jclinpath-2021-207768
13. Molin J, Lundstrom C, Fjeld M. A comparative study of input devices for digital slide navigation. *J Pathol Inform.* (2015) 6:7. doi: 10.4103/2153-3539.151894
14. Williams BJ, Jayewardene D, Treanor D. Digital immunohistochemistry implementation, training and validation: experience and technical notes from a large clinical laboratory. *J Clin Pathol.* (2019) 72:373–8. doi: 10.1136/jclinpath-2018-205628
15. Mukhopadhyay S, Feldman MD, Abels E, Ashfaq R, Beltaifa S, Cacciabeve NG, et al. Whole slide imaging versus microscopy for primary diagnosis in surgical pathology: a multicenter blinded randomized noninferiority study of 1992 cases (pivotal study). *Am J Surg Pathol.* (2018) 42:39–52. doi: 10.1097/PAS.0000000000000948
16. Araujo ALD, Arboleda LPA, Palmier NR, Fonseca JM, de Pauli Paglionni M, Gomes-Silva W, et al. The performance of digital microscopy for primary diagnosis in human pathology: a systematic review. *Virchows Arch.* (2019) 474:269–87. doi: 10.1007/s00428-018-02519-z
17. Williams BJ, Brett D, Aslam M, Barrett P, Bryson G, Cross S, et al. Guidance for remote reporting of digital pathology slides during periods of exceptional service pressure: an emergency response from the UK royal college of pathologists. *J Pathol Inform.* (2020) 11:12. doi: 10.4103/jpi.jpi_23_20
18. Hufnagl PZR, Haroske G. *Leitfaden Digitale Pathologie in der Diagnostik – Befunderstellung an Digitalen Bildern*. Berlin: Bundesverband Deutscher Pathologen e.V (2018).
19. Senaras C, Niazi MKK, Lozanski G, Gurcan MN. DeepFocus: detection of out-of-focus regions in whole slide digital images using deep learning. *PLoS One.* (2018) 13:e0205387. doi: 10.1371/journal.pone.0205387
20. Kohlberger T, Liu Y, Moran M, Chen PC, Brown T, Hipp JD, et al. Whole-slide image focus quality: automatic assessment and impact on AI cancer detection. *J Pathol Inform.* (2019) 10:39. doi: 10.4103/jpi.jpi_11_19
21. Janowczyk A, Zuo R, Gilmore H, Feldman M, Madabhushi A. HistoQC: an open-source quality control tool for digital pathology slides. *JCO Clin Cancer Inform.* (2019) 3:1–7.
22. University of Bern. *S. K. Automatized Quality Assessment of Whole Slide Images - An Exploratory Laboratory Study Medical Faculty*. Bern: University of Bern (2021).
23. van der Laak J, Litjens G, Ciompi F. Deep learning in histopathology: the path to the clinic. *Nat Med.* (2021) 27:775–84. doi: 10.1038/s41591-021-01343-4
24. Varga Z, Diebold J, Dommann-Scherrer C, Frick H, Kaup D, Noske A, et al. How reliable is Ki-67 immunohistochemistry in grade 2 breast carcinomas? A QA study of the swiss working group of breast- and gynecopathologists. *PLoS One.* (2012) 7:e37379. doi: 10.1371/journal.pone.0037379
25. Echle A, Rindtorff NT, Brinker TJ, Luedde T, Pearson AT, Kather JN. Deep learning in cancer pathology: a new generation of clinical biomarkers. *Br J Cancer.* (2021) 124:686–96. doi: 10.1038/s41416-020-01122-x
26. Paige. *PaigeProstate Detect.* (2022). Available online at: <https://www.paige.ai/> (accessed February 5, 2022).
27. Bychkov D, Linder N, Tiulpin A, Kucukel H, Lundin M, Nordling S, et al. Deep learning identifies morphological features in breast cancer predictive of cancer ERBB2 status and trastuzumab treatment efficacy. *Sci Rep.* (2021) 11:4037. doi: 10.1038/s41598-021-83102-6
28. Kather JN, Heij LR, Grabsch HI, Loeffler C, Echle A, Muti HS, et al. Pan-cancer image-based detection of clinically actionable genetic alterations. *Nat Cancer.* (2020) 1:789–99.
29. Abels E, Pantanowitz L, Aeffner F, Zarella MD, van der Laak J, Bui MM, et al. Computational pathology definitions, best practices, and recommendations for regulatory guidance: a white paper from the digital pathology association. *J Pathol.* (2019) 249:286–94. doi: 10.1002/path.5331
30. Polesie S, McKee PH, Gardner JM, Gillstedt M, Siarov J, Neittaanmaki N, et al. Attitudes toward artificial intelligence within dermatopathology: an international online survey. *Front Med.* (2020) 7:591952. doi: 10.3389/fmed.2020.591952
31. Zehra T, Shabbir A. Adoption of digital pathology in developing countries: from benefits to challenges. *J Coll Physicians Surg Pak.* (2021) 31:1120–2. doi: 10.29271/jcpsp.2021.09.1120
32. Chen PC, Gadepalli K, MacDonald R, Liu Y, Kadowaki S, Nagpal K, et al. An augmented reality microscope with real-time artificial intelligence integration for cancer diagnosis. *Nat Med.* (2019) 25:1453–7.

Advantages of publishing in Frontiers



OPEN ACCESS

Articles are free to read
for greatest visibility
and readership



FAST PUBLICATION

Around 90 days
from submission
to decision



HIGH QUALITY PEER-REVIEW

Rigorous, collaborative,
and constructive
peer-review



TRANSPARENT PEER-REVIEW

Editors and reviewers
acknowledged by name
on published articles

Frontiers

Avenue du Tribunal-Fédéral 34
1005 Lausanne | Switzerland

Visit us: www.frontiersin.org

Contact us: frontiersin.org/about/contact



REPRODUCIBILITY OF RESEARCH

Support open data
and methods to enhance
research reproducibility



DIGITAL PUBLISHING

Articles designed
for optimal readership
across devices



FOLLOW US

@frontiersin



IMPACT METRICS

Advanced article metrics
track visibility across
digital media



EXTENSIVE PROMOTION

Marketing
and promotion
of impactful research



LOOP RESEARCH NETWORK

Our network
increases your
article's readership